The role of external tufted cells in activity-dependent plasticity of the olfactory bulb

Hahn, Christiane

Awarding institution:
King's College London

The role of external tufted cells in activity-dependent plasticity of the olfactory bulb

Christiane Hahn

Institute of Psychiatry, Psychology and Neuroscience

King's College London

2018

Thesis is submitted for the degree of Doctor of Philosophy

Abstract

Neuroplasticity is a feature of the nervous system that allows organisms to adapt to changing environments. Understanding how individual cells in a neural network adjust and integrate their changes to alter circuit function is an important step in elucidating how systems in the brain functionally adapt to a changing sensory world. The olfactory bulb (OB) is a useful model system for studying neuroplasticity because of its stereotyped anatomy and the propensity of many of its components to adjust their properties in an activity-dependent manner. Additionally, inducing changes in OB activity levels can be achieved reliably with straightforward sensory manipulations. In this thesis, we use the OB to explore mechanisms of activity-dependent neuroplasticity on a cellular basis and observe how these adjustments influence the processing output of the network.

External tufted cells (ETCs) are excitatory interneurons found in the glomerular layer of the OB and are central to glomerular processing. Olfactory sensory neurons (OSNs) form monosynaptic contacts to ETCs, which drive the glomerular inhibitory circuitry. ETCs further provide a major source of feed-forward excitation to the glomerular output cells, the mitral and tufted cells (M/TCs). Despite their central role in glomerular processing, our knowledge of ETC activity-dependent plasticity is limited. In light of this, we investigated whether sensory experience alters ETC functional and morphological properties and, if so, whether the effects of any adjustments have any effect on glomerular output. We used 24 hours naris occlusion in mice to decrease OB activity. Whole-cell recordings in acute OB slices from control and occluded mice revealed that ETC intrinsic functional characteristics did not change after 24 h occlusion. This was mirrored by a lack of change in their gross morphological features.

When input of sufficient strength reaches glomeruli, ETCs and M/TCs are triggered to fire and release glutamate synchronously from their dendrites. This results in the generation of all-or-nothing glutamatergic long-lasting depolarising currents (LLCs), which are crucial for maintaining synchrony in the excitatory glomerular network, and are involved in shaping stimulus-evoked firing output of both ETCs and M/TCs. After short-term sensory deprivation, both ETCs and M/TCs portrayed larger LLCs under certain recording conditions. We demonstrate that OSN release probability does not change with occlusion, and thus likely does not contribute to the LLC phenotype. We also found that auto-evoked glutamatergic excitation in ETCs is not increased after 24 h sensory deprivation. These findings suggest that the locus of the LLC change is elsewhere in the network, potentially in mechanisms that enhance glutamate sensing or release at ETCs and/or M/TCs, and/or in adjustments in the local inhibitory circuitry. To explore whether the synaptic changes we observed with occlusion influence glomerular output, we

measured input-output responses by stimulating OSN axons and recording spike responses in ETCs and M/TCs. These experiments revealed that ETCs subtly increase their firing during a stimulus train under occluded conditions when inhibitory signalling is present, whereas M/TCs retain their response profiles both with and without the contribution of inhibitory signalling. Therefore, these properties seem to arise from an intricate interplay of local excitation and inhibition.

Our findings reveal that, surprisingly, the intrinsic properties of ETCs remain remarkably stable in response to short-term sensory deprivation despite their central role in glomerular processing. Additionally, we found that glomerular synaptic excitatory drive is enhanced with occlusion, although the mechanisms and implications of this change remain to be explored. This form of activity-dependent plasticity might control the gain of information flow through the circuit, thereby maintaining sensory performance in the face of external perturbations.

Declaration

The experiments and results presented in this thesis are the product of my own original research. Every effort has been made to highlight the efforts of others to this work in the text. Of particular note are the following contributions:

Dr. Marcela Lipovsek frequently made occlusion plugs for me to use for sensory manipulations.

Dr. Andres Crespo Vieira performed most of the genotyping of the mice used.

MATLAB scripts for analysing electrophysiological recordings of passive properties, single spiking properties, multiple spiking properties, spontaneous firing, OSN-evoked firing, auto-evoked glutamate release, and OSN release probability were written by Dr. Matthew Grubb. He further contributed substantially to the writing of MATLAB scripts for the analysis of sag potentials, LLCs, and OSN paired-pulse ratios.

The MATLAB script used for analysing AIS properties was written by Dr. Mark Evans.

Chapter 3:

All immunohistochemical data gathered for observing ETC gross dendritic morphology was obtained by Catherine Cunningham for her BSc research project. Under my supervision, she both optimised the staining protocol and traced all neurons to derive the data presented in figure 5, which she collected, and I analysed with statistical testing.

Chapter 4:

All immunohistochemical data for observing VGLUT1/2 expression presented in figures 3 and 6 were gathered by Ebrahim Bakhtar under my supervision for his BSc research project. He also performed all image analysis for these experiments. The subsequent normalisations and statistical analyses were performed by myself.

Acknowledgements

I would like to thank my supervisors, Dr. Matthew Grubb and Prof. Juan Burrone, for their invaluable insights and guidance on this project. I would particularly like to thank Matt for driving me to think about questions scientifically, develop critical reasoning skills, and helping me come to my own conclusions. I wold also like to thank both Matt and Dr. Elisa Galliano for introducing me to the world of electrophysiology. Especially Elisa has given me invaluable advice and training in this field, and has sacrificed a lot of time and effort to patiently introduce me to the skills and theory I would need to complete this project. She has been a great inspiration to me, and for that I cannot show enough gratitude.

I would also like to thank past and present members of the Grubb lab. All of them have provided invaluable advice and support, and made it a pleasure to be part of the scientific community. A special thanks goes out to two BSc students, Catherine Cunningham, and Ebrahim Bakhtar, that hugely helped me with my project by performing some experiments and analyses for me. Darren Byrne, my PhD colleague, has celebrated and struggled through countless experiments along-side me, and made the whole process feel less lonely. Dr. Marcela Lipovsek has kindly taken over the manual labour of making occlusion plugs, for which I cannot thank her enough! I would also like to particularly thank Dr. Andres Crespo-Vieria, our faithful technician that has saved me countless hours of work by helping me genotype animals, ensuring laboratory equipment runs smoothly, and making stock solutions for me to use. I would also like to thank everyone in the Centre for Developmental Neurobiology that have helped me throughout the years.

I also greatly thank my entire family and friends and my two cats, who have supported me profoundly with their love and kindness. To my mom, Tatjana, thank you for teaching me to keep a level head when the pressure is high, and to my dad, Jörg, thank you for inspiring me to be curious and wonder about how things work. I would also like to particularly thank Dr. Grant Otto, who has driven me to pursue this PhD and given invaluable advice and support throughout. To Dr. Katrin Augustin, thank you for your friendship and support, listening to my stories about the olfactory bulb and providing me with interesting conversations that are not related to science. Thank you also to Dr. Ruth Roberts, without whom my MATLAB skills wold have never developed as much as they did, and who provided constant encouragement. It goes without saying that I am profoundly thankful to my partner, Dr. Devdutt Sharma. You have encouraged me and emotionally supported me through all my successes and downfalls, and without you I would not have made it this far.

Finally, I would like to thank all the mice that enabled me to perform my research.

Contents

List of figures

Abbreviations

ACSF	Artificial cerebrospinal fluid
AHP	Afterhyperpolarisation potential
AIS	Axon initial segment
AMPA	Alpha-amino-3-hydroxy-5-methylisoxazole-4proinate
ANOVA	Analysis of variance
AOB	Accessory olfactory bulb
AP	Action potential
APV	2-Amino-5phosphonovalerate
Arc	Activity-regulated cytoskeleton-associated protein
BrdU	Bromodeoxyuridine
c-AMP	Cyclic adenosine monosphosphate
CCK	Cholecystokinin
ChR2	Channelrhodopsin
Cm	Whole-cell membrane capacitance
DIC	Differential interference contrast
DNA	Deoxyribonucleic acid
dV/dt	Change in voltage/change in time
EdU	5-Ethynyl-2'-deoxyuridine
EGR1	Early growth response protein 1
EPL	External plexiform layer
EPSC	Excitatory postsynaptic current
EPSP	Excitatory postsynaptic potential
ETC	External tufted cell
GABA	Gamma-aminobutyric acid
GC	Granule cell
GCL	Granule cell layer
GFP	Green fluorescent protein
GL	Glomerular layer
HCN	Hyperpolarisation-activated cyclic nucleotide-gated channel
HEPES	(4-(2-hydroxyethyl)-1-piperazineethanesulfonic acid
I	Current
IEG	Immediate early gene

I*h*	Hyperpolarisation-activated cation current
IPL	Internal plexiform layer
IPSC	Inhibitory postsynaptic current
IPSP	Inhibitory postsynaptic potential
ISI CV	Coefficient of variation of inter-spike intervals
JGC	Juxtaglomerular cell
LLC	Long-lasting depolarising current
M/TC	Mitral/Tufted cell
MCL	Mitral cell layer
mV	Milli Volt
NBQX	2,3-dioxo-6-nitro-1,2,3,4-tetrahydrobezno[f]quinoxaline-7-sulfonamide disodium salt
NFAT	Nuclear factor of activated T-cells
NMDA	N-methyl-D-aspartate
OB	Olfactory bulb
ONL	Olfactory nerve layer
OR	Olfactory receptor
OSN	Olfactory sensory neuron
PCR	Polymerase chain reaction
PGC	Periglomerular cell
PPD	Paired pulse depression
PPR	Paired pulse ratio
P*r*	Release probability
PTX	Picrotoxin
Ri	Input resistance
Rm	Membrane resistance
RNA	Ribonucleic acid
Rs	Series resistance
SAC	Short axon cell
SEM	Standard error of the mean
SVZ	Subventricular zone
TC	Tufted cell
TTX	Tetrodotoxin
VGLUT	Vesicular glutamate transporter
Vm	Membrane potential

Vmax	Maximum Voltage
Vthresh	Voltage threshold
WHH	Width at half height
WT	Wild-type

Chapter 1

Introduction

Neuronal plasticity occurs when neurons change their properties in response to changes in input information (Lamprecht and Ledoux, 2004). This phenomenon is critical to allow organisms with nervous systems to adapt to an ever-changing environment. Furthermore, neuroplasticity is vital during development of the brain, in learning and retention of memories, as well as in overcoming brain damage (Zhang and Linden, 2003). How individual neurons are able to respond to changes in incoming information is becoming increasingly well understood. Findings show that there can be a complex interplay between neurons changing their intrinsic excitability, synaptic properties, and even the structural arrangements of their components (Alkon, 1984; Brons and Woody, 1980; Ganguly et al., 2000; Grubb and Burrone, 2010; Chand et al., 2015). Now, more attention is being given to how these individual neuron-level changes can integrate at the network level. This will enable more in-depth understanding of how different networks function, as well as how whole-network adaptation occurs. This understanding may provide answers to topics such as how to re-generate a damaged circuit. In recent years, the rodent olfactory bulb (OB) has proven to be a valuable model network for studying plasticity. Many different cell populations occupying the OB are genetically tractable and the circuitry and individual odour processing steps are reasonably well known. Furthermore, manipulating activity levels in the OB circuitry can be reliably achieved with relatively simple sensory manipulations. Using these tools it has been found that many OB cell types have the capacity to undergo plastic changes (e.g. Chand et al., 2015; Cummings et al., 2014; Kosaka et al., 1987; for review see Wilson et al., 2004). Therefore, the OB has become an appropriate model system for deciphering how sensory information is computed by neural circuits, and how this computational prowess adjusts in response to changes in the environment.

1.1. The olfactory bulb

1.1.1. Odour input

Pre-neuronal determinants of olfactory processing

The OB is the first neural processing centre of olfactory information in the vertebrate brain. The processing of odour information starts in the nasal epithelium. Olfactory information is received and transduced by the olfactory sensory neurons (OSNs) that project their sensory cilia out of the olfactory epithelium into the nasal lumen to act as receptacles for odour molecules (Lowe,

2013). The nasal epithelium lies on top of anatomically distinct complex tissue folds, called turbinates, that form branched extensions of the ethmoid bone.

Multiple factors determine how odour molecules reach OSN cilia in this epithelial structure. In rodents, air flows through these channels during inspiration in a distinct pattern that maintains smooth parallel-layered airflow, i.e. laminar flow, as opposed to the less complex nasal passages in primates, where airflow is turbulent (Schoenfeld and Cleland, 2005). The nasal epithelium is lined with aqueous mucus in the terrestrial vertebrate nose. This serves to act as a selective barrier that absorbs inhaled vapours differently according to the sorptive properties of odour molecules. This means that distinct odour molecules migrate differently through the nose, where highly sorptive low-volatility hydrophilic molecules are retained more compared to less sorptive, high-volatility hydrophobic molecules (Schoenfeld and Cleland, 2005). This variability in odorant molecule migration is further impacted by fluctuations in inhalation dynamics, such as variations in flow rate, duration, and cycling. For example, the sorption of an odour molecule is reduced by higher air flow rates, whereas migration is enhanced under these circumstances (Mozell et al., 1991; Kent et al., 1996). Air flow variability arises due to several factors. First, rodents exhibit differential structures of medial and lateral nasal recesses though which air flow is pushed through at different rates (Kimbell et al., 1997). Additionally, one nostril gains higher air flow than the other, and the "dominant" nostril is switched every few hours. This difference in patency results in each nostril being differently optimised to sense different odorants, meaning that they transmit slightly different olfactory information to the brain (Sobel et al., 1999). This may be beneficial, because low- and high-sorptive odour molecules, which are best detected at various air-flow dynamics, can be detected by higher-order processing centres at the same time (by the summated activity of both nostrils) in this way (Schoenfeld and Cleland, 2005). Finally, active sniffing during odour-evoked behaviour further introduces variability in air flow (Sobel et al., 2000). Therefore, the structure of the nasal cavity and the olfactory epithelium within it, as well as the dynamics of air flow, are heavily involved in enhancing the differential migration of odorants according to their sorptiveness.

Olfactory transduction

Once odorants reach the OSNs, they bind to G-protein coupled olfactory receptors (ORs), which are located on the OSN cilia. Binding of an odorant to an OR results in G-protein activation, which activates adenylate cyclase that functions to increase intracellular cyclic AMP (c-AMP). Increased c-AMP results in the opening of ion channels that permit Na^+ and Ca^{2+} entry into the OSN, causing a depolarisation of the membrane. This depolarisation results in the generation of action potentials that are transmitted to the OB. Therefore, the OR-induced depolarisation and

subsequent action potential generation at the OSN is the initial step in which olfactory information is transduced (Nakamura and Gold, 1987). ORs are encoded by ~ 1000 genes in the mouse (Buck and Axel, 1991) and each mature OSN expresses only one of these genes, resulting in the expression of one OR-type and thus tuning the OSN to specific odour molecule families (Buck, 2004; Ibarra-Soria et al., 2014; Ressler et al., 1993).

Organisation of OSN input to the OB

Although each OSN only expresses one OR, individual ORs can bind multiple odorants, enabling distinct OSN types to detect multiple odorants (Malnic et al., 1999). OSNs are segregated into four broad zones along the mammalian nasal epithelium within which OSNs expressing particular ORs are seemingly randomly distributed (Vassar et al., 1994). However, there is considerable order in the way they send information to the brain. OSN axons coalesce in the olfactory epithelium, before projecting through the cribriform plate into the olfactory nerve layer (ONL) of the OB (Wilson and Mainen, 2006). From the ONL, OSNs project their axon terminals into the first processing structures of the OB - the glomeruli. These are neuropil filled "sacks" that contain a rich array of dendrites from cells within the OB and are surrounded by glial cells. Here, OSN axon terminals form axo-dendritic connections with postsynaptic targets, that then begin further odour processing (Lowe, 2013). Mammals have around 1000-3000 glomeruli, which approximates with the number of OR genes (Royet et al., 1987). From this observation stemmed the idea that OSNs must project their axons to spatially defined glomeruli. Indeed, early optical imaging and electrophysiological studies found that different odours activate different sets of glomeruli (Imamura et al., 1992; Kauer et al., 1987). Labelling OR mRNA in OSN terminals further demonstrated that specific OSNs project their axons to one, or a few, glomeruli that are bilaterally symmetric (Vassar et al., 1994). Furthermore, glomerular targeting is highly specified depending on which OR is expressed on which OSNs. Upon fluorescently labelling a specific OR type, the resulting fluorescently labelled OSNs associated with that OR projected to topographically fixed glomeruli in the mouse OB. Switching this fluorescently labelled OR for another resulted in an altered OSN projection pattern, where these axons now projected to a different set of glomeruli (Mombaerts et al., 1996).

Therefore, although the organisation of OSNs in the nasal epithelium appears somewhat chaotic, their axonal targets are distinctly specified which ensures individual glomeruli are activated by a distinct range of odour molecules, allowing them to respond to a set of odorants. Thus, odour information is transduced into a specified set of processing centres in the OB.

1.1.2. OB structure

Once OSNs release glutamate from their axon terminals (Ennis et al., 1996), the signal is further processed by multiple OB subnetworks comprised of distinct excitatory and inhibitory cell types.

Within the OB, histological studies using Golgi and Nissl staining, together with electron microscopy, have identified several morphologically distinct neuronal types that segregate into several layers of the OB (Pinching and Powell, 1971a,b; Price and Powell, 1970a,b). These observations further identified three initial groups of distinct neurons found in the OB; the juxtaglomerular cells (JGCs) surrounding glomeruli in the glomerular layer (GL), the principal mitral (MCs) and tufted cells (TCs; together M/TCs) forming the mitral cell layer (MCL) in deeper areas of the OB, and the granule cells (GCs), located at the heart of the OB and forming the largest layer, the granule cell layer (GCL). The JGCs were then divided into a further three subgroups based on gross morphology; the periglomerular cells (PGCs), the short axon cells (SACs), and the external tufted cells (ETCs) (Pinching and Powell, 1971a,b). Around 400 JGCs surround individual glomeruli, with the most numerous being PGCs, followed by around 40 ETCs, and then more sparsely SACs(around 1-2 per glomerulus, although this may be an underestimate; Adam and Mizrahi, 2011; Galliano et al., 2018). Each glomerulus further contains apical dendrites from around 70 M/TCs (Lowe, 2013).

Therefore, the JGCs form a heterogenous group and mostly consist of interneurons that do not innervate locations outside the OB (Nagayama et al., 2014). There is considerable soma-sparse space between the GL and MCL, called the external plexiform layer (EPL), that is occupied mostly by lateral M/TC dendrites and GC dendrites, as well as fibres originating from ETCs (Lowe, 2013). The space superficial to glomeruli is occupied by OSN axons converging to their specific targets, as well as supporting olfactory ensheathing cells (Ramón-Cueto and Avila, 1998), and is named the olfactory sensory neuron layer (ONL). Thus, the OB can be stratified into several discrete layers, and as will be described below, discrete functions. **Figure 1** displays a simplified depiction of OB structure and connectivity to provide a visual aid to the following descriptions.

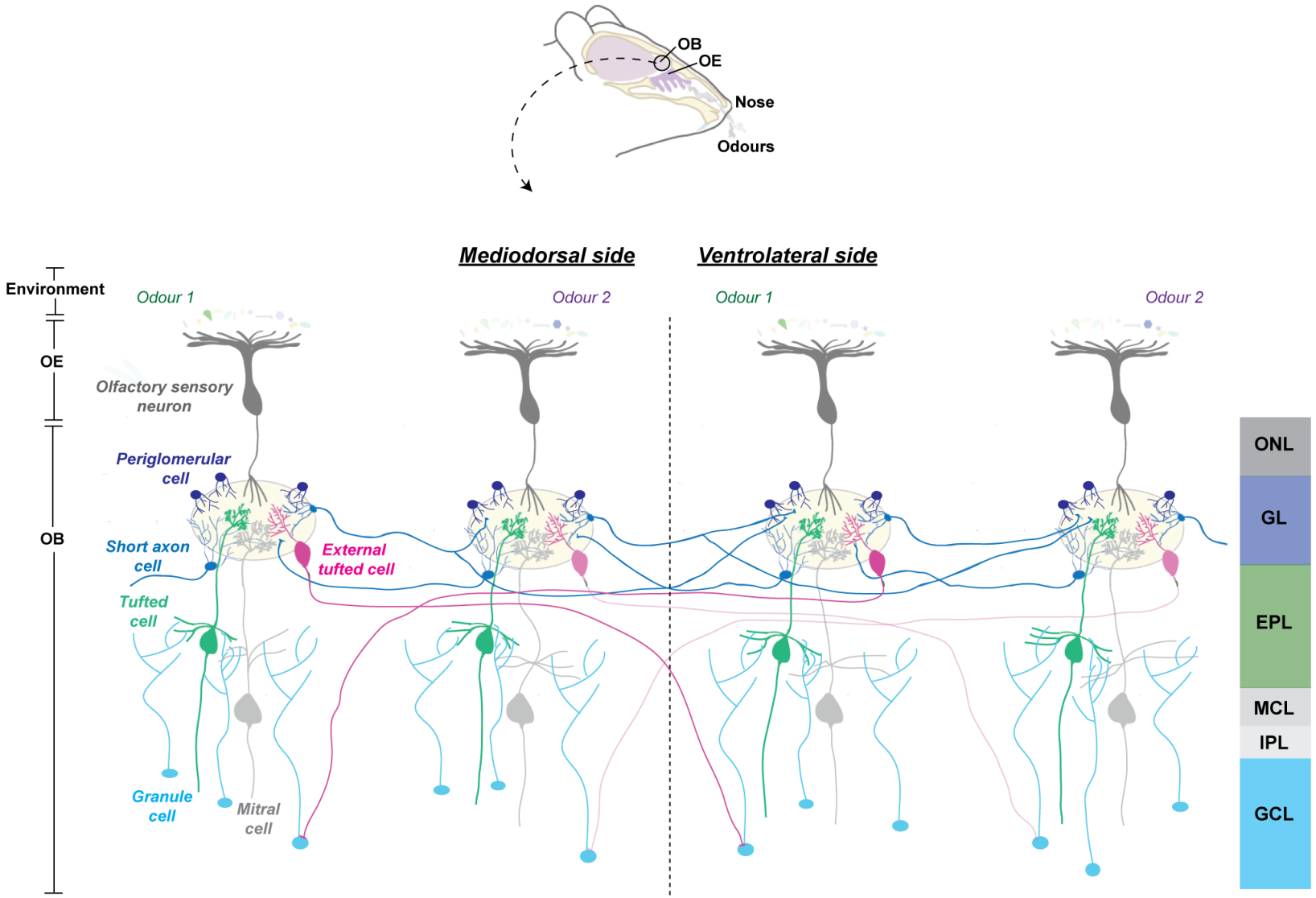
OB
OE
Nose
Odours
Mediodorsal side
Ventrolateral side
Environment
OE
OB
Odour 1
Odour 2
Odour 1
Odour 2
Olfactory sensory neuron
Periglomerular cell
Short axon cell
External tufted cell
Tufted cell
Granule cell
Mitral cell
ONL
GL
EPL
MCL
IPL
GCL

Figure 1. Rodent olfactory bulb (OB) structure.

Top: odours in the environment enter the nose and reach the olfactory epithelium (OE) where olfactory sensory neuron (OSN) sensory cilia are located. Bottom: OSNs express one type of olfactory receptor that recognises distinct odours. Hence, distinct odours activate different groups of glomeruli. OSNs project their axons to glomeruli in the glomerular layer (GL). Here, odour information is processed by local interneuron circuits. Periglomerular cells are axon-less and provide GABA neurotransmission, with some sub-types co-releasing dopamine. Short axon cells also provide GABA and dopaminergic neurotransmission but extend axons to other glomeruli. External tufted cells (ETCs) receive monosynaptic inputs from OSNs and provide excitatory drive to the glomerular circuit. ETCs target their axons to granule cells (GCs) that are involved in processing odours received by the same class of OSN receptor input at isofunctional glomeruli. Tufted cells are located in the deep external plexiform layer (EPL) and form part of the principal neuron population. Mitral cells are located in the mitral cell layer (MCL) and are also part of the principal neuron population. Both mitral cells and tufted cells form axon collaterals in the internal plexiform layer (IPL) that go on to target the olfactory cortex. The axon-less GCs are located in the granule cell layer (GCL) and project their dendrites into the EPL where they provide GABAergic reciprocal inhibition onto tufted and mitral cells.

Mitral and tufted cells

The large glutamatergic M/TCs located in the deep EPL and MCL are the principal cells of the OB circuit and are central to input-output functioning of the OB. They project their smooth primary apical dendrites through the EPL with little branching, into single glomeruli where they extensively ramify their dendrites. The apical dendrite is thus well-placed to receive modulated odour-evoked OSN input through glomerular signalling. MCs project their lateral dendrites into deeper areas of the EPL, whereas TCs generally extend lateral dendrites to more superficial areas of the EPL (Mori et al., 1983; Orona et al., 1983). M/TCs converge their axons to form the lateral olfactory tract that projects to output targets located in olfactory cortex (Lowe, 2013).

There is vast heterogeneity within these two categories of principal cells, the functional properties of which are still being investigated (Nagayama et al., 2014). Recent two-photon imaging revealed at least three types of MCs based on soma shape. Some are triangular, some are round, and some are fusiform (Kikuta et al., 2013). Additionally, some MCs express the $GABA_A$ receptor subunit α3, whereas others do not (Panzanelli et al., 2005). Furthermore, these cells have shown strong heterogeneity in their expression of voltage-gated K^+ channels and hyperpolarising-current activated cyclic nucleotide-gated (HCN) channels (Angelo et al., 2012; Padmanabhan and Urban, 2010).

Furthermore, there is heterogeneity in terms of axonal projection end-points. TCs mostly project axons to the anterior olfactory cortex, whereas MCs target axons widely throughout the entire olfactory cortex (Nagayama et al., 2010; Igarashi et al., 2012). It was further found, using clever rabies-virus dependent retrograde monotranssynaptic labelling, that individual cortical neurons receive M/TC axon contacts representative of several glomeruli, and different cortical areas represent different areas of the OB. For example, the piriform cortex appears to receive input from all areas of the OB, however the cortical amygdala receives projections from frontal parts of the OB (Miyamichi et al., 2011). Even M/TCs localised to the same glomerulus do not necessarily end up projecting their axons to the same cortical target (Miyamichi et al., 2011).

Granule cells

Most of the GCL is occupied by the somas of small GCs (Price and Powell, 1970b). These somas are stacked into horizontal rows where they are interspersed with MC and TC axons, as well as centrifugal fibres (Lowe, 2013). GCs are interneurons and are vastly numerous, consisting of many more cells compared to the MC and TC population. GCs are anaxonic and send spiny dendrites into the EPL where they form reciprocal dendrodendritic synapses with MCs and TCs

(Rall et al., 1966). So far, GABA has been the only identified neurotransmitter in these cells (Lowe, 2013).

GCs also form a heterogenous group of cells. Based on their dendritic extensions into the EPL, GCs have been grouped into at least three subgroups. Type I GCs have spiny dendrites at all depths in the EPL, type II GCs only extend dendrites into the deeper areas of the EPL, and type III extend their dendrites to superficial EPL areas (Mori et al., 1983). GCs also undergo extensive life-long neurogenesis, with ~ 10,000 GCs born each day in the subventricular zone (SVZ). Nevertheless, only around half of these newly generated cells are integrated into the existing network, and many existing GCs undergo apoptosis on a daily basis (Yamaguchi and Mori, 2005).

In summary, due to their position and projections, GABAergic GCs form an inhibitory feedback loop with M/TCs and are involved in modulating these cells (Lowe et al., 2013; see below).

Glomerular layer interneurons

Periglomerular cells

The PGCs have the smallest cell somas of all JGCs and project a spiny dendrite into only one, and very rarely multiple, glomeruli (Parrish-Aungst et al., 2007). The PGCs are generally termed as such to represent a group of JGCs, however even among PGCs there is high heterogeneity that encompasses multiple distinct subsets of cells. These subsets can be distinguished by their biochemical properties. Subsets have previously been identified via the expression of different calcium binding proteins, calretinin and calbindin, as well as the rate-limiting enzyme in dopamine synthesis, tyrosine hydroxylase (TH) (Kosaka and Kosaka, 2011). It was further demonstrated that most of these identified subclasses also express the GABAergic neuronal marker glutamate decarboxylase (GAD), either GAD65 or GAD67, establishing most PGCs as GABAergic interneurons (Nagayama et al., 2014). In mouse, cells expressing calbindin, calretinin and TH are largely non-overlapping. However, both the TH and calbindin populations preferentially express GAD67, whereas GABAergic calbindin expressing cells almost exclusively express GAD65 (Parrish-Aungst et al., 2007).

The connectivity of PGCs further segregates these cells into different subtypes. PGCs were initially classified into two subgroups depending on whether they project to glomerular areas containing OSN terminals, type I, or areas without OSN terminals, type II (Kosaka et al., 1987). Thus, it was considered that type I PGCs likely receive direct OSN input, whereas type II likely do not. Type I PGCs incorporate cells expressing both GAD and TH, whereas type II have been shown to contain GAD-, calbindin+, and calretinin+ PGCs (Kosaka and Kosaka, 2007). Particular interest was shown toward the TH-expressing PGCs as these were shown to co-release both GABA and

dopamine (Borisovska et al., 2013), as well as undergo life-long neurogenesis (Bonzano et al., 2014). Recent findings however, have shown that TH-expressing PGCs may further be subdivided into different populations based on morphological and functional properties. Recent evidence demonstrated that only the small anaxonic TH-expressing PGCs are postnatally generated (Galliano et al., 2018), and indeed it has been known for some time that there are likely two populations of JGCs that are dopaminergic based on soma size (Pignatelli et al., 2005). The small dopaminergic cells are likely "true" PGCs since they ramify into a single glomerulus, whereas the large subtype is likely a type of SAC (see below) due to their interglomerular dendritic and axonal ramification (Kiyokage et al., 2010). Collectively, dopaminergic JGCs of both types will be referred to as GABA/dopaminergic JGCs in this thesis.

Therefore, PGCs form a group of highly variable, mostly GABAergic, set of cells that are generally associated with one glomerulus. Due to their location and connectivity, they are anatomically well-placed to modulate initial odour-evoked input by providing inhibitory drive. The "true" PGCs, i.e. those associated with just one glomerulus, are especially anatomically well-placed to exhibit very local, intraglomerular modulation of input.

Short-axon cells

Despite their name, SACs actually possess relatively long axons that ramify across large areas of the GL. Original Golgi staining did not provide the penetration required to observe these long axons and thus arose the somewhat counter-intuitive nomenclature of these cells (Lowe, 2013). SACs also comprise a heterogenous population of cells based on their soma location, with some located close to the glomeruli, and some fairly deep in the OB (Kosaka and Kosaka, 2011). SACs have slightly larger soma sizes compared to PGCs and project their broad dendritic arbours to several glomeruli. Despite these projection targets, SACs do not seem to receive monosynaptic input from OSNs (Kiyokage et al., 2010). Indeed, it has recently been proposed that "true" SACs (mostly) do not directly project their dendrites into glomeruli at all, but rather, send these to targets between glomeruli (Kosaka and Kosaka, 2011).

Based on their polyglomerular morphology (Galliano et al., 2018; Kiyokage et al., 2010; Pinching and Powell, 1971a,b), as well as long-range functional data on interglomerular inhibition (Aungst et al., 2003; Whitesell et al., 2013), SACs appear to project their axons to several glomeruli, though the extent of this targeting is yet to be determined . SACs express the 67 isoform of GAD, as well as TH (Kosaka and Kosaka, 2011), and have been shown to release both GABA and dopamine (Liu et al., 2013). Due to these properties, SACs are largely thought to form part of the interglomerular inhibitory processing machinery (Kiyokage et al., 2010), and probably form

the population of the larger sized GABA/dopaminergic JGCs that are generated embryonically around E11-12 (Galliano et al., 2018).

External tufted cells

The glutamatergic ETCs exhibit the largest soma sizes of the JGCs and are located in the deeper parts of the GL (Pinching and Powell, 1971a). ETCs, as demarcated by their name, possess a tufted-looking apical dendrite, which they ramify into a single, or very rarely into two, glomeruli (Hayar et al., 2004a). These dendrites are mostly smooth, with only a few ETC dendrites containing sparely distributed spines (Hayar et al., 2004b). Most importantly, OSNs form extensive connections with ETCs, allowing ETCs to receive monosynaptic afferent input (Hayar et al., 2004b). Additionally, the extensive ETC dendritic ramification occupies more of a glomerulus compared to PGCs and even M/TC dendrites (Hayar et al., 2004b). Dendrodendritically, ETCs target PGCs (Hayar et al., 2004b; Gire et al., 2018), GABA/dopaminergic SACs (Banerjee et al., 2015), and M/TCs (De Saint Jan et al., 2009), and have been shown to provide excitatory inputs to all of these synaptic partners.

Targeted tracer experiments allowed for the observation that ETCs project their axons to isofunctional odour columns, meaning that they target mirror glomeruli innervated by OSNs expressing the same OR gene (Belluscio et al., 2002). These axons project into the internal plexiform layer (IPL), the layer formed between the MCL and the GCL, containing axon collaterals of MCs and TCs. Here, ETCs form synapses with GCs, which in turn project their dendrites into the EPL to form contacts with MCs and TCs associated with the isofunctional glomerulus (Lodovichi et al., 2003).

Similar to other JGCs, ETCs comprise a diverse group of cells that show morphological and functional differences (Antal et al., 2006). One group is located deeper in the GL, close to the EPL boundary, and contains lateral dendrites (Macrides and Schneider, 1982). Another group has no secondary dendrites, and only a single dendritic tuft ramifying in just one glomerulus (Liu and Shipley, 2008). Molecularly, ETCs can further be subdivided into several groups. Most ETCs are glutamatergic, expressing markers for VGLUTs (Ohmomo et al., 2009; Tatti et al., 2014). It was however, further found that a portion of VGLUT3 expressing ETCs also express GABAergic markers (Tatti et al., 2014). Additionally, some ETCs have been shown to release the neuropeptide cholecystokinin (CCK) as a neurotransmitter, and thus express CCK (Liu and Shipley, 1994), with a further subtype shown to release vasopressin (Tobin et al., 2010). ETC populations can further be subdivided based on their expression of $GABA_A$ receptor subunits. Some ETCs contain the α1 subunit, others the α3 subunit, and some containing both (Panzanelli et al., 2005). To date, the overlap of these distinct markers has not been extensively studied.

However, it appears that most ETCs that project lateral dendrites also express CCK and/or vasopressin (Liu and Shipley, 1994; Tobin et al., 2010) and preferentially the α3 subunit of $GABA_A$ receptors (Panzanelli et al., 2005). Additionally, ETCs expressing VGLUT3 dendrodendritically appear to exclusively excite TCs, and exhibit inhibitory input only to other ETCs (Tatti et al., 2014).

ETCs are generated in the later stages of mouse embryogenesis (E17.5 onwards) in both intra- and extrabulbar regions. Most are born in the ventricular zone of the OB region from radial glia where they migrate radially to their target location. However, a small number are generated up to perinatal ages in the lateral ventricle, where they migrate through the rostral migratory stream (RMS) (Winpenny et al., 2011).Their axonal development appears to occur mostly in early postnatal ages, where projections are first detectable at P7, with axons targeting broad regions that are initially input-independent. Subsequent axon specificity refinement is then dependent on odour input during the first weeks of life (Marks et al., 2006).

Thus, ETCs form a population of highly heterogenous, (mostly) glutamatergic JGCs that are well-positioned for receiving direct OSN input, providing intraglomerular excitation, and also appear to be involved in interglomerular processing.

The accessory olfactory bulb (AOB)

The main OB described above is not the only first-stage odour processing structure in the vertebrate brain. The AOB is another important structure involved in processing cues related to biological function, such as social recognition and mate selection (Holy, 2018). Whereas the main OB detects a broad variety of odorants, the AOB detects a more specific category of odorants related to pheromones and other semiochemicals. The AOB is located at the posterior end of the OB and receives inputs from vomeronasal sensory neurons (VSNs). These project their microvilli into the vomeronasal organ, a mucus-filled tube located in the nasal septum (Brennan and Keverne, 2004). As opposed to the OSNs in the main OB, VSNs are located away from the nasal airflow, and thus stimulation depends on a vascular pumping mechanism, allowing VSNs to detect non-volatile stimuli like urine deposits and saliva (Meredith, 1994). Processes in the AOB are transmitted via the amygdala and the bed nucleus of the Stria terminalis to hypothalamic areas where signals can induce behavioural and endocrine effects (Li et al., 1990). Additionally, the AOB receives noradrenergic, cholinergic, and serotonergic neuromodulatory input, and is thus heavily involved in the modulation of an animal's state (Holy, 2018).

The AOB is structurally similar to the main OB, however there are some key differences that likely contribute to different sensory processing mechanisms here. Vomeronasal receptors (VRs) are not as diverse as ORs. In the mouse, only 365 VR genes have so far been identified, arising

from three gene families, V1R, V2R, and formyl peptide receptors (FPRs) (Holy, 2018). Furthermore, as opposed to the main OB, many glomeruli in the AOB receive input from distinct VR-related VSNs. Additionally, the enzyme inducing activation in VSNs is phospholipase-C, as opposed to c-AMP in the OSNs (Halpern and Martinez-Marcos, 2003). The overall layered structure in the AOB is also different compared to the main OB. In the AOB, TCs (including ETCs) do not appear to be present, or at least are not structurally/morphologically distinguishable from MCs. Additionally, MCs have branched dendrites that ramify into multiple glomeruli, with some even being able to sample multiple VR-associated stimuli (Holy, 2018). As opposed to the main OB, MCs in the AOB are not found in a neat MCL, but rather, are scattered below the GL (Lowe, 2013). In addition to this, MCs in the AOB possess fewer secondary dendrites that are shorter in length compared to main OB MCs, thus positioning GC reciprocal synapses close to the MC primary dendritic tree (Halpern and Martinez-Marcos, 2003). Furthermore, MCs appear to form fewer contacts with GCs, and very few PGCs in the AOB seem to express TH (Mugnaini et al., 1984).

MCs of the AOB project to the bed nucleus of the stria terminalis and the vomeronasal corticostriatum, which form projections between each other as well as the hypothalamus (Holy, 2018). Furthermore, AOB MCs have been shown to target axons to the main OB, with electrophysiological confirmation that these axons are functional, suggesting that these two processing centres can interact early on in olfactory processing (Vargas-Barroso et al., 2016).

Given the important biological functions that the vomeronasal system is involved in, and the compact nature of the AOB, it is thus an excellent model system for elucidating the neural basis behind behaviours, enabling the study of how sensory input is converted to a behavioural output. Due to the potential crosstalk between the AOB and main OB (Vagras-Borroso et al., 2016), processes occurring in either system may potentially be impacted by and impact the activity of the other system. It may thus become important to consider these effects when interpreting findings from either processing centre. In light of this, the scope of this thesis focuses on processes occurring specifically in the main OB, however it is important to note that both systems may have been impacted during the course of the experiments.

1.2. Olfactory bulb circuitry and function

1.2.1. Odour representation in the OB

Initial odour representations in the OB consist of the activation of distinct glomeruli that reflect the combinatorial activation of ORs in the OE. It is this glomerular activity pattern that is thought to code for odour identity and concentration. The idea that glomerular activity patterns in

response to odorants are mapped in a certain order has been widely debated. Early findings have demonstrated that odour identity and concentration are uncovered by the relative activity of various glomeruli, with distinct glomeruli showing differences in how sensitive they are to odour stimulants (Bozza et al., 2004; Rubin and Katz, 1999). Though glomeruli responding to similar odour molecules appear to cluster together in the OB (Takahashi et al., 2004), conflicting evidence has shown that even in clustered sets of glomeruli, neighbouring glomeruli can be active upon stimulation with structurally dissimilar odorants (Wachowiak and Shipley, 2006). Furthermore, the pattern of active glomeruli has been shown to change with the concentration of odorants presented. For example, pentanal and 2-hexanone evoke different glomeruli at increasing concentrations, as more glomeruli are recruited from distal parts of the bulb at higher concentrations compared to lower concentrations (Johnson and Leon, 2000). Interestingly, in humans, increased concentrations of the above odours elicit differently perceived smells, supporting the idea that glomerular pattern of activation elicits differential odour perception. In addition to this, odour maps responding to the same stimuli appear to differ between individuals (Oka et al., 2006).

The spatial activity patterns of glomeruli are also temporally dynamic, where odour response patterns change over time during the response, because glomerular odour responses portray varying latencies and rise times in an odorant specific way. These temporal differences in the activation of different glomeruli are perceivable by mice, where they are able to discriminate the activation of different glomeruli during a respiration cycle at ~10ms resolution (Chong and Rinberg, 2018).

These temporal patterns appear to arise due to activity patterns displayed by OSNs and postsynaptic bulbar processes. OSNs display diverse temporal dynamics across glomeruli in an odorant-specific manner (Spors et al., 2006). These temporal dynamics are likely to impact postsynaptic cascades in the OB, and the collective temporal patterns of these processes give rise to the odour-specific temporal diversity in glomerular response patterns (Spors et al., 2012).

Thus, glomerular spatio-temporal activity patterns code for odorants, however this map is highly heterogenous and may not have any inherent order to it. Surprisingly, the pattern of glomerular activation in response to particular odorants is consistent between individuals, however this consistency likely arises due to a developmentally organised map rather than a functional neural map (Cleland et al., 2002).

Interestingly, there is discrepancy between the odour-evoked activation of glomeruli (i.e. OSNs) and the response properties of M/TCs. At lower odorant concentrations, OSNs and M/TCs show similar odour tuning responses. When odour concentrations increase, M/TCs revert to a more

selective odour tuning curve compared to OSN responses (Adam et al., 2014; Tan et al., 2010) and thus display response profiles that differ to initial input responses.

In addition to this, even though M/TCs projecting to the same glomerulus respond to the same input by OSNs, sister (i.e. associated with the same glomerulus) M/TCs can portray both uniform and heterogenous responses (Tan et al., 2010). M/TCs are narrowly tuned to distinct odour input activating the OR that is expressed by OSNs projecting axons to the corresponding glomerulus. However, the tuning curve of sister M/TCs receiving the same input becomes heterogenous with increasing odour concentration input (Tan et al., 2010). Additionally, in a recent study it was shown that the heterogeneity or uniformity of sister M/TC responses is determined by the relative affinity of a particular ligand to the associated OR, where the strongest ligand evokes uniform responses, however weaker ligands evoke heterogenous responses (Arneodo et al., 2018). Therefore, sister M/TCs appear to be selective in how they respond to the same OSN inputs.

For these activity patterns to occur, a set of complex glomerular processes occur that function to modulate input at the glomerular level. In this way, each glomerulus acts as a filter that fine-tunes glomerular output to functionally respond to particular odours, which is transmitted to the olfactory cortex that integrates these signals, resulting in odour perception.

OSN terminals

Glomeruli are activated by odour input through the binding of odours to ORs on OSNs. Upon activation, OSNs release glutamate onto their synaptic targets in glomeruli, and are capable of doing so in response to single odorant binding events (Lynch and Barry, 1989). OSNs have an unusually high release probability (P*r*) of ~0.8 of their glutamatergic vesicles (Murphy et al., 2004). Upon release, vesicles are slowly replenished, taking up to a minute to fully reinstate vesicle quantities (Vaaga and Westbrook, 2017).

Direct vs indirect activation of M/TCs by OSN input

OSNs primarily excite ETC and M/TC primary dendrites, though ETCs appear to have stronger connections here compared to M/TCs (De Saint Jan et al., 2009; Gire et al., 2012). A series of experiments have demonstrated that the excitatory pathway from OSN input to M/TC output is favourably wired through ETCs. Though direct contacts from OSNs to M/TCs exist (Najac et al., 2011), ETCs have hyperexcitable membrane properties (Hayar et al., 2004a), are excited by lower threshold stimuli (De Saint Jan et al., 2009), and have been shown to transmit glutamate to M/TCs via intraglomerular dendritic release (Zhou and Belluscio, 2008) and spillover communication (Gire et al., 2018). They have also been shown to spike earlier in the sniff cycle

in vivo, and respond to lower odour concentrations compared to M/TCs (Igarashi et al., 2012; Kikuta et al., 2013). Furthermore, input that *is* received by M/TCs is drastically shunted by connexin-36 gap-junction mediated currents (Gire et al., 2012). Thus, it is now widely accepted that under most circumstances, OSN input is first received by ETCs, which then transmit modulated signals to M/TCs. However, upon strong stimulus inputs, M/TCs are able to receive this input directly from OSNs (Gire et al., 2012; Najact et al., 2011; Vaaga et al., 2016).

Temporal Shaping of glomerular output

The properties of OSNs allow OSNs to release glutamate in response to a single odorant binding event (Lynch and Barry, 1989). Due to the "noisy" olfactory environment, many OSNs expressing different ORs are thus stimulated at once, making it difficult to transmit single odour identities to olfactory cortex. In addition to this, OSNs release glutamate at high P*r*, though vesicle replenishment is slow. These features therefore provide relatively transient, and "noisy" input to glomeruli.

However, despite transient and "noisy" input upon odour stimulation, M/TCs respond with prolonged firing patterns (Nagayama et al., 2004). This response pattern may be an essential determinant of final odour perception. In the piriform cortex, pyramidal neurons encode odour identity by being activated in certain patterns. Concentration of odorants has been suggested to be encoded by the temporal response profiles of these cells (Bolding and Franks, 2017). It is thus possible that the prolonged firing of M/TCs ensures pyramidal cells in the piriform cortex obtain reliable odour concentration information, and the activation of multiple M/TCs representing several glomeruli ensures odour identities are transmitted (Bozza et al., 2004; Rubin and Katz, 1999).

For M/TCs to exhibit prolonged firing upon odour input, a series of glomerular processes take place that serve to amplify or subdue initial input (Vaaga and Westbrook, 2017). This serves to provide strong excitatory drive to ensure M/TC prolonged firing, but also ensures weak inputs are subdued, providing a mechanism of contrast enhancement in a "noisy" olfactory environment. In addition to this, initial input is modulated by these processes, and together with feedback communication by GCs adjust the subsequent output properties of M/TCs. Thus, by modulating initial odour input as well as directly modulating M/TC firing, input information is filtered to ensure M/TCs project reliable odour identity and concentration coding to olfactory cortical areas.

1.2.2. Glomerular inhibitory circuitry and function

PGCs and SACs contribute a significant amount of inhibitory drive to the bulbar circuitry by shaping initial OSN input. This occurs both directly, and indirectly via modulating the activity of the excitatory network. These cells exhibit functional properties and local connectivity that are in place to drive inhibition in this first processing step which is thought to indirectly reduce excitatory drive to M/TCs (Lowe, 2013).

Intrinsic properties

PGCs have been shown to burst-fire both spontaneously and when evoked, a feature that is dependent on Ca^{2+} channel activation (McQuiston and Katz, 2001). This feature has been proposed to form part of a mechanism driving synchronous oscillations in the OB, however PGC burst-firing appears to be dependent on the activity of ETCs. Indeed, glutamate release from a single ETC is enough to trigger Ca^{2+} spikes facilitated by NMDA receptor activation in many PGCs (Murphy et al., 2005). Once PGC dendrites are depolarised, the consequential activation of P/Q type Ca^{2+} channels triggers the release of GABA (Murphy et al., 2005). PGCs further portray self-inhibition, where GABA released from a cell can directly activate $GABA_A$ receptors on the same cell. Though GABA could potentially provide excitatory drive to PGCs due to their high internal chloride composition, GABA appears to inhibit PGC firing by shunting excitatory signals (Smith and Jahr, 2002).

Upon depolarisation, most SACs exhibit accommodating trains of action potentials and produce a hyperpolarising sag potential (McQuiston and Katz, 2001). These cells also release GABA, but additionally have been shown to co-release dopamine (Borisovska et al., 2013; Vaaga et al., 2017). As with the PGCs, SAC activity is mainly driven by ETCs, as whole-cell recordings have demonstrated that these cells receive spontaneous, intermittent bursts of excitatory postsynaptic currents (EPSCs) likely originating from activity in ETCs (Hayar et al., 2004b).

Therefore, both PGC and SAC intrinsic activity and GABA/dopamine release seems to be set by the activity of ETCs. This means that PGCs and SACs are well-placed to provide feedback inhibition based on the levels of direct OSN-evoked activity coming into a given glomerulus.

Connectivity

Only around 20% of PGCs receive direct OSN inputs. Instead, the majority of PGCs receive disynaptic or polysynaptic input driven by ETCs (Hayar et al., 2004b). PGCs mainly project their dendrites to intraglomerular targets. PGCs form dendrodendritic synapses with neighbouring PGC dendrites, and thus inhibit each other with GABA release onto $GABA_A$ receptors (Murphy et al., 2005). In addition to this, during self-inhibition, spillover GABA from this transmission spreads laterally within the glomerulus that can act on other PGCs, SACs, and ET/M/TC dendrites

(Smith and Jahr, 2002). PGCs also form dendrodendritic synapses with ETCs (Hayar et al., 2004a), through which they receive most of their glutamatergic inputs.

As with PGCs, not all SACs receive direct synaptic input from OSNs, with only around 33% portraying such connectivity (Lowe, 2013), although whether they show such connectivity at all is still debated (Kosaka and Kosaka, 2011). SACs provide lateral inhibition onto glomeruli by targeting their axons to several glomeruli, and by ramifying their dendritic trees into several glomeruli (Aungst et al., 2003; Galliano et al., 2018; Kiyokage et al., 2010; Kosaka and Kosaka, 2011). SACs target ETCs where they provide inhibitory drive by chemical synapses, but also take part in a dual excitation-inhibition signal via electrical coupling to ETCs. ETCs are also the major source of glutamatergic input to SACs (Banerjee et al., 2015). SACs contribute to long-range interglomerular actions by providing GABAergic and dopaminergic signalling, thus contributing to glomerular inhibitory drive in this way.

Circuit function

The connectivity of PGCs and SACs allows them to modulate the excitatory network either directly via synaptic connectivity to ETCs, or indirectly by modulating the activity of OSN terminals. Their connectivity further provides a locus for the local inhibitory network to directly self-inhibit, which may function as a gain control mechanism.

Though there is sparse connectivity of OSNs with PGCs and possibly SACs, to date there has been no concrete observation of physical synapses of these cells onto OSN terminals by which modulation could occur. This indicates that all the OSN inputs received are through volume transmission and spillover communication. Nevertheless, the synaptic inhibitory drive from PGCs and SACs *can* act to modulate input at this first synapse. OSN terminals express $GABA_B$ and D_2-dopaminergic receptors (L Koster et al., 1999), the activation of which lowers P*r* and inhibits glutamate release (Aroniadou-Anderjaska et al., 2000; Murphy et al., 2005). Thus, the indirect (by ETCs) (Banerjee et al., 2015; Hayar et al., 2004b) or direct (by OSNs) (Maher and L Westbrook, 2008) activation of PGCs and SACs leads to GABA and dopamine release that can act on OSN terminals and subdue input to the glomerulus. This has recently been shown to occur with the endogenous release of GABA and dopamine by these cells (Vaaga et al., 2017).

PGCs and SACs also function to reduce excitatory drive by ETCs through an intricate feedback loop initiated by ETCs (Hayar et al., 2005), which indirectly impacts the amount of excitatory drive reaching M/TCs. PGC activation drives prolonged inhibition on ETC dendrodendritic synapses via $GABA_A$ receptor-mediated currents (Christie et al., 2001), which regulate burst properties in ETCs by reducing within-burst spike numbers (Hayar and Ennis, 2007). GABA release by SACs targets ETCs and results in $GABA_A$ receptor-mediated hyperpolarisation that

activates ETC I*h* currents. Dopamine released by these cells then binds to D_1-dopamine receptors which increases I*h* and results in increased rebound spiking in ETCs (Liu et al., 2013). Therefore, these opposing inhibitory and excitatory signals mediate an inhibition-excitation "switch" in ETCs and regulate their output (Liu et al., 2013). SACs have further been implicated in centre-surround inhibition of glomeruli, a process that is involved in generating contrast enhancement. SACs have been shown to send projections to ETCs at distant glomeruli to form inhibitory synapses there, and excitation in SACs significantly decreased M/TC excitatory input, through the inhibitory actions onto ETCs, implicating their role in lateral inhibition (Whitesell et al., 2013).

PGCs and SACs further impact the collective glomerular excitatory drive that is in place to amplify the transient OSN input. Input by OSNs is amplified through dendrodendritic excitation and spillover glutamate released by ETCs and M/TC dendrites, in the form of long-lasting depolarising currents (LLCs, further described below). LLCs are crucial for generating M/TC output, and LLC magnitude has been shown to directly impact the output these cells generate (Vaaga and Westbrook, 2017). It has previously been shown that $GABA_A$ currents received by ETCs directly reduce the probability of LLC generation (Gire et al., 2009; Whitesell et al., 2013), as well as their magnitude (Carlson et al., 2000), thus inhibition by the local glomerular inhibitory network strongly modulates the function of the excitatory circuitry.

Shaping M/TC responses to odorants

Due to their connectivity and function, the glomerular inhibitory circuit shapes M/TC output by providing inhibitory signalling that subdues OSN input and reduces the activity of ETCs. Since OSN input is most commonly first received by ETCs before being transmitted to M/TCs (Najac et al., 2011; Vaaga et al., 2016), the ETC-evoked as well as OSN-evoked inhibitory actions of PGCs and SACs back onto ETCs and OSNs profoundly modulate how much excitation is received by M/TCs, and thus indirectly shape the response profiles M/TCs exhibit. Indeed, it has been shown that interglomerular inhibition by SACs indirectly supresses M/TC responses to odorants (Banerjee et al., 2015; Economo et al., 2016). Furthermore, PGCs appear to be excited by lower threshold stimuli compared to M/TCs, and thus are recruited at weaker input intensities, which has been shown to supress M/TC responses to these stimuli. Upon stronger input intensities, an excitatory shift allows M/TCs to overcome inhibition and results in greater M/TC responses (Cleland and Linster, 2012; Gire et al., 2009). Whether the effects of glomerular inhibitory circuits directly impact M/TC output are still being explored. Recently it has been suggested that M/TCs can directly be inhibited by local glomerular inhibitory interneurons. Activation of putative PGCs in response to odorants was directly linked to hyperpolarisations in M/TCs, and was thus implicated in shaping M/TC response profiles (Fukunaga et al., 2014). However,

increasing evidence suggests that this modulation mostly occurs indirectly through inhibition targeted to OSN terminals and ETCs (Banerjee et al., 2015; Gire et al., 2009; Murphy et al., 2005).

1.2.3. GC inhibitory circuit and function

GCs function to provide a second wave of inhibitory drive onto M/TCs following initial input modulation by glomerular processes. This inhibition is directly targeted at M/TC secondary dendrites in the EPL and further shapes M/TC responses to odorants.

Connectivity

GCs are anaxonic and thus solely communicate via dendrodendritic communication. GCs connect with M/TCs through reciprocal dendrodendritic synapses of both chemical and electrical nature (Lagier et al., 2004). Virtually all vesicle-containing GC spines target M/TC dendrites, directly opposing M/TC release sites, both pre- and postsynaptically (Rall et al., 1966). Recent findings further showed that one type of GC even targets MC cell bodies rather than their dendrites (Naritsuka et al., 2009), and some superficial GCs also target TC and ETC lateral dendrites (Antal et al., 2006; Shepherd et al., 2007). GCs receive excitatory input from M/TCs via these dendrodendritic synapses, as well as from axons projected by ETCs. GCs further receive excitatory centrifugal input from olfactory cortex, which in turn inhibit M/TCs (Boyd et al., 2012; Markopoulos et al., 2012).

Thus, GCs receive input from the principal cells and centrifugal projections, and direct their output directly to M/TCs.

Circuit function

Since GCs do not project into the glomeruli and cannot receive direct OSN input, they have long been considered to take part in negative feedback inhibition driven by M/TCs. This is supported by electrophysiological experiments demonstrating that GCs transmit GABAergic M/TC-induced negative feedback inhibition (Friedman and Strowbridge, 2003) and specifically target their dendritic output to inhibitory synapses on M/TC dendrites (Shepherd et al., 2007). When a M/TC fires an action potential, this backpropagates to its lateral dendrites where it triggers the opening of high-voltage activated Ca^{2+} channels. This allows glutamate to be released, which is received by GCs that then depolarise, resulting in GABA release back to the M/TC, onto $GABA_A$ receptors (Shepherd et al., 2007). The amount of inhibition is directly related to the magnitude of Ca^{2+} influx into a stimulated M/TC, and thus provides a powerful locus for indirect M/TC self-inhibition (Isaacson and Strowbridge, 1998). This GABA inhibition occurs in the presence of Na^+

channel blockers, and hence does not even require the generation of an action potential in GCs (Jahr and Nicoll, 1982), though GCs are still capable of generating fast, Na^+-dependent spikes (Shepherd et al., 2007). Thus, this connectivity provides an extremely fast synaptic feedback loop between M/TCs and GCs (Friedman and Strowbridge, 2003).

GC inhibition further functions on a multiglomerular level. Since M/TC lateral dendrites can extend ~1000μm from the soma, connectivity with GC dendrites provides another locus for lateral inhibition between M/TCs of different glomeruli (Lowe, 2013). In addition to this, GCs provide disynaptic inhibition to MCs originating from different glomeruli (Shepherd et al., 2007). Lateral inhibition is further driven by ETC activity, as ETCs project their axons to form excitatory contacts with GCs that target the GC dendrites and provide inhibitory input to M/TCs associated with isofunctional glomeruli of the projecting ETC (Lodovichi et al., 2003).

GCs are therefore positioned to provide powerful feedback inhibition, including lateral inhibition to M/TCs.

Shaping M/TC responses to odorants

Due to their connectivity and functional properties, GCs are thought to be involved in providing contrast enhancement between M/TCs responding to different odours. The feedback inhibition to M/TCs provided by GCs can directly shape the output response of the same M/TCs as well as M/TCs at lateral locations. Indeed, this inhibition likely contributes to bulbar contrast enhancement and refining neuronal representations of odours (Lowe, 2013). For example, $GABA_A$-mediated transmission to M/TCs in the EPL synchronises the activity of M/TCs, and GCs have been found to exclusively regulate evoked γ-oscillations produced by M/TCs (Lagier et al., 2004). In addition to this, the activity of GCs can impact individual M/TC responses to odours, which may directly impact subsequent odour coding in the piriform cortex. As mentioned above, odour input results in the patterned activation of multiple glomeruli. Additionally, similar odours can evoke similar glomerular activity patterns, thus subsequent contrast enhancement by bulbar processing is vital if odorants in odour mixtures, as would appear in the olfactory environment, are to be distinguished. The inhibitory drive provided by GCs onto M/TCs appears to play a key role in this processing. For example, artificially increasing GC activity, and thus inhibition onto M/TCs, with ChR2, can increase selectivity in M/TC odour tuning and thus augment contrast enhancement (Gschwend et al., 2015). This effect is transmitted to olfactory cortex, and results in enhanced odour discrimination ability (Gschwend et al., 2015). The speed at which odours are discriminated by M/TCs can further be enhanced by GC activity. Upon artificially boosting GC synaptic drive onto M/TCs, Abraham et al., (2010) showed that the consequent enhanced inhibition onto M/TCs resulted in mice being able to discriminate similar odours more rapidly

than control animals. These effects are specific to discrimination of similar odours and may thus serve to adjust M/TC responses on a fine scale to differentiate between subtle differences in input.

Therefore, GCs serve to provide direct feedback inhibition onto M/TCs both locally, and through lateral inhibition. These functions likely contribute to contrast enhancement of odour input and serve to synchronise the M/TC network. GCs thus provide a key regulatory machinery that serves to adjust M/TC tuning to odour-evoked input.

1.2.4. Glomerular excitatory circuitry and function

The glomerular long-lasting depolarising currents

LLCs function to shape principal cell output

Glomerular recurrent excitation, in the shape of LLCs, strongly amplifies the transient initial OSN input reaching glomeruli and ensures M/TCs are able to respond with prolonged firing to inputs (Vaaga and Westbrook, 2017). LLCs are glutamatergic currents that occur due to synchronous glutamate released by all excitatory cells projecting to the same glomerulus in response to OSN input. They are thus long-lasting events that reflect polysynaptic amplification of glutamatergic signal (Carlson et al., 2000; De Saint Jan et al., 2009; Gire et al., 2009; Najac et al., 2011). LLCs therefore serve to amplify OSN inputs and are generated by dendrodendritic amplification and recurrent excitation among ETCs and M/TCs (De Saint Jan et al., 2007, 2009).

LLCs are crucial both for producing synchronised, or indeed any, firing responses in M/TCs (Gire and Schoppa, 2009), as well as tuning the response profiles of both ETCs and M/TCs (Vaaga and Westbrook, 2017). Dendrodendritic glutamatergic amplification among M/TCs appears to be stronger than in ETCs, resulting in M/TCs receiving comparatively larger LLCs than ETCs. The larger M/TC LLCs are responsible for producing prolonged firing in M/TCs in response to high-frequency OSN input that resembles active sniffing in rodents (Vaaga and Westbrook, 2017). This is in contrast to ETCs, which have smaller LLCs and portray more phase-locked responses to high-frequency input (Vaaga and Westbrook, 2017).

Apart from their function as drivers of M/TC activity, LLCs have also been highlighted as an important phenomenon during contrast enhancement of OSN inputs. Due to the “noisy” olfactory environment, dendrodendritic amplification of OSN inputs by M/TCs and ETCs in the form of LLCs is one mechanism by which the signal-to-noise ratio is improved due to the strong excitatory drive produced by an LLC. This is a crucial step in ensuring M/TCs are able to maintain a sustained response to odorants, that likely is integrated by higher-order areas to ensure

accurate olfactory perception (Bolding and Franks, 2017; Carlson et al., 2000; De Saint Jan and Westbrook, 2007; Vaaga and Westbrook, 2017).

Build-up of glomerular LLCs

LLCs have been shown to exist as all or nothing responses, the occurrence of which is dependent on the strength of OSN input and inhibitory drive by local inhibitory JGCs. The involvement of ETCs in ensuring M/TCs express an LLC has recently been highlighted. Action potentials induced in a single ETC can drive the activation of many M/TCs projecting to the same glomerulus with an underlying LLC (De Saint Jan et al., 2009), likely by providing extrasynaptic and gap-junction mediated glutamatergic currents to M/TCs (De Saint Jan et al., 2009; Gire et al., 2012). This relationship is not reciprocal (De Saint Jan et al., 2009), thus strengthening the hypothesis that OSN inputs first reach ETCs before being amplified and transferred to M/TCs. A further study pointed out that under weaker OSN input, this multi-step, feedforward excitatory pathway wired through ETCs takes place, however M/TCs are also excited directly upon strong OSN stimulation (Vaaga and Westbrook, 2016). Thus, ETCs are able to drive the amplification of weak inputs in order to ensure reliable transmission of signal to M/TCs.

The larger LLC observed in M/TCs compared to ETCs arises due to strong dendrodendritic recurrent excitation between M/TCs. Block of NMDA and mGluR1 receptors results in a decrease of M/TC LLC size, and thus has been suggested to be the mechanism by which M/TC dendrodendritic amplification is comparatively strengthened (De Saint Jan and Westbrook, 2007; Vaaga and Westbrook, 2017). These glutamatergic receptors can be activated extrasynaptically and are thus favourably located to sense spillover glutamate in the intraglomerular network (De Saint Jan and Westbrook, 2007). In addition to this, M/TCs express AMPA autoreceptors on their dendrites, which have been found to be involved in correlating M/TC spiking at a glomerulus (Schoppa and Westbrook, 2002b). AMPA autoreceptors have been further linked to driving dendrodendritic amplification of glutamatergic signalling with the finding that M/TC self-excitation is partly mediated through AMPA autoreceptors found on glomerular primary dendrites (Isaacson , 1999; Salin et al., 2001). In addition to this, sister M/TCs are electrically coupled to each other (Christie et al., 2005) and ETCs (De Saint Jan et al., 2009), providing another avenue for recurrent excitatory input.

Therefore, LLCs, built up by recurrent excitation in the glomerulus, allow M/TCs associated with one glomerulus to function in synchrony and drastically amplify excitatory signalling to ensure reliable functional output.

LLC modulation

Since the locus of LLC generation is in the glomerulus (Carlson et al., 2000), it is evident that LLC modulation by inhibition is primarily targeted at glomerular dendritic processes. $GABA_A$ currents have been shown to heavily impact LLC kinetics, by both decreasing the probability of an LLC occurring in the first place, as well as reducing its amplitude and time to decay (Carlson et al., 2000; Gire et al., 2009). The importance of ETCs in the regulation of M/TC output via LLCs is further highlighted by the evidence suggesting intra- and interglomerular inhibition is directly targeted at ETCs. Since both interglomerular and intraglomerular inhibition is heavily targeted to $GABA_A$ receptors located on ETC dendrites (Aungst et al., 2003; Banerjee et al., 2015; Hayar et al., 2004b; Murphy et al., 2005; Vaaga and Wesbtrook, 2016; Whitesell et al., 2013), and this inhibition has been shown to directly impact LLCs received by ETCs (Gire and Schoppa, 2009), feedback inhibition received by ETCs therefore indirectly influences the likelihood and magnitude of signal that is finally received by M/TCs.

Components of the excitatory network

M/TC intrinsic properties

Although both MCs and TCs project to olfactory cortical areas and perform similar functions, there are some marked differences between these cells. TCs have been shown to respond to lower odour concentrations compared to MCs and thus appear to have a lower detection threshold comparatively (Igarashi et al., 2012; Kikuta et al., 2013). Indeed, in slice experiments, TCs were shown to receive stronger direct OSN input compared to MCs, though this did not correlate with the differences observed during evoked firing (Burton and Urban, 2014). Nevertheless, TCs were found to be intrinsically at least twice as excitable as MCs. Thus, functionally, there may be some differences in how MCs and TCs receive and process OSN input.

Recent findings have further found that MC populations around a glomerulus express a distinct magnitude of I*h*-mediated sag potentials. MCs projecting to different glomeruli express highly heterogenous sag potentials, however even sister MCs, although more similar, also portray varying sag potential amplitudes (Angelo and Margrie, 2011). The magnitude of sag potential expressed by an MC impacts the excitability of the cell. It has been shown that MCs with larger sag potentials also spike more regularly and at lower rheobase (Angelo and Margrie, 2011). Similarly, TCs also exhibit heterogenous sag potentials, the amplitude of which correlates with TC firing regularity (Burton and Urban, 2014). Thus, I*h*-mediated currents are heavily involved in setting the excitability of both MCs and TCs.

M/TC connectivity

As stated above, OSNs do form direct connections with M/TCs, demonstrated with electron microscopy resolution (Najac et al., 2011), however input received here is heavily shunted by connexin-36 mediated gap-junctions (Gire et al., 2012). M/TCs further form gap junctions with each other, and it has been shown that these transmit depolarisations through the M/TC network, ensuring synchrony but also providing an additional source of excitatory drive (Christie et al., 2005). Furthermore, MCs communicate with each other via lateral chemical excitation. The locus of this is likely the apical dendrite and depends on AMPA receptor-mediated excitation (Pimentel and Margrie, 2008).

M/TCs further form chemical synapses with ETCs (De Saint Jan et al., 2009), though these appear to be sparse (Bourne and Schoppa, 2017). Nevertheless, ETC-MC communication is facilitated by gap-junctions (De Saint Jan et al., 2009), and is further thought to arise due to spillover glutamate in glomeruli (Gire et al., 2018).

Shaping M/TC responses

Though much of the bulbar processes discussed above shape M/TC output, some intrinsic features contribute to adjusting the responses these cells portray to odour-evoked input. For example, variability in sag potential magnitude has been hypothesised to exhibit the ability of M/TCs to integrate a broad range of odorants by displaying diverse integrative properties. Indeed, when sag potentials expressed by M/TCs were observed in a transgenic mouse line where all OSNs express the same OR, all M/TCs displayed similar sag potentials no matter which glomerulus they were associated with (Angelo et al., 2012). Thus, the magnitude of M/TC sag potential is involved in setting the response profiles these cells can portray.

It was further shown that sister M/TCs display highly correlated responses to odorants, however their spike timing was not homogenous across cells (Dhawale et al., 2010). This biophysical heterogeneity allows M/TCs to portray distinct spike responses to the same input. This population heterogeneity in responses allows cells to code for much more information compared to cells responding with similar outputs (Padmanabhan and Urban, 2010). Modelling M/TC response diversity to variable input has further suggested that stimuli are most effectively coded for when M/TCs possess a fine balance of response heterogeneity and similarity on a population level (Tripathy et al., 2013). This is because, on a population level, M/TCs create many spikes that could lead to “noisy” transmission. Ensuring input is transmitted homogeneously to some extent is vital to code for distinct input information, but subtle heterogeneity in responses increases the bandwidth of information that can be coded for.

Therefore, M/TCs not only generate integrated bulbar output to higher-order processing centres, but also actively take part in amplifying excitatory OSN input and integrating odour-specific information.

ETC intrinsic properties

There are several functional properties ETCs possess that allow these cells to perform their crucial functions in driving glomerular circuitry, and ultimately manipulating glomerular output. Most crucially, ETCs spontaneously fire bursts of action potentials both *in vivo* (Tatti et al., 2014) and *in vitro* (Hayar et al., 2004a), the frequency of which can be entrained by OSN input. This burst firing is generated by a persistent inward Na^+ current that is active at resting membrane potentials and persists in the presence of $GABA_A$ blockers, rendering this phenomenon an intrinsic feature of ETCs (Hayar et al., 2004a). Similar to the LLC behaviour mentioned above, ETCs respond to OSN inputs with all-or-nothing bursts of spikes, even at relatively low OSN input intensities (Hayar et al., 2004b). Furthermore, though ETCs related to one glomerulus spontaneously burst fire at various frequencies within the ranges of active and passive sniffing rates, the fact that OSN input can entrain and override ETC intrinsic frequency suggests that ETCs synchronise the activity within glomerular processing (Hayar et al., 2004a). A single OSN volley can thus be transformed into a correlated burst of spikes by many ETCs associated with the same glomerulus.

The specific mechanisms generating ETC burst firing are of high interest, because even though they are intrinsic, they can be influenced by the actions of the inhibitory circuitry. For instance, the I*h* current sets the ETC membrane potential which allows for other ionic conductances, persistent Na^+ currents and low-voltage activated Ca^{2+} currents, to generate the depolarisation envelope needed for generating burst firing (Liu and Shipley, 2008). Additionally, $GABA_A$ input appears to reduce ETC spike output by reducing the number of spikes within a spontaneous spike-burst (Hayar and Ennis, 2007). Thus, the intrinsic firing ETCs display is regulated by the inhibitory circuit, the activity of which is most commonly initiated by ETCs themselves.

Therefore, the hyperexcitable membrane properties ETCs display allow them to synchronise glomerular processing and provide strong excitatory drive that is responsible for shaping glomerular output. Furthermore, they are able to entrain the inhibitory glomerular network, which may provide a form of self-regulation and fine-tunes the amount of excitatory drive ETCs subsequently exhibit.

ETC connectivity

OSNs form monosynaptic connections with ETCs, which provides the major excitatory input these cells receive (Hayar et al., 2004b). ETC-PGC intraglomerular circuits are established by dendrodendritic synapses (Hayar et al., 2004a). This circuitry results in ETCs transmitting excitatory signal to PGCs, and in turn causes feedback inhibitory input to ETCs (Hayar et al., 2005). In addition to this, ETCs form both chemical and electrical synapses with GABA/dopaminergic SAC projections, providing a source of interglomerular communication (Banerjee et al., 2015).

Interestingly, there is controversy regarding whether or not ETCs form chemical synapses with each other, and indeed there is little evidence for strong chemical synaptic contacts between ETCs (Hayar et al., 2005). They do however, possess Ca^{2+} permeable AMPA autoreceptors on their primary dendrites and have been shown to undergo self-excitation (Ma and Lowe, 2007). These are thus placed in an optimal location to receive extrasynaptic spillover glutamate and contribute to glomerular recurrent excitation. Additionally, ETCs form gap junctions among themselves and with M/TCs (Hayar et al., 2005; De Saint Jan et al., 2009), and this gap-junctional communication, together with the pattern of OSN input, is thought to provide a mechanism by which ETCs around a glomerulus are synchronised.

Therefore, the connectivity of ETCs places them at the centre of glomerular processing, where they make extensive connections with OSN inputs and the local inhibitory circuit, and exhibit extrasynaptic glutamate receptors that aid in the amplification of glutamatergic input.

ETC-JGC excitation/inhibition circuit loops

Due to their anatomical and functional connectivity, ETCs receive direct OSN inputs and drive the inhibitory glomerular network, as inputs to inhibitory JGCs appear to mainly come from ETCs rather than the minimal inputs they receive from OSNs (Hayar et al., 2004b).

The actions of the glomerular inhibitory circuitry result in feedback communication that modifies ETC function. ETCs receive bursts of inhibitory postsynaptic currents (IPSCs) in response to fast excitatory input that is driven by ETCs, thus underlining the role of feedback inhibition provided by inhibitory JGCs that is directly driven by excitation in ETCs (Hayar et al., 2005). Furthermore, the I*h* current received by ETCs is directly modulated by the neurotransmitter release of GABA/dopaminergic JGCs. GABA release reaches $GABA_A$ receptors on ETC dendrites via dendrodendritic synapses to activate I*h* current. The co-release of dopamine by these JGCs acts on ETC D_1-dopaminergic receptors which increase this current. This in turn favours ETC rebound spiking and sets the resting membrane potential (Liu et al., 2013).

Interglomerular inhibition has also been shown to be routed through ETCs before reaching M/TCs. SACs provide inhibitory drive that supresses the gain of M/TCs in response to stimuli. This suppression can occur directly (Liu et al., 2016) but also indirectly through the inhibitory actions of these cells onto ETCs (Vaaga et al., 2017; Whitesell et al., 2013).

Thus, the actions of the inhibitory network on ETC function, mostly driven by ETCs in the first place, modulate ETC output which consequentially influences how much excitatory signal is transmitted to M/TCs.

The role of ETCs in the excitatory circuit

The local excitatory circuitry of the OB mainly consists of dendrodendritic interactions between ETCs and M/TCs (and within those cell classes), that serve to provide feedforward excitation onto M/TCs which integrate this information. ETCs heavily modulate the output of the glomerular network, through their communication with OSNs and inhibitory JGCs, and are a key component of bulbar excitatory function. In fact, it is now widely accepted that ETCs are the key component of a multi-step feedforward process from OSN to M/TCs, where they are the intermediary players that initially augment OSN signals. Though M/TCs do receive weak inputs upon OSN stimulation, strong input is generated through the ETC-mediated path, that is transmitted to the M/TCs (Gire et al., 2012). This provides a mechanism by which input is initially amplified, providing a major source of sustained glutamate release onto M/TCs, that is modulated by feedback inhibition through ETCs before it reaches M/TCs (De Saint Jan et al., 2009; Hayar et al., 2004a,b).

As is portrayed above, a network of ETCs and inhibitory JGCs lies between OSNs and M/TCs, which strongly impacts the information M/TCs receive. Since ETCs and M/TCs form few, if any, direct synaptic contacts (Bourne and Schoppa, 2017), there has been a long-standing question as to how M/TCs receive ETC input. Experimental evidence suggests this communication relies on spillover glutamate reaching M/TCs through extrasynaptic glutamate receptors (De Saint Jan and Westbrook, 2007; Gire et al., 2012). The relationship between ETCs and inhibitory JGCs has further been shown to be a key method of transmitting glutamatergic signal to M/TCs, as it has been demonstrated that much of the glutamate spillover received by M/TCs originates from ETC-JGC synapses (Gire et al., 2018). Through this synaptic connection, there appears to be a delicate balance of ETC excitation and JGC inhibition. Upon relatively strong input, the excitatory drive by ETCs on glomerular processing “wins”, overriding inhibition, resulting in output by the M/TCs. Contrastingly, when there is low input, the inhibitory network “wins” and inhibits the excitatory drive (Gire et al., 2018). Thus, it is evident that ETCs are heavily involved in gating odour input.

Therefore, through their functional properties, as well as their anatomical proximity to glomerular inhibitory and excitatory input, ETCs synchronise the glomerular network, amplify initial OSN input, and indirectly modulate how much excitation reaches MCs by driving glomerular dendrodendritic feedback inhibition and spillover glutamatergic signalling.

1.2.5. Centrifugal inputs

The OB is further a recipient of significant feedback information by centrifugal inputs, received from the anterior olfactory nucleus, piriform cortex, lateral entorhinal cortex, amygdala, and the nucleus of the lateral olfactory tract (Lowe, 2013). These inputs can have a significant effect on the output of the OB. Pyramidal cells in the olfactory cortex receive M/TC inputs, and send axons back to the OB to target GCs, and in this way indirectly drive disynaptic inhibition to M/TCs (Boyd et al., 2012). Additionally, there appears to be a cortical link between the two OBs, formed through the anterior olfactory nucleus pars external (AONpE). Again, these projections serve to modulate M/TC output through the activation of GCs. M/TCs from one glomerulus project to the AONpE, where neurons receive this information and send their axons to isofunctional odour columns (Yan et al., 2008).

Cholinergic input also impacts OB output. The OB receives many of its cholinergic inputs from the horizontal limb of the diagonal band of Broca. Optogenetic stimulation of cells there resulted in a reduction of spontaneous firing in M/TCs, PGCs, and GCs, demonstrating their capability of regulating OB output (Ma and Luo, 2012). Furthermore, acetylcholine has been shown to reduce spontaneous firing of GABA/dopaminergic JGCs in acute mouse OB slices (Pignatelli and Belluzzi, 2008). It is hypothesised that cholinergic inputs increase odour discrimination capability, because activation of these cells results in a sharpening of M/TC olfactory tuning curves, and broadly potentiates odour-evoked responses in PGCs and GCs (Ma and Luo, 2012). Serotonergic inputs from the raphne nuclei also provide innervation to the OB. Serotonin was shown to increase ETC excitability. More intriguingly, the activity of serotonin appears to modulate slower spontaneously bursting ETCs more heavily compared to faster bursting ETCs. Thus, it is hypothesised that serotonergic regulation of ETCs ensures the mean ETC burst frequency at a glomerulus is increased (Liu et al., 2012). The action of serotonin seems to impact ETCs indirectly, as it primarily targets the GABAergic PGCs which then exert their inhibitory actions onto ETCs (Petzold et al., 2009).

The circuitry of the OB is thus a complex one, involving multiple processing steps both within the OB as well as outside of it, that ensure odour information is reliably transmitted to higher cortical areas. All of the above findings highlight the intricate relationship between excitation and inhibition occurring during glomerular processing of odour input. At the glomerular level,

ETCs are a key player in determining glomerular output, since they directly and indirectly modulate how much excitatory signal reaches M/TCs. Furthermore, the complex nature of the intra- and interglomerular processing circuitry allows for contrast enhancement and reliable transmission of odour information, even though the sensory input is highly heterogenous. For this reason, it is unsurprising that many components of the OB circuitry have been shown to undergo various forms of activity-dependent plasticity, that serve to adjust the processing of odorants in the face of the ever-changing olfactory environment.

1.3. Plasticity in the olfactory bulb

The OB has been used extensively to uncover mechanisms of neuronal plasticity, both short- and long-term. From a technical point of view, not only is its circuitry genetically tractable and more easily accessible compared to deeper structures such as the hippocampus, but driving experience-dependent plastic changes can be achieved in a straight-forward manner with a variety of reliable sensory manipulations due to the proximity of the system to the sensory environment. In addition to this, as described above, the mechanisms of action by many OB components have been elucidated, and thus allow for the comprehensive study of plasticity on a cellular level, while observing net effects on the network. Furthermore, the OB is phylogenetically highly conserved, providing a model system that can be studied in a variety of model organisms to answer specific questions experimentally (Wilson et al., 2004).

Using the simple, yet reliable technique of manipulating the olfactory environment to drive changes in OB input, plasticity in many components of the OB circuitry has been revealed. From ORs to higher-order cortex participants, multiple cell types have been shown to produce changes from membrane excitability adjustments, synaptic changes, and even extreme forms of plasticity like adult neurogenesis and apoptosis.

1.3.1. The use of sensory manipulations to study plasticity in the OB

Unilateral naris occlusion

Unilateral naris occlusion is perhaps the most-used sensory manipulation to drive activity-induced changes in the bulb. The principle is simple and provides a method of depriving the bulb of sensory input by the blockage of the nostril corresponding to that bulb. Additionally, the OE to OB connectivity is exclusively ipsilateral, meaning that sensory input is only blocked to the bulb corresponding to the blocked nostril. The earliest use of this method was performed in the late 1800s by Bernhard von Gudden, who described that the blockage of one nostril in new-born

rabbits produced a remarkable effect of drastically reducing the size of the ipsilateral OB 6 weeks later (Coppola, 2012).

Sensory deprivation has been used extensively via various methods to drive plastic changes in the OB. Sensory deprivation is achieved by removing or somehow blocking sensory input through the OSNs. One way is to perturb the airflow to a nostril by blockage with an occlusion "plug", which can be removed to study the effects of both deprivation and recovery (Cummings et al., 1997), or by heat-cauterization of the nostril (Coppola, 2012). Other methods consist of removing OSN input in the bulb via chemical (Nadi et al., 1981) or surgical deafferentation of the OSNs (Kawano and Margolis, 1982).

All these methods appear to produce similar changes in the OB, implicating the robustness of the effects of sensory deprivation. For example, one study found that naris occlusion produced similar effects and on a similar time scale as zinc-sulphate induced denervation of the OB (Baker et al., 1993). The remarkable ability for OB regeneration after external perturbations has also been studied using the occlusion paradigm, further underlining the remarkable ability of this system to be bidirectionally plastic. For example, OB volume was dramatically decreased when occlusion occurred from P1-P20, but this recovered to control measures after 40 days of plug removal (Cummings et al., 1997). Thus, this simple manipulation is highly effective in driving plastic changes that are reversible upon recovery.

Controversy in control conditions for the naris occlusion paradigm

When studying the effects of naris occlusion, it may be tempting to use the contralateral, un-occluded OB as the control condition. This would provide a powerful internal within-subjects control (Coppola, 2012). Nevertheless, because airflow to the nostril of the occluded OB is perturbed, the un-occluded side must compensate, resulting in the open nostril carrying much larger airflow compared to unperturbed conditions (Farbman et al., 1988). Additionally, due to the block of one nostril, the shift of the "dominant" nostril gaining more airflow than the other is disturbed (Maruniak et al., 1990). The effect of increased airflow to the open nostril has marked effects on downstream odour processing. For example, the open side experiences a loss of OSNs in rostral regions of the epithelium with prolonged occlusion (3 months) (Maruniak et al., 1990). Additionally, OSNs on the open side have been shown to downregulate their transcription of OR genes (Coppola and Waggener, 2012). These findings demonstrate that upon naris occlusion, the free/open-side OB does not receive "normal" odour input, and may therefore not be ideal for comparative purposes.

These findings have led to the idea that using the contralateral, free OB as the control condition when drawing comparisons on the effects of occlusion may not be appropriate (Coppola, 2012).

Instead, it may be more relevant to use unperturbed animals as controls. Additionally, a sham occlusion paradigm can be employed on control animals that do not undergo naris occlusion. In this way, the exposure to anaesthetic and potential mechanical damage of nostril occlusion is replicated in control animals, but the shammed OB is not exposed to excessive airflow that results in altered odour input, and thus is more representative of a true control (Kass et al., 2013a).

Olfactory enrichment

Sensory enrichment has also been used to explore the effects of odour over-exposure on the bulbar neural circuitry. This manipulation is driven by passive over-exposure to odorants for a certain period of time. The enrichment paradigm is perhaps more complex however. Different odours activate different patterns of glomeruli, therefore deciphering neural changes in response to enhanced input becomes complex when aiming to distinguish between circuits that have been "enhanced" versus circuits that have not, with a particular odour. Nevertheless, studies employing enrichment are numerous and comprehensive. They have further gained strength through the advent of being able to genetically target particular ORs, which enables the visualisation of particular glomeruli associated with that OR through the expression of the OR gene at OSNs (Mombaerts et al., 1996). For these genetically targeted ORs, known ligands have been discovered (Arneodo et al., 2018; Bozza et al., 2004), thus enriching animals with these OR-known ligands and then exploring the effects at the associated glomeruli overcomes the above-mentioned problems (Jones et al., 2008).

For example, odour enrichment can drive activity changes in the activity of glomerular patterns. Upon exposing animals to odours with increased concentrations, the response latencies of active glomeruli that were tuned to these odours reduced, and more glomeruli were recruited to be active (Spors and Grinvald, 2002). Consistent odour enrichment for 10 days can increase the number of cells associated with enriched glomeruli that express a cell-activity marker, the immediate-early gene Zif268, in response to an odorant (Mandairon et al., 2008). Even short-term odour exposures can drive changes in the OB. For example, 20 minutes of odour exposure to adult rats can markedly reduce MC numbers responding to not just the exposed odour, but also novel odours (Buonviso et al., 2003). Even exposure to odours for less than a minute can fine-tune the receptive fields of MCs (Fletcher and Wilson, 2003).

Associative olfactory experience

Odour memory plays an important role in odour-guided behaviours in many animals (Wilson et al., 2004). Thus, the learning of associations with specific olfactory cues has been used as

another paradigm to study plasticity in the bulb. For example, when rats are trained to discriminate between odours associated with different rewards, M/TCs modulate their activity during behaviours exhibiting odour sampling, and this modulation is dependent on the predicted value of each odour (Kay and Laurent, 1999). Thus, bulbar processing can be modulated by active experience, as well as the passively-experienced olfactory environment.

Therefore, inducing plastic changes in the OB circuitry can robustly be achieved by sensory manipulations that reduce or increase input to the circuit, and even by associative learning tasks to specific odorants. Various techniques to achieve these sensory manipulations have widely been used to adjust OB activity, which has allowed for the observation of the many ways in which neuroplasticity occurs in the OB.

1.3.2. Plasticity in olfactory sensory neurons

OSN neurogenesis

OSNs exhibit the remarkable ability to regenerate throughout adult life. Mature OSNs appear to have a limited life-span of only about 30-90 days (Graziadei and Graziadei, 1979; Mackay-Sim and Kittel, 1991). Continuous mitotic division of stem cells in the olfactory epithelium are the source of this life-long neurogenesis, and under physiological conditions, there is constitutive on-going neurogenesis of OSNs (Schwob, 2002).

There is however, also neurogenesis that underlies the reconstitution of the OE. When the nasal epithelium is damaged, mature OSNs undergo apoptosis and immature OSNs replace these by connecting their axons to appropriate glomeruli, a process that takes around 8 weeks to return to control levels of OSN innervation (Schwob et al., 1999). Though OSN turnover occurs throughout the life of an animal, it appears that this turnover slows down as an animal ages (Kondo et al., 2010).

The neurogenesis of OSNs in the adult is activity-dependent, as sensory input is required to restore OSN innervation after injury. Chronic imaging of OSNs revealed that OSNs functionally regenerate their response magnitudes and restore the functional topography of glomeruli to odour stimuli by 12 weeks after epithelial injury (Cheung et al., 2013). When looking at the physical properties of generation, when mature OSNs are killed with methimazole, the olfactory epithelium is restored with OSNs after 28 days of recovery. However, if the nostril is occluded during a critical period of 7-14 days after injury, there is a reduction of newly generated OSNs

as well as an increase in apoptotic OSNs compared to the non-deprived side (Kikuta et al., 2015). Furthermore, it has recently been found that the effect of sensory deprivation on OSN densities has variable effects on different OR-expressing OSNs. For instance, three weeks of naris occlusion had no effect on the density of M71-expressing OSNs, whereas it drastically reduced the number of MOR23-expressing OSNs (Molinas et al., 2016). Thus, sensory input is important for the restoration of OSNs after injury, and may have variable effects on OSNs expressing different types of ORs.

Olfactory experience can further have dramatic effects on OSN generation that is genetically passed on to several generations. Using a transgenic mouse-line that had the M71 OR and consequently OSNs associated with this OR fluorescently labelled, Jones et al., (2008) showed that fear-conditioning associated with a particular odour that activates M71 ORs resulted in an increased generation of M71 OR-expressing OSNs 3 weeks later. Fascinatingly, the offspring of the fear-conditioned mice also expressed more M71 OR-associated OSNs and higher behavioural sensitivity to the odorant that specifically stimulates M71 ORs (Dias and Ressler, 2014). This inheritance persisted even in the F2 generation offspring and depended on gamete inheritance from the initial fear-conditioned animals.

OSN targeting of distinct glomeruli is activity-dependent

Even in the first step of olfactory transduction, experience-dependent plastic changes can occur that do not involve neurogenesis. In fact, the refinement of OSN axons to glomerular targets appears to be dependent on sensory input. Early in development, OSNs expressing distinct ORs converge on multiple glomeruli, but between P10-P60 (in mice), OSNs refine their targeting to produce the distinct glomerular maps associated with particular ORs. This duration of this maturational refinement is specific to particular ORs, as it has been shown that some OR-associated glomerular specification occurs much later compared to others (Zou et al., 2004). Sensory experience is crucial for this refinement however, as sensory deprivation, by unilateral naris cauterisation, from P0 disrupts maturational axon refinement, leading to numerous glomeruli being innervated by OSNs representing multiple ORs by P40-P90 (Zou et al., 2004).

It has further been found that activity is required to maintain OSN connectivity with appropriate glomeruli. The genetic block of spontaneous synaptic release by OSNs does not impair the correct targeting of the appropriate glomerulus during development, however if there is a failure to establish stable synaptic connectivity, those OSNs disappear and the corresponding glomerulus is not maintained (Yu et al., 2004).

OSNs portray activity-dependent synaptic adjustments in the established circuit

Even at the earliest stage of odour processing, the transduction of olfactory information into electrical signalling, has been shown to be activity-dependent. For instance unilateral naris occlusion delivered by cauterisation 1 day after birth results in a marked increase of adenylate cyclase expression in OSNs 24 days later (Coppola et al., 2006). Since adenylate cyclase catalyses the production of c-AMP, the production of which allows OSNs to reach depolarising thresholds, this suggests that OSNs under these condition may be able to transduce odour inputs more efficiently.

OSNs further show the capability of undergoing synaptic changes in response to sensory manipulations. For example, 2 weeks of naris occlusion resulted in OSNs increasing their release probability (P*r*) of glutamate, a likely compensatory effect that may be in place to increase sensory transmission transduction when there is minimal odour input (Tyler et al., 2007). Additionally, it has been shown that there is continuous turnover of OSN synaptic terminals. However, with 3 weeks of sensory deprivation, the rate of this turnover is downregulated in both mature and immature OSNs (Cheetham et al., 2016). Thus, OSNs appear to be able to remodel their synapses in an activity-dependent manner.

OSNs have also been shown to undergo long-term changes in their synaptic strength to post-synaptic targets. The first study to highlight this found a somewhat unusual mechanism of inducing long-term potentiation (LTP) at the OSN-M/TC synapse. Here, brief tetanic stimulation of OSNs *in-vitro* potentiated NMDA-receptor dependent spiking in M/TCs, but did not involve AMPA receptors (Ennis et al., 1998). It was previously reported that LTP likely is expressed by AMPA-receptor mediated responses, thus the dependence on NMDA for LTP induction and expression at this synapse demonstrated a novel form of synaptic plasticity. Computational modelling of these results revealed that the mechanism behind LTP at this synapse likely stems from an increased P*r* at the OSN, and an upregulation of NMDA receptors on M/TC primary dendrites (Ennis et al., 1998). Contrastingly, when OSNs are electrically stimulated at low frequencies in young postnatal acute OB slices, long-term depression (LTD) at the OSN-M/TC synapse occurs, and has been linked to alterations in presynaptic efficacy through the activation of metabotropic glutamate receptors (Mutoh et al., 2005). Associative odour learning can also drive synaptic changes in OSNs. Upon foot-shock conditioning associated with a particular odour, the synaptic output of OSNs, measured by imaging vesicle release of OSN synapses labelled with synapto-pHluorin is facilitated when the animal is exposed to the conditioned odour (Kass et al., 2013b).

These observations reveal that sensory experience can shape the OB circuitry at its earliest processing stages.

1.3.3. Plasticity in inhibitory JGCs

The bulbar interneuron network in general shows extreme forms of structural plasticity in terms of lifelong neurogenesis. Cells are continuously generated in the SVZ and migrate to the OB where they differentiate into GCs and inhibitory JGCs (Altman, 1969; Lois and Alvarez-Buylla, 1994). In the GL, plasticity has mainly been observed in the GABA/dopaminergic JGCs, with many studies not differentiating between the types of PGCs or even PGCs and SACs. Nevertheless, taken together, experimental findings demonstrate that sensory experience can profoundly impact multiple properties of these cells, from their generation to functional adjustments.

Activity-dependent expression of tyrosine hydroxylase

Perhaps the most striking and influential findings on plasticity in the bulb demonstrate the malleability of the dopamine synthesising enzyme TH expression in GABA/dopaminergic JGCs in response to sensory manipulations. The level of TH expression appears to be dependent on the magnitude of glutamate that is released by OSNs (Puche and Shipley, 1999), thus the olfactory environment can impact TH expression profoundly. For example, even after 4 days of naris occlusion in adult mice, TH immunoreactivity drastically decreases (Baker et al., 1993). The *activity* of TH was also shown to decrease with 14 days of sensory deprivation, an effect that remained 6 months later (Cho et al., 1996). Even upon relatively short-term sensory deprivation (24 hours), TH expression in the JGCs is decreased, as measured with immunohistochemistry (D. Byrne, E. Galliano, unpublished data). The effect of sensory experience on TH expression is bidirectional, as recovery from OB deafferentation results in an increase of TH expression comparable with control levels (Nadi et al., 1981). The effect of sensory deprivation on TH expression is so robust that it is now often used as a positive control to demonstrate that sensory deprivation did indeed occur in particular experiments (Cockerham et al., 2009; Coppola, 2012; Platel et al., 2018; Wilson and Sullivan, 1995).

Inhibitory JGCs undergo activity-dependent adult neurogenesis

Neurogenesis under physiological conditions

Another famous finding is that the survival of newly generated GABA/dopaminergic JGCs and other PGCs depends on sensory input. First and foremost, long-term *in vivo* time lapse imaging has allowed for the chronic imaging of particular OB neuronal subtypes for several months. In the case of GABA/dopaminergic JGCs, 9 months of chronic imaging revealed that this population is highly dynamic. There appeared to be a clear addition and loss of these JGCs in the GL, with progressively more addition than loss occurring as the animal aged. This led to the assumption

that GABA/dopaminergic JGCs do not merely replenish their populations, but that the interneuron bulbar network changes throughout adulthood (Adam and Mizrahi, 2011).

Activity-dependent neurogenesis

The survival of new-born inhibitory JGCs has originally been thought to be determined during a critical window of around 8 weeks post neurogenesis, during which time a high amount of cell loss has been reported. Sensory input appears to facilitate the survival of these cells, as nostril occlusion during this critical period drastically increases apoptosis among newly generated inhibitory JGCs. (Mandairon et al., 2006). Nevertheless, it has recently been shown that under physiological conditions, new-born JGC death occurs very rarely. This observation stems from long-term chronic tracking of thousands of new-born JGCs showing that when genetically targeting these cells under physiological conditions, little cell death occurs. A similar result was found when labelling these cells with EdU to immunohistochemicaly observe cell numbers (Platel et al., 2018). The same study found that during the critical period, many new-born JGCs tend to undergo apoptosis when labelled with high doses of EdU and BrdU, as was performed in the original study by Mandairon et al., (2006), and suggests that using standard doses of this labelling technique is toxic to new-born JGCs. However, the dependence on sensory input by new-born JGC for their survival was again shown, as sensory deprivation via unilateral naris occlusion during the critical period of JGC generation resulted in a significant amount of new-born cells undergoing apoptosis (Platel et al., 2018).

The lack of sensory input appears to impact the survival neurogenic capabilities of both mature and immature inhibitory JGCs. Upon long-term sensory deprivation via naris occlusion (42 days), the number of new-born as well as resident GABA/dopaminergic JGCs was reduced (Bastien-Dionne et al., 2010). The use of *in vivo* imaging further allowed for the live observation that specifically GABA/dopaminergic JGCs require sensory input to aid survival. 28 days of occlusion resulted in a drastic loss of surviving GABA/dopaminergic JGCs due to an increase in apoptosis in these cells. However, this manipulation did not affect calretinin+ or calbindin+ PGC survival. New-born GABA/dopaminergic JGCs were not spared from this effect, and indeed under occluded conditions there was a decreased survival of these new-born cells labelled by genetically targeting GFP expression to TH-expressing JGCs. This effect was shown to be reversible, as nostril reopening after 56 days resulted in an increased number of new-born GABA/dopaminergic JGCs and increased number of surviving resident GABA/dopaminergic JGCs (Sawada et al., 2011). With the use of *in vivo* two-photon imaging, it was further shown that even just 7 days of naris occlusion induces a reduction in GABA/dopaminergic JGCs and their synapses due to increased apoptosis of these cells. This was linked to a marked increase in

microglial density and activation, showing an increased frequency of wrapping GABA/dopaminergic JGC somas (Grier et al., 2016). Thus, there appears to be an activity-dependent link between GABA/dopaminergic JGC death and microglial activation.

Contrastingly, odour enrichment appears to enhance the survival capabilities of GABA/dopaminergic JGCs as well as PGCs. Prolonged exposure (>30 days) to a range of 20 aromatic odours markedly increases TH immunoreactivity in GABA/dopaminergic JGCs and occurs due to an increase in cell number rather than an increase in TH expression (Bonzano et al., 2014). When taking the whole PGC population into account, it was further found that new-born PGC survival is enhanced with 3 weeks of olfactory enrichment. Indeed, the survival of these cells was markedly dependent on odour input, as removal of odour enrichment resulted in less new-born PGCs surviving 3 weeks after odour over-exposure was removed (Bovetti et al., 2009).

Therefore, sensory experience shapes the bulbar interneuron circuitry by determining how many new players are incorporated into the established system, and how many of the resident participants survive.

Inhibitory JGCs exhibit structural plasticity

Activity-dependent structural changes have also been observed in the GABAergic JGC populations. Under physiological conditions, new-born PGCs appear to maintain highly dynamic structural plasticity in that they continuously form and remove synapses well after they have matured (Mizrahi, 2007a). *In vivo* chronic imaging of the presynaptic marker PSD95 tagged with GFP on PGCs revealed that sensory enrichment results in an increase of PSD95-GFP expression on adult-born PGCs in glomeruli that reaped the effects of enrichment (Livneh et al., 2009). This effect of increased PSD95-GFP expression implies that these new-born cells undergo more synaptogenesis when sensory experience is enhanced.

Contrastingly, “mature” PGCs appear to be able to stabilise their synaptogenesis rates with sensory experience. Though 10 days of enrichment does not seem to impact the extent of dendritic ramification into glomeruli by mature PGCs, the rate of synaptogenesis and synapse removal is drastically decreased even after the second day of odour enrichment. Though the total ratio of new synapses and lost synapses is not affected by enrichment, mature PGCs seem to be able to adjust their synaptic turnover rate by drastically decreasing the amount of new synapses they generate, and old synapses they remove, an effect that remains for a relatively long period of time (Livneh and Mizrahi, 2011). Thus, both mature and new-born PGCs are structurally plastic in as they can modulate synaptic turnover in the face of external modifications.

In the dopaminergic population of JGCs, axon-bearing GABA/dopaminergic JGCs also have the capability of adjusting their axon initial segment (AIS). The AIS is an axonal structure where many voltage-gated ion channels reside at high densities. Most, if not all, action potentials are generated at this site in cells that contain an axon. Changes in the length and distance of the AIS in relation to the cell soma have been correlated with changes in the excitability of a cell (Grubb and Burrone, 2010b). In the OB, artificially exposing dissociated GABA/dopaminergic JGCs to chronic depolarisation, as would likely be the case under odour enriched environments, results in their AISs lengthening and proximally relocating towards the soma (Chand et al., 2015). Upon 24 hour naris occlusion, the opposite effect can be observed *ex vivo*, where GABA/dopaminergic JGC AISs shorten in length, a structural alteration which has been linked to a decrease in intrinsic excitability of these cells (E. Galliano, unpublished data).

Therefore, sensory experience can shape the morphological properties of bulbar inhibitory JGC population in more than one way.

Inhibitory JGCs portray experience dependent functional plasticity

The addition and loss of inhibitory JGCs, as well as their ability to structurally change in response to sensory experience must have functional consequences then, if it is to modulate OB processing of odorants.

Recent findings demonstrate that adult-born PGCs do indeed functionally integrate into the network, as these cells responded with spiking behaviours to odorants when recorded *in vivo,* with less mature adult-born cells being more likely to respond (Livneh et al., 2014). These odour responses appear to be developed to different degrees depending on sensory experience. When PGCs are born during a two-week odour enriched environment, these PGCs appear to decrease their odour responsiveness, making them more selective to odour stimulation. The resident population of PGCs however, is not affected, and continues to respond to odours with the same tuning curves as before the enrichment occurred (Livneh et al., 2014). Thus, new-born PGCs functionally integrate into the network but obtain distinct odour-response profiles that are tuned by the olfactory environment the animal was in when these cells were generated.

Sensory experience further shapes the functional properties of inhibitory JGCs contained within the mature circuit. Even short-term naris occlusion (3 days) can increase glutamate receptor-mediated quantal scaling in these cells that likely occurs due to an increased expression of AMPA and NMDA receptors on PGC dendrites, thus exhibiting more channels through which glutamate can enter the cells (Tyler et al., 2007). Synaptic efficacy changes have further been observed in GAD67 expressing PGCs. Weeks of naris occlusion reduces the number of SACs expressing GAD67 (Parrish-Aungst et al., 2011). Additionally, upon chemical OB deafferentation, PGCs

release less GABA onto ETCs, an effect likely arising due to a reduction in the synaptic contacts GAD67+ PGCs make with ETCs (Lau and Murthy, 2012). Therefore, the functional properties displayed by PGCs and SACs appears to be dependent on sensory experience.

These findings demonstrate the vast amount of experience-dependent plastic changes inhibitory JGCs can undergo. Given their role in the bulbar circuit, adjustments in these cells can profoundly impact the output of a glomerulus. As mentioned in the introductory part of this chapter, inhibitory JGCs are heavily involved in modulating the magnitude of the excitatory circuit, which ultimately affects the output at the M/TC level. Additionally, given that both GABA and dopamine inhibit glutamate release at OSN terminals (Aroniadou-Anderjaska et al., 2000; Maher and Westbrook, 2008), and GABA/dopaminergic JGCs are able to regulate their TH expression, it is further likely that these cells are capable of modulating incoming odour information at the level of initial input. Therefore, the sensory experience-driven plastic changes these cells undergo may function to continuously adjust the bulbar circuitry to maintain functional odour perception.

1.3.4. Plasticity in granule cells

GCs are heavily involved in the modulation of M/TC activity (Chen and Shepherd, 1997), and thus GC activity fine-tunes the output of bulbar circuits. As with JGCs, activity-dependent plasticity in GCs has been observed on multiple levels. Not only are these cells plastic to the extent of life-long neurogenesis, but structural and functional adjustments are also induced by sensory experience during adulthood.

Activity-dependent neurogenesis and survival

Many reports have shown that there is continuous turnover of the GC population. Under normal conditions, though ~10,000 new GCs are generated each day (Yamaguchi and Mori, 2005), around 50% of these new-born GCs undergo apoptosis within 1 month (Petreanu and Alvarez-Buylla, 2002). The decision of life or death is made after new GCs have developed synaptic connectivity in the EPL, and is thus highly influenced by olfactory experience. The turnover of GCs throughout life has a functional effect and appears to ensure intact odour discrimination. When GC apoptosis is inhibited with a caspase inhibitor, odour discrimination becomes substantially worse (Mouret et al., 2009). Thus, the life-long structural dynamics GCs undergo appear to play a critical role in functioning odour perception.

The survival of GCs is dependent on sensory input, as anosmia causes a drastic decrease in GC survival rates compared to functional olfactory systems (Petreanu and Alvarez-Buylla, 2002). With sensory deprivation new-born GCs do not appear to survive as well as their control

counterparts. Interestingly, there seems to be a critical window in which GCs require sensory input to allow them to survive. This critical window appears to be during the 14th to 20th days of GC maturation, as occlusion during this time-period, but not outside of it, causes the drastic decrease in survival rate that is observed after 28 days of occlusion (Yamaguchi and Mori, 2005). It was further shown that long-term occlusion also decreases the rate of GC generation (Mandairon et al., 2006; Saghatelyan et al., 2005). Nevertheless, as with the inhibitory JGCs, it has recently been found that under physiological conditions, new-born GCs survive quite well, and only the deprivation of sensory input during the critical period results in the vast amount of GC loss observed (Platel et al., 2018). Thus, sensory experience likely maintains GC survival, but perturbations during the critical period of GC development results in a loss of these new-born cells.

In contrast, over-exposure of odorants increases the generation of new GCs as well as their survival (Martončíková et al., 2011; Rochefort et al., 2002). Sensory experience appears to determine GC survival by influencing the functional incorporation of GCs into the pre-existing circuit, and this has been found to depend on the intrinsic activity levels of newborn GCs in a cell-autonomous manner. This is because genetically increasing the excitability of newborn GCs via artificially increasing sodium channel expression blocks cell death in these cells, whereas decreasing the intrinsic excitability of newborn GCs via increasing potassium channel expression, decreases their survival rates (Lin et al., 2010). To this end, it has further been found that the critical maturational time-window where GCs require sensory input to survive, corresponds to the time-window in which GCs form extensive synaptic contacts with the resident network (Yamaguchi, 2014). Thus, synaptic input through sensory experience during this critical period appears to crucially facilitate GC survival.

GCs exhibit activity-dependent structural plasticity

Upon network integration, GC structural plasticity continuously occurs. Indeed, chronic *in vivo* imaging techniques have enabled the observation that GCs of all maturational ages continuously add and eliminate around 20% of their dendritic spines, a function thought to optimise odour information processing (Sailor et al., 2016). Interestingly, a recent finding demonstrated that specifically mature GCs are able to relocate their spines in an activity-dependent manner within minutes of stimulation. The direction of relocation was determined by M/TC activity, where GCs actively relocate their spines from inactive M/TCs towards dendrites of active M/TCs (Breton-Provencher et al., 2016). This form of short-term plasticity may function to adjust the bulbar network to rapidly changing odour environments.

Sensory experience can further modulate these structural properties. Upon sensory deprivation, GCs exhibit reduced spine numbers as well as less branching in their dendritic tree (Dahlen et al., 2011). When looking at gross morphology, this effect appears to impact specifically new-born GCs during the life-or-death critical window, as mature GCs seem to be resistant to this change (Breton-Provencher et al., 2016; Saghatelyan et al., 2005). However, when distinguishing between different parts of GC dendrites, it was found that even mature GCs undergo structural changes in the face of long-term (3 weeks) occlusion. In this scenario, GCs appear to increase their synaptic densities only in their proximal dendrites (Kelsch et al., 2009). In new-born GCs, the effect of sensory deprivation on decreased spine number is restricted to the distal and basal compartments of the dendrite (Kelsch et al., 2009; Saghatelyan et al., 2005). Olfactory learning has the opposite effect. In mice that learned to discriminate between two odours with repeated exposure, new-born GC spine densities were enhanced in the distal, proximal and basal domains of their dendrites (Lepousez et al., 2014). This form of plasticity may be in place to enhance long-range functional connectivity during olfactory learning (Lepousez et al., 2014). Therefore, sensory experience impacts the structural maturation of new-born GCs and further modulates integrated GC synaptic connectivity.

GC functional plasticity in response to input changes

GCs are also plastic in terms of their functional activity, a property that is influenced by the olfactory environment. Using Ca^{2+} imaging to look at the sensory maps of GCs, it was found that long-term (5-6 weeks) sensory deprivation inhibited new-born GCs from expanding their sensory maps, whereas mature GCs were unaffected (Quast et al., 2016). Contrastingly, upon odour enrichment delivered through a go-no-go task, the expansion of immature GC sensory maps are enhanced (Quast et al., 2016). Nevertheless, this study used Cre-lines to drive expression in newborn GCs, which may have impacted the results, as a further study using targeted lentiviral injections to label newborn GCs found somewhat contradicting results (Wallace et al., 2017). Here, the authors found that newborn GCs exhibit broader odour tuning curves compared to their mature counterparts during the first two weeks of maturation. Newborn GCs then refine their tuning curves by 3 weeks of maturation. However, upon odour enrichment during this time, newborn GCs appear to continue exhibiting a broad odour tuning curve (Wallace et al., 2017). Despite their contrasting results, these studies imply that immature GCs require sensory input to develop sensory maps, but also tune their odour responses in an input-dependent manner.

These functional differences between mature and immature GCs in the face of changing odour environments were further demonstrated with the use of IEGs to mark activity. Once new GCs

synaptically integrate into the established system, developmentally young GCs show increased IEG expression in response to novel odours compared to the established resident population when mice were exposed to an odour-rich environment. Interestingly, upon habituation to odour exposure, established, mature GCs exhibited a decrease in their IEG expression (Magavi et al., 2005). Thus, sensory experience not only shapes the response profiles of new-born GCs, but also alters properties of the existing GC population.

The functional plasticity GCs possess influences bulbar output. In response to repeated tetanic OSN stimulation, a paradigm that may have similar effects as odour enrichment on OB circuitry, the frequency of *γ*-oscillations in the OB is increased. This increase has been linked to the increased activation of GCs, which may provide a larger inhibitory drive onto M/TCs (Friedman and Strowbridge, 2003). Indeed, even GC intrinsic excitability can be adjusted in an experience-dependent manner, which impacts bulbar output. Saghatelyan et al., (2005) demonstrated that even though less GCs are born after sensory deprivation, the ones that *are* generated are intrinsically more excitable compared to their control counterparts. This effect may function to maintain inhibitory drive onto M/TCs in the face of external perturbations. Similarly, cholinergic input onto GCs has been shown to potentiate GC intrinsic excitability by converting after-hyperpolarisation into after-depolarisation. This in turn increased M/TC inhibition, and has been proposed to be a method by which cholinergic inputs could be regulating short-term plasticity in glomerular output (Pressler et al., 2007). Though this is not a direct example of experience-driven plasticity, it does reveal an example of short-term plasticity that may function to sharpen GC responses in response to repetitive stimulation, as cholinergic inputs have previously been implicated in the adaption of the bulbar circuit to repetitive sniffing-like input (Linster and Cleland, 2002). Thus, functional adjustments in GCs have the potential to profoundly impact M/TC output, and can also be induced by sensory experience.

In summary, even at this later stage in olfactory processing, the various forms of plasticity GCs exhibit can aid in the adjustment of the circuit to changes in the olfactory environment.

1.3.5. Plasticity in mitral and tufted cells

Though M/TCs do appear to adjust some of their properties in an experience-dependent manner, these adjustments, on an intrinsic level, are far less extensive compared to the inhibitory network. Indeed, on a cellular level, most of the plasticity occurring in the OB has almost always been linked to the inhibitory interneuron population. It is further likely that many changes observed in MCs and TCs in response to changing odour environments stem from altered inhibitory actions. A classic demonstration of how M/TCs adjust to long-term sensory deprivation showed that M/TCs enhance their response profiles to odours. This effect was

mimicked by application of a D_2-receptor antagonist, thus this change in M/TCs could reflect an adjustment in other parts of the circuitry (Wilson and Sullivan, 1995).

M/TCs express remarkable dendritic structural stability

Following on from the idea that M/TCs retain stability in changing odour environments, it has been shown that M/TC dendrite morphology is remarkably stable. Using chronic imaging techniques *in vivo*, it has been shown that M/TC dendrites in the adult mouse do not undergo any adjustments with long-term odour enrichment (40 days). Though chronic application of a $GABA_A$ antagonist increases the firing rate of these cells as well as the rate of synapse pruning and sprouting, the overall dendritic architecture remains stable even in these un-physiological conditions (Mizrahi and C Katz, 2003). This phenomenon was interpreted as MCs and TCs retaining dendritic stability throughout an ever-changing olfactory environment, that may provide a scaffold to maintain the organisation of the local (inhibitory) circuits that do change phenomenally with experience.

Interestingly, it appears that for M/TCs to retain their dendritic stability, they require OSN axons to be functionally established. Indeed, if OSN axons are abolished during the developmental period in which M/TCs are maturing, these cells undergo atrophy in their dendrites and fail to develop normally (Kobayakawa et al., 2007; Leo and Brunjes, 2003). Furthermore, if OSN axons are damaged after the circuitry is established in the adult, M/TC dendrites also retract their dendrites and attenuate their responses to odours. Once this occurs, it is difficult to re-establish OSN-M/TC connectivity even after OSN projections have recovered (Murai et al., 2016). Thus, MCs and TCs appear to retain stable dendritic morphology in the face of sensory perturbations, however if the initial input circuitry is physically damaged, they appear to lose this ability.

Activity-dependent generation of M/TCs

Despite their apparent dendritic stability, MCs and TCs do show some other examples of plasticity that are induced by sensory experience. For example, it has been shown that sensory experience during bulbar circuitry development after birth can directly impact the number of M/TCs that are incorporated into the system. Unilateral neonatal sensory deprivation results in a significant and permanent loss of M/TCs in the occluded bulb, an effect that occurs within 25 days after nasal blockage (Meisami and Safari, 1981). The opposite effect is seen when rat pups are exposed to odour enrichment. In this case, after 4 weeks of odour enrichment, M/TC numbers were much higher both in the main OB as well as the AOB (Rosselli-Austin and Williams, 1990).

In addition to the apparent developmental effect sensory experience has on M/TC number, the mature population also responds to olfactory experience, though in the opposite direction. With repetitive and prolonged (30 days) exposure to a purely olfactory cue, i.e. that would specifically stimulate only the OB, adult mice (3 months and 1 year olds) exhibit a reduced number of M/TCs (Johnson et al., 2013). Thus, olfactory experience can profoundly influence the population density of MCs and TCs, which likely has impacts on odour processing and perception.

Sensory experience shapes M/TC responses to odours

Changes in sensory experience also seem to induce M/TCs to adjust their response profiles to odours in the mature and immature animal. When adult rats are repetitively exposed to odorants for 6 days, the proportion of M/TCs responding to the exposed odours is decreased. Interestingly, this effect is not specific to the exposed odorants, as this decreased responsiveness also occurs in response to previously un-exposed odours. This plastic effect is long-lasting, as it persists for at least 10 days after odour enrichment (Buonviso et al., 1998). Even shorter periods of olfactory enrichment seem to affect MC and TC odour response profiles. When odours are presented repeatedly (over a short experimental period) with 5 minutes of inter-stimulus intervals, odour-induced M/TC spiking responses decrease. M/TCs are able to restore original firing responses when given a recovery period, and thus this adjustment likely represents habituation (Chaudhury et al., 2010). Contrastingly, M/TCs have also been found to enhance their responsiveness to novel odours. Upon odour stimulation with a novel odour molecule that was shown to best activate particular M/TCs, those M/TC odorant receptive fields undergo a shift toward the experienced odorant. This effect is relatively long-lasting, and remains for at least 60 minutes (Fletcher and Wilson, 2003). Thus, even a single demonstration of a novel odorant can enhance M/TC responsiveness to that odour, and indicates that past experience can shift M/TC odour feature tuning toward familiar odorants. Therefore, M/TCs can adjust their odour tuning curves to either decrease their odour responses when stimuli become irrelevant (i.e. habituation), but also are able to enhance their receptive fields to increase their ability of responding to novel input.

Sensory deprivation also appears to modulate M/TC responsiveness to odours. When sensory deprivation occurs early during rat postnatal development (P2), though M/TCs do not adjust their response profiles to odours *per se*, they do appear to decrease their spontaneous activity and portray a higher incidence of responding to odours compared to the unperturbed condition (Guthrie et al., 1990).

Nevertheless, it has been argued that these adjustments likely represent alterations in the inhibitory circuit that exhibit their effects onto M/TCs. For example, it has been shown that

internal GCs of the AOB can adjust their intrinsic excitability, which impacts M/TC output. When an intruder male mouse is placed in the same cage as a resident male mouse, internal GCs impacted by the odour cues of the intruder male in the resident males' AOB exhibit increased intrinsic excitability. The subsequent increased inhibitory drive onto M/TCs was shown to subdue M/TC responses to input stimulation (Cansler et al., 2017). Furthermore, since cholinergic inputs can influence the firing frequency in M/TCs, PGCs, and GCs (Ma and Luo, 2012), it is likely that sensory experience in awake animals also influences these connections, which can further modulate bulbar output. Indeed, when mice learn to associate an odour with a sugar reward, there is an increase in noradrenaline release by centrifugal projections from the locus coeruleus into the OB. This is in addition to an increase in the ratio of glutamate release, presumably from M/TCs, to GABA release, presumably from GCs (Brennan et al., 1998). Hence, multiple modulatory processes appear to be plastic together, which may prevent the observation of endogenous plasticity displayed by M/TCs.

Despite these controversies however, recent chronic two-photon Ca^{2+} imaging *in vivo* in awake animals has demonstrated that M/TCs could in fact increase their odour responsiveness intrinsically. Upon repeated odour exposure, M/TCs weakened their responses to the odours they were exposed to, an effect that lasted for months after odour exposure. After recovering to original response levels, they could then again weaken their odour responses to a different set of odorants that were presented in an enriched format post-recovery. This effect was likely not due to changes in the GC network because GCs also weakened their responses to exposed odorants. Since GCs mainly target M/TCs then, it is unlikely that the changes in M/TCs observed were due to an overall increase in GC activity. These results therefore imply that M/TCs are intrinsically capable of tuning their odour response curves, though this study did not examine the effects on JGCs. Interestingly, when mice were anaesthetised, this effect of sensory experience on M/TCs was no longer evident (Kato et al., 2012), which highlights the importance of considering the state of the animal when interpreting data.

M/TCs undergo activity-dependent synaptic plasticity

M/TCs have further been shown to adjust their synaptic efficacy in an activity-dependent manner. M/TCs form connexin-36-mediated gap junctions with each other which contributes to M/TC excitatory transmission as well as the synchronisation of M/TC firing in cells associated with the same glomerulus. Many more gap junctions are present at developmentally early stages, which rapidly decrease with age after P10 as chemical transmission becomes more prominent. This plastic change has been shown to require sensory input. If sensory deprivation occurs at birth, M/TCs develop more slowly and fail to reduce the number of gap-junctions they

form (Maher et al., 2009). Hence, M/TCs appear to undergo an experience-dependent maturational transition from electrical conductance to chemical *and* electrical transmission.

In the mature circuitry, M/TCs are also likely to adjust the extent of dendritic lateral chemical excitation with other M/TCs in an activity-dependent manner. It has been shown, using paired recordings, that different M/TCs projecting to the same glomerulus exhibit different strengths of lateral excitation. Upon theta-burst stimulation, lateral excitation is potentiated in connections that are small, but depressed in connections that are large. The direction and amplitude of this plasticity correlates with changes in presynaptic P*r* of glutamate, where P*r* is increased during potentiation and decreased during depression (Pimentel and Margrie, 2008). This example of synaptic plasticity therefore demonstrates that M/TCs can undergo instantaneous dendrodendritic plasticity and suggests that the strength of these connections is determined either developmentally and/or by recent activity history.

The M/TC-GC connection is also a likely candidate for activity-dependent plasticity in the mature circuit. Stimulation of M/TCs evokes the expected excitatory postsynaptic potential (EPSP) in GCs consisting of both AMPA and NMDA potentials. Interestingly, this EPSP is reversibly inhibited with the application of noradrenaline. As a result, M/TCs display a reduced number of spontaneously occurring inhibitory postsynaptic potentials (IPSPs), an effect that is likely due to decreased synaptic efficacy originating from the M/TCs (Trombley and Shepherd, 1992). Thus, not only does noradrenaline appear to have a disinhibitory effect on the OB, but it also appears to reduce M/TC-mediated GC excitation, that may directly increase M/TC excitability due to decreased feedback inhibition. Though this study did not directly determine whether this plasticity results from a change in sensory experience, it does suggest that M/TCs have the *capability* to adjust their synaptic strength with GC partners. Furthermore, since noradrenaline appears to be involved in olfactory learning (Brennan et al., 1998), an effect that ultimately arrives due to sensory experience, the effects of enhanced noradrenaline release by centrifugal inputs due to presentation of the learned odorant could directly modulate M/TC synaptic drive, which in turn modulates GC activity, and thus results in modulated M/TC output.

M/TCs are thus able to adjust a number of their properties as a result of sensory experience. As described above, it is difficult to distinguish whether some of these changes, particularly response profiles, occur intrinsically or as a result of the highly malleable local inhibitory circuit, or even centrifugal inputs. Nevertheless, some findings do directly demonstrate the endogenous plastic properties of M/TCs, and others strongly suggest that they have the *capability* to undergo activity-dependent functional plasticity. Therefore, even at the output level of initial processing, plastic changes occur in response to changes in the olfactory environment.

1.3.6. Impacts activity-dependent plasticity in ETCs would have on bulbar processing

As already indicated above, ETCs perform vital functions in the glomerular circuitry. They are directly implicated in driving feedforward excitation onto M/TCs (De Saint Jan et al., 2009) and appear to be the major target of OSN inputs (De Saint Jan et al., 2009; Gire et al., 2012; Najac et al., 2011). Thus, these cells are now viewed as the intermediary pathway by which M/TCs gain input from the outside world. ETCs further drive the inhibitory glomerular network and are therefore a major source of triggering feedback inhibition (Hayar et al., 2004a). They further drive the synchronous activity observed in glomeruli (Hayar et al., 2004a), and thus are heavily involved in setting the response profile of a glomerular circuit. In summary, ETCs directly receive OSN inputs and appear to drive the glomerular circuitry as a response, providing modulated feedforward excitation for M/TCs to amplify into an excitatory output. Interestingly, ETCs do not appear to be present in the AOB (Lowe, 2013), and thus may have developed to perform functions specifically for odour processing, rather than processing information related to other biological functions such as mate choice.

As ETCs are so central to initial odour processing, experience-driven plasticity in any of their properties could have profound impacts on glomerular processing and eventual M/TC output. Because all other major components of the OB circuitry are able to adjust at least some of their properties in response to external perturbations, it seems likely that ETCs would also display forms of experience-driven plasticity, and may in fact trigger the plastic changes observed in other parts of the circuit.

1.3.7. Are ETCs plastic?

Despite their crucial involvement in OB circuitry, activity-dependent plasticity in ETCs has not been heavily explored. One major finding though, was that as opposed to M/TCs, long-term sensory deprivation (4 weeks) since birth does not induce a change in the number of ETCs (Marks et al., 2006).

In fact, the only form of activity-dependent plasticity in these cells discovered so far has been demonstrated in terms of ETC axonal projections to isofunctional glomerular columns. ETCs form part of the intrabulbar map, where they connect isofunctional glomerular columns via their axonal targeting (Lodovichi et al., 2003). As this intrabulbar map forms and develops, ETCs initially portray broad axonal targeting that gradually refines to the targeting of distinct glomerular columns by around 7 weeks of age in mice (Marks et al., 2006). If sensory deprivation occurs during this developmental period for prolonged periods of time (3 weeks), the intrabulbar

map appears to broaden to the extent seen in very young (1 week old) mice (Marks et al., 2006). The opposite effect occurs if glomeruli are enriched with odour input, as this results in an accelerated refinement of the intrabulbar map (Marks et al., 2006).

When observing the mature circuit, sensory experience can still affect these ETC intrabulbar projections. Upon sensory deprivation in adult mice, ETC axonal projections broaden to levels resembling the immature circuit and exhibit a reduced branch point density (Cummings and Belluscio, 2010; Marks et al., 2006). This effect has been shown to be reversible, as removing the sensory block results in a re-refinement of ETC axonal projections and increases in branch point density after a recovery period (Cummings and Belluscio, 2010). Thus, sensory experience can shape the intrabulbar map created by ETCs in immature as well as mature animals.

Since the target of intrabulbar axonic connections is GCs, which are involved in modulating M/TC activity, this plasticity in ETC projection targeting could therefore impact the amount of inhibition received by M/TCs associated with isofunctional odour processing. Interestingly, there is a delicate interplay between GC generation and ETC axonal targeting. When neurogenesis is inhibited in the adult, ETCs expand their axonal targeting to similar levels as seen with occlusion. Furthermore, when nares are allowed to recover from occlusion but neurogenesis is inhibited, ETCs are unable to re-refine their axonal targeting to control levels (Cummings et al., 2014). Thus, there is a requirement for new-born GCs to maintain established ETC intrabulbar maps, as well as for the re-refinement of axonal projections in response to external perturbations.

Despite these findings however, the functional consequences of this projection plasticity, or indeed the exploration of any further plastic capabilities portrayed by ETCs, were not further explored. Since ETCs are so heavily involved in glomerular processing, it would thus be interesting to observe whether these cells change any of their other properties that modulate their function. If ETCs are malleable, and are able to respond to changes in olfactory environment, they may provide a major avenue by which glomerular processing and final output is adjusted.

1.4. Thesis aims – an exploration of ETC activity-dependent plasticity

As described above, on a cellular basis, multiple components of the OB demonstrate the ability to adjust multiple properties in response to external perturbations, both in the mature and immature OB. How these changes integrate to adjust bulbar processing as a whole is still being investigated, but many findings suggest that these adjustments function in concert to produce a modified output and adjust odour processing in an ever-changing olfactory environment. This

may crucially function to ensure odour information is reliably transmitted to the olfactory cortex, where processes there use this information to navigate the organism through the olfactory world.

Even though ETCs are so central in the OB circuit, very little is known about how ETCs respond to the constant changes in olfactory environment. Given their central role in the glomerular circuit, any plastic adjustment of ETC properties likely would impact multiple levels of bulbar processing, and would thus place these cells at the heart of glomerular adjustments.

This thesis therefore, aims to shine some light on the plastic capabilities ETCs exhibit. More specifically, we want to know whether ETCs are intrinsically plastic in response to sensory perturbations. If this is indeed the case, we further aim to elucidate whether ETC plasticity functionally adjusts the OB network when changes occur in olfactory environment. To enable this exploration, we use sensory deprivation by unilateral plug naris occlusion to drive experience-dependent changes in the juvenile mouse main OB. Our occlusion paradigm consists of short-term sensory deprivation (24 hours), as this has been shown to be enough time to drive changes in the glomerular inhibitory circuit (D. Byrne, E. Galliano, unpublished data).

Using patch clamp physiology in acute OB slices as well as immunohistochemical analysis, we characterise various ETC functional and morphological properties and compare these properties in occluded conditions to control conditions. We first explore the possibility that ETCs alter their intrinsic excitability and gross morphology upon naris occlusion (chapter 3). Using a large sample size, we find no experience-driven differences in the many different intrinsic functional and morphological properties ETCs display. However, we did find a significant increase in the magnitude of LLCs ETCs experience in occluded conditions (chapter 4). This spurred us on to explore how this form of synaptic plasticity arises, and whether it impacts the output of the glomerular network (chapter 5).

Overall, we found that there is an intricate interplay of alterations in glomerular excitation and inhibition upon short-term sensory deprivation. This may be involved in maintaining set levels of M/TC output in response to external perturbations, which may be crucial for maintaining sensory perception when there are changes in the sensory environment.

Chapter 2

Materials and methods

All chemicals were purchased from Sigma-Aldrich, unless otherwise specified.

2.1. Animals

All experiments were performed in accordance with UK Home Office guidelines under C. Hahn's Personal Licence and M. Grubb's Project Licence for animal experiments. Mice of either gender were used and all experiments were performed between postnatal day (P) 20-35. C57B16 mice were acquired from Charles River and were either used as experimental animals, or to back-cross each generation of transgenic animals. CCK-IRES-Cre (Taniguchi et al., 2011) founders were kindly donated by Prof. Beatriz Rico, and crossed with a floxed tdTomato (tdT) reporter line (The Jackson laboratory stock number 008601) to produce transgenic animals that labelled all cells expressing CCK with tdT (CCK-tdT). Transgenic mice were genotyped for the expression of tdT and Cre from ear-notched tissue using PCR. All mice were housed under a 12h light-dark cycle in an environmentally controlled room. The mice had free access to water and food. Every effort was made to minimize both the number of animals used and their suffering during the experimental procedures.

2.2. Sensory manipulation

To perform unilateral naris occlusion, mice were briefly anaesthetised (<5 min) with isoflurane. In the occluded group, a custom-made ~6 mm Vaseline-lubricated plug of silicone and nylon (Ethylon polymide, non-absorbable suture, Ethicon, UK) (Cummings et al., 1997) (made by either C. Hahn or M. Lipovsek) was inserted into the right nostril and left for 24 hours. At the termination of each experiment, post-hoc visual observation of the nasal cavity was always performed to ensure that the plug had remained in place. Occluded mice where the plug could not be found, were not used for experiments.

For control animals, our initial aim was to characterise ETC responses in both sensory deprived and enriched conditions. We thus obtained some data from some experiments, mentioned in the text, where the control group was unperturbed and remained in the home-cage until experimental use. Upon abandoning the aim of exploring sensory enrichment, we decided to incorporate a more accurate control for our occluded group by performing a sham occlusion on control animals to control for both anaesthetic exposure and any potential nasal damage caused by the plug. In this case, the mouse was anaesthetised with isoflurane and a naris plug was

inserted but immediately removed. In just one experiment (chapter 4, **Fig 4**) both unperturbed and sham-treated animals were represented in the data-set, and no difference was found between the two types of control. As noted in the text, all experiments from chapter 4, Fig. 4 onwards used exclusively sham-treated mice as controls.

2.3. Slice electrophysiology

Mice were deeply anaesthetised with isoflurane and then swiftly decapitated. Subsequently, the OB was removed and transferred into ice-cold slicing medium containing (in mM): 240 sucrose, 5 KCl, 1.25 Na_2HPO_4, 2 $MgSO_4$, 1 $CaCl_2$, 26 $NaHCO_3$ and 10 D-Glucose, bubbled with 95% O_2 and 5% CO_2. Horizontal slices (300µm thick) of the olfactory bulb were cut using a vibratome (VT1000S, Leica) and afterward stored in ACSF containing (in mM): 124 NaCl, 5 KCl, 1.25 Na_2HPO_4, 2 $MgSO_4$, 2 $CaCl_2$, 26 $NaHCO_3$ and 20 D-Glucose, bubbled with 95% O_2 and 5% CO_2. Some experiments, indicated in the text (chapter 4) were performed with ACSF containing 0 Mg^{2+}. Slices were allowed to recover for at least 45 minutes at room temperature before the experiments started. Experiments were performed at physiologically relevant temperature (34 ± 2°C) with an in-line heater (TC-344B, Warner Instruments), and the bath was continuously perfused with oxygenated ACSF (1.33ml/min). Slices were secured in place using a harp (Warner Instruments).

WT ETCs were visualized using an upright microscope (Axioskop Eclipse FN1, Nikon) equipped with a 40X water immersed objective. DIC optics were employed to enhance contrast of signal which aided the visualisation of live-imaged cells captured via a camera (DMx 31BF03, Scientifica). Alexa fluorescence was revealed by epifluorescent illumination with appropriate excitation and emission filters (CoolLED pE-100) once the dye had dialysed the cells in the whole-cell configuration. We included only cells that were located in the deeper parts of the GL, that showed a characteristic tufted morphology, that fired spontaneously in bursts in current clamp *I*=0, and that displayed a characteristic depolarising sag when injected with prolonged negative current steps in current clamp mode (see chapter 3). CCK-tdT ETCs were visualised by finding tdT+ cells using epifluorescence and their location in the GL. The same stringent criteria for ETC identification applied to CCK-tdT ETCs. M/TCs were identified by their large soma size and location in the MCL.

Pipettes were pulled from borosilicate glass (1.5mm outer diameter, 1.17mm inner diameter, Harvard Apparatus; or 1.5mm outer diameter, 0.84mm inner diameter, World Precision Instruments) with a resistance of 2.5-7.5MΩ using a vertical P10 puller (Narishige). For whole-

cell recordings in ETCs, patch-pipettes were fire-polished with a microforge MF-900 (Narishige) before the experiment. Unless stated otherwise, recording electrodes were filled with an intracellular solution containing (in mM): 124 K-Gluconate, 9 KCl, 10 KOH, 4 NaCl, 10 HEPES, 28.5 Sucrose, 4 Na_2ATP, 0.4 Na_3GTP, 0.15% Biocytin (pH 7.25-7.35; osmolarity 290 mOsm) and Alexa 488 (1:150) (Thermo Fisher Scientific). pH was adjusted with KOH. As indicated in the text, we further included 10mM glutamate in the patch pipette for recordings of glutamate potentials (see chapter 4) to avoid glutamate rundown (Ma and Lowe, 2007). Liquid junction potential between ACSF and the internal solution was not corrected for but was calculated in the Clampex software as 12.1mV for standard solutions. For experiments containing 10mM glutamate in the recording electrode, the liquid junction potential was 12mV.

To record OSN evoked responses, we electrically stimulated OSN fibres using ACSF-filled monopolar patch-pipettes with a brief pulse of manually selected amplitudes delivered by an isolated stimulator (0.01-10mA, ISO-Flex, A.M.P.I). The stimulating electrode was placed into the ONL nearby the targeted glomerulus, and care was taken to avoid placing the electrode directly onto a glomerulus.

Patch-clamp recordings were performed using an Axopatch amplifier 700B (Molecular Devices). Signals were digitized (Digidata 1550, Molecular Devices) and Bessel-filtered at 3kHz. Fast capacitance was compensated in the on-cell configuration. In the whole-cell configuration, membrane potential (Vm) was measured immediately after rupture in current-clamp mode. A protocol for test series was included before and after each recording. This test series consisted of, in voltage clamp, a voltage step of -10mV for 10ms and +10mV for 10ms. This produced traces from which series resistance (from the current peak), membrane resistance (from the steady holding current at the new voltage), and membrane capacitance (from the area under the exponentially decaying current from peak to holding current) could be calculated. For whole-cell recordings in ETCs, traces were excluded if series (Rs) or input (Ri) resistances were respectively bigger than 30 MΩ or smaller than 100 MΩ, and if they varied by > 20% over the course of the experiment. For whole-cell recordings in M/TCs, traces were excluded with the same criteria as for ETCs, except that cells were excluded if their Ri was smaller than 70MΩ. For cell-attached recordings, traces were excluded if the test series showed that a giga-seal (>1000 MΩ) was not formed.

Some experiments were performed in the presence of 10µM picrotoxin (PTX, Sigma-Aldrich) in the recording solution. For auto-evoked glutamate potentials, responses were recorded in ACSF to obtain baseline measures of glutamate potentials, followed by wash-in of 10µm 2,3-dioxo-6-nitro-1,2,3,4-tetrahydrobezno[f]quinoxaline-7-sulfonamide disodium salt (NBQX, Sigma-

Aldrich) and 50µm DL-2-amino-5-phosphonopentanoic acid (APV, Cambridge Bioscience) that eliminated the responses (further described in chapter 4). Bridge balance was not compensated for, except for glutamate potential recordings performed in chapter 4.

Current-clamp experimental protocols

In current-clamp mode, evoked spikes and sag potentials were measured with V_{hold} set to −55 ± 3 mV. Spontaneous firing was recorded for 30 seconds with 0 pA current input (I=0). For multiple spiking measures, we injected 500-ms-duration current steps from 0pA of increasing amplitude (Δ10pA) until the neuron passed its maximum firing frequency. For action potential waveform measures, we injected 10ms-duration current steps of increasing amplitude (Δ10pA) until the current threshold for reliable action potential generation was reached. For sag-potential measures, we injected 500ms-duration current steps from -300pA of increasing amplitude (Δ25pA) until 0pA current injection was reached. Some cells were not tolerant to a -300pA hyperpolarisation. In these cases, if cells recovered, we began our step-current from -200pA. For auto-evoked glutamate potential measurements, action potentials were induced with a 2ms-duration current step of 800pA.

Voltage-clamp experimental protocols

In voltage-clamp mode, spontaneous LLCs were recorded at a holding potential of -55mV for one minute. To record OSN-evoked LLCs, a brief 0.1ms-duration OSN stimulation was given at 20ms inter-stimulus intervals. At least 4 sweeps were recorded in this way to determine average amplitude and charge of the evoked LLCs. To record paired-pulse ratio (PPR) responses in ETCs, OSNs were electrically stimulated with 0.1ms-duration pulses with an inter-pulse interval of 50ms. OSNs were given 60s between pulse-trains to fully replenish their synaptic vesicles after this paired stimulus (Vaaga and Westbrook, 2017). To ensure we were recording EPSCs evoked with roughly comparable stimulus intensities across cells, the first evoked EPSC needed to display an amplitude between 200-500pA. At least 3 sweeps were recorded per cell in this configuration. We further used a repetitive OSN stimulation protocol to record EPSCs in the whole-cell configuration to quantify release probability (P*r*) and provide another measure of PPR at 20ms inter-pulse intervals. OSNs were stimulated at a frequency of 50Hz with 20 pulses. A 60s recovery period was given between pulse trains. At least 3 sweeps were recorded per cell in this configuration. To record OSN-evoked spiking, we used the same OSN stimulation protocol. We further adapted the protocol to record OSN-evoked spiking when 20 pulses were delivered at 5Hz. For these recordings, at least 5 sweeps were recorded for each cell.

2.4. Analysis of electrophysiological recordings

For all electrophysiological analyses, the experimenter was blind to the treatment condition until all data in an experiment were analysed and de-coded.

Intrinsic spiking properties

Exported traces were analysed using custom-written routines in MATLAB (Mathworks) written by M. Grubb, which have been used routinely in the laboratory (Chand et al., 2015; Dumitrescu et al., 2016; Galliano et al., 2018). Before differentiation for dV/dt, recordings at high temporal resolution (5µs sample interval) were smoothed using a 20 point (100µs) sliding filter. For quantification of action potential properties (AP), voltage threshold (Vthresh) was taken as the potential at which dV/dt first passed 10 V/s. AP height (Vmax) was determined as the difference between maximum spike voltage and voltage threshold. Spike width (WHH) was measured at the midpoint between voltage threshold and maximum voltage. Afterhyperpolarisation values (AHP; and relative AHP) were measured from responses to 500ms current injection. AHP was measured from the local voltage minimum after the first spike fired at rheobase, the minimum current required to generate an AP. Relative AHP (Rel. AHP) was measured as the difference between the AP threshold voltage and the AHP. Maximum rate of AP rise was determined by measuring maximum dV/dT (Max. dV/dt), calculated from the first derivative of the AP. First spike delays were measured as the time it took to reach Vmax from the initiation of the current step.

For quantification of multiple spiking properties, input-output curves were constructed by counting the number of spikes fired at each level of injected current and plotting the number as a function of input current density (pA/pF). The coefficient of variation for inter spike interval (ISI CV) was calculated for each sweep with at least 3 spikes, and the mean of these values was taken from all the sweeps of that cell. Maximum number of spikes were determined by counting the maximum number of spikes of any given sweep per cell. Spike numbers were segmented into 100ms time-bins across the 500ms current injection to view differences in spiking patterns (Goldfarb et al., 2007).

Measuring the sag potential

The sag potential was quantified by calculating the sag index (Chittajallu et al., 2013) for the recorded cell. This was calculated using a custom-written MATLAB script (C. Hahn and M. Grubb). The sag index was calculated using the following formula:

$$Sag\ index = \frac{Vrest - Base\ plateau}{Vrest - Sag}$$

Where Vrest = resting membrane potential, Base plateau = the voltage at which the sag reaches baseline before the hyperpolarising step is ended, and Sag = the minimum voltage the sag of the cell reaches during the hyperpolarising step (depicted in chapter 3, **Fig 9 Ai**, red box = base plateau, purple box = Vrest, green box = Sag). With this calculation, the lower the sag index, the larger the sag potential. These measures were taken from raw traces, with values from multiple traces then fitted with polynomial curves in order to quantify the sag index at the same voltage base for each cell (chapter 3, **Fig 9 Aii-iv**). Pilot data for several different voltage bases were taken to define what voltage base would result in the most comprehensive results (i.e. at what voltage base did most cells have a measurable sag potential; data not shown). From these data, a voltage base of -90mV was chosen for subsequent analysis.

Auto-evoked glutamate potentials

Tail potential amplitudes were measured from the baseline occurring before AP initiation, to the peak of the amplitude 30ms after the AP (see **Fig. 7** in chapter 4). PPR was quantified by dividing the second peak amplitude by the first peak amplitude.

LLC analysis

Spontaneous LLCs were selected by eye in Minianalysis (Synaptosoft). Detection thresholds were set to the following parameters: threshold, ~10pA (set by the amount of RMS noise, 5x multiplication factor); period to search a local maximum, 50 000µs; time before a peak for baseline, 90 000µs; period to search a decay time, 200 000µs; fraction of peak to find a decay time, 0.37; period to average a baseline, 5000µs; number of points to average for peak, 1. Upon detecting all LLCs in that trace, all events were grouped to create an average LLC in the group analysis and curve fitting window. The x and y points of the average event were exported into a text file, which was subsequently used to re-plot the average LLC profile in MATLAB for subsequent analysis (C. Hahn and M.Grubb). The amplitude was calculated from the difference between mean baseline current and mean peak current. The mean peak current was calculated by taking the mean of the ± 7 closest points to the minimum current measured. The charge was calculated by measuring the area under the curve from the first current deflection (the start, defined by the first point after the last baseline measure point) of the LLC, to 500ms after this point (Gire and Schoppa, 2009). Evoked LLC traces were directly imported into MATLAB and analysed in the same way as spontaneous LLCs, but with an LLC start point commencing

immediately after the stimulus artefact. For ETCs and M/TCs, evoked LLCs were measured at suprathreshold stimulus intensities, when LLCs occurred reliably across sweeps without monosynaptic components (see **Fig 2** in chapter 4). For M/TCs with variable-amplitude evoked LLCs (see **Fig 10**, chapter 4), these were not further quantified. For coefficient of variation (CV) analysis of LLC amplitudes, individual LLCs recorded in a cell were analysed for amplitude, and the CV was calculated per cell by dividing the mean LLC amplitude by the standard deviation. For histogram analysis of LLC "quantal" properties, all spontaneous or evoked LLC events from either all ETCs or all M/TCs were normalised for the median amplitude of LLC in each cell. To quantify M/TC evoked LLCs in this way, traces where the multistep LLCs were observed were included, rather than using suprathreshold stimulation recordings. The resulting values were then plotted against the frequency of occurrence, using the automatic binning function in GraphPad Prism to plot the histograms. Single Gaussian distributions were fitted to the resulting histograms to observe the spread of the data points.

OSN release probability analysis

To quantify PPR from the paired-pulse OSN stimulation protocol, we recorded current responses in ETCs that displayed monosynaptic OSN-evoked responses. To obtain a measure of PPR, we divided the amplitude of the second evoked EPSC by the amplitude of the first using a custom-written MATLAB routine (C. Hahn and M. Grubb). The first EPSC amplitude was measured from the mean baseline current before stimulus onset to the peak of the EPSC response. To estimate the baseline of the second EPSC, decay curves were fitted with single-exponential functions using a least-squares minimalization algorithm to the decay of the first EPSC and extended to where it met the second EPSC peak on the x-axis. This measure was then considered the baseline from which to calculate the amplitude of the second EPSC in the same way the first EPSC amplitude was derived. The same analysis was performed for PPR recordings obtained from the 50Hz OSN stimulus train protocol, measuring the amplitudes of the first two EPSCs.Estimations of OSN P*r* based on 50Hz OSN-stimulus trains were performed using a custom-written MATLAB script (M. Grubb). P*r* was calculated by dividing the first evoked EPSC by the size of the readily releasable pool. The readily releasable pool was estimated using two separate methods. The Schneggenburger, Meyer, and Neher (SMN) method involved fitting a linear fit to the last 5 EPSCs on a plot displaying the cumulative EPSC amplitude against the stimulus number. The readily releasable pool was then measured as the y-intercept of the fitted line (Schneggenburger et al., 2002). The Elmqvist-Quastal (EQ) method involved fitting the fast EPSC amplitude against the cumulative EPSC amplitude. A line was fitted to the first 3 EPSCs, where the x-intercept shows the estimated size of the releasable pool (Elmqvist and Quastel, 1965). These calculations have previously been used to reliably quantify OSN P*r* (Vaaga and Westbrook, 2017).

OSN-evoked spiking properties

For quantification of OSN-evoked on-cell spikes, using a custom-written MATLAB script (C. Hahn and M. Grubb), spikes were counted automatically, based on manually-established upper and lower thresholds for each trace. Spikes were counted during the 10s window before stimulus onset, during the stimulus period, as well as during the recovery period. Spike frequency was normalised by subtracting the measured spike frequency from baseline firing frequency recorded 10s before stimulus onset. Temporal filters were measured by calculating the percentage of spikes that occurred after each stimulus from the total number of spikes throughout the stimulus train (Vaaga and Westbrook, 2017). ISI CV for spontaneously-fired spikes was calculated in the same way as for the intrinsic spiking properties described above.

2.5. Immunohistochemistry on fixed acute slices

Confirming CCK immunoreactivity in patched cells from WT tissue

After ETC recordings were complete, acute slices were fixed in 1% paraformaldehyde (PFA; in 3% sucrose, 60mM PIPES, 25mM HEPES, 5mM EGTA and 1mM $MgCl_2$) overnight and then processed for immunohistochemistry. The position of the cell in the OB was noted during the recording protocol to enable subsequent localisation with confocal microscopy. Free-floating slices were washed with phosphate-buffered saline (PBS) and incubated in 200 µl/well 5% normal goat serum (NGS, Sigma-Aldrich) for blocking, and PBS/Triton/azide (0.25% triton, 0.02% azide, Sigma-Aldrich) for permeabilization, for 6h at room temperature. The slices were incubated with 200 µl/well of a mixture of primary antibody (rabbit IgG anti-CCK, 1:200, Immunostar) diluted in PBS/Triton/azide for two days at 4°C. Slices were washed 5 times for 5 minutes with PBS and then incubated with 200 µl/well of a mixture of appropriate secondary antibodies and streptavidin conjugated to Alexa Fluor 488 (Life Technologies, Alexa Fluor, 1:1000 diluted in PBS/0.25% Triton/0.02% azide , Streptavidin Alexa Fluor 488 conjugate, S32354) for 2h at room temperature. Slices were washed again 5 times for 5 minutes with PBS. The slices were then mounted with Mowiol (Calbiochem) on glass slides (Menzel-Gläser).

Immunolabelling of patched CCK-tdT ETCs for analysis of dendrite morphology

After ETC recordings were complete, acute slices were fixed in 4%PFA (in 3% sucrose, 60mM PIPES, 25mM HEPES, 5mM EGTA, and 1mM $MgCl_2$) for a minimum of 20 minutes and a maximum of 3 hours, before being processed for immunohistochemistry for the characterisation of biocytin-filled patched ETCs. The position of the cell in the OB was noted during the recording protocol to enable subsequent localisation with confocal microscopy. Free-floating slices were

washed with PBS 3 times for 5 minutes and stored in PBS + 0.02% azide until the commencement of the staining protocol. Immunohistochemistry and subsequent imaging and tracing of neurons were exclusively performed by Catherine Cunningham under C. Hahn's and M. Grubb's supervision. Free-floating slices were washed in PBS 5 times for 10 minutes and then incubated for 2 hours at room temperature in a PBS solution containing 2% NGS, 0.025% triton and streptavidin Alexa Fluor 633 conjugate (1:1000, Life Technologies), which binds to the biocytin located in the patched cells. After this, slices were incubated overnight at 4ºC. Following the incubation period, slices were washed in PBS 8 times for 10 minutes and then mounted with Mowiol on glass slides.

2.6. Immunohistochemistry on slices obtained from transcardially fixed animals

Mice were anaesthetised with an overdose of pentobarbital delivered with intraperitoneal injection. Mice were then transcardially perfused with 20mL PBS containing heparin (Alfa Aesar; 20 units/mL^{-1}) to prevent blood coagulation and clear blood from the blood vessels. This was followed by transcardial perfusion with 20mL of 1% or 4% PFA. The OBs were then dissected and post-fixed for either 2 days in the case of 1% PFA perfusion, or 1 day in the case of 4% PFA perfusion. OBs were embedded in 5-8% agarose and sliced coronally at 50µm using a vibratome (VT1000S, Leica).

Labelling of axon initial segments (AIS)

Free-floating slices that were fixed in 1% PFA were washed 3 times for 5 minutes in PBS and were then incubated for 2 hours at room temperature in 200µl/well in a PBS-based blocking and permeabilising solution containing 5% NGS, 0.25% triton, and 0.02% azide. Following this, slices were incubated with 200µl/well of a mixture of primary antibodies diluted in a PBS solution containing 5% NGS, 0.25% triton, and 0.02% azide for two days at 4°C. The primary antibodies used were: mouse IgG2a anti-Ankyrin-G (1:500, NeuroMab, monoclonal clone N106/36), and rabbit IgG anti-CCK (1:200) in WT tissue. Following primary antibody incubation, slices were washed 5 times for 5 minutes with PBS and then incubated for 2-3 hours at room temperature with 200µl/well species-appropriate secondary antibodies diluted in a PBS solution containing 5% NGS, 0.25% triton, and 0.02% azide (Alexa Fluor-conjugated, 1:1000, Life Technologies). After this incubation period, slices were washed 3 times for 5 minutes with PBS and mounted on glass slides with Mowiol.

Staining for expression of relevant markers

2-4 4% PFA-fixed OBs were co-embedded in agarose before slicing, to produce slices that could be co-stained to form part of one experimental set that was labelled under exactly the same conditions to normalise our comparison of fluorescence intensities upon further analysis. Agarose blocks were cut into different shapes in order to identify which OB belonged to which animal post-hoc. The co-stained sets always included at least one control sample.

For CCK labelling in CCK-tdT tissue, slices were stained for CCK with the same protocol used for AIS labelling. The staining and subsequent image analysis for glomerular VGLUT1 and VGLUT2 expression was performed by Ebrahim Bakhtar under C. Hahn's and M. Grubb's supervision. Slices were incubated in a PBS solution containing 10% NGS, 0.25% triton and 0.02% azide for 2 hours at room temperature. Slices were then incubated with 250µl/well of a mixture containing primary antibody diluted in PBS containing 10% NGS, 0.25% triton, and 0.02% azide for 2 days at 4ºC. The primary antibodies used were: rabbit IgG anti-VGLUT1 (1:500, Synaptic Systems) and rabbit IgG anti-VGLUT2 (1:500, Synaptic Systems, UK). Following this incubation period, slices were washed 3 times for 5 minutes in PBS, and were then incubated with 250µl/well of the species-appropriate secondary antibody diluted in PBS containing 10% NGS, 0.25% triton, and 0.02% azide (Alexa Fluor-conjugated, 1:1000, Life Technologies) for 4 hours at room temperature. Slices were then washed with PBS 3 times for 5 minutes, after which they were incubated with 2 drops/mL of the nuclear marker NucRed (ThermoFisher, UK) for 20 minutes at room temperature. Slices were then mounted on glass slides with Mowiol.

For staining of Arc, c-Fos, EGR1, and NFAT, CCK-tdT OB slices were incubated in a PBS solution containing 10% NGS, 0.25% triton and 0.02% azide for 5 hours at room temperature. Slices were then incubated with 250µl/well of a mixture containing primary antibody antibody diluted in PBS containing 10% NGS, 0.25% triton, and 0.02% azide for 2 days at 4ºC. The primary antibodies used were: mouse IgG2a ant-Arc (C-7) (1:200, Santa Cruz Biotechnology, monoclonal), rabbit IgG anti-EGR1 (1:200, Santa Cruz Biotechnology), rabbit IgG anti-NFATC4 (1:500, Santa Cruz Biotechnology), and mouse IgG anti-c-Fos (1:500, Santa Cruz Biotechnology). Following this incubation period, slices were washed with PBS 3 times for 5 minutes before being incubated for 2 hours at room temperature with 250µl/well of species-appropriate secondary antibody diluted in PBS containing 10% NGS, 0.25% triton, and 0.02% azide (Alexa Fluor-conjugated, 1:1000, Life Technologies). Slices were then washed for 5 minutes 3 times in PBS and then mounted on glass slides with Mowiol. For successful Arc staining, antigen retrieval was performed before blocking and permeabilization by incubating slices in 10mM sodium citrate (pH 6) for 20 minutes before being transferred to the NGS-containing blocking solution. Due to the heating step, the agarose around OB slices melted and it was not possible to distinguish

which OB belonged to which treatment condition. For this reason, the heating temperature and time left in these conditions was varied to optimise this protocol in order to minimise agarose melting. We further placed some trials into the fridge after heat treatment to re-solidify partially melted agarose. Nevertheless, upon further attempts using antigen retrieval, as well as standard immunohistochemical protocols as performed for EGR1, c-Fos and NFAT staining, and even with repetition of the exact same protocol as performed initially, we could not observe suitable Arc staining (see chapter 3).

2.7. Imaging

The tissue was imaged with a laser scanning confocal microscope (Zeiss LSM 710) using appropriate excitation and emission filters, a pinhole of 1 AU and a 40x oil immersion objective. Laser intensity and gain were set manually to avoid signal saturation in AIS, VGLUT1, and VGLUT2 signals. For imaging of Streptavidin signal, laser intensity and gain were set to saturate the signal to allow for clear observation of even small and thin processes.

Imaging CCK label in patched cells

Patched cells from a WT background were found by looking for cells clearly expressing Alexa 488, and by checking that that particular cell corresponded with the location of the recorded cell (noted by the experimenter during the recording experiment). Images were taken in z-stacks of 0.45µm steps and inspected on orthogonal projections to clearly observe co-label of the filled cell with CCK staining.

Imaging CCK-tdT ETCs for morphological analysis

To locate patched and Alexa-filled ETCs, a 10x water-immersion objective was used. Once found, ETCs were imaged with a 40x oil immersion objective. Images were taken with 3x zoom, 1024x1024 pixels (0.07µm/pixel) and in z-stacks with 0.58µm steps. Overlapping tile-stacks including cell soma, primary dendrite, and dendritic tuft were imported into ImageJ and stitched together to create a whole-cell stack using the Grid/Collection Stitching plugin (Schindelin et al., 2015; Preibisch et al., 2009). Manual neuron reconstruction in Fiji (ImageJ) using the Simple Neurite Tracer plugin (Schindelin et al., 2012; Longair et al., 2011) was performed in 3 dimensions. Cells were excluded that portrayed incomplete filling, cut-off dendrites, or inadequate signal-to-noise. Primary dendrite length was obtained directly from individual patch reconstruction, where the segment was defined as ending at the first branch point of the dendrite. The reconstructed images were further used for Sholl analysis using the Fiji plugin Sholl Analysis (Ferreira et al., 2014). The centre of analysis was placed at the first branch point of the

primary dendrite. Analysis only included dendrites within the tuft. The radius step size between concentric spheres was set to 2µm. Sholl profiles were imported into MATLAB for calculating area under the curve using custom code (Garcia-Segura and Perez-Marquez, 2014).

Imaging AISs

Imaging and subsequent analysis were performed blind to experimental group. Laser intensity and gain were set to permit clear delineation of the axon using the CCK label in WT tissue, or the endogenous tdT label in CCK-tdT tissue. To ensure AISs belonged to a particular soma, the experimenter visually observed whether the Ankyrin-G label clearly co-localised with the CCK or tdT labelled axon projecting from that particular cell. Images were taken in z-stacks (0.45µm steps) with 3x zoom, 512x512 pixels (0.138µm/pixel). AIS lengths and distances from the soma were quantified using ImageJ with the 5d viewer plugin (ImageJ plugin, Heintzmann, 2010) for 3D analysis, and using a custom-written MATLAB script to quantify the ImageJ values (M. Evans). The axon start was determined as the first point after the clear end-point of the soma, defined by the perimeter of the CCK or tdT signal of a cell. The AIS start was defined as the first point where the Ankyrin-G signal began, and the AIS end point was defined as the proximally last point of the Ankyrin-G signal that was clearly in continuation from the first point.

Imaging CCK staining to confirm co-localisation of CCK with tdT+ cells in CCK-tdT tissue

Single-plane images of both the tdT signal channel and CCK signal channel were taken with 0.7x zoom, 1024x1025 pixels (0.296µm/pixel). Images were exported into ImageJ and co-localisation of tdT and CCK signals was manually counted using Cell Counter. Counting was performed by first placing different style cell counters onto either tdT+ or CCK+ cells in separate channels. This gave a total count of tdT+ and CCK+ cells. Then, signal channels were merged into a composite RGB image for co-localisation counting. A separate style of cell counters was placed on cells that had both tdT and CCK counters placed on them in the initial separate-channel counting. This then gave a count of how many cells were both tdT+ and CCK+.

Imaging VGLUT1 and VGLUT2 staining

The experimenter was blind to the treatment slices belonged to during imaging and subsequent analysis. Two slices from each animal were imaged. Before image acquisition, glomeruli located in several different regions of each slice in an experimental set were scanned in the VGLUT signal channel in order to set the laser intensity and gain manually to avoid signal saturation. The same

laser intensity and gain were then used for imaging the entire set to produce comparable fluorescence intensity values. All imaging was performed on the top 10µm of the tissue to avoid inconsistency in brightness due to antibody penetration variations. Single-plane images were taken with 1.5x zoom, 512x512 pixels (0.278µm/pixel). Glomeruli were clearly identifiable by the NucRed signal, as nuclei are scattered around individual glomeruli. We thus first identified glomeruli in the NucRed signal channel, before taking the image with both VGLUT and NucRed signal channels. This was to avoid bias towards picking specific regions in the VGLUT signal channel. Images were exported into ImageJ to measure fluorescence intensities. In the NucRed signal channel, glomeruli were manually outlined, and fluorescence intensities of those regions were measured in the VGLUT signal channels. 3 small squares were manually defined in areas of low fluorescence intensity around glomeruli and their intensities were noted. These values were used for background subtraction from the VGLUT fluorescence intensity values. Fluorescence intensities of both control and occluded samples in an experimental set were further normalised to the mean fluorescence intensity of control samples in the set.

Imaging cell-activity markers

Single-plane images were taken with 1x zoom, 512x512 pixels (0.415µm/pixel). Images were exported in ImageJ and visually inspected for CCK and activity marker co-localisation.

2.8. Statistical analysis

Statistical analysis was carried out using Prism (GraphPad), MATLAB or SPSS (IBM). All values are represented as mean ± SEM and α-values were set to 0.05 unless using Bonferroni correction (indicated in the text), in which case α was divided by the number of comparisons. All comparisons were two-tailed. Data sets were assessed for normality with the D'Agostino and Pearson omnibus test, and sometimes additionally with a custom-written script in MATLAB (M. Grubb) that calculates the percentage variance of a given distribution accounted for by a best-fit Gaussian function (data accepted for parametric analyses if >90% of variance was explained by a Gaussian fit). Data were then analysed using parametric or non-parametric tests accordingly. Some datasets were square-root (sqrt) or $\log_{10}$ transformed to render normality, as mentioned in the text.

Details regarding the specific statistical test carried out on specific data sets are indicated in the results sections. Broadly, pairwise group comparisons were performed using unpaired t-tests. If variances between the data sets differed significantly, Welch's correction was applied. If data were not normally distributed, Mann-Whitney U tests were used instead of unpaired t-tests.

Repeated measures were analysed using mixed model analysis as indicated in the text. For group comparisons taking into account genotype or cell type, and analysis of Sholl profiles, two-way ANOVAs were performed. For these comparisons, we checked whether variances between the data sets did not differ significantly using Lavene's Test of Equality of Error Variances in SPSS. None of the compared groups displayed differences in their variances. To compare the mean one-phase decay fits across data sets quantifying OSN-evoked spiking frequency and temporal filter, *k* parameters of the fits were compared with an extra sum of squares *F*-test. All data sets analysed for correlations were normally distributed and were thus analysed using Pearson's correlations. For comparing VGLUT fluorescence intensity, we wanted to account for the variability across values obtained from different experimental sets. We thus employed multilevel analysis where normalised fluorescence values were compared using linear mixed models (SPSS) with experimental set as the subject variable (Aarts et al., 2014).

Chapter 3

External tufted cells do not adjust their intrinsic excitability or gross morphological properties with short-term sensory deprivation

3. 1. Introduction

The activity of various JGCs of the OB is heavily involved in modulating incoming odour information at a glomerulus (Mori et al., 1999). Due to the nature of the olfactory world,

incoming odour information is highly heterogenous. How can odour information be coherently transmitted to olfactory cortex if there are constant changes in incoming information? Overall, OB responses can alter in response to changes in incoming odour input, however at the cellular level, plastic changes in the face of sensory manipulation have almost always been reported in the inhibitory interneuron populations either in the GL (Baker, 1990; Kosaka et al., 1987; Livneh et al., 2014) or in the GCL (Dahlen et al., 2011; Saghatelyan et al., 2005) (see chapter 1, Introduction).

Interestingly, evidence for activity-dependent plasticity in the excitatory interneuron population is lacking. ETCs are principal excitatory glutamatergic interneurons that are located deep in the GL, close to the EPL. These cells protrude a single dendritic "tuft" into a glomerulus through which they receive monosynaptic input from OSN axon terminals. ETC axons project to isofunctional odour columns, meaning that they connect glomeruli that process information received from the same olfactory receptor type (Lodovichi et al., 2003). Furthermore, ETCs drive the glomerular inhibitory network via dendro-dendritic communication. ETCs provide excitatory monosynaptic input onto JGCs, causing subsequent feedback inhibition (Hayar et al., 2004a). Most crucially, most of the direct, excitatory transfer of information from OSNs to M/TCs is now thought to be routed through ETCs (De Saint Jan et al., 2009; Gire et al., 2018; Zhou and Belluscio, 2008). Due to these properties, ETCs are therefore major modulators of odour input reaching M/TCs. Morphologically, ETCs are known to be able to change their axon targeting specificity in response to a long-term deficit of sensory experience (Cummings et al., 2014), however little is known about their ability to change their functional intrinsic and synaptic properties in the face of changing input information.

Since ETCs are a key player in determining glomerular output, the capability of these cells to undergo activity-dependent plasticity could hold great potential in adapting glomerular processes in response to a changed odour input. In this chapter, we aimed to explore whether ETCs change any of their intrinsic properties in an activity-dependent manner. To investigate this, we used 24h unilateral naris occlusion to induce odour deprivation in juvenile mice in order to compare ETC properties in these conditions to control conditions. Activity-dependent plasticity can come in several broad forms, which we wished to explore. Plastic changes at the intrinsic level can occur morphologically (Dahlen et al., 2011, Chand et al., 2015; Grubb and Burrone, 2010) and/or functionally (Aizenman and Linden, 2000; Saghatelyan et al., 2005; Turrigiano et al., 1998), so we explored both using immunohistochemical and electrophysiological approaches in *ex vivo* tissue.

3.2. Results

3.2.1. Targeting and identifying ETCs in acute slices

To identify ETCs in acute slices in WT OBs, a series of published criteria were used (**Fig 1**). First, ETCs are found in the deep area of the GL, very close to the bordering EPL (**Fig 1 Ai**). Second, these cells have a characteristic balloon-shaped soma of around 10µm in diameter, and are mostly the only cell type of that size in that area. Furthermore, ETCs portray a prominent apical dendrite resembling a tuft, that ramifies into a single glomerulus (Hayar, Karnup et al., 2004; Liu and Shipley, 2008) (**Fig 1 Aii**). We targeted cells in the deep GL, and patched ETCs in WT tissue that visibly had a balloon shaped soma and tufted apical dendrite, visualised with Alexa 488 dye that filled the cell during whole-cell recordings. All targeted cells considered ETCs portrayed these morphological characteristics. Once cells of the correct morphology and location were recorded in the whole-cell configuration, ETC identity was additionally defined by a number of physiological characteristics consisting of spontaneous burst firing (**Fig 1 Bi**), a hyperpolarising sag potential (indicative of I_h current) (**Fig 1 Bii**), and a resting membrane potential (Vm) of ~ -55mV (Liu and Shipley, 2008). We accepted cells that satisfied most of these criteria. Cells always needed to be located in the deep GL and portray an apical tuft. Not all populations of ETCs burst-fire spontaneously (Antal et al., 2006), so if cells did not exhibit this property but satisfied all other criteria, they were accepted as ETCs. We further allowed for a high range of resting membrane potential (-40mV to -70mV) as this property could potentially change with occlusion and has also been described previously as being heterogeneous due to the heterogeneity of the ETC population (Antal et al., 2006; Liu and Shipley, 2008). Additionally, not all cells portrayed a sag potential, consistent with previous findings (Antal et al., 2006), however if they fired spontaneously and met the morphological criteria, we considered them as ETCs. For final confirmation of ETC identity in a subset of recorded neurons, cells were filled with byocitin, and then were fixed and stained for the ETC marker CCK (Cheetham et al., 2015; Nagayama et al., 2014) (**Fig 1C**) and Streptavidin. In total, 20 previously patched cells were found using confocal microscopy, of which 18 were clearly CCK+. For the remainder of the found cells, it was unclear whether they were CCK+ due to the sub-optimal CCK label – this is a common problem with CCK antibodies (O. Marin, personal communication). Taking all of these measures of identification into account, we can be confident that the cells patched in WT tissue are truly ETCs.

As a further indicator of ETC identity, CCK-IRES-Cre mice (Taniguchi et al., 2011) were crossed with a floxed tdTomato (tdT) reporter line (Madisen et al., 2009) producing offspring that theoretically have all CCK+ cells labelled with tdT. Using these CCK-IRES-Cre/Rosa-tdT mice (CCK-

tdT) would therefore allow us to identify ETCs in acute slices by this label, both confirming our ability to accurately target ETCs in WT tissue, and simplifying the approach for ETC identification in acute slices. CCK is a non-specific marker of ETCs, as superficial tufted cells and some deep short axon cells also express CCK (Seroogy et al., 1985). Thus, we still used location (**Fig 1 Ai**, right) in the GL as a criterion for selecting tdT+ cells to patch. We also filled these cells with Alexa (488) during patch experiments to confirm morphological identification (**Fig 1 Aii**, right). Cell shape could be easily seen; however, due to high background fluorescence of other tdT+ cells it was difficult to observe characteristic tuft morphology in these slices. A total of 38 quality control-passing ETCs were patched from 8 CCK-tdT animals in order to compare intrinsic properties of these cells with those acquired during WT recordings (**Table 1**). From these recordings, it was evident that identified tdT+ ETCs also fired spontaneously (**Fig 1B i,** right), and displayed a characteristic sag potential (**Fig 1 Bii**, right). Immunohistochemistry on 50µm olfactory bulb slices from CCK-tdT mice at P24 revealed that many tdT+ cells co-localise with immunohistochemical CCK label at the edge of the GL close to the EPL where ETCs are targeted in acute slices (**Fig 1 C**, right). However, tdT+ cells also appear on the superficial edge of the GL close to where the OSN axons meet the glomeruli, as well as throughout the mitral cell layer and scattered across the EPL (data not shown). Quantification of CCK-tdT co-localisation revealed that in the deep GL where we would normally target ETCs, 52% of tdT+ cells were also CCK+ (n=6 glomeruli, N=2, data not shown). The high number of tdT+ cells that were not CCK+ (48%) could be attributed to the sub-optimal label the CCK antibody produced. Furthermore, some cells may have expressed CCK during development, thus activating the *Cre* recombinase permanently. Therefore, CCK-tdT mice may not be useful for selectively targeting ETCs.

Regardless of the non-specificity towards ETCs in this transgenic mouse-line, we further patched 36 WT and 38 CCK-tdT putative ETCs to quantitatively compare their properties. All patched CCK-tdT ETCs presented with intrinsic functional properties that closely resembled these properties in WT ETCs (**Table 1**). A few significant differences between the two groups were observed, however. First, the series resistance (Rs) of the recordings was lower in the WT data compared to CCK-tdT data. (WT ETC: mean ± SEM 11.55 ± 0.64MΩ *n=33*; CCK-tdT ETC: 19.27 ± 0.64 MΩ *n=38*; *unpaired t-test*, $p<0.001$). There is a technical explanation for this difference: the electrophysiological recording set-up was relocated between WT and CCK-tdT recordings, thus this difference possibly arises due to lack of experimenter familiarity at the new set-up location. We also observed a significantly lower membrane capacitance (Cm) in CCK-tdT ETCs. This difference may arise due to the way Cm was calculated, as it was estimated from the area under the curve during test-pulses that were used to calculate Rs. Thus a change in Rs will give rise to a change in the estimate of Cm. Indeed, when correlating Rs with Cm, both in WT and CCK-tdT

ETCs a lower Cm significantly correlated with higher Rs (WT: *Pearson's correlation coefficient*, r^2 = 0.19, p=0.02; CCK-tdT: *Pearson's correlation coefficient*, r^2 = 0.46, p<0.0001, data not shown). Two more functional properties differed between WT and CCK-tdT ETCs. CCK-tdT ETCs had a slightly lower resting membrane potential (Vm) compared to their WT counterparts. Furthermore, CCK-tdT ETCs had a slightly lower after-hyperpolarisation potential (AHP), compared to WT ETCs (Vm: WT ETC mean ± SEM -57.33 ± 0.92mV, *n=36*; CCK-tdT 53.48 ± 1.23mV, *n=33*; *unpaired t-test*, p=0.01; Cm: WT ETC mean ± SEM 45.08 ± 2.30pF, *n=33*; CCK-tdT ETC 38.00 ± 2.11pF, *n=38*; *unpaired t-test*, p=0.03; AHP: WT ETC mean ± SEM -52.04 ± 0.45mV, *n=23*; CCK-tdT ETC: -49.64 ± 0.49mV, *n=24*; *unpaired t-test*, p=0.0008). Nevertheless, ETCs identified in WT and CCK-tdT slices possessed extremely similar overall functional properties (**Table 1)**. The population of ETCs is highly heterogenous (Macrides and Schneider, 1982) thus the differences in AHP and Vm likely reflect a slightly more homogeneous group of ETCs patched in CCK-tdT animals as opposed to WT animals. Thus, histochemical and functional findings indicate that CCK-tdT mice could potentially be useful when looking for ETCs in acute slices, provided the search is performed in the correct GL area.

The functional results in this chapter exclusively stem from ETCs patched in WT tissue, as we have confirmed that they can be reliably targeted in acute slices. As noted where appropriate, some histochemical and all dendrite morphological analyses were performed on ETCs identified in CCK-tdT tissue.

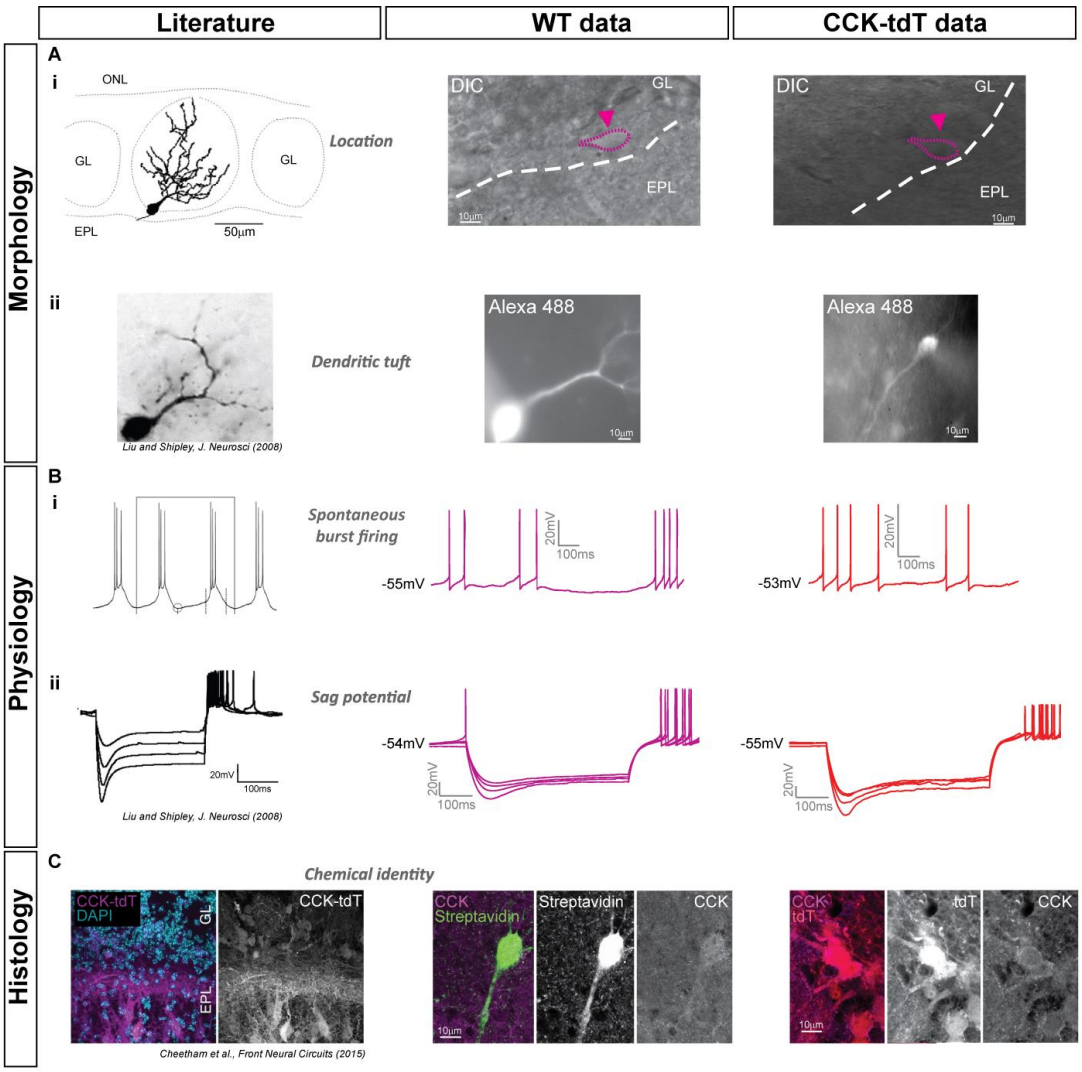

Fig 1. Live targeting and post-hoc identification of external tufted cells (ETCs).

(**A**) ETCs are found at the deeper half of the glomerular layer (GL), close to the external plexiform layer (EPL), and display a characteristic apical dendritic tuft. (**Ai**) Published results on ETC location in the GL, followed by example bright-field images of ETCs (magenta triangle) found in WT tissue (middle) and CCK-tdT tissue (right). (**Aii**) Published results on ETC morphology portraying a balloon-shaped soma and dendritic tuft. Middle and right: Alexa488-filled ETCs in WT (middle) and CCK-tdT (right) tissue corresponding with published data. Dendrite morphology in the CCK-tdT ETC is difficult to distinguish due to background fluorescence from other tdT+ cells. (**B**) Electrophysiological properties of ETCs. (**Bi**) Published data highlight characteristic bursting spontaneous firing (left), which is matched with our recordings in WT (middle) and CCK-tdT (right) tissue. (**Bii**) Published data highlight characteristic hyperpolarising sag potential (left), which is matched with our recordings in WT (middle) and CCK-tdT (right) tissue. (**C**) Published data show ETCs express cholecystokinin (CCK) (left). In the middle is a patched cell that fulfilled the above functional criteria for ETC identification, filled with Alexa and biocytin and fixed for post-hoc CCK labelling to confirm ETC identity. On the right, CCK-tdT tissue has been labelled with CCK to show that tdT+ cells express CCK.

	WT	CCK-tdT			
Property	**Mean ± SEM, N**	**Mean ± SEM, N**	**p-value**	**Statistical test**	**Significance**
Passive properties					
Rs (MΩ)	11.55 ± 0.64, N=33	19.27 ± 0.64, N=38	< 0.0001	unpaired t-test	***
Holding I (pA)	-1.53 ± 5.01, N=31	-28.2 ± 10.30, N=31	0.112	Mann-W hitney test	n.s.
Rm (MΩ)	246.1 ± 21.83, N=33	296.8 ± 31.63, N=38	0.584	Mann-W hitney test	n.s.
Vm (mV)	-57.33 ± 0.92, N=36	-53.48 ± 1.23, N=33	0.0147	unpaired t-test	*
Cm (pF)	45.08 ± 2.30, N=33	38.00 ± 2.11, N=38	0.026	unpaired t-test	*
First spike properties					
Vthresh (mV)	-36.64 ± 0.84, N=23	-36.09 ± 0.74, N=24	0.6238	unpaired t-test	n.s.
Vmax (mV)	19.02 ± 1.35, N=23	19.44 ± 1.03, N=24	0.8017	unpaired t-test	n.s.
First spike delay (ms)	187.3 ± 23.36, N=23	223.2 ± 26.60, N=24	0.3177	unpaired t-test	n.s.
WHH (ms)	0.6783 ± 0.03, N=23	0.7229 ± 0.03, N=24	0.1043	Mann-W hitney test	n.s.
AHP (mV)	-52.04 ± 0.45, N=23	-49.64 ± 0.49, N=24	0.0008	unpaired t-test	***
Rel. AHP (mV)	15.41 ± 0.85, N=23	13.56 ± 0.82, N=24	0.1247	unpaired t-test	n.s.
Max dV/dt (mV/ms)	142.3 ± 7.98, N=23	143.4 ± 5.26, N=24	0.7096	Mann-W hitney test	n.s.
Multiple spiking properties					
Max. spike number	61.23 ± 4.39, N=30	73.46 ± 4.51, N=24	0.0597	unpaired t-test	n.s.
ISI CV	0.3281 ± 0.04, N=30	0.34 ± 0.05, N=24	0.6698	Mann-W hitney test	n.s.

Table 1. WT and CCK-tdT external tufted cells (ETCs) differ in some of their intrinsic properties.

Table shows statistical results from patched ETC data in WT and CCK-tdT animals, showing passive properties, first spike properties, and multiple spiking properties. Rs=series resistance, HoldingI=holding current, Rm=membrane resistance, Vm=membane potential, Cm=membrane capacitance, Vthresh=Voltage threshold for action potential, Vmax=maxium voltage, WHH=width at half height, AHP=after hyperpolarising potential, Rel. AHP= relative AHP, MaxdVdt=peak rate of rise, Max. spike number=maximum spike number, CV=coefficient of variation of inter-spike intervals (ISI) . *, $p<0.05$, ***, $p<0.001$.

3.2.2. Using naris occlusion (24 hours) to investigate ETC activity-dependent plasticity

Naris occlusion has been used extensively to drive activity-dependent changes in the OB (Coppola, 2012). This manipulation is usually employed on a longer time-frame, however preliminary data from our laboratory indicate that plastic changes can occur with short-term, 24h, sensory deprivation (D. Byrne, E. Galliano, C. Hahn, unpublished data). In our experiments, we occluded juvenile mice (P20-P35) for 24 hours using a custom-made plug that is inserted into one nostril (see Methods, chapter 2). For our control conditions, control animals were either left unperturbed, or received a sham occlusion where the occlusion plug was briefly inserted into one nostril and immediately taken out again (**Fig 2A**). In this chapter, all occluded animals were compared to unperturbed control animals

Following occlusion, OBs were extracted for acute slicing, or mice were intracardially perfused with PFA for subsequent histochemical analysis of fixed OBs (**Fig 2B**). ETCs were identified in acute OB slices and patched to compare intrinsic and synaptic properties (**Fig 2 Ci**). Confocal microscopy was used to image fixed OB slices labelled with various markers (**Fig 2Cii**).

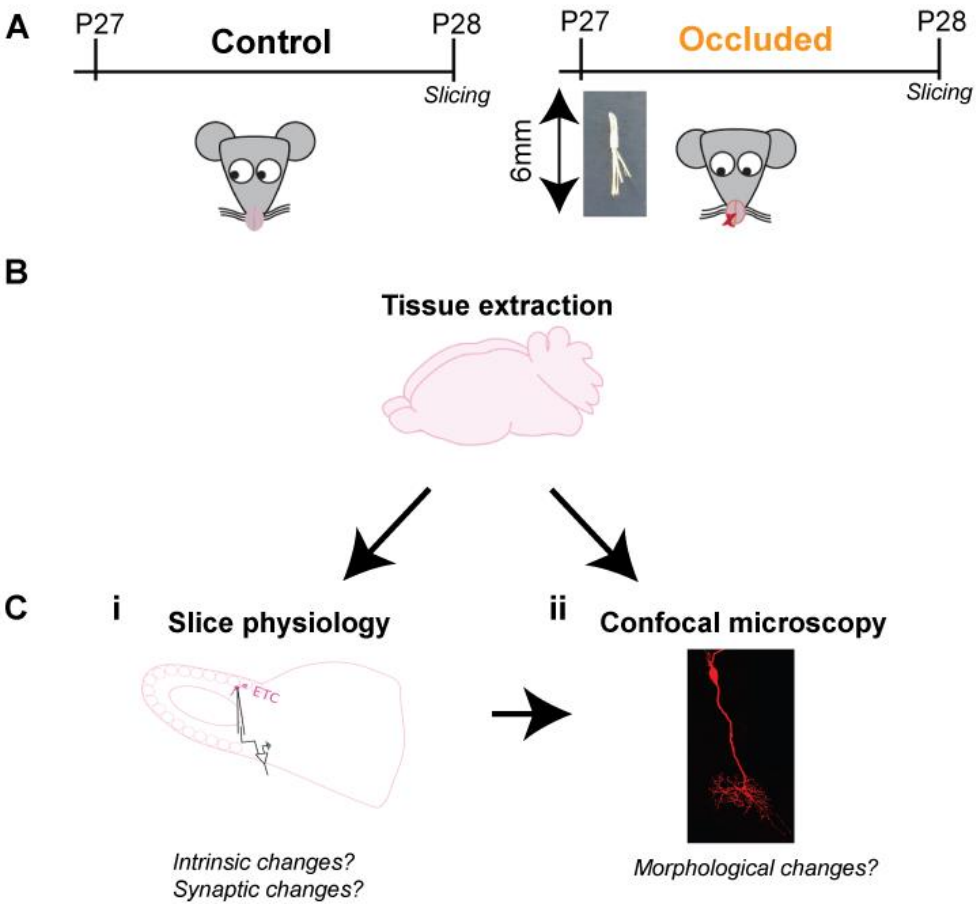

Fig 2. Experimental design to compare external tufted cells (ETCs) functionally and morphologically in control versus occluded mice.

(**A**) Mice, aged between P20-P35, were either occluded with a custom-made plug inserted into one naris or left unperturbed. (**B**) Olfactory bulbs were either acutely sliced, or fixed via transcadial perfusion with either 1 or 4% PFA. (**C**) Comparing control vs occluded ETC functional properties and morphological properties. (**Ci**) Acute slices were made in order to use patch physiology for functional characterisation. (**Cii**) Fixed slices (either fixed acute slices or slices from PFA-perfused animals) were labelled with antibodies to compare morphological features via confocal microscopy.

3.2.3. We could not identify reliable activity-dependent markers of ETC activity

Preliminary data have shown that 24h naris occlusion causes expression changes in the immediate early gene (IEG) c-Fos, where c-Fos immunoreactivity markedly decreased in GABA/dopaminergic JGCs (D. Byrne and E. Galliano, unpublished data). c-Fos immunoreactivity has been used extensively to observe activity changes in different types of neurons (Schilling et al., 1991). For example, c-Fos was expressed by cells that were active *in vivo* and not by inactive cells in the monocular visual cortex after enucleation (Barnes et al., 2015). Thus, our first exploration of ETC activity-dependent plasticity involved the quantification of ETC c-Fos expression in control and occluded conditions. For this, we employed immunohistochemical labelling with a c-Fos antibody, and confocal imaging of OB glomeruli in CCK-tdT mice, where most tdT+ cells in the deeper GL should represent ETCs. However, ETCs do not appear to express c-Fos, or at least not at detectable levels in our hands under these conditions (**Fig 3A**).

We thus strove to find a more appropriate activity-dependent marker that is expressed in at least some ETCs under control conditions. We first began our trials with Arc immunolabelling. Arc is a known activity-dependent IEG that has been shown to change expression levels in the GL in mice that were exposed to amyl acetate, a non-biological odorant (Bepari et al., 2012). Indeed, we were able to replicate this labelling, and clear co-localisation with CCK-tdT was evident in some cells (**Fig 3B**). Unfortunately, this successful labelling was never reproduced after the first time, despite extensive efforts to replicate, and then systematically vary, the staining protocols used. We thus continued our marker hunt and trialled another activity-dependent IEG known to change expression levels in the GL, EGR1 (Bepari et al., 2012). Though EGR1 expression did appear to co-localise with CCK-tdT+ cells (**Fig 3C**), our labelling with this marker unfortunately produced confocal images that were of very poor quality, and thus could not be used for the thorough semi-quantitative analysis we wished to perform. A further marker we chose to try was NFAT. This marker is not an IEG; however activity-dependent expression changes in NFAT can result in NFAT translocating to the nucleus, indicating a recent history of cell activity (Masuyama et al., 2012). From our experiments, all tdT+ cells appeared to express NFAT in their cytoplasm, rather than the nucleus (**Fig 3D**), thus we concluded that it was not an appropriate marker for observing activity changes in ETCs in our conditions.

Therefore, we were unable to produce reliable immunohistochemical data showing that ETC activity was reduced with occlusion. Nevertheless, plug occlusion has been a reliable tool for decreasing OB activity in general (Kikuta et al., 2015), and has been specifically shown to be effective in decreasing activity levels in OB glomerular neurons after 24 h (D. Byrne and E.

Galliano, unpublished data), so we continued our comparison of ETC morphological and functional properties after this manipulation.

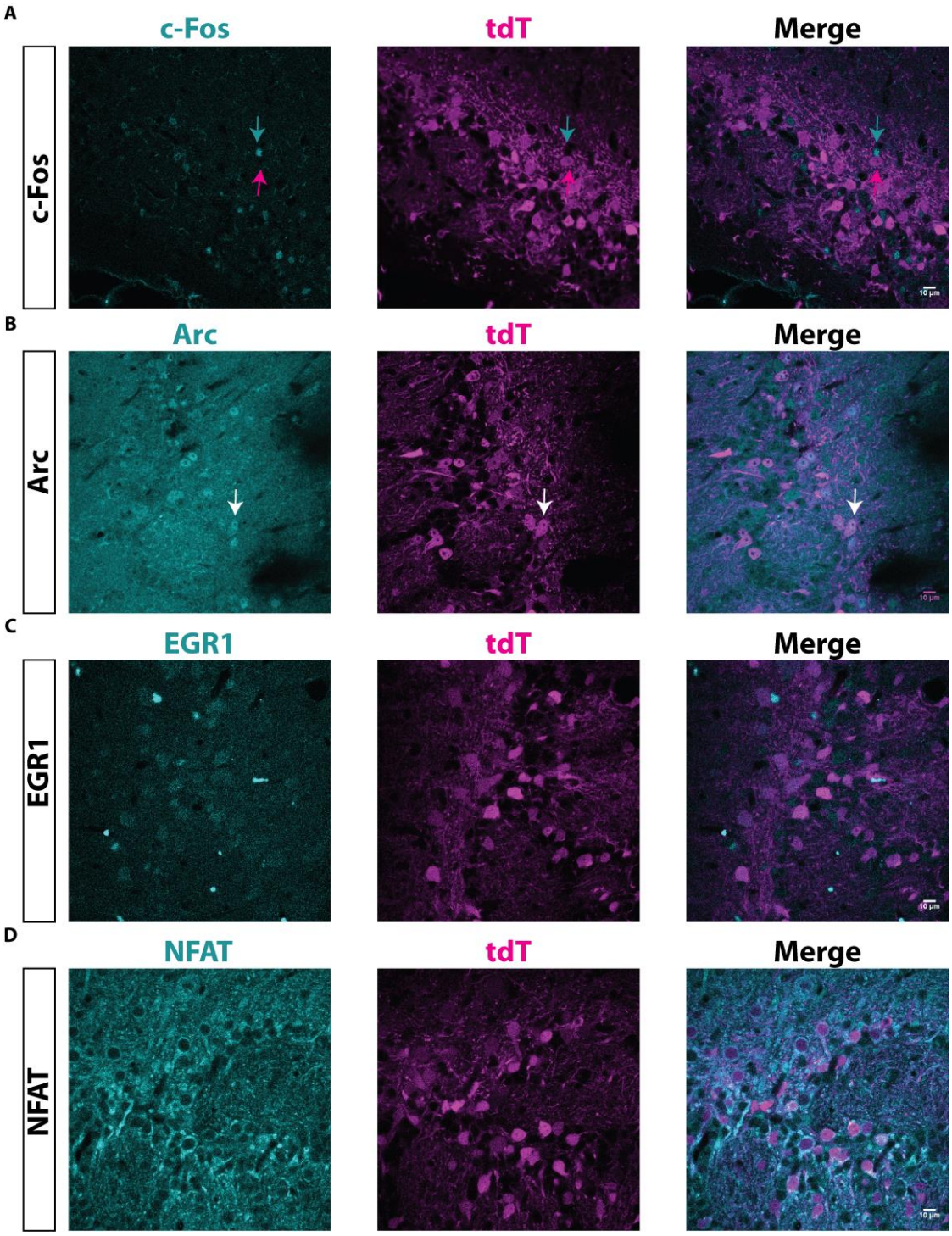
A
c-Fos
tdT
Merge
c-Fos
B
Arc
tdT
Merge
Arc
C
EGR1
tdT
Merge
EGR1
D
NFAT
tdT
Merge
NFAT

Fig 3. Lack of reliable activity-dependent markers in external tufted cells (ETCs).

Single plane example images from CCK-tdT OBs showing co-labelling with various activity-dependent markers. (**A**) c-Fos; the arrow in teal points to a c-Fos+ cell, which does not co-localise with tdT. The arrow in magenta shows a tdT+ cell, which does not co-localise with c-Fos. (**B**) Arc was expressed by tdT+ cells. White arrow points towards example co-localisation of Arc and tdT. Unfortunately, this staining could not be reproduced. (**C**) EGR1 appears to be expressed by some tdT+ cells, but the immunolabelling is not precise enough for quantification. (**D**) NFAT labelling is always restricted to tdT+ cell cytoplasm, thus it is not an appropriate marker for observing activity changes in ETCs.

3.2.4. ETC axon initial segment (AIS) lengths and distance from the soma were not affected by occlusion

We first sought to observe whether ETCs exhibited any activity dependent morphological changes after 24 h occlusion. The AIS is a highly specialised axonal structure formed of a high density of specialised scaffolding molecules and Na^+ channels near the soma of a neuron, and is the site of action-potential generation in most neurons (Grubb and Burrone, 2010b). Due to its properties, it is highly implicated in the modulation of neuronal excitability. The AIS is not necessarily a permanent fixture, as it can change its properties in an activity-dependent manner, often closely correlated with changes in neuronal excitability (Bender and Trussell, 2012; Grubb and Burrone, 2010a; Kaphzan et al., 2011; Kuba et al., 2010). For example, chronic depolarisation of hippocampal cells in culture resulted in a relocation of the AIS to a more distal location from the soma, correlated with decreased excitability in these cells (Grubb and Burrone, 2010a). A similar effect was shown in hippocampal organotypic slices, a preparation where neuronal diversity is more conserved compared to dissociated cells in culture. Chronic depolarisation (48h) of pyramidal neurons in this system induced a relocation of their AISs further from the soma, an effect that resulted in delayed firing upon stimulation (Wefelmeyer et al., 2015). Additionally, adjustments in AIS length have also been shown to correlate with changes in neural activity. For example, a lengthening of the AIS in response to relatively long-term sensory deprivation or neural abnormalities in a mouse model of Angelman syndrome, increased neural excitability (Kaphzan et al., 2011; Kuba et al., 2010). Even short-term manipulations can induce changes in AIS length. Upon 3h of optogenetic stimulation, dissociated cultured dentate granule cells of the hippocampus showed a shortening of AISs that was correlated with decreased excitability (Evans et al., 2015). In the OB, activity-dependent plasticity has previously been shown in dissociated GABA/dopaminergic JGCs. Here, chronic depolarisation resulted in an AIS lengthening as well as relocation closer to the soma (Chand et al., 2015)

Due to the potential functional implications of AIS plasticity, and due to the fact it has been reported previously in the OB, we next wanted to observe whether ETC AISs undergo activity-dependent plasticity. We thus labelled AISs with a known marker, Ankyrin-G (Ank-G) (Jenkins and Bennett, 2001), on ETCs in control and occluded conditions. For this experiment we used both WT and CCK-tdT animals. WT tissue was additionally processed for CCK labelling to identify ETCs. ETCs clearly contained AISs in both control and occluded conditions (**Fig 4A**). AISs were close to the cell somas (~2.5µm) and sparsely distributed in the GL and EPL. They further tended to align in the same direction (away from the superficial GL), thus it was straightforward to

visualise which AIS belonged to which ETC. A total of 76 AISs from 6 WT and 1 CCK-tdT control animals, and 84 AISs from 3 WT and 2 CCK-tdT occluded animals were measured (see methods, chapter 2).

Quantification of AIS lengths revealed that ETCs slightly lengthened their AISs after occlusion, but this effect was not significant. There were no significant differences between WT and CCK-tdT ETC AIS lengths (**Fig 4B**) (WT: control mean ± SEM 18.54 ± 0.38µm; occluded 19.94 ± 0.59µm; CCK-tdT: control mean ± SEM 16.92 ± 1.12µm; occluded 20.63 ± 1.24µm; *two-way mixed models ANOVA*, effect of treatment, $F_{(1,156)}$ = 2.56, p=0.15, effect of genotype, $F_{(1,156)}$ = 0.33, p=0.57, interaction, $F_{(1,156)}$ = 1.36, p=0.26). AISs can also change their distance from the soma (Grubb and Burrone, 2010a; Chand et al., 2015). We thus measured these distances in control and occluded ETCs (**Fig 4C**). Again, occlusion did not have a significant effect on ETC AIS distances from the soma. Furthermore, WT and CCK-tdT ETC AIS distances from the soma did not differ significantly from each other (WT: control mean ± SEM 2.67 ± 0.23µm; occluded 2.50 ± 0.22µm; CCK-tdT: control mean ± SEM 1.60 ± 0.39µm; occluded 3.51 ± 0.40µm; *two-way mixed models ANOVA*, effect of treatment, $F_{(1,156)}$ = 0.01, p=0.92, effect of genotype, $F_{(1,156)}$ = 3.06, p=0.11, interaction, $F_{(1,156)}$ = 4.62, p=0.051).

These results suggest that though ETCs may slightly lengthen their AISs with occlusion, this change is very subtle and does not reach significance. Thus, occlusion does not seem to impact ETC AIS structure.

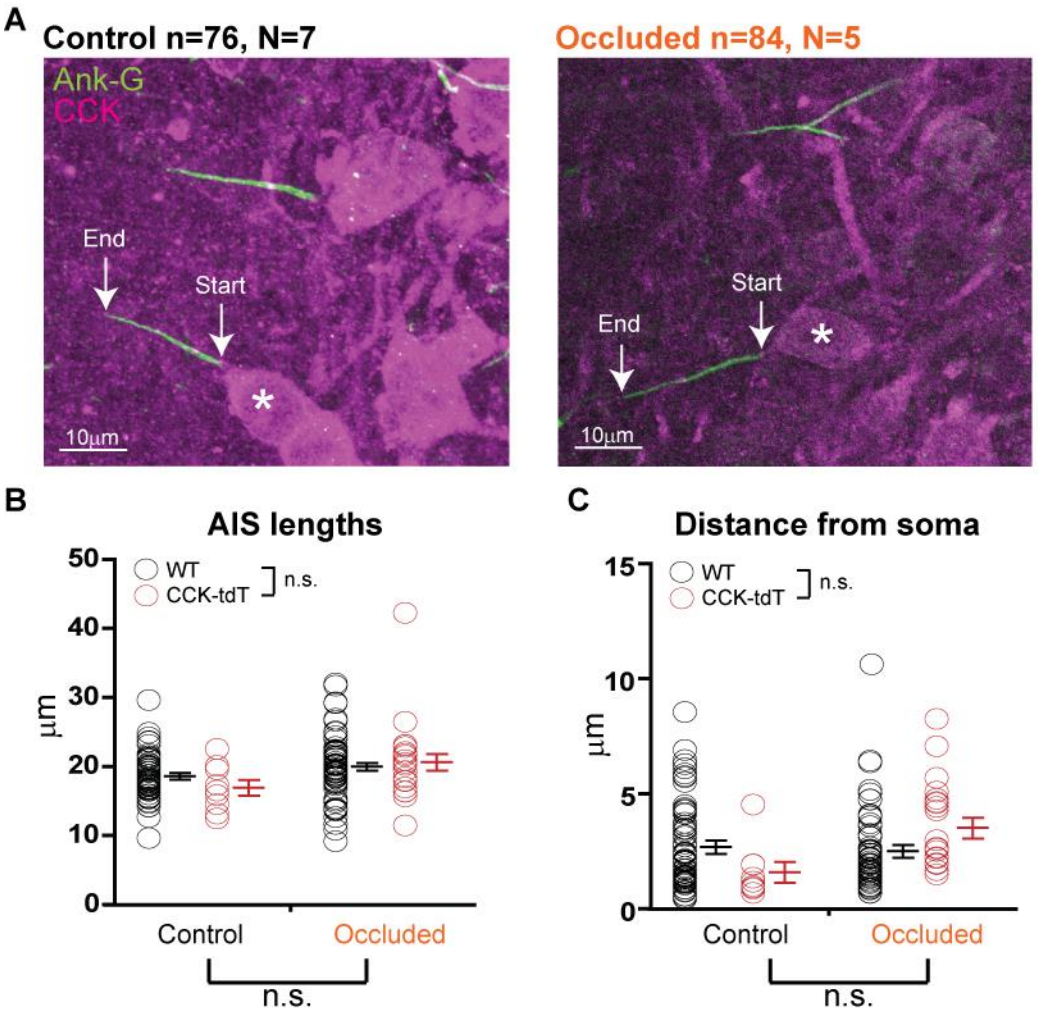

Fig 4. Occlusion does not alter the axon initial segment (AIS) of external tufted cells (ETCs).

(**A**) Confocal single-plane images of control (left) and occluded (right) ETCs, labelled for CCK (magenta) and Ank-G (green), an AIS marker. White arrows show the start and end points of example AISs; asterisks show the cell bodies to which those AISs belong. (**B**) Mean ± SEM AIS length in WT (black) and CCK-tdT (red) animals. Each circle represents one AIS. (**C**) Mean ± SEM AIS distance from the soma in WT (black) and CCK-tdT (red) animals. n.s., non-significant.

3.2.5. Occlusion does not impact ETC primary dendrite morphology

In previous reports, it has been shown that ETCs can change their axonal targeting in an activity-dependent manner, where sensory deprivation caused an expansion in ETC axonal target specificity (Cummings et al., 2014). Dendrite morphology can also be adjusted in an activity-dependent manner. For example, GC dendritic branching and spine number can decrease upon short-term (48h) sensory deprivation (Dahlen et al., 2011). Since dendro-dendritic transmission between ETC primary dendrites and other JGCs as well as M/TCs has been extensively shown to modulate OSN input (Gire et al., 2018), we sought to observe whether ETC tuft morphology is impacted by occlusion. We further wished to correlate any morphological changes to functional changes, and thus analysed ETC morphology from electrophysiologically characterised cells.

All data on ETC dendrite morphology were acquired from CCK-tdT animals. In total, 10 control and 4 occluded patched and byocitin-filled ETCs were fixed and labelled with streptavidin, allowing for the accurate tracing and reconstruction of apical dendrites for morphological analysis (**Fig 5A**). An initial analysis of primary dendrite length and total dendrite length revealed that ETCs, especially in the higher n control group, showed high variability (**Fig 5Bi-ii**), corresponding with previous reports that ETCs are a heterogenous population of cells (Antal et al., 2006; Macrides and Schneider, 1982). No significant differences between control and occluded groups were found (**Fig 5Bi-ii**). There was a slight trend towards ETCs in the occluded group having slightly lower total dendrite length, however this was not significant and the values here fell within control values (Primary dendrite length: control mean ± SEM 97.78 ± 11.20µm; occluded 77.09 ± 17.23µm, *Mann-Whitney test*, p=0.45; total dendrite length: control mean ± SEM 1985.00 ± 183.8µm; occluded 1488.00 ± 84.32µm; *Mann-Whitney test*, p=0.054).

We further performed a Sholl analysis, which provides a measurement for distribution and density of branching (Sholl, 1953). The centre of analysis was placed on the first branch point of dendrites, and analysis only included measures taken from the apical tuft. This placement was chosen as we were interested in glomerular effects of occlusion so we chose to focus our attention on morphological features projecting into a glomerulus rather than axon and lateral dendrite morphology. Additionally, since axons and lateral dendrites can be severed during the slicing process, we focused on tuft morphology as these were likely to stay intact. Statistical analysis of these Sholl profiles revealed no significant differences between control and occluded ETCs (*Two-way ANOVA*, effect of treatment, $F_{(1,9)} = 1.91$, p=0.20, effect of radius, $F_{(64,576)} = 6.03$, p<0.0001, interaction, $F_{(64,576)} = 0.54$, p=0.999). The area under the Sholl curve represents the total degree of dendritic coverage, the maximum number of intersections describes the

distribution of dendritic density, and the inclusion radius reflects the reaching extent of dendritic arborisations from the first branch points. These measures could be taken from the Sholl analysis. We found that none of these measurements in ETCs differed significantly between control and occluded groups (**Fig 5 Cii-iv**), but there was a trend towards occluded ETCs showing less ramification. This could be due to the low n of occluded ETCs in our analysis, as again occluded ETC values fell within control values (Area under Sholl curve: control mean ± SEM 13378.0 ± 136.10; occluded 968.5 ± 88.05; *Mann-Whitney test*, p=0.11; maximum intersections: control mean ± SEM 40.10 ± 3.88; occluded 33.75 ± 3.15, *Mann-Whitney test*, p=0.49; inclusion radius: control mean ± SEM 83.80 ± 7.99; occluded 67.00 ± 6.58, *Mann-Whitney test*, p=0.15).

Therefore, after having compared multiple measures of dendritic tuft morphology, we conclude that ETCs do not significantly change their gross apical dendritic morphology in response to occlusion.

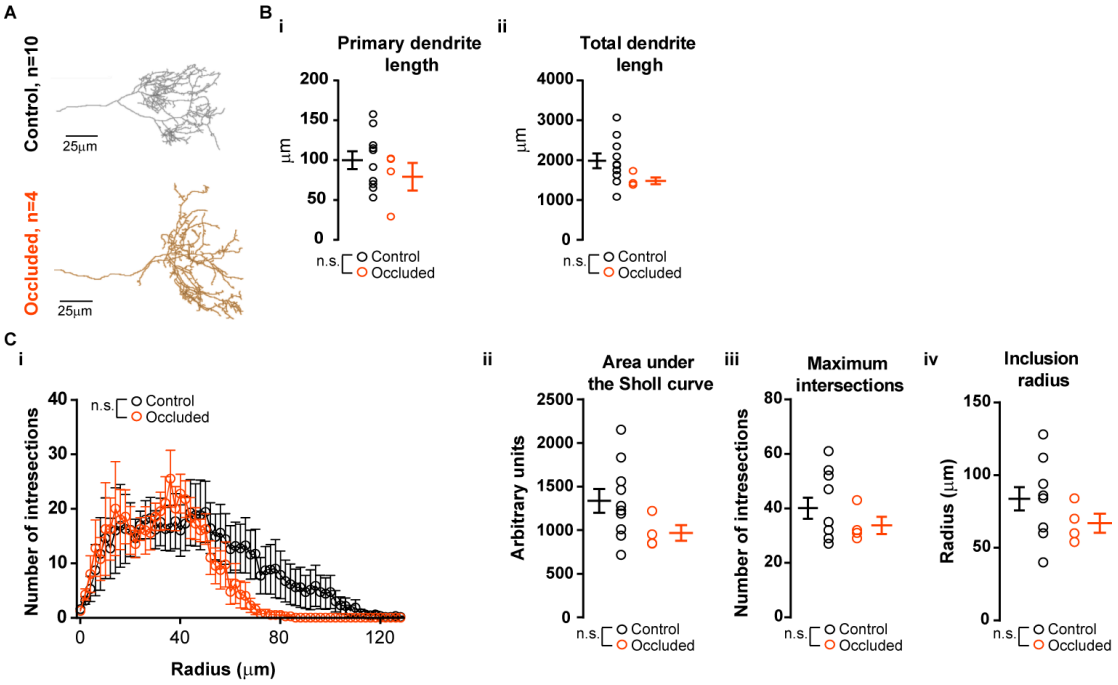

Fig 5. External tufted cell (ETC) primary dendritic tuft morphology is not affected by occlusion.

All reconstructions were performed on biocytin-filled cells after patch recordings in CCK-tdT animals. (**A**) Example reconstructed apical dendrites from control (top) and occluded (bottom) ETCs. Reconstructions start from the soma border, at the left. (**B**) Quantification of dendrite length. (**Bi**) Quantification of primary dendrite length. (**Bii**) Quantification of total dendrite lengths. Each circle represents one cell. Control mean ± SEM are on the left of control plots, and occluded mean ± SEM are on the right of the occluded plots. n.s., non-significant. (**C**) Sholl analysis. (**Ci**) Mean ± SEM Sholl profiles of control and occluded ETC apical tufts. The focal point was placed on the first branch point of the primary dendrite. (**Cii-iv**) Quantification of Sholl measures taken from area under Sholl curve, maximum intersections, and inclusion radius. All conventions as for B.

3.2.6. ETCs do not adjust their spontaneous firing properties after occlusion

Measuring the intrinsic excitability of neurons can sometimes reveal experience-dependent changes. For example, in the accessory OB, internal GCs can become more excitable when an intruder male mouse is presented to a resident male mouse (Cansler et al., 2017). In the main OB, new-born GCs in sensory-deprived animals are more excitable compared to their control counterparts (Saghatelyan et al., 2005). Morphologically, ETCs do not seem to change with 24 h occlusion (see above), so we next wanted to assess whether ETC intrinsic excitability could change after sensory deprivation. We patched ETCs from 21 mice in control conditions, and 20 mice in occluded conditions. This rendered a total of 36 control, and 57 occluded ETCs that passed rigorous quality control and identification criteria (see above; Methods, chapter 2). All recordings were performed in the presence of picrotoxin (PTX) to eliminate the contribution of fast GABAa currents in our recordings. Passive membrane properties, quantified using series resistance (Rs), holding current, membrane resistance (Rm), resting membrane potential (Vm), and membrane capacitance (Cm) did not differ between the two groups (**Table 2**). Cm and Rm are potential indicators of cell size. Cm is an indicator of cell membrane area, however the way we estimated this from our test series may not be entirely reliable (Golowasch et al., 2009). Rm produces a measure of overall cell leakiness, which can scale with size, however also with leak channel density. Therefore, observing no changes in these functional properties correspond to our previous data reflecting no differences in primary dendrite morphology. We were thus interested in whether these measures would correlate with some of the dendrite measures, notably total dendritic length, inclusion radius, and area under the Sholl curve, which also indicate cell size. Nevertheless, no significant correlations were found, and these were not affected by occlusion (data not shown).

ETCs have an intrinsic capability to fire spontaneously in slices (Hayar et al., 2004b). We performed 30s whole-cell current-clamp recordings without any current injection (I=0) and found that 21 control (63.6%) and 32 occluded (66.7%) ETCs fired spontaneously (**Fig 6A**). These proportions did not differ significantly between the two groups (*Fisher's exact test*, p>0.99). Comparisons of spike frequency (**Fig 6Bi**), and spike patterns, measured by the coefficient of variation (CV) of inter-spike intervals (ISI) (**Fig 6Bii**) revealed no differences between control and occluded ETCs (Frequency: control mean ± SEM 2.73 ± 0.77Hz; occluded 4.51 ± 1.28Hz; *Mann-Whitney test,* p=0.41; ISI CV: control mean ± SEM 3.2 ± 0.47; occluded 2.55 ± 0.35; *unpaired t-test*, p=0.26). Upon correlating resting membrane potential with spontaneous firing frequency, there were significant correlations between firing frequency and membrane potential in both conditions (**Fig 6Biii**) (control, *Spearman's correlation*, p<0.0001, r=0.75; occluded, *Spearman's*

correlation, p<0.0001, *r*=0.78). This conforms to previous findings that ETCs portraying higher resting membrane potentials tend to spontaneously fire at higher frequencies (Antal et al., 2006)

Therefore, occlusion does not appear to impact intrinsic ETC spontaneous firing pattern or frequency.

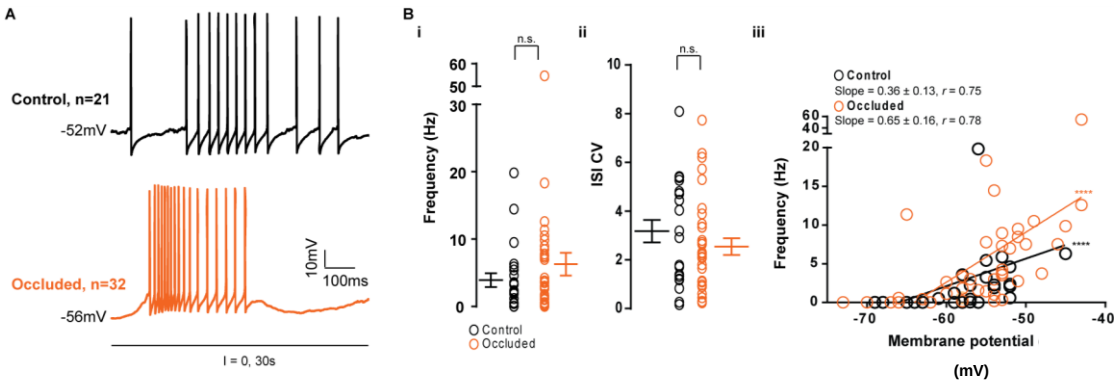

Fig. 6. Occlusion does not affect external tufted cell (ETC) spontaneous firing.

(**A**) Example traces of spontaneous firing recordings from WT ETCs recorded in current-clamp mode. (**B**) Quantification of spontaneous firing in control and occluded ETCs. Each circle represents one cell. Control mean ± SEM are on the left of each control plots, and occluded mean ± SEM are on the right of the occluded plots. (**Bi-ii**) Quantification of firing frequency and coefficient of variation (CV) of inter-spike intervals (ISI (**Biii**) Plot showing resting membrane potential (mV) plotted against firing frequency (Hz). Each circle represents one cell, *r* was derived from Spearman's correlation. n.s., non-significant. ****, p<0.0001.

3.2.7. ETCs do not change their single action potential properties with occlusion

Analysing action potential waveforms produces classic measures of several key functional properties that give rise to spikes, and that may be intrinsically adjusted (Bean, 2007). For instance, the voltage threshold (Vthresh) at which a spike can be fired, as well as the after-hyperpolarising potential (AHP), first spike delay, width at half height (WHH), spike height (Vmax) and the maximum rate of rise of an action potential (Max dV/dT) are all indicators of ion conductances that could be adjusted in an activity-dependent manner. Due to the capacity for these properties to change, we next wanted to observe whether ETC single spike properties were changed with occlusion. This was assessed by injecting 10ms current pulses of increasing amplitude until the cell fired at threshold. 23 control and 39 occluded ETCs that passed rigorous quality control measures fired single action potentials in this configuration and were included in the analysis (**Fig 7A**).

The afterhyperpolarisation potential (AHP), though a single-spike property, can only be calculated from a prolonged depolarisation protocol that induces repetitive firing, thus this measure was taken from our multiple-spiking protocol. There was a small, but insignificant trend towards increased relative afterhyperpolarisation potential (Rel. AHP) in occluded ETCs (control mean ± SEM 15.41 ± 0.85mV; occluded 17.18 ± 0.57mV, *unpaired t-test*, p=0.08). No other single spike properties appeared to show any differences between the groups (**Table 2**); Voltage threshold (Vthresh, mV), spike height (Vmax, mV), width at half height (WHH, ms) (**Fig 7 Bi-iii)**. Additionally, the latency to the first action potential, taken from a multiple spiking protocol, did also not significantly differ between control and occluded conditions (**Fig 7 Biv**) (control mean ± SEM 187.3 ± 23.36ms; occluded 176.9 ± 22.24ms, *unpaired t-test*, p=0.76). These results are in agreement with our AIS data showing that AISs do not change with occlusion, as positive correlations have been found between AIS length and spike height (Dumitrescu et al., 2016) and maximum rate of spike rise (Evans et al., 2015). Therefore, a lack of these functional properties changing with occlusion were supported by our finding that AISs also do not change.

These data indicate that ETC intrinsic action potential waveforms are not affected by 24 h occlusion.

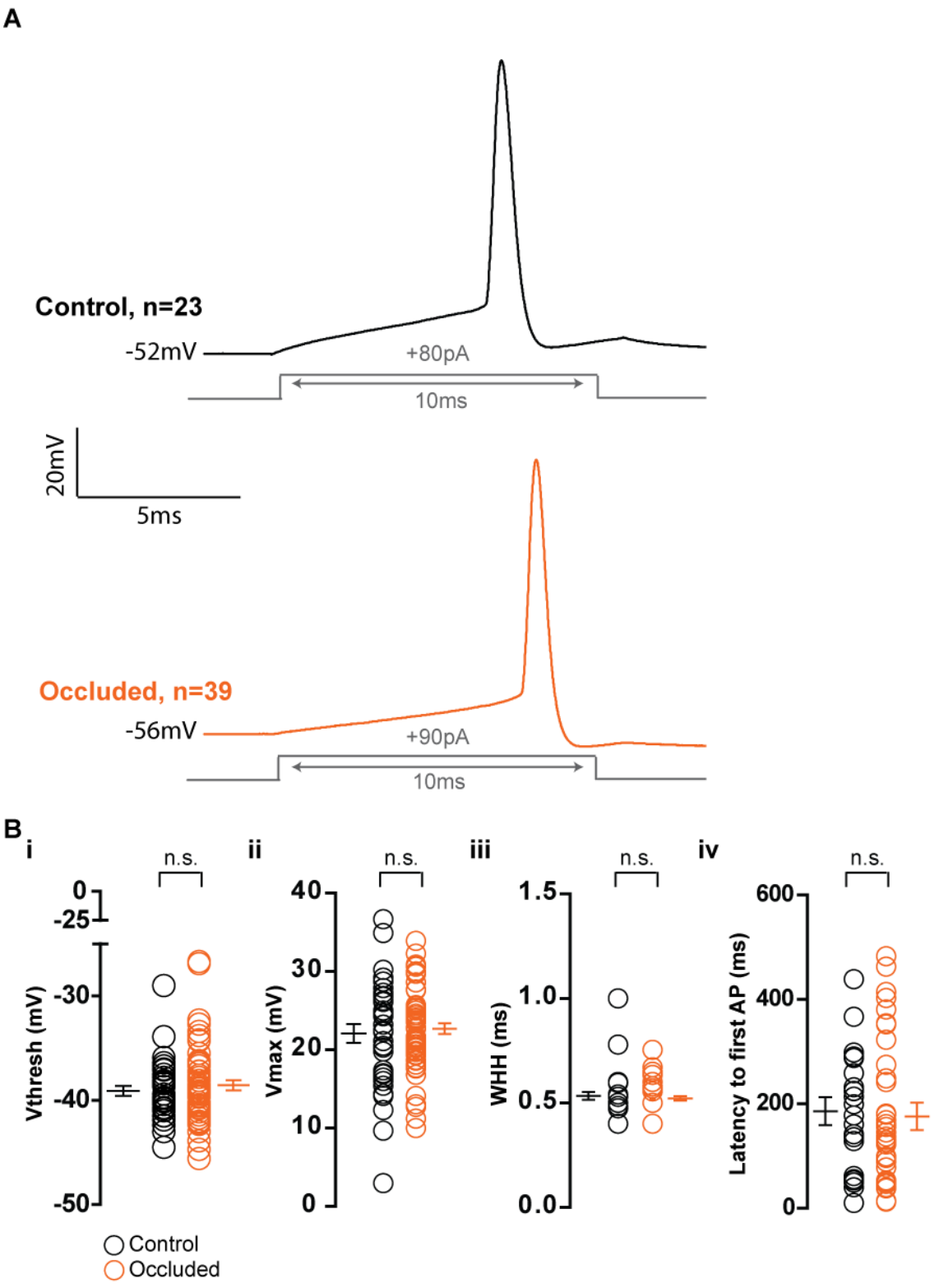

Fig 7. External tufted cell (ETC) single action potential properties are not affected by occlusion.

(**A**) Example traces from WT ETCs showing a single spike obtained by a 10ms threshold current injection. (**B**) Quantification of spike properties. Each circle represents one cell. Control mean ± SEM are on the left of each control plots, and occluded mean ± SEM are on the right of the occluded plots. (**Bi-iiv**) Plots showing voltage threshold (Vthresh, mV), maximum voltage (Vmax, mV), width at half height (WHH, ms), and latency to first action potential (AP, ms) in control and occluded conditions. n.s., non-significant.

3.2.8. Multiple spiking properties in ETCs are unaffected by occlusion

Since single spike properties were unaffected by occlusion, we next wanted to observe whether ETCs changed their multiple spiking behaviour, another measure of intrinsic excitability. Eliciting a train of action potentials with a current injection reveals how many spikes a cell can intrinsically fire at a given additional current density, as well as the firing patterns in terms of burstiness or distribution of spikes across the current injection.

We assessed spike train properties by using 500ms duration current pulses of increasing amplitude in current-clamp mode and recording the elicited spikes from a total of 30 control and 46 occluded ETCs that passed quality control criteria for these measures (**Fig 8A**). This analysis also revealed that ETCs do not change their multiple spiking behaviour in response to sensory deprivation.

Although there was a trend towards ETCs in the occluded group firing less spikes at any given current injection, this difference was not significant (**Fig 8 Bi**) (mixed model analysis, $F_{(2,72)} = 2.93$, effect of treatment, p=0.056, treatment x current density interaction, $F_{(2,72)}=1.17$, p=0.23). Occlusion had no effect on ISI CV or maximum number of spikes (**Fig 8 Bii-iii**) (ISI CV: control mean ± SEM 0.33 ± 0.04; occluded 0.39 ± 0.04; *Mann-Whitney test*, p=0.56; Maximum spike number: control mean ± SEM 61.23 ± 4.37; occluded 55.65 ± 3.06; *unpaired t-test*, p=0.28). There was a slight decrease in ETC instantaneous frequency firing rate with occlusion, however this slight decrease was again not significantly different to control conditions (**Fig 8C**) (mixed model analysis, effect of treatment, $F_{(2,72)} = 3.02$, p=0.051, interaction, $F_{(2,72)}=1.123$, p=0.29).

We further segmented spike trains into 100ms time bins throughout the 500ms current injection (**Fig 8D**). This analysis can reveal potential spike pattern changes that may otherwise be masked by only looking at the whole spike train (Goldfarb et al., 2007). This analysis revealed a trend towards ETCs in occluded conditions firing less in each time bin, corresponding to the result we found when quantifying the number of spikes elicited as a function of input current density (**Fig 8 Bi**). Nevertheless, again, this effect was not significantly different to control conditions (**Fig 8D**), and there was no effect of the interaction with time bins. The only significant effect was that of time bin, which was expected (*Mixed model analysis*, effect of treatment, $F_{(1,75)} = 3.152$, p=0.08, effect of time bin, $F_{(4,300)} = 50.51$, p<0.001, interaction, $F_{(4,300)} = 0.62$, p=0.65).

Our recordings allowed us to perform thorough investigations into different measures of multiple spiking behaviour with a reasonably large dataset, and in no scenario were any of these properties significantly affected by occlusion. We thus suggest that ETC multiple firing properties are likely not affected by short-term sensory deprivation.

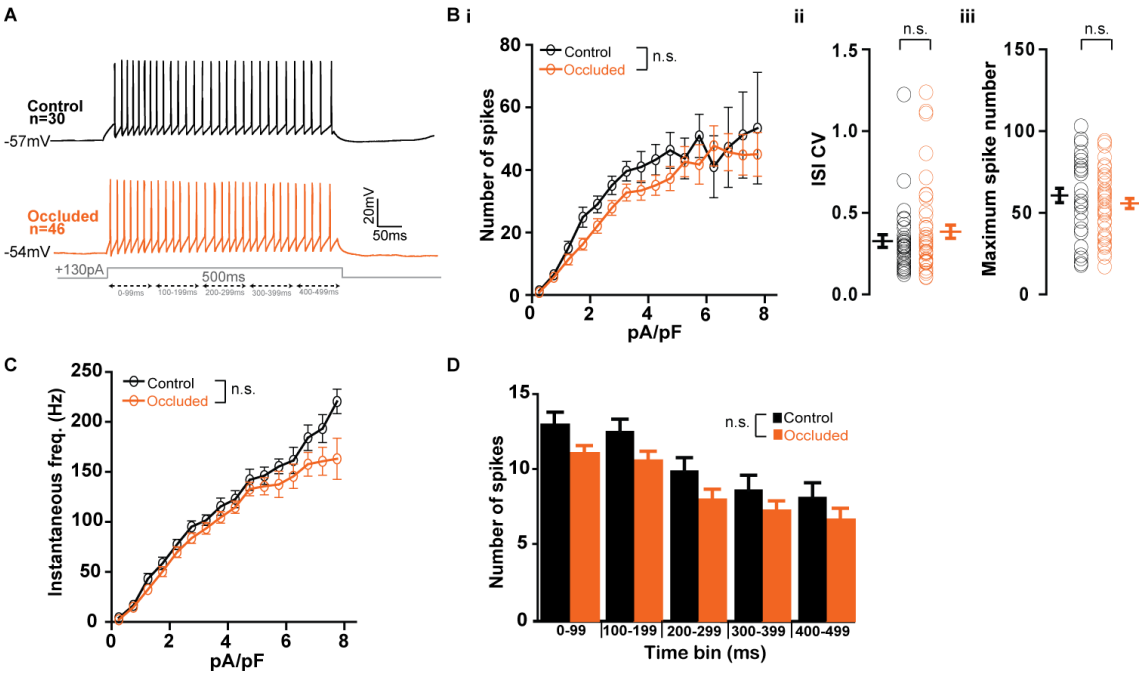

Fig 8. Occlusion has no significant effect on external tufted cell (ETC) multiple firing properties.

(**A**) Example traces from WT ETCs of multiple spiking, obtained by a threshold current injection for 500ms. (**B**) Quantification of multiple spiking properties. (**Bi**) Input-output curve of mean spike number in control and occluded conditions as a function of input current density (pA/pF). Error bars indicate ± SEM. (**Bii-iii**) Quantification of coefficient of variation (CV) of inter-spike intervals (ISI), and maximum spike number elicited. Each circle represents one cell. Control mean ± SEM are on the left of each control plots, and occluded mean ± SEM are on the right of the occluded plots. (**C**) Input-output curve of mean instantaneous frequency in control and occluded groups as a function of input current density (pA/pF). Error bars indicate ± SEM. (**D**) Bar graph showing the number of spikes in each defined time bin in control and occluded groups. The 500ms recordings were divided into 5x 100ms bins and spike numbers were counted for each of the 5 time periods. Error bars indicate ± SEM. n.s., non-significant.

	Control	Occluded			
Property	**Mean ± SEM, N**	**Mean ± SEM, N**	**p-value**	**Statistical test**	**Significance**
Passive properties					
Rs (MΩ)	11.55 ± 0.64, N=33	11.67 ± 0.47, N=48	0.87	unpaired t-test	n.s.
Holding Current (pA)	-1.53 ± 5.01, N=31	-1.84 ± 5.41, N=57	0.63	Mann-Whitney test	n.s.
Rm (MΩ)	246.10 ± 21.83, N= 33	235.90 ± 18.57, N= 48	0.54	Mann-Whitney test	n.s.
Vm (mV)	-57.33 ± 0.92, N=36	-56.58 ± 0.94, N=64	0.58	unpaired t-test	n.s.
Cm (pF)	45.08 ± 2.30, N=33	41.75 ± 1.77, N=48	0.25	unpaired t-test	n.s.
First spike properties					
Vthresh (mV)	-36.64 ± 0.84, N=23	-35.10 ± 0.71, N=39	0.18	unpaired t-test	n.s.
Vmax (mV)	19.02 ± 1.35, N=23	19.39 ± 0.91, N=39	0.81	unpaired t-test	n.s.
First spike delay (ms)	187.30 ± 23.36, N=23	176.90 ± 22.24, N=39	0.76	unpaired t-test	n.s.
WHH (ms)	0.68 ± 0.03, N=23	0.65 ± 0.01, N=39	0.56	Mann-Whitney test	n.s.
AHP(mV)	-52.04 ± 0.45, N=23	-52.28 ± 0.59, N=39	0.75	unpaired t-test	n.s.
Rel. AHP (mV)	15.41 ± 0.85, N=23	17.18 ± 0.57, N=39	0.08	unpaired t-test	n.s.
Max dV/dt (mV/ms)	142.30 ± 7.98, N=23	147.10 ± 4.93, N=39	0.30	Mann-Whitney test	n.s.
Multiple spiking properties					
Max. spike number	61.23 ± 4.37, N=30	55.65 ± 3.06, N=46	0.28	unpaired t-test	n.s.
ISI CV	0.33 ± 0.04, N=30	0.39 ± 0.04, N=46	0.56	Mann-Whitney test	n.s.

Table 2. WT control and occluded external tufted cells (ETCs) do not differ in their intrinsic properties.

Top Table: table shows statistical results from patched ETC data in WT control and occluded ETCs, showing passive properties, first spike properties, and multiple spiking properties. Rs=series resistance, HoldingI=holding current, Rm=membrane resistance, Vm=membane potential, Cm=membrane capacitance, Vthresh=Voltage threshold for action potential, Vmax=maxium voltage, WHH=width at half height, AHP=after hyperpolarising potential, Rel. AHP= relative AHP, MaxdVdt=peak rate of rise, Max. spike number=maximum spike number, CV=coefficient of variation os inter-spike intervals (ISI) . n.s., non-significant.

3.2.9. ETC sag potential is not impacted by occlusion

I*h* currents are currents activated by hyperpolarising potentials that can be important for setting a cell's resting membrane potential, as well as active properties (Nolan et al., 2007). ETCs portray a characteristic sag potential upon hyperpolarisation in the whole-cell configuration which is indicative of I*h* current. I*h*-mediated sag potential amplitudes have been shown to be highly heterogenous in M/TCs, which are segregated into functional units that respond to different inputs. It is thus suggested that changes in sag potential magnitude would result in different functional outputs (Angelo and Margrie; Angelo et al., 2012). To test this in ETCs, we wanted to quantify whether occlusion has an effect on the ETC sag potential. For this analysis, a total of 22 control and 38 occluded ETCs passed quality-control and were used for the analysis. Most cells in our recordings exhibited a noticeable sag potential (**Fig 9 Ai**).

A sag index (Chittajallu et al., 2013; see Methods, chapter 2) (**Fig 9 Aii-Aiv**) was obtained from these cells in order to quantify sag potential amplitude. Comparisons of control and occluded ETC sag indexes revealed that occlusion did not affect the sag potential when measured at a - 90 mV plateau (**Fig 9B**) (control mean ± SEM 0.83 ± 0.02; occluded 0.86 ± 0.02; *Mann-Whitney test*, p=0.34). Moreover, even when taking the sag index from other voltage plateaus tested, no significant differences were observed (data not shown).

These results correspond with findings that ETC membrane potential (**Table 2**) and intrinsic burst firing (**Fig 6**) do not change with occlusion, as the sag index, indicative of the magnitude of the sag potential which is heavily implicated in the regulation of these properties in this cell type (Liu and Shipley, 2008; Liu et al., 2013), is also unaffected by occlusion.

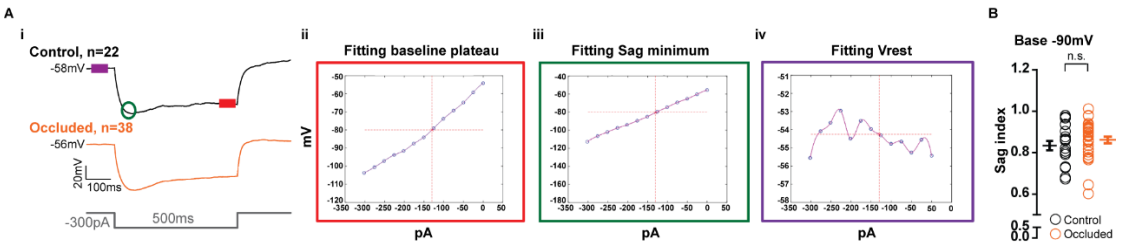

Fig. 9. Occlusion has no effect on external tufted cell (ETC) sag potential.

(**Ai**) Example traces of control and occluded WT ETC sag potentials obtained by injecting a negative current for 500ms. (**Aii-iv**). Calculating the sag index from polynomial fits of sag baseline measures (baseline plateau, red square), minimum sag measures (sag minimum, green square), and holding potential (Vrest, purple square). In the control trace in Ai, the two boxes and circle are colour coded to match where each measure is taken for the polynomial fits. (**B**) Quantification of the sag index taken from -90mV baseline voltage. Each circle represents one cell. Control mean ± SEM are on the left of each control plots, and occluded mean ± SEM are on the right of the occluded plots. n.s., non-significant.

3.3. Discussion

In this chapter, we wanted to explore whether ETCs were capable of adjusting any of their intrinsic properties in an activity-dependent manner. Our initial exploration of ETC activity-dependent plasticity revealed that with short-term (24h) sensory deprivation, ETCs do not appear to adjust any of the morphological or functional properties we investigated.

3.3.1. Live targeting of ETCs in acute slices

Our first obstacle in characterising ETC functional properties was being certain that cells patched in WT acute slices were indeed ETCs. We therefore used published results on ETC location (Liu and Shipley, 2008), morphology (Liu and Shipley, 2008), function (Hayar et al., 2004b), and immunolabelling (Cheetham et al., 2015; Nagayama et al., 2014) to guide our targeting. Using these criteria it was clear that our targeting of ETCs was accurate (**Fig 1**). Though not all patched ETCs were recovered or found for post-hoc analysis of CCK expression, 18 out of the 20 found cells were CCK+, with the remaining 2 showing unclear CCK labelling due to the poor-quality staining achieved with the CCK antibody.

To further strengthen our argument that patched cells were indeed ETCs, we obtained CCK-tdT animals to identify CCK+ cells labelled live in acute slices. Not only did we want to compare our control WT data with ETCs patched in the same way in CCK-tdT animals, but also use this live labelling of ETCs to aid our ETC targeting in the future. Immunohistochemical labelling of OBs from these mice revealed that CCK is expressed by various cells in the OB, not just ETCs. Nevertheless, tdT+ cells co-localised well with the CCK label in the deeper GL, the location we would target ETCs in WT tissue. To ensure we were patching ETCs in these CCK-tdT animals, we also used the strict criteria for identifying ETCs in WT tissue. A comparison of WT ETCs with CCK-tdT ETCs revealed that both groups are very similar in their functional properties (**Table 1**), but differed significantly in a few features: series resistance, membrane capacitance, resting membrane potential, and after-hyperpolarisation potential. CCK-tdT ETCs had a higher series resistance compared to WT tissue. This difference could have arisen due to a change in electrophysiology set-up location, as all CCK-tdT ETCs were patched there, whereas WT ETCs were patched at the previous location. This could have influenced our recordings due to lack of familiarity with the new location by the experimenter. The slightly lower membrane capacitance observed in CCK-tdT ETCs thus likely results from the changed series resistance we recorded, as the capacitance was calculated from the same voltage step recordings as the series resistance.

The slightly lower resting membrane potential and after-hyperpolarisation potential observed in CCK-tdT ETCs could be caused by the fact that ETCs are a very heterogenous population of

cells (Macrides and Schneider, 1982). Indeed, our tuft morphological analysis on CCK-tdT ETCs (**Fig 5**) showed that all imaged cells possessed lateral dendrites (data not shown). It has previously been shown that ETCs with lateral dendrites show slightly different functional properties compared to those that do not (Antal et al., 2006), thus it could be possible that some of the ETCs patched in WT tissue did not have lateral dendrites and thus drove this small discrepancy in our WT vs CCK-tdT comparison. Notably, differences in after-hyperpolarisation potential have previously been reported, with one group of ETCs exhibiting a larger AHP than the other, though again the variability within a group was high (Antal et al., 2006). Resting membrane potential differences could be attributed to differences in I*h*-mediated sag potentials, as these have been shown to set the membrane potential in ETCs (Liu et al., 2013). M/TCs display heterogenous sag potential amplitudes that functionally segregate into several single-glomerulus processing units (Angelo and Margrie, 2011). Though we did not compare WT and CCK-tdT ETC sag potentials (due to the high variability in our WT data), differences in expression of the sag potential could have led to this small difference in membrane potential.

Since we did not aim to discriminate between different ETC populations, our WT ETCs could have come from various pools of ETC populations that show slightly different functional properties. Contrastingly, the ETCs expressing tdT in CCK-tdT animals could have stemmed from a more refined population , or a slightly different combination of ETC subgroups, thus rendering these small differences. Regardless of these differences, overall WT and CCK-tdT ETC functional properties were highly similar, thus we used our stringent targeting of ETCs in both WT and CCK-tdT models to gain consistent results in this chapter.

These data demonstrate that CCK-Cre is not an effective driver line for specifically targeting ETCs. This may especially be true for experiments that strive to target ETCs *in vivo* in the intact OB, for example with ChR2, as this would render extremely unspecific targeting of non-ETCs. An alternative driver line to use instead of CCK-IRES-Cre could be the Pcdh21-Cre line crossed with the tdT reporter line. Expression in Pcdh21-Cre line crossed with the Rosa26-loxP-stop-loxP-CFP line revealed more restricted labelling of M/TCs (Nagai et al., 2005), however in the GL expression also seemed to be restricted to the deep GL layer, and these labelled cells are likely ETCs (Mitsui et al., 2011; Schoenefeld et al., 1985). However, even in these mice, we would still be unable to target individual subtypes of ETCs. Single-cell sequencing approaches could provide a future avenue to characterise individual ETC populations at a molecular level, and thus allow for the clean targeting of specific ETC subgroups, or even all ETCs without the noise from other labelled cells.

3.3.2. Lack of reliable activity-dependent markers of gene expression in ETCs

The first place we wanted to look for activity-dependent plasticity in ETCs was gene expression changes as an indicator of changes in ETC activity levels after occlusion. Immunohistochemical analysis of such markers has revealed that expression changes of certain genes are correlated with activity. For example, the IEG c-Fos is expressed by cells in layer 2/3 monocular visual cortex that are active *in vivo* but not by inactive cells (Barnes et al., 2015). c-Fos expression is activity-dependent, as increased c-Fos expression correlates with increased neuronal firing (Yassin et al., 2010). In the OB, c-Fos expression has also been shown to be plastic. Long-term sensory deprivation (2 months) caused a decrease in glomerular layer c-Fos expression (K Jin et al., 1996). Additionally, preliminary data revealed that GABA/dopaminergic JGCs decrease their c-Fos expression upon short-term (24h) sensory deprivation (D. Byrne, E. Galliano, unpublished data). M/TCs can also show activity-dependent changes in c-Fos expression. Upon application of NMDA receptor antagonists, M/TC c-Fos expression was increased due to decreased feedback inhibition from GCs onto M/TCs (Wilson et al., 1996).

Since markers for c-Fos have been used previously to demonstrate recent activity in cells (Barnes et al., 2015; D. Byrne, E. Galliano, unpublished data; (Kawashima et al., 2014), and may thus indicate whether changes in activity levels occurred, we sought to elucidate whether ETC c-Fos expression would decrease with sensory-deprivation. However, ETCs did not seem to appear to express c-Fos in our control conditions (**Fig 3**). Since ETCs spontaneously fire in slices (Hayar et al., 2004b), as well as *in vivo* (Tatti et al., 2014), this result is somewhat peculiar, as active cells usually do express c-Fos. However, not all active cells express c-Fos. For example, in the striatum, GABAergic medium spiny cells do not express c-Fos at all (Vazdarjanova et al., 2006). Indeed, even in the OB, it has been shown that c-Fos expression is not uniform or ubiquitous. M/TCs, which are also spontaneously active in slices and *in vivo* (Heyward et al., 2001; Kuba et al., 2010), show lower *Fos*, a product of c-Fos expression, expression compared to GCs (Guenthner et al., 2013). Thus, it could be possible that ETCs do not express c-Fos at all. Again, the use of single-cell sequencing approaches in the future will be helpful in identifying whether ETCs express c-Fos. Additionally, c-Fos expression induced by activity changes can be fast and transient (Moratalla et al., 1993). Thus, perhaps ETCs do express c-Fos when they are active in control conditions, but this expression does not last very long. We would then only be able to observe c-Fos+ ETCs on very rare occasions, and perhaps our sample size was not large enough to pinpoint these cells. Alternatively, perhaps ETCs only express c-Fos upon extreme activity, which may not be the case in our control conditions.

Another commonly used marker of activity changes is Arc (Link et al., 1995; Lyford et al., 1995). Arc expression in the OB GL has been shown to be induced by novel odour exposure (Bepari et al., 2012). Since no reports, to our knowledge, have characterised Arc expression specifically in

ETCs, and since expression of Arc is plastic in the GL, we next chose to investigate whether Arc expression could be used as an indicator of ETC activity level changes. Arc was indeed expressed by ETCs (**Fig 3**), but unfortunately the immunohistochemical labelling producing this result could never be replicated, despite applying various antibody retrieval techniques and changes in antibody concentrations. One explanation for this irreproducibility is the Arc antibody half-life. The antibody aliquot was kept in the fridge, as instructed by the manufacturer. However, it could be possible that this form of storage allowed the aliquot to degrade extremely rapidly, as oxidation and proteolytic degradation has more of an effect at higher temperatures. Thus, a strategy to try for reliable Arc labelling of ETCs would be to obtain fresh Arc aliquots for each experiment.

We further probed for the activity-dependent IEG EGR1. This marker is also commonly used to track neural activity (Saffen et al., 1988). Again, it has previously been shown that EGR1 is upregulated in JGCs of the GL upon odour exposure (Bepari et al., 2012). EGR1 appeared to be expressed by some ETCs (**Fig 3**), but the quality of staining produced with the EGR1 label could not be used for quantitative analysis.

A final marker of neural activity we chose to test was NFAT. NFAT is located in its phosphorylated form in the cytoplasm of resting cells. When a neuron is active, there is an influx of Ca^{2+} which binds to calmodulin. This activates the phosphatase calcineurin, which then dephosphorylates NFAT. Upon dephosphorylation, NFAT translocates to the nucleus where it can regulate gene function. Thus, the recent history of a cell's activity can be mapped by staining for NFAT and observing its cellular location (Masuyama et al., 2012). If ETCs showed activity level changes, we would expect some cells, in control conditions at least, to express NFAT in their nuclei, and some in their cytoplasm. Our labelling revealed that in fact all ETCs appeared to express NFAT in their cytoplasm (**Fig 3**). Thus, in ETCs, under our conditions, NFAT is likely not a reliable marker for activity level changes. Just as this is a possibility with c-Fos expression, perhaps the activity threshold for NFAT translocation in ETCs is extremely high. Another possibility for lack of translocation could be that ETCs do not express calcineurin, however calcineurin expression has previously been reported in the OB (Zhu et al., 2009), and the GL (Allen Brain Atlas).

Investigating gene expression changes using immunohistochemistry gives rise to difficulties in the quantification of such changes. Since immunohistochemistry relies on antibodies binding to target locations, and since the specificity of antibodies is never perfect, off-target binding can increase the background noise in the sample. This background noise may not be the same in all areas of the sample, so even upon normalising for background, the measures taken from the sample will always be an estimate. Furthermore, it is difficult to use immunohistochemistry to compare across samples. Even with our technique of staining multiple samples in the same well

under the same conditions (see Methods, chapter 2), the same problem of background noise arises. Furthermore, the penetration capacity of antibodies through the tissue and onto target locations can vary across samples, due to differences in initial fixation quality for example, and produce inconsistent results.

Recently, the rise of the patch-seq technique has arisen as a powerful tool for measuring gene expression in functionally characterised cells (Cadwell et al., 2015; Fuzik et al., 2016). In this technique, a cell is patched and then aspirated through the patch pipette. The contents can then be processed for RNA sequencing. With the use of this technique therefore, we could sequence ETC RNA in control and occluded conditions, screen for activity markers such as Arc (since we know ETCs do express Arc), as well as identify whether other genes have changed expression levels during occlusion. This technique is particularly useful for cells, like ETCs, that have not had a specific genetic driver line identified yet.

Though we were not able to reliably quantify ETC activity levels in control and occluded animals, plug occlusion has been shown to decrease OB activity in general. For example, long-term (28 days) occlusion significantly reduced the overall OB responses to odours (Kikuta et al., 2015), and even short-term (24h) occlusion has been shown to decrease c-Fos levels in GABA/dopaminergic JGCs (D. Byrne and E. Galliano, unpublished data). Due to the strong connections ETCs have with OSN inputs, it is likely that ETCs would decrease their activity levels after occlusion, as less input at the OSNs would result in a lower level of ETC activation as a consequence. However, we cannot rule out the possibility that ETCs do not change their activity in occlusion.

3.3.3. ETC morphology was unchanged by occlusion

Activity-dependent changes in cell morphology may provide a mechanism by which a functional adjustment can occur. Here we analysed two important morphological features of ETCs – the AIS, and the apical tuft – and found that neither was significantly changed by 24 h occlusion.

The AIS

In this chapter, we describe for the first time, to our knowledge, that ETCs contain an AIS. The lengths of ETC AISs are surprisingly short (~ 19µm), more resembling hippocampal dentate granule cells (~ 19µm; Evans et al., 2015), compared to other excitatory neurons such as pyramidal (~ 30µm; Wefelmeyer et al., 2015) and M/TCs (~ 26µm; E. Galliano, unpublished data). This could be due to ETCs being smaller and potentially having a shorter axon than other principal neurons. ETC axons may further not be myelinated due to these features. This is the case for dentate granule cells, which are known to have unmyelinated axons (Amaral et al.,

2008) and shorter AISs. Furthermore, it has been shown that acute demyelination can result in shorter AISs of neocortical layer 5 neurons (from ~ 34µm to ~ 31µm) (Hamada and Kole, 2015). Thus, perhaps ETC axons are not myelinated, which may be linked to their shorter AISs.

We investigated whether ETCs would show activity-dependent plasticity of their AISs as a first step in our morphological analysis. We predicted that occlusion would either increase AIS lengths, relocate AISs closer to the soma, or both, since similar reports noted these forms of AIS plasticity in excitatory cells (Grubb and Burrone, 2010a; Kaphzan et al., 2011; Kuba et al., 2010), and such changes would likely compensate for any decreased activity produced by sensory deprivation. Nevertheless, our results demonstrate that ETC AISs showed little, if any at all, plastic changes (**Fig 4**). There was a hint of a trend of AISs lengthening in the occluded group, however this trend was insignificant and the lengths were only ~1.5µm longer on average than their control counterparts. Our sample size was fairly large (76 control and 84 occluded AISs), so if any reliable differences, even if small, were occurring, they would be evident. It could be possible that ETCs require longer periods of sensory deprivation for the induction of AIS plasticity. Indeed, in experiments reporting AIS length changes *ex vivo* in the chick, these changes occurred after relatively long-term (7 days) sensory deprivation (Kuba et al., 2010). However, AIS plasticity can also occur with short-term manipulations (Evans et al., 2015). In the OB specifically, though AIS changes were observed in dissociated cultures, chronic depolarisation lasted for just 24 hours (Chand et al., 2015). Thus, it is likely that sensory deprivation for 24h would be able to induce AIS plasticity *ex vivo* as well. Indeed, preliminary data have shown that AISs shorten after 24h naris occlusion in the GABA/dopaminergic JGCs *ex vivo* (E. Galliano, unpublished data). Therefore, we conclude that after 24h odour deprivation, ETCs do not adjust their AISs, which is a first indicator that ETC intrinsic excitability may not be changing with such short-term naris occlusion.

Primary dendrite morphology

Morphological plasticity has previously been shown in ETC axons, with long-term (3 weeks) sensory deprivation resulting in an expansion of ETC axonal targeting zones (Cummings et al., 2014). Since ETCs therefore show the capacity to change morphologically, and since neurons in the OB have the capacity to change the features of their dendrite morphology (Dahlen et al., 2011), we next wanted to identify whether occlusion would induce a change in the morphology of the primary dendritic tuft, and whether any of these changes could be correlated with functional changes we might see.

Our results corresponded with previous findings that ETC morphology, even within a specific ETC population, is highly variable (Antal et al., 2006), thus making it difficult to draw strong

conclusions from our relatively small sample size. We chose to characterise only the primary dendrite of ETCs, as the slice preparation often leads to severed axons and lateral dendrites, whereas primary dendrites are localised enough to remain fully intact. We found that overall, gross tuft morphology of ETCs was not affected by occlusion (**Fig 5**). There was a trend towards decreased total dendritic length with occlusion, a trend that was unsurprisingly supported by Sholl AUC also being smaller in the occluded group. This suggests that the dendritic tree is smaller in the occluded group. However, these trends were not significant, and it was difficult to draw a conclusion from this as our n was low (4) for the occluded group. Additionally, the slightly lower values in the occluded group fell within the range of the control group. Thus, upon analysis of gross tuft morphology, ETCs do not seem to be adjusting these in response to short-term occlusion. This is similar to previous findings in M/TCs, where long-term (40 days) olfactory enrichment resulted in no change in M/TC dendrite arborisation (Mizrahi and Katz, 2003). It could be possible that perhaps the excitatory cells involved in glomerular processing retain their dendrite morphology as a scaffold to allow the allow the highly malleable inhibitory circuitry to organise around (Mizrahi and Katz, 2003).

24h sensory deprivation may not be enough time for ETCs to change their dendrite morphology, after all, the OB GC phenotype of decreased dendritic branching occurred after 48h of sensory deprivation. Nevertheless, studies in other systems have revealed that short-term manipulations can effectively drive dendrite morphological changes. For example, pyramidal neurons in the hippocampus of ground squirrels drastically reduce their dendritic lengths and branching during hibernation, an effect that was rapidly reversed within two hours of leaving the hibernating state (Popov et al., 1992). In the optic tectum of *Xenopus laevis*, enhanced visual stimuli resulted in increased dendritic arborisation of tectal projection neurons in as little as 4 hours (Sin et al., 2002). Thus, a more detailed study on a finer scale of ETC morphology may reveal changes in the future. In our study, we did not look at spine morphology, which has the capacity to change in response to changes in activity. As mentioned above, GCs are able to reduce their spine number in the face of relatively short-term sensory deprivation (Dahlen et al., 2011). Furthermore, persistently high rates of spine turnover have been reported in GCs (Sailor et al., 2016). Spine plasticity in GC dendrites has further been demonstrated to occur at an extremely fast rate (within minutes) in response to odour stimuli, where GC spines relocated closer towards activated M/TCs (Breton-Provencher et al., 2016). Thus, a finer-scale measure of ETC morphology could involve the characterisation of their spinal phenotype, and whether this is affected with occlusion. In the OB, an appropriate technique for visualising such fine-scale changes has been characterised. Using longitudinal *in vivo* imaging of viral-targeted neurons through a cranial window, it has been shown that that adult-born spiny JGCs do not adjust their

gross morphology throughout time, however spine turnover was relatively high (Mizrahi, 2007b). Thus, this technique could be applicable when tracking individual live-labelled ETCs over time, to observe whether spine turnover or morphology is changing with occlusion. Live-labelling could be achieved by using the Pcdh21-Cre driver line. Additionally, sparse labelling could be achieved by targeting ETCs *in-utero,* at E17.5 when they are generated (Winpenny et al., 2011), with an electroporated fluorophore-expressing plasmid or through the injection of a viral construct expressing a fluorophore.

In summary, due to lack of AIS plasticity and gross tuft changes in response to occlusion, we suggest that ETCs do not show large-scale activity-dependent morphological changes with short term sensory deprivation. However, further investigation on a finer scale may reveal potential adjustments in these cells under these conditions.

3.3.4. ETCs do not adjust their intrinsic excitability in response to occlusion

We were highly interested in whether ETCs would change some of their functional properties in response to occlusion. Given the central role of ETCs in determining glomerular input-output functions (see chapter 1; Introduction), changes here could potentially have a huge impact on glomerular output. Nevertheless, so far, to our knowledge, ETC functional activity-dependent plasticity has never been investigated, thus we sought to elucidate how, functionally, ETCs may adjust glomerular processing in the face of a changed odour environment. Occlusion did not have an impact on basic ETC morphological properties, however it may affect some of their functional properties.

Overall, our results strongly suggest that intrinsic excitability is unchanged with occlusion. We have performed a thorough analysis of multiple properties using a large sample size with stringent inclusion criteria, thus any differences should have been clearly evident, even in this heterogenous set of cells. The basic passive properties (Rs, Rm, Cm) of ETCs in control and occluded groups were highly similar, thus we could be fairly confident that even the recording conditions were similar for both groups. Furthermore, the lack of any significant differences between the two groups underlines our ability to target ETCs in acute slices (see above).

ETCs in slices intrinsically burst-fire spontaneously (Hayar et al., 2004b) and the number of spikes per burst is regulated by the ionotropic actions of glutamate and GABA (Hayar and Ennis, 2007). This ETC spontaneous firing has been shown to synchronise glomerular activity (Hayar et al., 2004a; Wachowiak and Shipley, 2006), thus we sought to observe whether perhaps this property was adjusted with occlusion. Our recordings of spontaneous firing revealed that ETCs do not adjust their spike frequency or pattern in response to occlusion (**Fig 6**). Since we were always

blocking $GABA_A$ signalling, this lack of change is likely not due to inhibitory network changes. Nevertheless, ETC spontaneous firing is entrained by OSN inputs (Hayar et al., 2004b), thus perhaps these inputs adjusted their properties to maintain signal input in the face of occlusion. This possibility will be explored further in chapter 4.

Spontaneous firing is not the only intrinsic feature that can be adjusted. Single action potential waveforms can be intrinsically adjusted in response to changes in input (Bean, 2007). For example, pyramidal neurons in layer V of the visual cortex have been shown to decrease their voltage threshold for firing an action potential in response to repeated stimulation (Cudmore and Turrigiano, 2004). Changes in action potential waveforms provide insights as to which ionic currents are involved in this process. Our results from control and occluded ETCs demonstrate that all basic features of single spike waveforms are unchanged with occlusion (**Fig 7**). These data fit together well with our AIS data as ETC AIS length and distance from the soma also did not seem to change with occlusion. The action potential voltage threshold and rate of rise have been shown to correlate with AIS phenotype. For example, AIS lengthening in response to sensory deprivation in the nucleus magnocellularis neurons of the auditory brainstem was correlated with a faster spike rate of rise and lower voltage threshold (Kuba et al., 2010). Furthermore, when correlating AIS length with spike threshold on a cell-by-cell basis in dissociated dentate granule cells, a significant negative relationship was found (Dumitrescu et al., 2016). Since occlusion did not affect ETC AIS lengths, the lack of changes in voltage threshold and rate of spike rise therefore correspond well with our AIS non-phenotype.

The frequency of spiking and timing between spike bursts are powerful means of transmitting specific signals. Thus, multiple spiking behaviour provides another avenue for which a cell can adjust its intrinsic excitability, which could indirectly function to adjust a network in response to input changes. For example, in response to persistent stimulation, deep cerebellar nuclear neurons have been shown to increase their intrinsic excitability by increasing the number of spikes they produce upon intracellular current injection steps, a phenotype relying on Ca^{2+} influx (Aizenman and Linden, 2000).

In our data, we found that ETCs do not change their multiple spiking behaviour in response to occlusion (**Fig 8**). Though ETCs appeared to fire slightly less compared to controls, this trend was not significant, and given our large sample size, we conclude that occlusion does not affect this intrinsic property of ETCs either. These data again match with our lack of AIS phenotype, as it has been shown that AIS length changes were particularly correlated with changes in multiple spiking (Dumitrescu et al., 2016; Evans et al., 2015).

The sag potential

ETCs further express a characteristic sag potential, a proxy for I*h* currents, upon hyperpolarising current steps (Liu and Shipley, 2008). Activity-dependent changes in sag potential magnitudes have previously been reported and have shown that this can influence intrinsic excitability. In hippocampal neurons, inducing long-term potentiation (LTP) to potentiate input resulted in decreased neural excitability that occurred due to a larger sag potential under these conditions (Fan et al., 2005). In another study, the I*h* was artificially increased resulting in decreased firing rates of CA1 pyramidal neurons (van Welie et al., 2004). In the OB, sag potential heterogeneity among M/TCs has been hypothesised to arise due to short-term plasticity. Furthermore, the same study demonstrated that a larger sag potential correlated with regular spiking, whereas M/TCs displaying no sag appeared to fire much less in general (Angelo and Margrie, 2011). It was then shown that M/TCs responding to the same odorants form functional processing units that all express similar sag potential amplitudes (Angelo et al., 2012), further suggesting that different input characteristics could result in sag potential plasticity. Thus, there seems to be a strong link between sag potential magnitude and neuronal excitability.

The sag potential in ETCs has been shown to set the resting membrane potential and contribute to rebound burst-firing (Liu and Shipley, 2008). Since this property has a propensity to change, and since it is implicated in setting intrinsic excitability, we were interested to see whether this feature was changing in occluded ETCs. Again, occlusion did not appear to affect the sag potential in ETCs, though similar to previous reports (Angelo and Margrie, 2011), sag potentials were very heterogenous across cells (**Fig 9**). Nevertheless, our sample size was large (22 control and 38 occluded ETCs), thus even small differences arising due to occlusion should have been evident.

In ETCs, the sag potential has been shown to be activated by $GABA_A$ mediated signalling, which is further enhanced by D_1-Dopamine receptor activation resulting in an inhibition-excitation switch as this increases ETC rebound spiking (Liu et al., 2013). Since we always blocked $GABA_A$ currents in our recordings, a lack of sag phenotype cannot be accounted by changed regulatory activity of $GABA_A$. However, we did not block dopamine transmission. We could imagine a scenario where ETCs adjusted their sag potentials by increasing the sag potential amplitude, perhaps by increasing I*h* conductance. However, if GABA/dopaminergic JGCs reduced their dopamine release, this could off-set the potential ETC sag potential effect we would see, as less D_1-Dopamine receptor-mediated amplification of the sag potential would occur compared to control conditions. To test this hypothesis, we could thus perform our patch experiments in the

presence of both $GABA_A$ and D_1-Dopamine receptor blockers and observe whether we could then see an occlusion effect on the sag potential.

Nevertheless, a lack in sag potential changes actually correlates with a lack of change in resting membrane potential (**Table 2**). We therefore again suggest that this intrinsic property of ETCs remains unchanged with 24h occlusion.

3.4. Conclusions

The morphological and functional data gathered in this chapter strongly indicate that ETCs do not alter their intrinsic excitability with short-term sensory deprivation. Though we could not determine reliable activity markers for ETCs, plug occlusion decreases OB activity (D. Byrne, E. Galliano, unpublished data; Kikuta et al., 2015), thus we know that using this experimental paradigm was a powerful tool for driving plastic changes in the OB. We show that ETC primary dendritic and AIS morphology are unaffected by occlusion. This is closely matched by our findings that none of the extensive list of functional intrinsic properties we analysed changed with occlusion. Thus, even though ETCs are glomerular gatekeepers of initial odour processing, they do not appear to show any plastic change in their intrinsic properties after 24h sensory deprivation. In the next chapter, we further explore whether perhaps ETC synaptic inputs are altered in the face of occlusion.

Chapter 4

Short-term occlusion enhances excitatory signalling in glomeruli

4.1. Introduction

In the previous chapter we have shown that ETC intrinsic excitability, gross morphology, and passive properties are unchanged after 24h sensory deprivation. However, functional changes can also occur on a synaptic level. As discussed in chapter 3, synaptic plasticity is a powerful tool for changing the way signals are processed. For example, long-term occlusion (2 weeks) increases the release probability (P*r*) of OSNs, an effect that is intrinsic to OSN synapses (Tyler et al., 2007). Contrastingly, tetanic stimulation of OSNs induces pre-synaptic long-term depression (LTD) at M/TC synapses (Mutoh et al., 2005) which may be a compensatory function in the face of odour over-exposure. It has further been shown that M/TCs show heterogeneity in their synaptic dendrodendritic lateral excitation. The efficacy of transmission here, and thus potential for synaptic plasticity, was correlated with sniffing frequency (Pimentel and Margrie, 2008). ETCs have also been shown to undergo synaptic plasticity. Short-term sensory deprivation (3d) is enough time to induce compensatory synaptic changes in ETCs, where mEPSC amplitudes recorded from ETCs increased. This resulted due to an increase in ETC glutamate receptor densities, suggesting that sensory deprivation strengthens ETC glutamate sensing (Tyler et al., 2007). Ultimately, all of these synaptic adjustments hold great potential in adjusting or maintaining odour processing in the face of changes in the olfactory environment.

A crucial synaptic feature that impacts functional output of both ETCs and M/TCs is the glomerular LLC. ETCs and M/TCs projecting to the same glomerulus form part of the excitatory glomerular network that acts in synchrony, ensuring reliable output is transmitted from the M/TCs (De Saint Jan et al., 2009; Gire et al., 2012; Hayar et al., 2004a; Schoppa and Westbrook, 2001). ETCs have been shown to drive M/TC activity and are thus considered to function as the intermediary step between OSN input and M/TC output, amplifying initial OSN inputs (De Saint Jan et al., 2009; Gire et al., 2012). A crucial step in this amplification and synchronisation is the glomerular LLC (Schoppa and Westbrook, 2001). LLCs are slow, polysynaptic glutamatergic currents that arise due to dendrodendritic excitatory amplification by ETCs and M/TCs projecting to the same glomerulus. Although the trigger for LLCs has not been identified, there is evidence to suggest that OSN inputs are responsible for the initiation of LLCs (Gire and Schoppa, 2009; Schoppa and Westbrook, 2001), which then acquire their magnitude through spillover glutamatergic dendrodendritic amplification, by M/TCs, ETCs, and/or both cell types (De Saint Jan et al., 2009; Najac et al., 2011; Vaaga and Westbrook, 2017). LLCs are thought to be initially amplified by ETCs, since they form stronger connections with OSNs and are excited at lower thresholds compared to M/TCs (De Saint Jan et al., 2009). Additionally, ETC spiking can evoke an LLC in M/TCs, a relationship that is not reciprocal (De Saint Jan et al., 2009). Thus, the main

model for LLC generation is that it occurs through sequential steps originating from glutamate release due to OSN input. This migrates through the ETC network, where it is initially amplified, before being transmitted to the M/TC network for further amplification with recurrent excitatory loops at the ETC and M/TC stages. (**Diagram 1**).

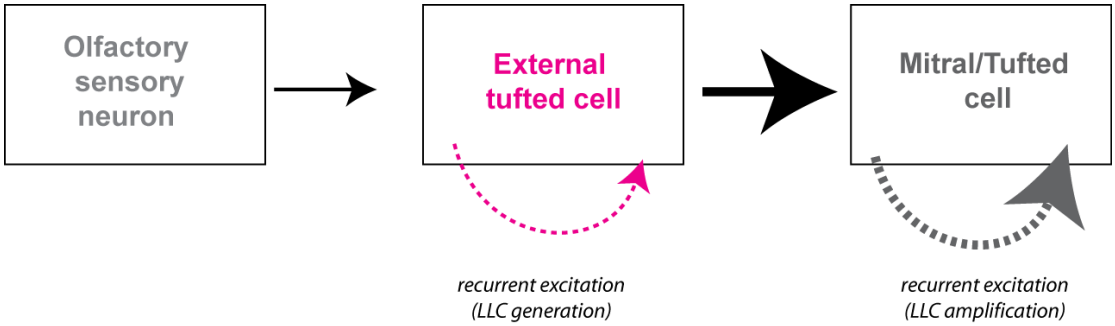

Diagram 1. Illustration picturing LLC generation.

OSN inputs reach ETCs which transmit this information to M/TCs. ETCs initially amplify OSN inputs (magenta arrow) among themselves, which is further amplified by dendrodendritic amplification at M/TCs (grey arrow).

LLCs not only synchronise excitatory glomerular processing, but also define the output profile of cells that are receiving the LLC. Indeed, they are so crucial for M/TC function, that when they do not occur, most M/TCs projecting to the same glomerulus do not fire at all (Gire and Schoppa, 2009). ETC spike responses to OSN inputs are phase locked and are thus transient, whereas M/TC spike responses are more prolonged. The ability for M/TCs to sustain firing is highly dependent on NMDA and mGluR1 receptors, as pharmacological block of these results in M/TC responses being converted to resemble ETC responses (i.e. phase locked) (Vaaga and Westbrook, 2017). NMDA and mGluR1 receptors also play a vital role in the M/TC LLC, as blocking these receptors pharmacologically eliminates LLCs (De Saint Jan and Westbrook, 2007). Therefore, M/TCs can only produce their characteristic prolonged firing in response to input if they receive large LLCs due to strong dendrodendritic amplification (Vaaga and Westbrook, 2017). Thus, the spiking output profiles of ETCs and M/TCs are driven by the magnitude of dendrodendritic amplification of OSN signals, portrayed as LLCs, therefore highlighting the importance of LLCs in driving overall function in these cells.

LLCs are further modulated by the inhibitory JGC network. Previous reports have stated that LLCs are a binary phenomenon, where they either occur at full magnitude, or do not occur at all (Gire and Schoppa, 2009). The probability of an LLC occurring in response to OSN input is regulated by $GABA_A$ currents, received from inhibitory intra- and inter-glomerular JGCs, likely

acting on ETCs (Aungst et al., 2003; Gire and Schoppa, 2009). These can completely block the occurrence of an LLC, and thus have been suggested to prevent LLC-evoked M/TC firing in response to weak odour inputs by manipulating the LLC occurrence probability (Gire and Schoppa, 2009). Furthermore, $GABA_A$ signalling can impact the magnitude of the all-or-nothing LLC. $GABA_A$ antagonists have been shown to result in an increased amplitude and time decay of LLC (Carlson et al., 2000) which further suggests that under relatively physiological conditions, the all-or-nothing LLC probability as well as magnitude is modulated by $GABA_A$ inhibition.

Therefore, LLCs form part of a synaptic amplification process that starts in ETCs, is further dendrodendritically amplified by M/TCs, and regulates both synchrony and the spike profile of its targets, and thus glomerular output. The build-up and modulation of LLCs suggests that there are several avenues in which they can be adjusted, which may result in a profound impact on initial odour processing. Therefore, to investigate occlusion effects on ETC synaptic function, in this chapter we focused on exploring whether, and how short-term sensory deprivation can influence the ETC LLC.

4.2. Results

4.2.1 After 24 h naris occlusion, ETCs portray larger spontaneously occurring LLCs

We wanted to investigate whether any synaptic plasticity was occurring in ETCs as a result of occlusion. In our initial exploration, we recorded spontaneous synaptic inputs onto ETCs in the whole-cell configuration, voltage-clamped at their resting membrane potential of -55mV (Liu and Shipley, 2008). These recordings were performed in the presence of the $GABA_A$ receptor blocker picrotoxin (PTX) as we were predominantly interested in any effects occurring in the excitatory glomerular layer network (**Fig 1A**). These recordings were achieved in WT animals, from the same cells that were patched for our intrinsic excitability data set (chapter 3).

Fast excitatory synaptic inputs were rarely seen (**Fig 1 Bi-Bii,** red asterisks), corresponding with previous reports that they occur infrequently (Hayar et al., 2004a). We did not investigate these events further due to their rare occurrence, and due to the inability of distinguishing where these inputs were coming from, as sources could include OSNs, other ETCs, M/TCs, or even cortical feedback. This would make it very difficult to interpret any specific network effects from these results.

LLCs, however, occurred spontaneously in our recordings (**Fig 1 Bi**, green star) and were clearly evident by their large amplitudes and slow onset and decay kinetics (lasting from ~ 500-1000ms), closely resembling published reports of these events (Carlson et al., 2000; Gire and Schoppa, 2009). LLCs occurred spontaneously in 17 control and 26 occluded ETCs (**Fig 1C**). LLCs occurred at similar frequencies in both groups (control; mean ± SEM 0.10 ± 0.02Hz; occluded 0.07 ± 0.01Hz; *unpaired t-test* using Welch's correction, $t_{(22.38)}$ = 1.51, p=0.15, data not shown). However, occlusion significantly increased the amplitude of spontaneously occurring LLCs in ETCs (**Fig 1D**. left). Furthermore, the charge of LLCs, calculated for a 500ms window from the start of the LLC at baseline, also significantly increased with occlusion (**Fig 1D**, right) (amplitude: control; mean ± SEM 49.95 ± 4.48pA; occluded 69.95 ± 6.43pA; *unpaired t-test* using Welch's correction, $t_{(40.32)}$ = 2.51, p=0.03; charge: control; mean ± SEM 10.83 ± 1.24pC; occluded 16.86 ± 1.37pC; *unpaired t-test,* $t_{(41)}$ = 3.06, p=0.004).

These data suggest that ETCs receive increased polysynaptic excitatory input after short-term occlusion.

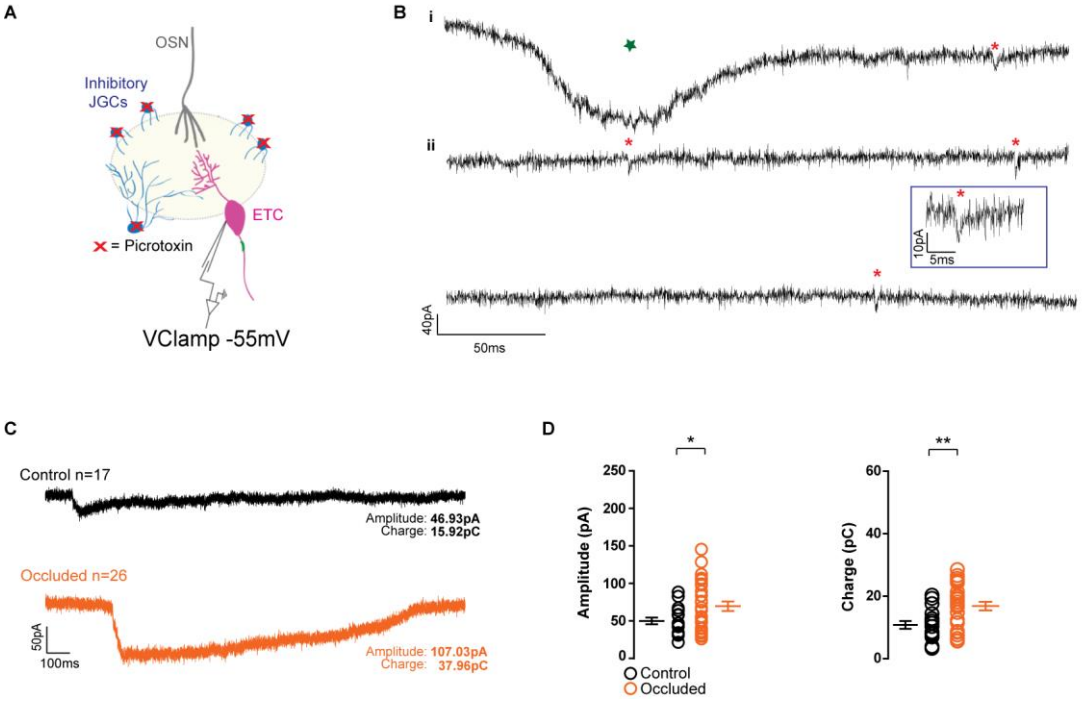

Fig 1. Spontaneous long-lasting depolarising currents (LLCs) become larger with occlusion in external tufted cells (ETCs).

(**A**) ETCs were recorded in the whole-cell configuration, clamped at -55mV. 10µm picrotoxin (PTX) was included in the recording solution to block $GABA_A$ currents received from inhibitory juxtaglomerular cells (JGCs). (**B**) Example recordings of spontaneous events. Fast inward currents are demarcated with a red asterisk. LLC is demarcated with a green star (**Bi**) Example recording showing a spontaneously occurring LLC, followed by a fast excitatory inward current. (**Bii**) Example trace showing infrequent occurrence of fast synaptic excitatory input. Inset shows zoom-in of one recorded inward current taken from the trace above it. (**C**) Example traces of control and occluded spontaneous LLCs. (**D**) Quantification of LLC amplitude (left) and charge (right). Each circle represents one cell. Error bars indicate SEM. *, p<0.05; **, p<0.01.

4.2.2. Evoked ETC LLCs become larger with occlusion.

Given the importance of LLCs in the synchronisation of glomerular output (see above, introduction), and since we found an increased magnitude of spontaneous LLCs with occlusion in ETCs, we wanted to explore the significance of this phenotype more thoroughly. LLCs are thought to be triggered by input from OSNs (Carlson et al., 2000; De Saint Jan et al., 2009), and spontaneous LLCs in acute slices are likely triggered by spontaneous release of glutamate at OSN terminals (Carlson et al., 2000; De Saint Jan et al., 2009).

We thus chose to record ETC LLCs that were evoked by electrical stimulation of OSNs. This allowed us to study the effects of 24 h occlusion on LLCs in a more temporally controlled manner, employing reliable stimulation of the excitatory network in a given glomerulus. ETCs were patched in the whole-cell configuration and voltage clamped at -55mV, while OSNs were electrically stimulated every 20 seconds. All recordings were performed in the presence of PTX in CCK-tdT animals (**Fig 2A**). Electrical stimulation strengths needed to be carefully tuned on a cell-by-cell basis, based on the types of evoked responses recorded in ETCs (**Fig 2B**). LLCs are thought to occur in a binary all-or-nothing manner(Gire and Schoppa, 2009), where they either do not occur at all (**Fig 2B**, top), or always occur with the same magnitude (**Fig 2B**, middle two traces) depending on how strong the afferent stimulation intensity is. In ETCs, only the lowest threshold responses evoked by OSNs result in LLCs. If OSNs are stimulated strongly, however, a fast monosynaptic EPSC superimposes upon the LLC (**Fig 2B**, bottom, red asterisk). For our analysis, we recorded "pure" LLCs that were not infiltrated with monosynaptic responses, at suprathreshold stimulus intensities that always produced reliable LLCs. A total of 14 sham control and 17 occluded ETCs were recorded in this configuration.

OSNs were stimulated by placing the stimulating electrode in the ONL clearly visible with DIC optics, far away from the GL. However, to ensure that LLCs were evoked by stimulating OSN fibres rather than post-synaptic dendrites directly, we performed two control experiments (**Fig 2C**). In the first, we recorded evoked LLCs in three separate ETC recordings and then washed in tetrodotoxin (TTX) to eliminate spike-mediated transmission. This resulted in the elimination of the evoked LLC in all separate recordings (**Fig 2 Ci**). In the second control experiment, we again evoked LLCs in three separate ETC recordings, but this time washed in the AMPA receptor blocker NBQX, which should effectively block the transmission from OSNs to ETCs. In all three separate recordings, the evoked LLCs were eliminated (**Fig 2 Cii**). These data indicate that LLCs were evoked as a result of OSN stimulation - if ETCs were stimulated directly by the stimulating electrode, we would still observe responses in the presence of these blockers.

Both sham control and occluded ETCs displayed evoked LLCs in response to OSN stimulation (**Fig 2Di**). In 12 ETCs from each treatment group, both evoked and spontaneous LLCs were recorded and could be compared on a within-cell basis (**Fig 2 Diii-Div**). Both sham control and occluded ETC evoked LLC amplitudes significantly and positively correlated with their spontaneous LLC amplitudes (**Fig 2 Diii**), consistent with the reported binary nature of these responses (Carlson et al., 2000; Gire et al., 2009; sham control: *Pearson's correlation*, p=0.008, *r*=0.72; occluded; *Pearson's correlation*, p=0.001, *r*=0.84). However, evoked LLCs were consistently larger compared to spontaneously occurring LLCs in the same ETCs which could be due to inconsistent excitatory input reaching recorded ETCs under spontaneous recording conditions (Charge: sham control; spontaneous mean ± SEM 6.21 ± 1.27pC; evoked 18.22 ± 2.41pC; *Mann-Whitney test*, p<0.0001; occluded; spontaneous mean 7.76 ± 1.65pC; evoked 29.15 ± 4.23pC; *Mann-Whitney test*, p<0.0001; Amplitude: sham control; spontaneous mean ± SEM 38.63 ± 5.84pA; evoked 70.44 ± 8.41pA; *Mann-Whitney test*, p=0.002; occluded; spontaneous mean ± SEM 58.82 ± 8.97pA; evoked 109.70 ± 15.81pA, *Mann-Whitney test*, p=0.01). Alternatively, or in concert, there could be a modulatory effect of the initial amplitude triggered by OSN stimulation that may impact LLC size. Indeed, when correlating spontaneous LLC charge with evoked LLC charge, the correlation was positive but not significant (**Fig 2 Div**), implying that the initial amplitude received by ETCs may have an effect on LLC duration (sham control: *Pearson's correlation*, p=0.19, *r*=0.40; occluded; *Pearson's correlation*, p=0.57, *r*=0.18). This illustrates that spontaneously recorded LLCs do not always involve the full local excitatory subnetworks, which are, in contrast, reliably activated by OSN stimulation.

Evoked ETC LLCs again were significantly impacted by occlusion, as both amplitude and charge, calculated in the same way as for spontaneous LLCs, were significantly larger in occluded ETC LLCs compared to sham controls (**Fig 2 Dii**) (amplitude: sham control; mean ± SEM 65.51 ± 7.93pA; occluded 105.80 ± 12.92pA; *unpaired t-test*, $t_{(29)}$ = 2.46 p=0.02; charge: sham control; mean ± SEM 16.74 ± 2.30pC; occluded 26.27 ± 3.44pC; *unpaired t-test*, $t_{(29)}$ = 2.20, p=0.04).

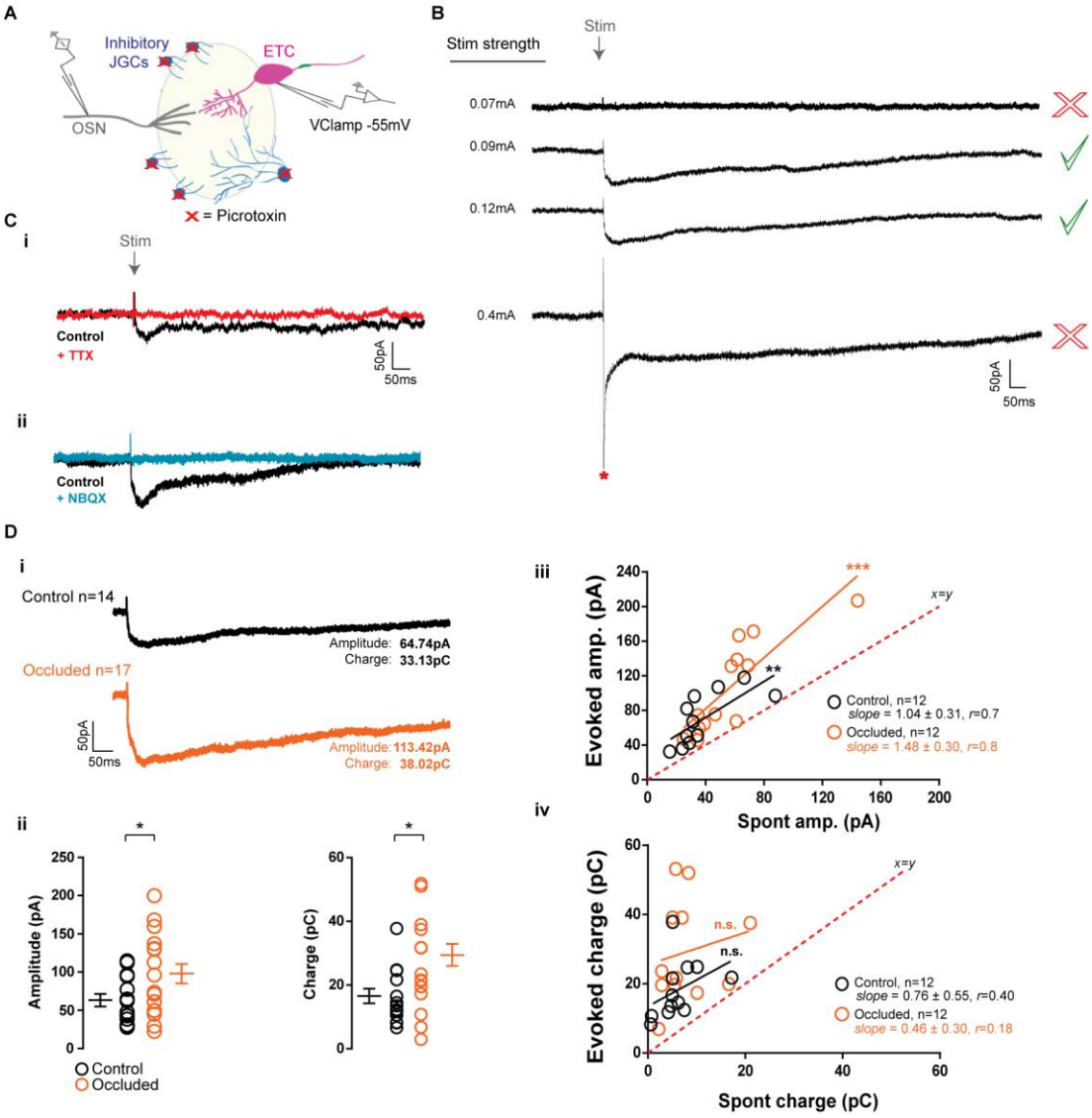
A
Inhibitory JGCs
ETC
OSN
VClamp -55mV
= Picrotoxin
B
Stim strength
Stim
0.07mA
0.09mA
0.12mA
0.4mA
50pA
50ms
C
i
Stim
Control
+ TTX
50pA
50ms
ii
Control
+ NBQX
D
i
Control n=14
Amplitude: 64.74pA
Charge: 33.13pC
Occluded n=17
Amplitude: 113.42pA
Charge: 38.02pC
50pA
50ms
ii
Amplitude (pA)
Charge (pC)
Control
Occluded
iii
Evoked amp. (pA)
Spont amp. (pA)
x=y
Control, n=12
slope = 1.04 ± 0.31, r=0.7
Occluded, n=12
slope = 1.48 ± 0.30, r=0.8
iv
Evoked charge (pC)
Spont charge (pC)
n.s.
Control, n=12
slope = 0.76 ± 0.55, r=0.40
Occluded, n=12
slope = 0.46 ± 0.30, r=0.18

Fig 2. Evoked long-lasting depolarising currents (LLCs) in external tufted cells (ETCs) become larger after occlusion.

(**A**) ETCs were recorded in the whole-cell configuration and clamped at -55mV in the presence of 10μm picrotoxin (PTX). During the recordings, olfactory sensory neuron (OSNs) fibres were electrically stimulated with 20s inter-stimulus intervals. (**B**) Electrical stimulus intensity was adjusted to obtain a pure LLC recording. Top: stimulus intensity was too low to evoke an LLC. Middle two traces: at these two stimulus intensities, LLCs were reliably evoked. Evoked LLCs were always of the same magnitude. Bottom: stimulus intensity was too strong and evoked a monosynaptic response (red asterisk) as well as an LLC. (**C**) Control experiment to show that LLCs reflected synaptic input by OSN stimulation as opposed to direct electrical stimulation of the recorded ETC. (**Ci**) Example trace showing the elimination of the evoked LLC (black trace) with a wash-in of 1μm tetrodotoxin (TTX) (red trace). (**Cii**) Example trace showing the elimination of the evoked LLC (black trace) with a wash-in of 10μm NBQX, teal trace. (**D**) Recording and quantification of control and occluded ETC LLCs. (**Di**) Example traces of evoked LLCs in control and occluded conditions. (**Dii**) Quantification of amplitude (left) and charge (right) of control and occluded ETC LLCs. Each circle represents one cell. Error bars indicate SEM. (**Diii**) Correlation of evoked and spontaneous LLC amplitude in control and occluded data. Each circle represents one cell. Red dotted line shows linear fit. Solid black (control) and orange (occluded) lines show best-fit. *r* was derived from Pearson's correlation. (**Div**) Correlation of evoked and spontaneous LLC charge in control and occluded data. *., $p<0.05$; **., $p<0.01$; ***., $p<0.001$; n.s., non-significant.

4.2.3. Evoked LLCs are more stereotyped than spontaneous LLCs.

We next explored whether evoked LLCs indeed portray a more reliable binary phenotype compared to spontaneous LLCs. We hypothesise that the discrepancy between spontaneous and evoked LLC magnitudes may occur due to varying stereo typicity when recording LLCs in different configurations. Spontaneously occurring LLCs may be less stereotyped in their magnitudes compared to evoked LLCs as spontaneously occurring LLCs my be evoked by the activation of glomerular excitatory "sub-compartments" that may not always employ the full network. Contrastingly, evoking LLCs via OSN stimulation may activate most/all of the excitatory network and thus produce a more reliable response.

We first performed histogram-style analysis on all spontaneously occurring and evoked LLCs to evaluate the quantal nature of LLCs in both scenarios (Fig 3A). This would indicate whether LLCs really are all-or-nothing phenomena in both recording conditions. For each cell recorded, spontaneous LLC amplitudes were normalised to the median of all spontaneous LLC amplitudes of that cell. In the same way, evoked LLC amplitudes were normalised for each cell where this was recorded. These normalised LLC amplitude values were then plotted, from all cells, against the frequency at which they occurred (Fig 3A). Gaussian curves were fitted to the resulting histograms to explore the quantal nature of these events. Upon visual observation, it is evident that although spontaneous LLCs centre around a peak of 1 (indicative of the binarity of release), there is a higher spread of variability compared to the more tightly centred evoked LLC distribution. The goodness of the gaussian fits were calculated as r^2=0.86 for spontaneous LLCs and r^2=0.99 for evoked LLCs.

To further explore this phenomenon, we analysed the per-cell coefficient of variation (CV) of spontaneously occurring and evoked LLC amplitudes (Fig 3 B). With this analysis, values below 1 indicate more stereotyped events. Values around 1 portray a more random distribution, and values above 1 indicate high variability between events. We further compared CV values in control and occluded conditions to observe whether there were any occlusion effects on LLC amplitude variability. These data complement the histogram analysis by demonstrating that spontaneous LLC amplitude CV values were significantly higher compared to evoked LLC CV values. Additionally, occlusion did not impact the variability of LLC amplitudes (control: spontaneous, mean ± SEM 0.51 ± 0.10; evoked, 0.14 ± 0.02; Occluded: spontaneous, mean ± SEM 0.42 ± 0.03; evoked, 0.137 ± 0.03; two-way ANOVA on log10-transformed values, effect of stimulus type, $F_{(1,59)}$=69.34, p<0.0001, effect of treatment, $F_{(1,59)}$=0.15, p=0.70, interaction, $F_{(1,59)}$=0.02, p=0.89).

These results demonstrate that recorded evoked LLCs are more homogenous in their magnitudes compared to spontaneously occurring LLCs.

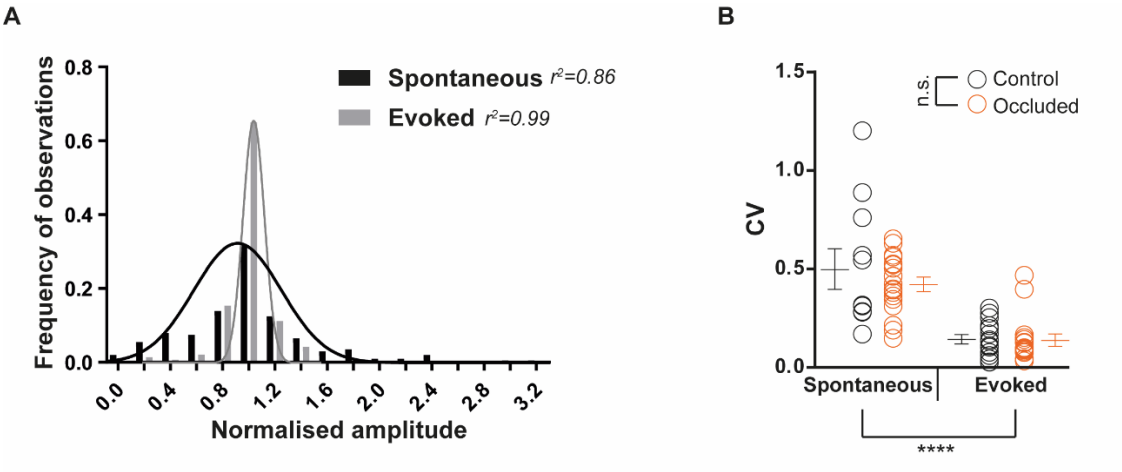

Fig 3. Evoked long-lasting depolarising currents (LLCs) in external tufted cells (ETCs) are more stereotyped than spontaneous LLCs.

(**A**) Histograms of all median-normalised amplitudes (pA) of spontaneously occurring (black) and evoked (grey) LLCs plotted against the frequency of observations (Hz). Single Gaussian curves were fit to spontaneous (black) and evoked (grey) LLC histograms. r^2 indicates goodness of fit. (**B**) Quantification of the coefficient of variation (CV) of spontaneous and evoked LLC amplitudes in control (black) and occluded (orange) conditions. Each circle represents one cell. Error bars indicate SEM. ****., $p<0.0001$; n.s., non-significant.

4.2.4. OSN release probability is not impacted by 24h sensory deprivation

We next wanted to decipher the locus of the larger ETC LLC after 24 h naris occlusion. The evidence presented above suggests that LLCs may not be truly binary, as spontaneous and evoked LLC charges do not show a significant positive correlation when compared within neurons. In addition, evoked LLCs were larger than spontaneous LLCs recorded in the same cells, so perhaps the initial input received by ETCs may modulate the magnitude of the charge of the subsequent polysynaptic response. This initial input could arrive from release by OSNs. Perhaps, therefore, the pre-synaptic properties of these triggering inputs are changing with occlusion, resulting in the larger LLCs we observe. It has previously reported that OSNs can increase their P*r* after long-term (2 weeks) sensory deprivation (Tyler et al., 2007). Thus, we wondered whether OSNs were increasing their P*r* after 24h occlusion, which may be tied to our LLC phenotype.

Glomerular immunofluorescence for VGLUT2 at OSN terminals is not affected by occlusion

In the GL, OSNs strongly express VGLUT2 in their axons and synaptic terminals, and are the major source of VGLUT2 immunofluorescence within the glomerular neuropil (Gabellec et al., 2007). We therefore measured the fluorescence intensity of VGLUT2 staining in sham control and occluded fixed CCK-tdT OBs. This would indicate the level of VGLUT2 expression by OSNs which allowed us to observe whether the relative level of VGLUT2 protein in a glomerulus changes with occlusion (**Fig 4 Ai**).

To identify glomerular structures reliably, we used the nuclear marker NucRed, as cells in the GL are mostly located at glomerular boundaries. We then measured the normalised VGLUT2 fluorescence intensity of whole glomeruli. We performed 8 sets of experiments using 4 sham control and 7 occluded animals, where multiple samples were co-stained in the same co-embedded slice preparation to allow for appropriate standardisation and normalisation of staining intensity (see Methods, chapter 2). A total of 278 sham control and 277 occluded glomeruli were incorporated into the analysis. To take into account inter-set variability across our samples, we used multilevel ANOVA analyses, where normalised fluorescence values were compared between control and occluded samples, nested in set subjects (see methods). Data was normally distributed when fitted to a Gaussian distribution in MATLAB, where the variance of distribution accounted for by the best fit to the Gaussian function was 94.1%. This analysis revealed that occlusion did not have any effect on glomerular VGLUT2 fluorescence intensity

(**Fig 4 Aii**) (sham control normalised intensity, mean ± SEM 1 ± 0.02; occluded 0.99 ± 0.02; *multilevel ANOVA*, effect of treatment, $F_{(1, 430)} = 0.168$, p=0.682).

The powerful statistical analysis performed on these data demonstrates that relative VGLUT2 protein levels in glomeruli are not affected by occlusion.

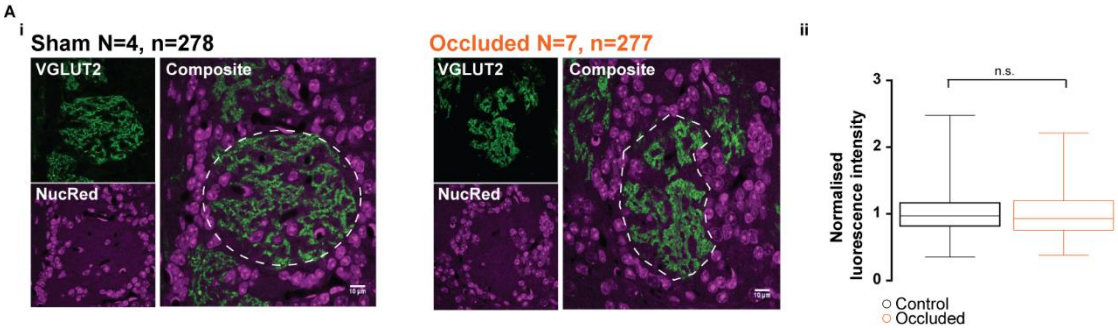

Fig 4. VGLUT2 expression in glomeruli is not affected by occlusion.

(**A**) Measuring VGLUT2 staining of glomeruli, a marker for pre-synaptic olfactory sensory neurons (OSNs) terminals. (**Ai**) Single-plane confocal images showing control and occluded glomeruli stained for VGLUT2. Slices were further incubated with the nuclear marker NucRed to aid the identification of glomerular borders. Glomeruli are outlined with white dotted lines, as seen in the composite image. (**Aii**) Quantification of normalised fluorescence intensity of VGLUT2 in control and occluded samples, taken from the entire area of the glomerulus that was imaged. Error bars indicate SEM. n.s., non-significant.

Functional approaches indicate that occlusion does not impact OSN P*r*

A functional measure that indirectly describes presynaptic release properties is the measurement of paired pulse ratio (PPR) in monosynaptic evoked post-synaptic inputs. This measurement has been used previously to show that OSN P*r* is surprisingly high, portrayed by the paired-pulse depression (PPD) recorded in monosynaptic responses of various JGCs (Murphy et al., 2004). We thus performed PPR protocols as a proxy measure of P*r* to observe whether occlusion has an effect on OSN P*r*.

We recorded PPR responses from ETCs in control and occluded conditions. We electrically stimulated OSNs at stimulation strengths eliciting a characteristic monosynaptic EPSC in ETCs patched in the whole-cell configuration and voltage clamped at -55mV (**Fig 5 Ai**). Two pulses were given 50ms apart to record paired-pulse responses. In an initial set of experiments, we recorded from 5 sham control, 29 unperturbed control, and 25 occluded ETCs in this way. 14 control and 11 occluded ETCs were recorded in CCK-tdT animals (**Fig 5 Bi**). As stated in the methods (chapter 2), we made the later decision to incorporate sham controls in our experiments as a more reliable control condition, and this experiment is the only one in this thesis that employs both control types. Additionally, shammed and unperturbed conditions only existed in the CCK-tdT group. There was no difference in OSN-evoked 50ms PPR between unperturbed and sham controls (sham control PPR mean ± SEM 0.48 ± 0.03; unperturbed control PPR 0.49 ± 0.05; *Mann-Whitney test*, p=0.80, data not shown).

In this first set of experiments, occlusion significantly decreased the PPR, which is indicative of OSN P*r* increasing (**Fig 5 Bii,** left) (control mean ± SEM 0.53 ± 0.02; occluded 0.41 ± 0.03; *Mann-Whitney test*, p=0.001). When taking a small but significant effect of genotype into account, occlusion still had this significant effect, and there was no significant effect of the interaction between the two factors (**Fig 5 Bii**, right; WT: control; mean ± SEM 0.57 ± 0.03; occluded; 0.43 ± 0.05; CCK-tdT: control; mean ± SEM 0.49 ± 0.03; occluded; 0.35 ± 0.03; *two-way ANOVA*, effect of treatment, $F_{(1,55)} = 13.72$, p=0.0005, effect of genotype, $F_{(1,55)} = 4.52$, p=0.04, interaction, $F_{(1,55)} = 0.0003$, p=0.99).

We next planned to establish whether OSN P*r* was intrinsically increasing, or whether presynaptic modulation by the glomerular inhibitory network was changing after 24h occlusion. Dopamine and GABA, released by inhibitory JGCs, strongly supress P*r* at OSNs via D_2-dopaminergic and $GABA_B$ receptors (Aroniadou-Anderjaska et al., 2000; Maher and Westbrook, 2008). Since occlusion has been shown to decrease TH expression and excitability in GABA/dopaminergic JGCs (D. Byrne, E. Galliano, unpublished data; Baker, 1990) we thought it

possible for these cells to exhibit less GABA and/or dopamine transmission to OSNs, which could result in the increased P*r* seen above after 24h sensory deprivation. Therefore, we performed a second set of experiments to measure PPR with the inclusion of several pharmacological agents (**Fig 5 Ci**). However, in this second set of experiments, even under identical conditions with standard ACSF, we could not reproduce our original occlusion effect on PPR (**Fig 4 Cii**) (sham control mean ± SEM 0.62 ± 0.04, *n=9* WT ETCs; occluded 0.58± 0.06, *n=6* WT ETCs; *Mann-Whitney test*, p=0.53).

Considering that VGLUT2 expression did not change with occlusion, and one set of experiments found no difference in PPR, these data suggest that OSN P*r* is not affected by short-term odour deprivation. However, since we obtained inconsistent results in our PPR data, we performed another set of experiments to measure OSN P*r* more directly. In this approach, we again electrically stimulated OSN fibres to induce monosynaptic evoked EPSCs in whole-cell voltage-clamped patched ETCs (**Fig 6 Ai**). Electrical stimulation then consisted of 20 pulses delivered at 50Hz (**Fig 6 Aii**). The recorded responses could then be quantified to calculate PPR from the first two responses, as well as direct measures of P*r* using two independent methods that estimate the size of the readily releasable pool from monosynaptic responses to high-frequency stimulus trains (Thanawala and Regehr, 2016). These methods are appropriate for estimating releasable pool size at the OSN synapse because vesicle replenishment is low and P*r* is high (Vaaga and Westbrook, 2017), and these methods produce an accurate estimate for synapses such as this (Thanawala and Regehr, 2016).

In total, we included reliably recorded responses in 11 sham control and 16 occluded WT ETCs in our analysis (**Fig 6 Bi**). We first measured the PPR from the first two EPSCs elicited in order to include a third experimental set to our PPR analysis. The amplitudes of EPSCs were calculated with the same method as in the initial PPR experiments, with the only difference being the inter-pulse interval, which was 20ms in this case. Occlusion again did not significantly affect the PPR (**Fig 6 Bii**) (sham control mean ± SEM 0.42 ± 0.03; occluded 0.43 ± 0.03; *Mann-Whitney test*, p=0.94). We then used two measures of calculating the size of the readily releasable pool in order to estimate P*r* from this stimulation protocol (**Fig 6 Biii-iv**). The Scheggenburger, Meyer, and Nehr (SMN) method plots the cumulative EPSC against stimulus number and then fits a line through the last 5 responses. The y-intercept indicates the total size of the readily releasable pool and the first EPSC is then divided by the readily releasable pool to obtain an estimate of P*r*. The Elmqvist-Quastal (EQ) method fits the fast EPSC amplitude against the cumulative EPSC amplitude and fits a line to the first 3 EPSCs to calculate the readily releasable pool at the x-intercept. P*r* is then calculated the same way as for the SMN method. Both measures were used in order to provide independent routes to the same measurement of P*r*, derived from different

underlying assumptions. We would then expect the final calculations to converge on a common output. In our cells, the SMN method seemed to estimate higher OSN P*r* (**Fig 6 Biii**) than the EQ method (**Fig 6 Biv**), and both methods estimate Pr to be much lower than other estimates previously reported for this synapse (Murphy et al., 2004; Tyler et al., 2007; Vaaga and Westbrook, 2017). However, compared to previous studies, we did not include the use of $GABA_B$ and D_2-Dopamine receptor blockers which may explain this discrepancy. The two methods revealed a positive, though not significant, correlation of P*r* estimation (*Pearson's correlation*, p=0.14, *r*=0.47, data not shown). However both estimates converged on the same result - occlusion did not significantly affect estimated OSN P*r* (**Fig 6 Biii-Biv**) (SMN: sham control P*r* mean ± SEM 0.64 ± 0.04; occluded P*r* 0.58 ± 0.02; *unpaired t-test*, $t_{(25)}$ = 1.39, p=0.18; EQ: sham control P*r* mean ± SEM 0.49 ± 0.02; occluded P*r* 0.48 ± 0.02, *unpaired t-test*, $t_{(25)}$ = 0.53, p=0.59).

Having taken multiple measures to estimate OSN P*r*, or indirectly quantifying indicators of pre-synaptic properties, we conclude overall that short-term sensory deprivation does not affect P*r* at sensory neuron inputs to ETCs. The LLC phenotype we observe in occlusion therefore, does not seem to be due to changes in OSN input properties.

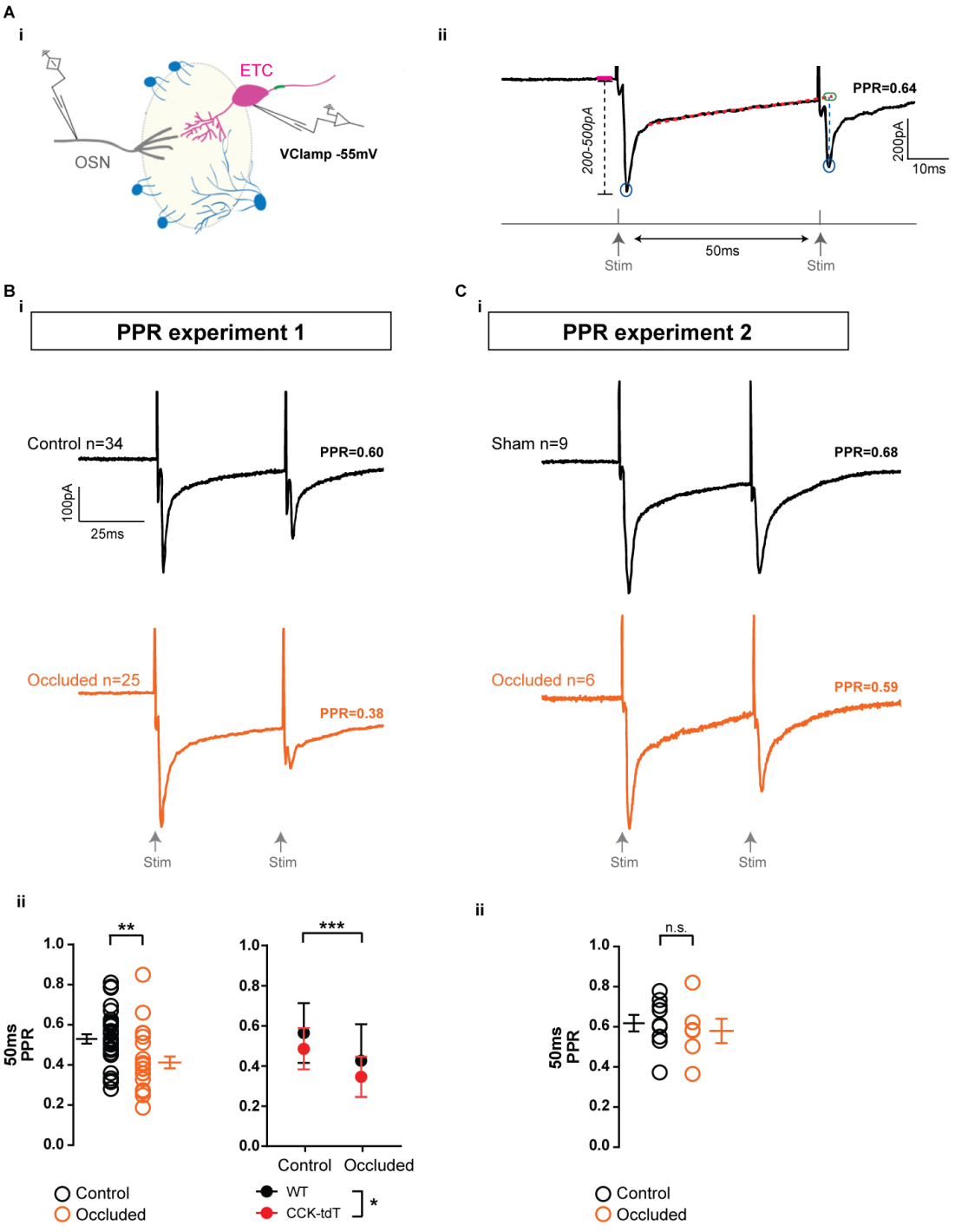
A
i
ETC
OSN
VClamp -55mV
ii
200-500pA
PPR=0.64
200pA
10ms
50ms
Stim
Stim
B
i
PPR experiment 1
Control n=34
PPR=0.60
100pA
25ms
Occluded n=25
PPR=0.38
Stim
Stim
C
i
PPR experiment 2
Sham n=9
PPR=0.68
Occluded n=6
PPR=0.59
Stim
Stim
ii
50ms PPR
**
***
Control
Occluded
WT
CCK-tdT
*
ii
50ms PPR
n.s.
Control
Occluded

Fig 5. Inconsistent results on paired pulse ratio (PPR), an indicator of release probability in olfactory sensory neuron (OSN) inputs.

(**A**) Protocol for obtaining PPR measures. (**Ai**) OSNs were electrically stimulated to evoke monosynaptic responses in whole-cell patched external tufted cells (ETCs), clamped at -55mV. (**Aii**) Two pulses were given with an inter-stimulus interval of 50ms. 1 minute was given between pulse trains. For responses to be included in the subsequent analysis, the first monosynaptic EPSC needed to be between 200-500pA in amplitude (dotted grey line). The first EPSC was measured from baseline, demarcated with a magenta line, to its peak (blue circle). A linear line was fitted from the decay of the first EPSC and extrapolated to the peak time of the second EPSC (red dotted line) to estimate the approximate baseline from which to calculate the second EPSC (green circle). The amplitude of the second EPSC was calculated from this estimated baseline to its peak (blue circle). To obtain a PPR measure, the amplitude of the second EPSC was divided by the first. (**B-C**) PPRs obtained from recordings several months apart. Each circle represents one cell. Error bars indicate SEM. (**Bi**) Example traces from control an occluded ETCs in a first set of experiments. (**Bii**) Left: quantification of PPR recordings obtained from a mix of WT and CCK-tdT animals. Each circle represents one cell. Error bars indicate SEM. Right: plot displaying the effect of genotype in this analysis. Error bars indicate SEM. (**Ci**) Example traces and quantification of PPR recordings from control and occluded WT ETCs in a second set of experiments, performed a few months after the first. (**Cii**) Quantification of PPR recordings obtained from second PPR experiment. Each circle represents one cell. Error bars indicate SEM. **., $p<0.01$; ***., $p<0.001$; n.s., non-significant.

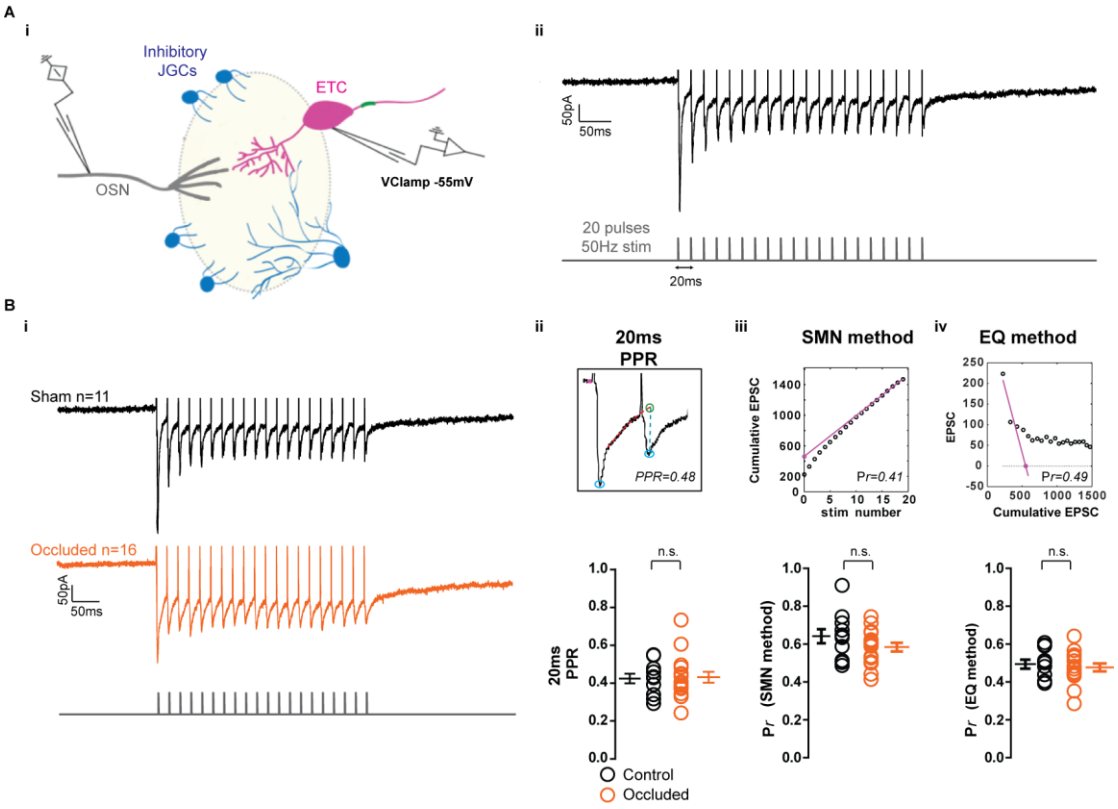

Fig 6. Olfactory sensory neuron (OSN) release probability (Pr) does not change after 24h occlusion.

(**A**) Protocol for obtaining P*r* measures. (**Ai**) OSNs were electrically stimulated to produce monosynaptic responses in whole-cell patched external tufted cells (ETCs) clamped at -55mV. (**Aii**) ETCs were patched whole-cell to record EPSCs in response to OSN stimulation (top). Trains of 20 electrical pulses were given to OSNs at 50Hz, with an inter-trace interval of 1 minute (bottom). (**B**) Obtaining measures of paired pulse ratio (PPR) and P*r* from stimulation trains. (**Bi**) Control and occluded ETCs responded to 50Hz OSN stimulation with monosynaptic EPSCs. (**Bii**) PPR was calculated from the first two OSN stimulation responses (with an inter-pulse interval of 20ms). Top: PPR measures were obtained by dividing the amplitude of the second EPSC by the first EPSP. The first EPSC amplitude was calculated from the baseline recording (magenta line, left) to its peak (blue circle). A linear line was fitted from the decay of the first EPSC (red dotted line) and extrapolated to the peak time of the second EPSC to estimate the baseline of the second EPSC (green circle). The amplitude of the second EPSC was calculated from its peak (blue circle, right) to the estimated baseline. Bottom: quantification of PPR. Each circle represents one cell. Error bars indicate SEM. (**Biii**) Size of the readily releasable pool calculation based on the Schneggenburger, Meyer, and Neher (SMN) method. Top: cumulative EPSC amplitude was fitted against stimulus number, fit by a line through the last 5 EPSCs. The readily releasable pool was calculated by the y-intercept of this linear fit. The first EPSC was then divided by the readily releasable pool to estimate P*r*. Bottom: Quantification of P*r* using the SMN method. Each circle represents one cell. Error bars indicate SEM. (**Biv**) Size of the readily releasable pool calculation based on the Elmqvist-Quastal (EQ) method. Top: the fast EPSC amplitude was fitted against the cumulative EPSC amplitude. A line was fit to the first 3 EPSCs to calculate the size of the readily releasable pool, the x-intercept. P*r* was calculated with the same method as in the SMN method. Bottom: quantification of P*r* using the EQ method. Each circle represents one cell. Error bars indicate SEM. n.s., non-significant.

4.2.5. VGLUT1 glomerular protein density is not affected by occlusion

Since OSN P*r* is unlikely contributing to the LLC phenotype we see in occlusion, we next sought to explore whether intraglomerular dendro-dendritic recurrent excitation could be the mechanism by which this increase occurs.

We first began our exploration with an indirect method of quantifying recurrent excitation in whole glomeruli. The expression of VGLUT1 in glomeruli is localised to presynaptic glutamatergic terminals from ETCs and M/TCs (Gabellec et al., 2007; Tatti et al., 2014). It has previously been shown that two weeks of sensory deprivation resulted in increased VGLUT1 expression in glomeruli, a phenotype tied to quantal scaling of AMPA and NMDA receptors in JGCs (Tyler et al., 2007). Thus, we explored the possibility of 24h occlusion also resulting in an increase of VGLUT1 glomerular expression.

We performed immunohistochemistry on fixed sham control and occluded CCK-tdT OBs to compare the fluorescence intensity of VGLUT1 in whole glomeruli. NucRed was again employed to aid the identification of glomerular borders (**Fig 7 Ai;** see **Fig 4**, VGLUT2). A total of 438 control and 426 occluded glomeruli were quantified for VGLUT1 fluorescence intensity from 7 sham control and 11 occluded animals in 13 sets of co-stained samples that always included a sham control sample. We again performed a powerful multilevel statistical analysis to take the set variable into account. Data was normally distributed when fitted to a Gaussian distribution in MATLAB, where the variance of distribution accounted for by the best fit to the Gaussian function was 98.6%. Using this analysis, we found that there was significant variation across sets of experiments, however occlusion had no effect on normalised VGLUT1 fluorescence intensity (**Fig 7B**) (sham control mean ± SEM 1.00 ± 0.02; occluded 1.04 ± 0.03; *multilevel ANOVA*, effect of treatment, $F_{(1, 665)} = 2.61$, p=0.12).

These results suggest occlusion does not impact glomerular VGLUT1 expression, which implies that excitatory presynaptic properties may not be adjusted with this short-term manipulation.

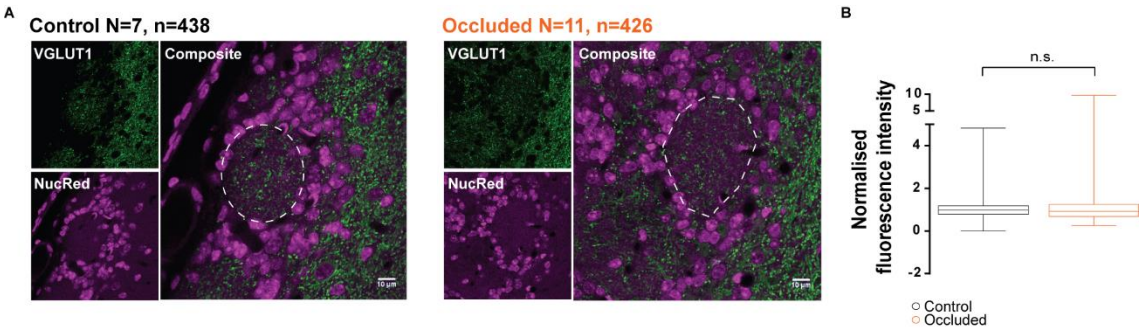

Fig 7. Glomerular VGLUT1 expression does not change with occlusion.

(**A**) Single-plane confocal images of control (left three panels) and occluded (right three panels) glomeruli stained against VGLUT1, a marker of post-synaptic excitatory terminals in glomeruli. Olfactory bulb slices were further incubated with NucRed to aid in the identification of glomeruli. Dotted line in the composite images show the boundaries of glomeruli. (**B**) Quantification of VGLUT1 normalised fluorescence intensity taken from whole-glomeruli images. Error bars indicate SEM. n.s., non-significant.

4.2.6. Auto-evoked recurrent excitation is not affected by occlusion

Increasing VGLUT1 protein density is not the only way synapses can increase recurrent excitation, and only shines light on one, out of many, possible mechanisms in which this could occur. We thus continued our investigation using a functional approach. Previous studies on ETC and M/TC recurrent excitation have demonstrated a paradigm in which auto-evoked glutamatergic potentials can be measured as a proxy for recurrent excitation (De Saint Jan et al., 2009; Ma and Lowe, 2007). When an ETC is driven to spike, it will release glutamate, which in turn will activate other excitatory cells, presumably through glutamate spillover at ETC-JGC synapses (Gire et al., 2018). The neighbouring cells will then release glutamate that may act on the initial cell (**Fig 8 Ai**). Additionally, it is possible for glutamate released from an ETC to act upon the same cell, as self-evoked excitation has been reported on ETCs (Ma and Lowe, 2007). We thus quantified auto-evoked recurrent excitation through ETCs in sham control and occluded conditions. Cells were patched whole-cell in current clamp in order to record glutamatergic tail potentials. Two spikes were initiated with a large depolarising current pulse (800pA), 50ms apart (**Fig 8 Bii**). Spikes were initiated to induce glutamate release from the recorded cell. This caused a voltage rebound following each spike, indicative of the glutamatergic tail potential. To avoid glutamate rundown due to consecutive depolarisation steps (De Saint Jan et al., 2009), we included 10mM glutamate in our internal solution. Additionally, due to the high contribution of NMDA-mediate currents to these potentials, we excluded Mg^{2+} in our recording solution to maximise tail potential observations. Upon initial experiments, we patched ETCs with a holding potential of - 55mV as in all our other experiments. With this holding potential, we could clearly observe tail potentials following spikes (**Fig 8 Bi,** left). However, following wash-in of NBQX+APV, these potentials were not completely eliminated (**Fig 8 Bi**, right) suggesting that another current, possibly Ca^{2+} (Ma and Lowe, 2007), is contributing to the response at this voltage. We wanted to obtain a purer measure of the glutamatergic potential, thus we trialled several holding potentials and found that - 65mV produced reliable evoked responses that were mostly eliminated with NBQX and APV (**Fig 8 Bii**).

In an ideal scenario, tail potentials would then be quantified by measuring the amplitude of the tail potentials from the baseline established by NBQX+APV elimination (**Fig 8B**). However, reliably washing in pharmacological agents resulted in very few cells recorded that could be used for analysis. We thus performed a trial analysis from recordings obtained from 6 cells where both baseline and NBQX/APV recordings were made. This analysis was then used to estimate a time point at which we could quantify tail potentials in recorded cells where NBQX/APV wash-

in was unsuccessful. We first measured tail potentials after 20, 30, 40, and 50ms of each spike from baseline measures (**Fig 9 Ai**). We then measured tail potentials at the same time points following NBQX/APV wash-in (**Fig 9 Aii**). We could then subtract the initial response from the NBQX/APV response at the same time point (**Fig 9 Aiii**) and calculate the percentage of the initial response that was due to glutamate at that time point post-spike, for all time points measured. From this analysis, we found that almost all of the potential is glutamatergic 30ms after each spike (**Fig 9 Aiii**, right). We thus used this information to analyse subsequent recordings in which pharmacological wash-in was not successful, but initial tail potentials were reliably recorded in ACSF external, by measuring base-to-peak amplitudes 30ms after each spike.

In total, we obtained reliable recordings from 14 sham control and 14 occluded CCK-tdT ETCs (**Fig 9 Bi**). Interestingly, in our recordings the two elicited tail potentials displayed paired-pulse facilitation, rather than depression as previously reported (De Saint Jan et al., 2009). Our analysis further revealed that tail potentials were becoming slightly, but not significantly, smaller with occlusion (**Fig 9 Bii**) (Peak 1: sham control; mean ± SEM 1.42 ± 0.33mV; occluded 1.13 ± 0.45mV; *Mann-Whitney test*, p=0.08; Peak 2: sham control; mean ± SEM 2.85 ± 0.85mV; occluded 1.41 ± 0.27mV; *Mann-Whitey test,* p=0.29). We further quantified the PPR of the tail potential as a proxy of whether P*r* was increasing in the glomerular excitatory network after occlusion. PPR was calculated by dividing the Peak 2 amplitude by Peak 1 amplitude. Nevertheless, occlusion did not significantly impact PPR (**Fig 9 Bii**, right) (sham control PPR mean ± SEM 2.17 ± 0.37mV; occluded PPR 2.48 ± 0.68mV; *Mann-Whitney test*, p=0.80).

These data suggest that recurrent excitation triggered by ETC glutamate release is not impacted by short-term occlusion.

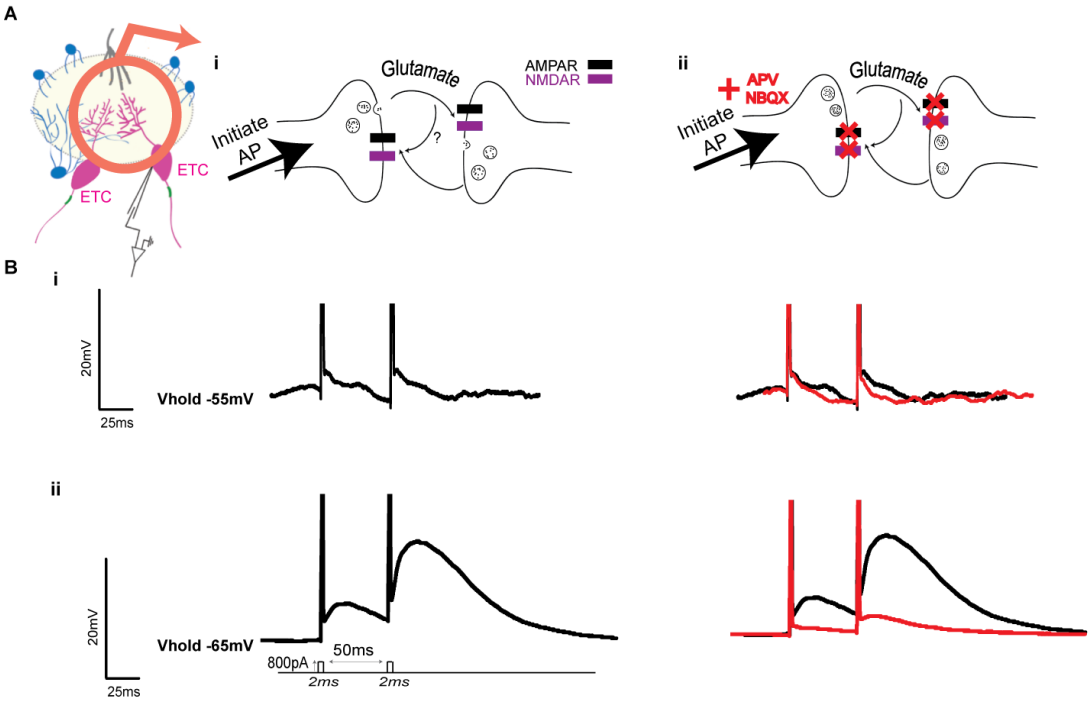

Fig 8. External tufted cell (ETC) auto-evoked recurrent excitation at different holding potentials.

(**A**) Diagrams showing experimental paradigm. Multiple ETCs may be involved in glomerular recurrent excitation and one ETC was patched to obtain a readout of this. Due to the large contribution of NMDA-mediated currents to this phenomenon, the recording solution contained no Mg^{2+} (**Ai**) Two action potentials were initiated to trigger release of glutamate from the patched cell. This release can act on neighbouring ETC dendrites that may further release glutamate back to the original cell. Glutamate released from the patched cell may also potentially act on the same cell. (**Aii**) In order to quantify the amount of recurrent excitation occurring, glutamatergic signalling was blocked with 50µm APV and 10µm NBQX after obtaining a baseline measure. AMPAR, AMPA receptor; NMDAR, NMDA receptor. (**B**) Optimising the recording protocol. (**Bi**) Two spikes were initiated 50ms apart with a 2ms duration 800pA current injection in current clamp. The aim was to quantify auto-evoked recurrent glutamatergic tail potentials that occurred immediately after each spike. When cells were held at -55mV, tail potentials were evident (left), however NBQX and APV did not completely block these responses (right), suggesting that these are not recurrent glutamatergic potentials. (**Bii**) Cells held at -65mV showed tail potentials (left) that were largely eliminated with NBQX and APV (right). We thus used a holding potential of -65mV to record these responses in control and occluded conditions.

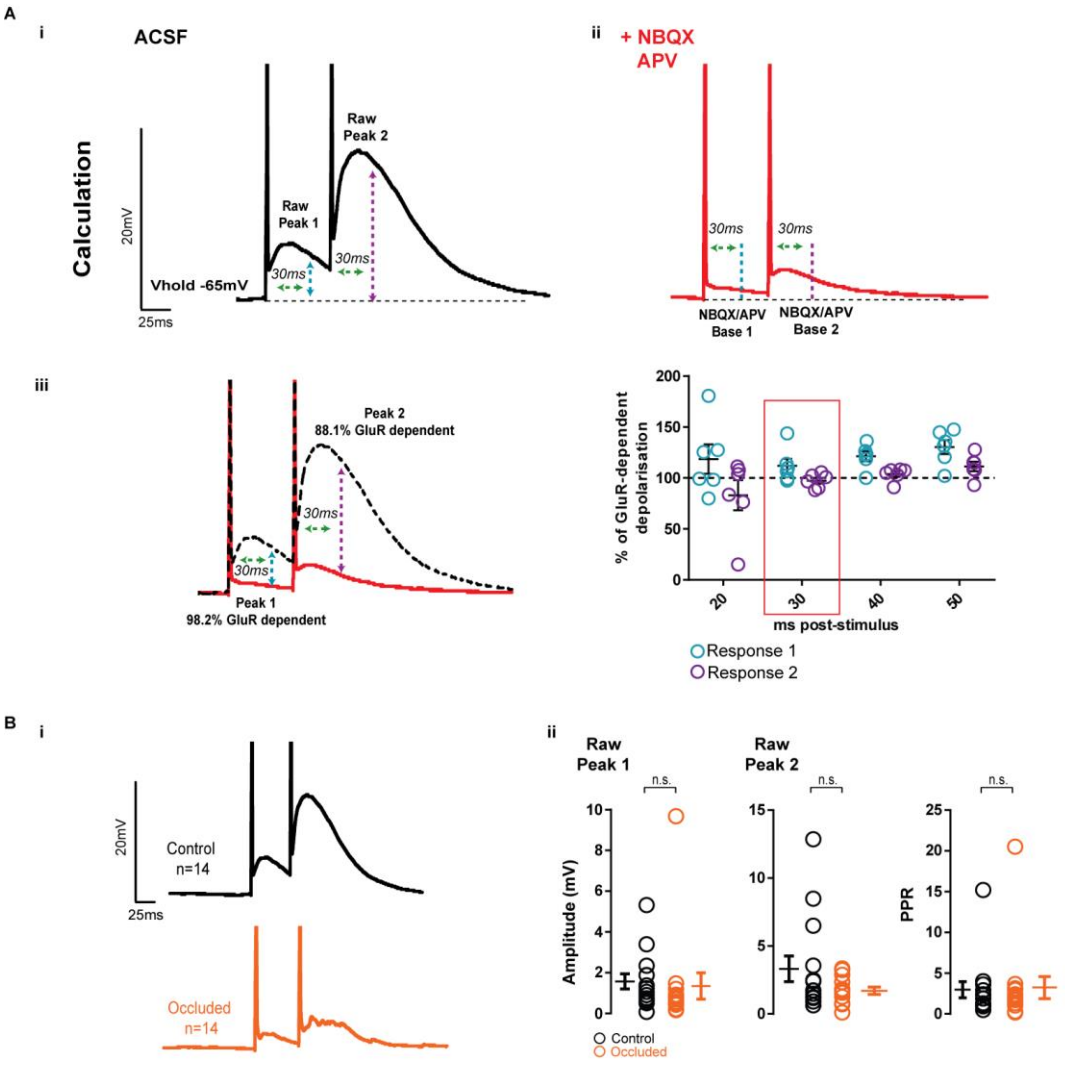

Fig 9. External tufted cell (ETC) auto-evoked recurrent excitation is not affected by occlusion.

(**A**) Calculation of tail potential peaks. (**Ai**) Peak tail potentials in ACSF were measured 30ms after spike onset for both peaks from baseline. (**Aii**) Tail potentials were mostly eliminated with NBQX and APV after 30ms post-spike. (**Aiii**) A trial analysis using cells where both ACSF baseline and NBQX/APV baselines were recorded revealed that at 30ms post-stimulus, most of the glutamatergic (GluR) dependent depolarisation was eliminated with NBQX and APV. Plot shows % of GluR elimination at different times post-stimulus. This time point was used for subsequent analyses of peak-to-base measures in cells where wash-in of drugs was unsuccessful. (**B**) Quantifying auto-evoked recurrent excitation in control and occluded ETCs. (**Bi**) Example traces showing control and occluded ETC recordings with glutamatergic tail potentials. (**Bii**) Quantification of tail potential amplitudes (peak 1 and peak 2) measured 30ms post-stimulus in ACSF traces. Paired pulse ratio (PPR) was calculated by dividing the second peak by the first. Each circle represents one cell. Error bars indicate SEM. n.s., non-significant.

4.2.7. M/TC LLCs are built up differently to ETC LLCs

During our investigation of what might be causing the LLC phenotype in occlusion, we did not find evidence for presynaptic changes in OSNs or changes in ETC-evoked recurrent excitation contributing to this phenotype. It has previously been shown that M/TC dendrodendritic amplification of excitatory signal is greater than in ETCs. The much larger M/TC LLC magnitude was shown to be underlying this effect (Vaaga and Westbrook, 2017). Though we could not decipher what underlies the LLC change, it is likely that M/TC LLCs are built up from multiple ETC LLC subnetworks (De Saint Jan et al., 2009; Gire et al., 2012; Najac et al., 2011). Thus, we were next interested in observing whether occlusion had an effect on M/TC LLCs.

In initial experiments, we electrically stimulated OSNs in order to evoke LLCs recorded in whole-cell patched M/TCs clamped at - 55mV (**Fig 10 B**). Interestingly, in 10 out of 24 total sham control and occluded M/TCs, recorded LLCs were not binary, all-or-nothing events (**Fig 10 B**), contrary to previous reports (Carlson et al., 2000; Gire and Schoppa, 2009). In these cells, evoked LLCs occurred with clear two- to three magnitude levels when OSNs were stimulated at the same threshold intensity. ETCs on the other hand, responded with near identical LLC magnitudes when evoked at threshold in all cases (**Fig 10 A**). Additionally, spontaneously recorded M/TC LLCs were much larger compared to ETC LLCs. Their amplitudes were significantly larger, and their charge was trending towards being higher compared to ETC LLCs. This corresponds with previous findings that M/TCs portray comparatively more dendrodendritic amplification of excitatory signal (Vaaga and Westbrook, 2017) (Amplitude: M/TC sham control mean ± SEM 111.6 ± 20.39pA, n=9; ETC control 49.95 ± 4.48pA, n=17; *unpaired t-test*, $t_{(24)}$ = 3.90, p=0.0007; Charge: M/TC sham control mean ± SEM 22.67 ± 5.26pC, n=9; ETC control 10.83 ± 1.24, n=17pC; *unpaired t-test* using Welch's correction, $t_{(8.89)}$ = 2.19, p=0.06; data not shown). We further performed histogram style analysis on spontaneous and evoked M/TC LLC median-normalised amplitudes as previously done for ETC LLCs (**Fig 3**) to determine the quantal nature of M/TC LLCs to support the notion that M/TC LLCs are not binary as previously thought. Plotting Gaussian curves to the resulting histograms reveals that most M/TC LLCs per cell are centred around 1 both in spontaneous and evoked recording conditions, with curves between both recording conditions heavily overlapping (**Fig 10C**) (goodness of fit; spontaneous LLCs, r^2=0.84, evoked LLCs, r^2=0.89).

This is indicative of the binary nature of LLCs in general, however we further wished to observe whether M/TC LLCs portray higher variability in their amplitudes compared to ETCs, as this would indicate that whereas ETC LLCs are all-or-nothing events when evoked "fully" (i.e. OSN stimulation), M/TC LLCs are built up of multiple pools of excitatory signal. We again employed

CV analysis of per-cell LLC amplitudes. We first checked for occlusion effects on the variability of LLC amplitudes in M/TCs (**Fig 10D**). As in ETCs, occlusion had no effect on the variability of M/TC LLC amplitudes. As expected, and in contrast to ETCs, M/TC evoked LLCs were as variable in their amplitudes as spontaneous M/TCs LLCs, indicating the non-binary nature of M/TC LLC magnitudes (control: spontaneous, mean ± SEM 0.51 ± 0.10; evoked, 0.41 ± 0.05; Occluded: spontaneous, mean ± SEM 0.42 ± 0.06; evoked, 0.41 ± 0.07; *two-way ANOVA,* effect of stimulus type, $F_{(1,38)}$=0.63, p=0.43, effect of treatment, $F_{(1,38)}$=0.54, *p*=0.53, *interaction,* $F_{(1,38)}$=0.51, *p*=0.48). To explore whether M/TC LLC magnitudes are more variable than ETC LLCs, and thus supporting the notion that M/TC LLCs are built up if multiple "pools" of excitatory signal, we compared LLC amplitude CV values between all ETCs and M/TCs where spontaneous and evoked LLCs were recorded (**Fig 10E**). This analysis revealed a strong effect of spontaneous vs evoked LLC magnitudes, where ETC evoked LLCs had significantly more stereotyped amplitudes as compared to both spontaneous and evoked M/TC LLC magnitudes (*two-way ANOVA on sqrt-transformed values*, effect of stimulus type, $F_{(1,112)}$=11.42, p=0.001, effect of cell-type, $F_{(1,112)}$=21.96, p<0.0001, interaction, $F_{(1,112)}$=7.31, *p*=0.007). This further demonstrates that when the presumably entirety of the glomerular excitatory network is stimulated, ETC LLC magnitudes are binary, whereas M/TC LLC magnitudes show a non-binary, non-stereotyped phenotype, likely due to the multi-step build up of the M/TC LLC.

Therefore, due to their larger size, and their apparently non-binary nature, M/TC LLCs appear to be built up in a different way to ETC LLCs. These data support the hypothesis that multiple separate ETC LLC subnetworks feed into M/TC LLC responses.

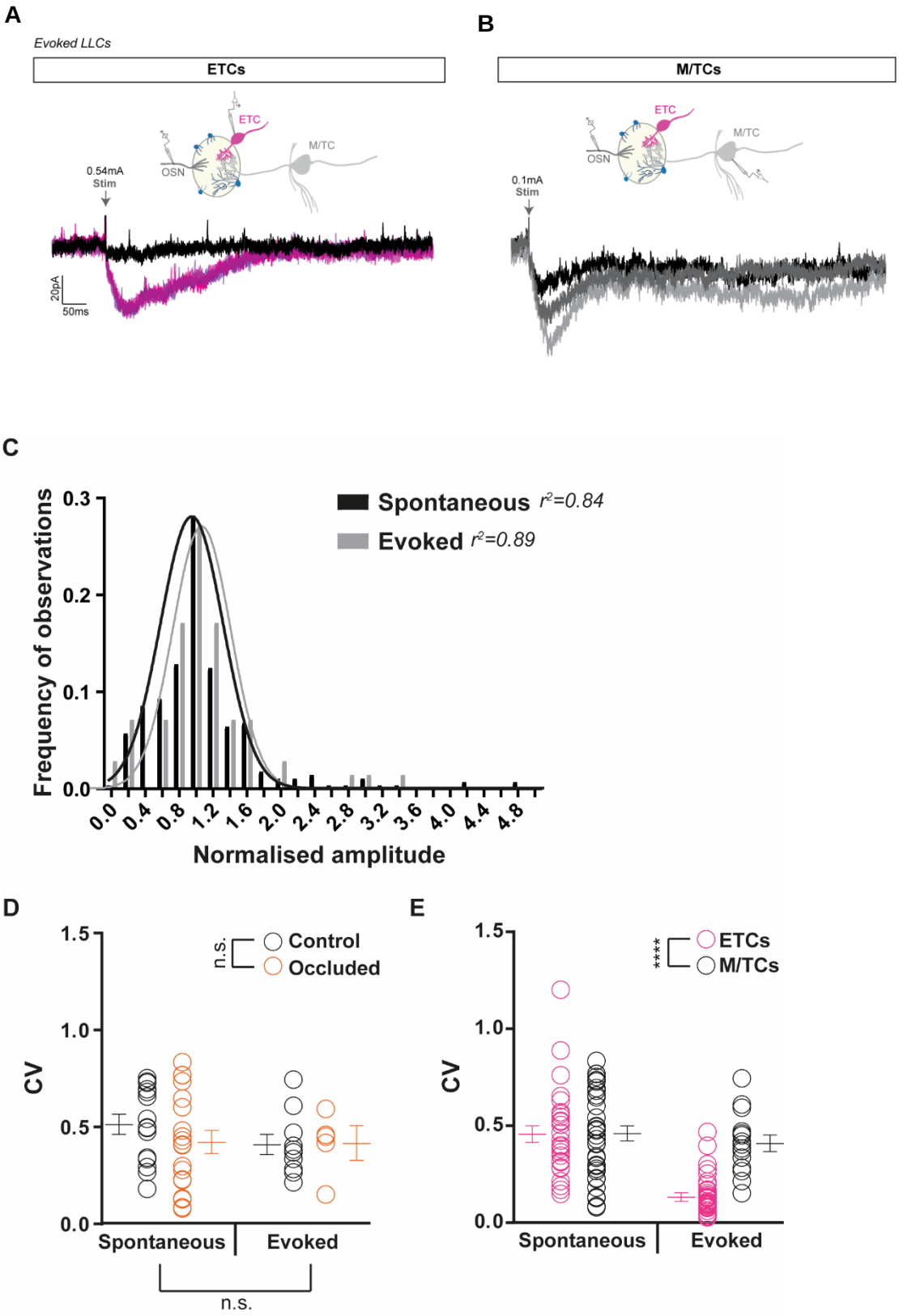
A
Evoked LLCs
ETCs
ETC
M/TC
OSN
0.54mA
Stim
20pA
50ms
B
M/TCs
ETC
M/TC
OSN
0.1mA
Stim
C
Spontaneous r²=0.84
Evoked r²=0.89
Frequency of observations
0.0
0.1
0.2
0.3
0.0 0.4 0.8 1.2 1.6 2.0 2.4 2.8 3.2 3.6 4.0 4.4 4.8
Normalised amplitude
D
n.s.
Control
Occluded
CV
1.5
1.0
0.5
0.0
Spontaneous
Evoked
n.s.
E
****
ETCs
M/TCs
CV
1.5
1.0
0.5
0.0
Spontaneous
Evoked

Fig 10. Mitral/tufted cell (M/TC) long-lasting depolarising currents (LLCs) are different to external tufted cell (ETC) LLCs.

(**A**) ETCs portray classic all-or-nothing LLC at perithreshold stimulus intensities. Example trace shows multiple sweeps from the same recording. Black trace indicates a null-response, shades of pink represent evoked LLCs. (**B**) M/TC LLCs do not portray the all-or-nothing LLC. At the same stimulus intensity, M/TCs can exhibit multiple LLC magnitudes. Example trace shows multiple sweeps from the same recording. Different shades of grey indicate different size evoked LLCs. (**C**) Histograms of all median-normalised amplitudes (pA) of spontaneously occurring (black) and evoked (grey) M/TC LLCs plotted against the frequency of observations (Hz). Single Gaussian curves were fit to spontaneous (black) and evoked (grey) LLC histograms. r^2 indicates goodness of fit. (**D**) Quantification of the coefficient of variation (CV) of spontaneous and evoked LLC amplitudes in control (black) and occluded (orange) conditions. Each circle represents one cell. Error bars indicate SEM. (**E**) Comparison of CV values of spontaneous and evoked LLC amplitudes between ETCs (magenta) and M/TCs (black).****., $p<0.0001$; n.s., non-significant.

4.2.8. M/TC LLCs become larger with occlusion under certain conditions

Analysing evoked LLCs in M/TCs proved to be a technical challenge due to the multi-level nature of the M/TC LLC in certain, but not all, cells. It was thus difficult to interpret which of the multi-level LLC responses to include in our comparison. Additionally, finding the right location to electrically stimulate OSNs to evoke an LLC in M/TCs was further technically challenging. Since we observed an ETC LLC phenotype in spontaneous recordings, we therefore decided to characterise LLCs in M/TCs with this method instead, where cells were whole-cell patched and clamped at - 55mV, in the presence of PTX.

We recorded from 9 sham control and 12 occluded M/TCs, and both control and occluded M/TCs portrayed spontaneously occurring LLCs (**Fig 11 Ai**). Occlusion did not impact the frequency of LLCs (sham control; mean ± SEM 0.15 ± 0.07Hz; occluded 0.13 ± 0.02Hz; *Mann-Whitney test*, p=0.33, data not shown). Furthermore, occlusion slightly, but not significantly, increased M/TC LLC charge and had no effect on LLC amplitude (**Fig 11 Aii**) (Amplitude: sham control mean ± SEM 111.60 ± 20.39pA; occluded 113.80 ± 19.53pA; *unpaired t-test* on $\log_{10}$ transformed values, $t_{(19)} = 0.11$, p=0.92; Charge: sham control mean ± SEM 22.67 ± 5.26pC; occluded ± SEM 27.62 ± 5.12pC; *unpaired t-test on* $\log_{10}$ transformed values, $t_{(19)} = 0.89$, p=0.39).

Since $GABA_A$ currents are known to reduce the amplitude of LLCs in M/TCs (Carlson et al., 2000), perhaps M/TC spontaneous LLC magnitudes were reaching a ceiling level due to the block of $GABA_A$ currents when recording in PTX. If M/TCs were driven to become large due to PTX, they may not have been able to increase their magnitude any further, and this may thus have concealed any occlusion effect. Due to this possibility, we performed another set of whole-cell voltage clamped M/TC recordings to record M/TC LLCs in regular ACSF, thus keeping $GABA_A$ signalling intact, in order to avoid this potential ceiling effect. In total, we recorded from 14 sham control and 12 occluded M/TCs in this way.

Under these conditions, LLCs were still spontaneously generated in both control and occluded conditions (**Fig 11 Bi**), however LLC frequency, though not different between treatment groups, was lower than when recorded in PTX (sham control; mean ± SEM 0.08 ± 0.03Hz; occluded 0.08 ± 0.04Hz; *Mann-Whitney test*, p=0.76, data not shown). In terms of LLC magnitude, occlusion had a significant effect on both M/TC amplitude and charge under these recording conditions (**Fig 11 Bii**) (Amplitude: sham control mean ± SEM 56.37 ± 8.48pA; occluded 86.6 ± 14.51pA; *unpaired t-test* on $\log_{10}$ transformed values, $t_{(24)} = 2.29$, p=0.03; Charge: sham control mean ± SEM 7.45 ± 1.55pC; occluded ± SEM 19.68 ± 3.48pC; *unpaired t-test on* sqrt transformed values, $t_{(24)} = 3.72$, p=0.001). These data further support the notion that the inclusion of PTX in the recording solution drove M/TC LLCs to ceiling levels, as LLCs recorded in PTX reached similar

charges and amplitudes observed in ACSF-recorded occluded M/TC LLCs, whereas ACSF-recorded sham control M/TC LLCs were much smaller in comparison (**Fig 11 Bii**, dotted error bars).

To elucidate whether an enhanced synaptic drive onto M/TCs contributes to the larger LLC magnitudes we see in occlusion in ACSF, we further recorded spontaneous excitatory postsynaptic currents (sEPSCs) in sham and occluded M/TCs both in ACSF as well as in the presence of PTX (**Fig 11 Ci, Di**). Comparing the cell-average sEPSC amplitude and frequency, we did not observe a significance in these parameters either in ACSF or in ACSF+PTX between sham control and occluded conditions (ACSF: Amplitude: sham control mean ± SEM 24.81 ± 2.84pA; occluded 26.69 ± 2.58pA; *unpaired t-test*, $t_{(20)}$ = 0.49, p=0.63; Frequency: sham control mean ± SEM 0.04 ± 0.02Hz; occluded ± SEM 0.19 ± 0.12Hz; *Mann-Whitney test*, p=0.25. ACSF+PTX: Amplitude: sham control mean ± SEM 20.74 ± 2.17pA; occluded 21.26 ± 1.65pA; *unpaired t-test*, $t_{(20)}$ = 0.19, p=0.85; Frequency: sham control mean ± SEM 0.14 ± 0.03Hz; occluded ± SEM 0.10 ± 0.04Hz; *Mann-Whitney test*, p=0.45). Nevertheless, other synaptic blockers to observe individual vesicle release events were not included in the recording solution, therefore it is difficult to conclusively state whether or not a change in synaptic drive occurred.

These data suggest that M/TC LLCs are also becoming larger with occlusion, an effect precluded by the likely ceiling effect of PTX inclusion, but strongly evident in ACSF recordings. Therefore, our findings so far suggest that increases in ETC LLC magnitudes are associated with increases in M/TC LLC magnitude, and are consistent with the notion that the M/TC LLC is built up from multiple ETC LLC responses.

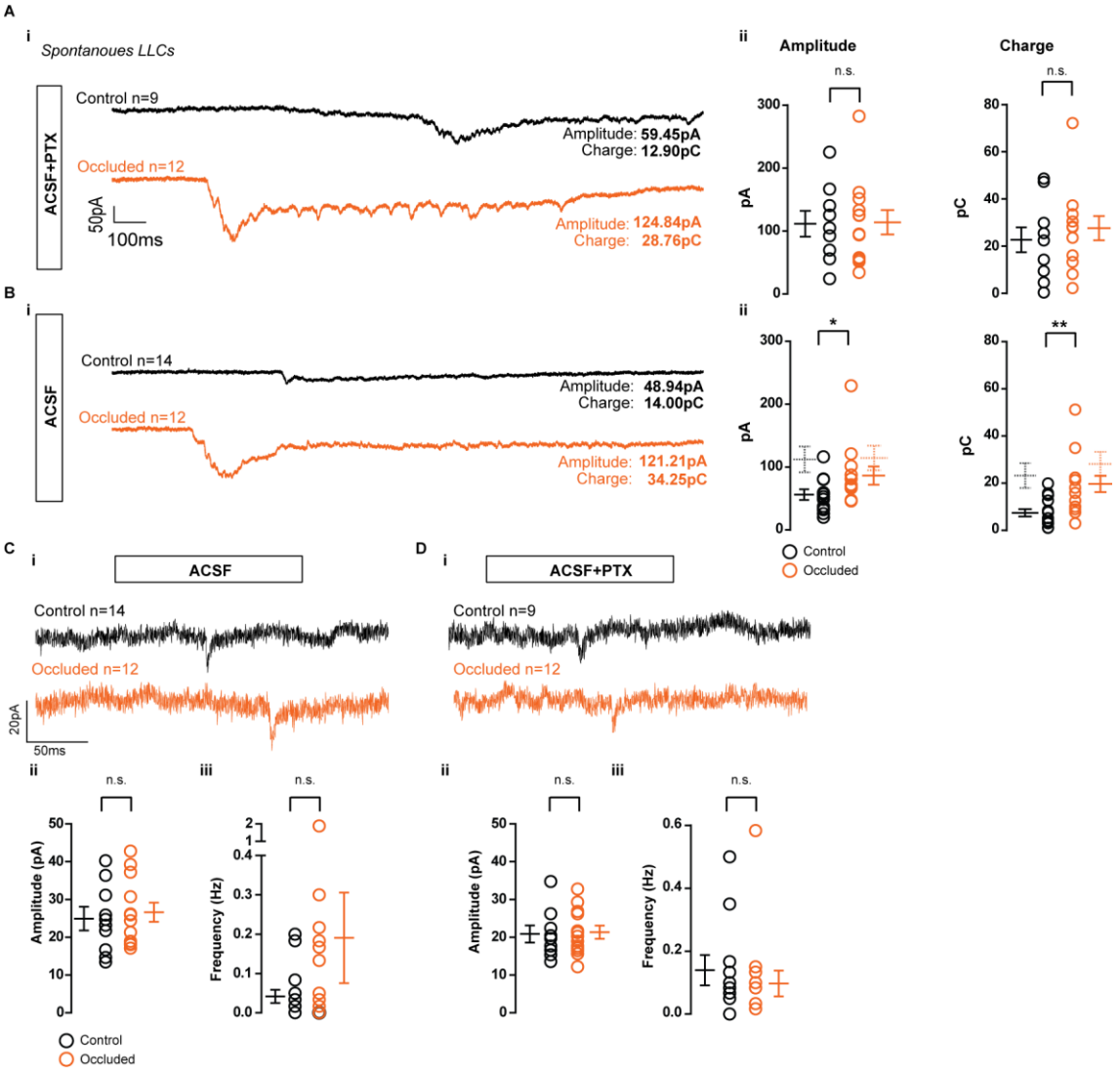
A
i
Spontanoues LLCs
ACSF+PTX
Control n=9
Amplitude: 59.45pA
Charge: 12.90pC
Occluded n=12
Amplitude: 124.84pA
Charge: 28.76pC
50pA
100ms
ii
Amplitude
Charge
n.s.
pA
pC
B
i
ACSF
Control n=14
Amplitude: 48.94pA
Charge: 14.00pC
Occluded n=12
Amplitude: 121.21pA
Charge: 34.25pC
ii
*
**
Control
Occluded
C
i
ACSF
Control n=14
Occluded n=12
20pA
50ms
ii
iii
Amplitude (pA)
Frequency (Hz)
Control
Occluded
D
i
ACSF+PTX
Control n=9
Occluded n=12
ii
iii

Fig 11. Mitral/Tufted cell (M/TC) long-lasting depolarising currents (LLCs) become larger with occlusion under certain conditions.

(**A**) Spontaneous M/TC LLCs are not affected by occlusion in the presence of 10μm picrotoxin (PTX). (**Ai**) Example traces of control and occluded spontaneous M/TC LLCs. (**Aii**) Quantification of amplitude (left) and charge (right) of control and occluded spontaneous M/TC LLCs. Each circle represents one cell. Error bars indicate SEM. (**B**) Spontaneous M/TC LLCs become larger with occlusion when recorded in regular artificial cerebrospinal fluid (ACSF). (**Bi**) Example traces of control and occluded spontaneous M/TC LLCs. (**Bii**) Quantification of control and occluded M/TC spontaneous LLC amplitude (left) and charge (right) in ACSF. Each circle represents one cell. Error bars indicate SEM. Dotted error bars indicate mean ± SEM of spontaneous LLC amplitude and charge in the presence of PTX for comparison. (**C-D**) Spontaneous excitatory postsynaptic currents (sEPSCs) are not impacted by occlusion regardless of whether $GABA_A$ inhibition is intact. (**Ci**) Example traces showing sEPSCs in control and occluded conditions recorded in ACSF. (**Cii-iii**) Quantification of amplitude and frequency of sEPSCs in control and occluded conditions. Each circle represents one cell. Error bars indicate SEM. (**Di**) Example traces showing sEPSCs in control and occluded conditions recorded in ACSF in the presence of 10μm PTX. (**Dii-iii**) Quantification of amplitude and frequency of sEPSCs in control and occluded conditions. Each circle represents one cell. Error bars indicate SEM. *., $p<0.05$; **., $p<0.01$; n.s., non-significant.

4.2.9. ETC LLCs do not increase with occlusion when $GABA_A$ signalling is left intact

Finally, given that M/TC LLC magnitudes increased with occlusion in the presence of $GABA_A$ signalling, we next wanted to explore whether ETC LLCs were affected by occlusion under the same circumstances. PTX appeared to push M/TC LLC magnitudes toward ceiling levels, masking the occlusion effect. We therefore wanted to observe whether PTX was increasing ETC LLC magnitudes under baseline conditions as well, and further wanted to investigate whether the occlusion effect on ETC LLCs was enhanced when $GABA_A$ signalling persisted.

We recorded spontaneously occurring LLCs from 17 sham control and 22 occluded ETCs in regular ACSF (**Fig 12A**). As predicted, ETC LLCs in both control and occluded conditions were comparatively smaller compared to ETC LLCs in the presence of PTX (**Fig 12B**, dotted error bars). Again, LLC frequency was not affected by occlusion, and as opposed to M/TC LLCs, frequencies did not differ when recorded with or without PTX in the recording solution (sham control; mean ± SEM 0.13 ± 0.03Hz; occluded 0.08 ± 0.02Hz; *unpaired t-test* using Welch's correction, $t_{(34.96)} = 0.64$, p=0.52). Intriguingly, however, occlusion did not affect LLC magnitude under these conditions (**Fig 12B**) (Amplitude: sham control mean ± SEM 33.48 ± 3.05pA; occluded 40.78 ± 5.78pA; *unpaired t-test* on $\log_{10}$ transformed values using Welch's correction, $t_{(34.96)} = 0.64$, p=0.52; Charge: sham control mean ± SEM 6.28 ± 1.07pC; occluded ± SEM 5.61 ± 0.88pC; *unpaired t-test on* sqrt transformed values, $t_{(37)} = 0.55$, p=0.58).

Therefore, these data imply that increases in ETC LLC magnitude in response to occlusion can only be observed when $GABA_A$ signalling is blocked.

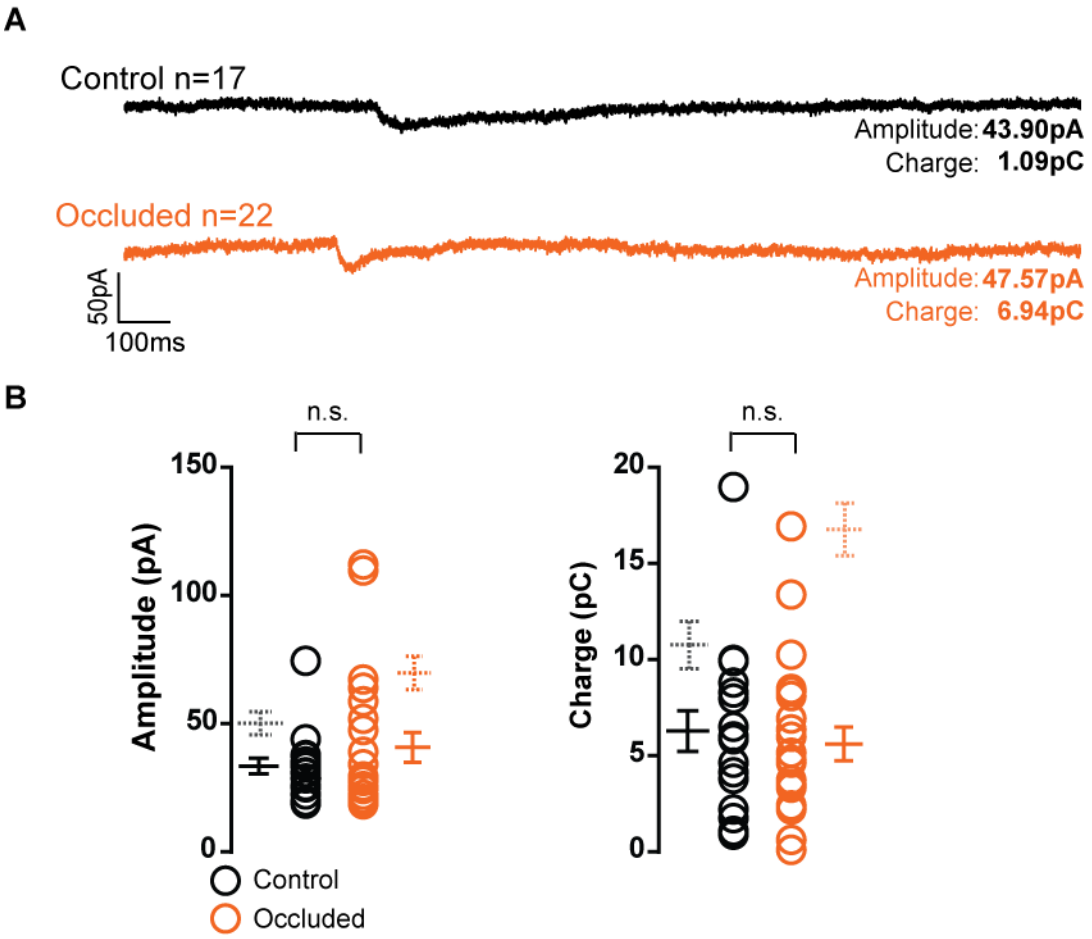

Fig 12. External tufted cell (ETC) long-lasting depolarising currents (LLCs) are not affected by occlusion when recorded in regular artificial cerebrospinal fluid (ACSF).

(**A**) Example traces of spontaneously occurring LLCs in control and occluded ETCs recorded in ACSF. (**B**) Quantification of spontaneous LLC amplitude (left) and charge (right) recorded in ACSF. Each circle represents one cell. Error bars indicate SEM. Dotted error bars indicate mean ± SEM of spontaneous LLC amplitude and charge recorded in the presence of 10μm picrotoxin (PTX) for comparison. n.s., non-significant.

4.3. Discussion

Our data demonstrate that LLCs may not be a binary feature as previously thought, as OSN-evoked M/TC LLCs could portray several magnitudes of LLC at the same threshold stimulus intensity and the charge of an evoked LLC did not correlate well with the charge of spontaneously occurring LLCs. Furthermore, we show that ETC *and* M/TC LLCs can become larger after short-term sensory deprivation under certain conditions. We have shown that this change likely is not due to changes in the presynaptic properties of OSNs, as these were unaffected by 24h occlusion. This would suggest that the excitatory glomerular network postsynaptic to OSNs is able to adjust dendrodendritic amplification of excitatory signalling after sensory deprivation, though there appears to be a complex interplay with local inhibition involved in this effect.

4.3.1. OSNs do not alter their Pr with short-term sensory deprivation

Interestingly, we noted that the magnitude of spontaneously occurring LLCs did not necessarily correlate with the magnitude of evoked LLCs, and indeed only the amplitude, not charge, correlated well across the two recording methods (**Fig 2**). Previous reports observed LLCs as an all-or-nothing phenomenon (Carlson et al., 2000; Gire and Schoppa, 2009), however our data suggest there is room for manipulating LLC magnitude by initial amplitude. It could be possible, for example, for initial LLC amplitude to exist in a binary fashion, but the resulting dendrodendritic amplification responsible for defining how much charge is transferred could be manipulated depending on how much input is reaching these cells for them to amplify. In our evoked LLC recordings, OSN stimulation likely resulted in the recruitment of many more LLC contributors compared to spontaneous recordings where we were not stimulating the circuit. Under evoked conditions, the LLC amplitude, although well-correlated with the amplitude of spontaneous LLCs, is still larger than spontaneous LLC amplitudes. This small effect of amplitude is likely amplified over the 500ms duration we measured for charge, which could create this stronger discrepancy between spontaneous and evoked LLC charges. Therefore, a way in which ETC LLCs could increase their magnitude in the face of occlusion could result from increased pre-synaptic input.

We therefore wished to identify whether OSN input could be the locus for the LLC change we observe with occlusion. It has previously been found that OSNs are able to increase their P*r* intrinsically in response to two-weeks of sensory deprivation (Tyler et al., 2007). Additionally, OSN P*r* is regulated by the local inhibitory JGC network, where GABA and Dopamine released by these cells causes activation of both $GABA_B$ receptors and D_2-Dopamine receptors which strongly supress release of OSNs (Aroniadou-Anderjaska et al., 2000; Maher and Westbrook,

2008; Wachowiak and Cohen, 1999). Due to these observations, we wanted to identify whether 24h occlusion resulted in any P*r* change at OSN terminals. If P*r* is increased, either intrinsically or due to changes in the inhibitory network, this could provide more glutamatergic currents for the excitatory network to amplify, which may result in the larger LLCs we see in occlusion.

We performed several different methods that have been validated previously to estimate OSN P*r*. These included indirect measurements of VGLUT transporters on OSN terminals (**Fig 4,** Gabellec et al., 2007), PPR as an indicator of P*r* (**Fig 5,** Tyler et al., 2007), and estimations of the readily releasable pool of vesicles to calculate P*r* directly (Thanawala and Regehr, 2016; Vaaga and Westbrook, 2017) (**Fig 6**). Occlusion did not appear to significantly impact the estimated P*r* using any method of estimation. However, in our dataset, OSN P*r* estimations were lower compared to findings from previous studies (Murphy et al., 2004; Tyler et al., 2007). These other studies blocked $GABA_B$ and D_2 dopaminergic receptors in their recordings whereas we did not, which may explain this discrepancy. Out of all our sets of experiments, only one set of experiments showed that PPR was significantly decreased with occlusion (**Fig 5**), an effect that could not be recapitulated with a separate set of recordings. A decrease in PPR implies an increase in P*r*. Since OSN P*r* *can* change with longer-term occlusion (Tyler et al., 2007), it could be possible that 24h occlusion results in a very subtle increase of OSN P*r* that was revealed in our initial, larger, data set. However, this very slight increase may not be reliable and this is why we did not observe it in a second or third, smaller, data set examining PPR (**Fig 5, Fig 6**). Regardless of the reasons behind this variability, OSN inputs are likely not the locus of the LLC change we observe in occlusion.

4.3.2. M/TC LLCs do not display a binary phenotype

We further wondered whether the occlusion effects on ETC LLCs were translated to M/TC LLCs. As previously mentioned, the glomerular LLC is involved in synchronising firing of M/TCs projecting to the same glomerulus (De Saint Jan et al., 2009), and allowing them to respond with sustained transmission upon OSN input (Vaaga and Westbrook, 2017). A change in the magnitude of LLC received by M/TCs could therefore influence the output of these cells.

Our initial experiments revealed that evoked M/TC LLCs are much larger compared to ETC LLCs. This observation ties in with the observation that dendrodendritic amplification of glutamatergic signals is stronger in M/TCs compared to ETCs (Vaaga and Westbrook, 2017), and suggests that upon initial glomerular LLC generation, M/TCs may further amplify this signal among themselves. We further observed that M/TC LLCs, as opposed to ETC LLCs, did not always occur at the same magnitude when stimulated with the same stimulation intensity (**Fig 3; Fig 10**), suggesting that M/TC LLCs do not adhere to the all-or-nothing phenotype previously described

(Carlson et al., 2000; Gire et al., 2009). Indeed, although both ETC and M/TC portray LLC magnitudes that appear to adhere to a relatively "quantal" phenomenon (**Fig 3; Fig 10**), M/TC LLC magnitudes portray more heterogenous amplitudes when compared to ETC LLCs (**Fig 10**).

As opposed to other studies, we may have observed the "multi-level" M/TC LLC because we recorded LLC responses using narrower stimulus intensity steps. We often increased or decreased stimulus intensities by 0.05mA, whereas the other studies multiplied their threshold stimulus intensities. The subtler stimulus intensity steps we used may have allowed us to record LLCs at different build-up states, which may have revealed the multiple components of the M/TC LLC build up. Indeed, we did not observe multi-level M/TC LLCs at *all* stimulus intensities, suggesting that in order to be able to observe them, a very specific amount of OSN input needs to reach the glomerular circuit. Additionally, Gire et al., (2009) used young rats (P10-16) in their experiments. This could influence the magnitude of the LLCs they recorded, as it has previously been shown that LLCs are developmentally regulated, increasing in magnitude from ~ P11-P16 (De Saint Jan and Westbrook, 2007). We always recorded from juvenile mice post P20, thus we may have observed a more mature picture in our recordings.

How, then, are M/TCs able to recruit the ETC LLC to amplify it further? The charge of the M/TC LLC has previously been shown to depend not only on NMDA receptors, but also on mGluR1 receptors (De Saint Jan and Westbrook, 2007). Upon OSN stimulation, the activation of mGluR1 receptors recruits low-voltage activated T-type Ca^{2+} channels in primary dendrites, and together these receptor mediated currents account for a large proportion of LLC magnitude (Johnston and Delaney, 2010). No one, to our knowledge, has explicitly looked at whether the same mechanism operates in ETCs. However recent findings imply that M/TC LLCs are larger than ETC LLCs due to increased dendrodendritic amplification via NMDA and mGluR1 receptors. In this study, pharmacological block of these receptors converted M/TC LLCs into magnitudes more comparable to ETC LLCs (Vaaga and Westbrook, 2017). ETCs receive stronger OSN input compared to M/TCs (De Saint Jan et al., 2009; Gire et al., 2012; Vaaga and Westbrook, 2016), therefore ETCs could be driving the initiation of the glomerular LLC, perhaps due to higher-efficacy AMPA receptors and/or Ca^{2+} permeable AMPA autoreceptors (Ma and Lowe, 2007), which is further amplified through NMDA/mGluR1 mediated dendrodendritic amplification in M/TCs. To support this notion, it has been shown that ETCs can respond to weaker OSN inputs, whereas direct OSN-M/TC input tends to only occur as a result of very strong OSN input (Najac et al., 2011). Thus, this initial amplification step by ETCs could be a way in which relatively weak odour inputs are reliably converted to a M/TC response. Additionally, we have indicated that the glomerular LLC may be formed of multiple excitatory "subnetworks", which may be interpreted differently by ETCs and M/TCs. From our CV analysis on spontaneous versus evoked

LLC amplitudes, we found that evoked ETC LLCs are fairly stereotyped compared to spontaneously occurring LLCs (**Fig 3**). This may occur because when LLCs are evoked by OSN stimulation, the entirety of the excitatory network is being triggered, whereas spontaneously occurring LLCs may reflect the activity of relative excitatory subnetworks. Interestingly, when observing the M/TC LLCs, evoked LLCs are still more heterogenous than evoked ETC LLCs, and in fact do not differ to spontaneously occurring M/TC LLC amplitudes (**Fig 10**). Therefore, the multi-level LLCs we recorded in M/TCs may have revealed the different steps involved in LLC generation. Perhaps the several sizes we observed represent initial LLC generation by ETCs, which are subsequently amplified by dendrodendritic mechanisms to generate the larger M/TC LLCs. This could explain why ETCs only show either "off" or "on" LLCs (**Fig 10**), as this extra amplification does not occur at their synapses.

To test this hypothesis, we could perform several additional experiments. To observe whether we recorded "ETC LLCs" in our evoked M/TC LLC recordings (the smaller magnitude LLCs), we could perform the same OSN-evoked LLC recordings again, and find stimulus intensities that reveal the multi-level M/TC LLCs. We would then wash in mGluR1 and NMDA blockers after baseline recordings. If the evoked LLC then reverted to a binary state, and became more comparable in size to one of the smaller LLCs in the multi-level LLC (presumably an ETC LLC), this would suggest that indeed M/TCs read in ETC LLCs before amplifying these to a full M/TC LLC. This experiment would be strengthened even more with a dual patch approach. If both an M/TC and an ETC projecting to the same glomerulus are recorded in synchrony, we could observe the magnitude of either cell's LLC at baseline levels, as well as after pharmacological block of NMDA and mGluR1 receptors. We would then be able to see, on a cell-by-cell basis, whether the ETC LLC remains intact in the M/TC LLC recording.

4.3.3. Can changes in glomerular recurrent excitation explain the LLC magnitude increases in ETCs and M/TCs following occlusion?

Immunofluorescence approaches to deciphering presynaptic function

Since we observed larger LLCs recorded in ETCs under $GABA_A$ block in occluded conditions, and since it is unlikely that presynaptic OSN inputs are contributing to this change, we sought to investigate whether recurrent excitation as a whole is increased after occlusion. This would imply that the LLC change we observe is linked to the dendrodendritic amplification of glutamatergic currents by the excitatory network, potentially via glutamate sensing enhancement mechanisms described below. We initially screened for effects in VGLUT1

expression in glomeruli. VGLUTs are crucial for filling synaptic vesicles with glutamate (Bellocchio et al., 2000), thus if changes occurred in VGLUT1 density, it could imply that cells may be becoming more efficient at filling their vesicles with glutamate, and in turn, become more efficient at transmitting glutamatergic signal to the recurrent network. Alternatively, or in addition, it could imply that there are more glutamatergic release sits that enhance recurrent excitation. Our screen of VGLUT1-label fluorescence intensity failed to show any effect of occlusion (**Fig 7**). Nevertheless, VGLUT expression in ETCs, for example, is heterogenous, with some subtypes expressing either VGLUT1, VGLUT3, or both (Tatti et al., 2014). Some have even been suggested to express VGLUT2 (Ohmomo et al., 2009). Therefore, presynaptic function could be enhanced by increases in expression of various VGLUTs or other elements of the presynaptic machinery.

PSD-95 is a postsynaptic scaffolding protein that recruits receptors, ion channels, and signalling proteins (Stathakis et al., 1997). Specifically, it has been shown to recruit AMPA receptors to the synapse (Schnell et al., 2002). The number of AMPA receptors at a synapse directly impacts the quantal size of that synapse, and has further been correlated with the P*r* of that synapse (Murthy et al., 2001). Thus, if postsynaptic terminals were increasing their PSD-95 protein levels, it could enhance the excitatory function of that terminal and would be interesting to quantify in occluded ETCs to see whether this is the case. Therefore, a more sensitive approach compared to VGLUT staining to deciphering structural synaptic function, could be achieved with the use of intrabodies. Intrabodies are recombinant antibody-like proteins that bind to target proteins. The genes expressing intrabodies are then fused with genes expressing GFP, allowing for the real-time observation of these proteins in a reducing environment such as the cell cytoplasm (Nizak et al., 2003). Recently, intrabodies have been developed to target postsynaptic proteins in excitatory terminals, specifically PSD-95. Additionally, these intrabodies have been designed to tie their regulation of expression with endogenous expression of PSD-95, ensuring that the signal transmitted by the intrabody gives an accurate readout of how much PSD-95 is endogenously present (Gross et al., 2013). With the use of intrabodies targeting PSD-95 therefore, we could compare fluorescence intensities in control and occluded ETCs to observe whether postsynaptic function is enhanced, and therefore elucidate whether this is linked to an increase in recurrent excitation. To achieve the level of sensitivity for this approach, we would need to be able to sparsely label ETCs in order to quantify expression of the intrabody at punctate postsynaptic terminals using confocal microscopy. Achieving sparse labelling is difficult, as ETC genetic driver lines have not yet been developed (see chapter 3). Thus, the use of *in utero* electroporation or viral injection of a vector containing the PSD-95 intrabody would need to be optimised to achieve this level of sparse label, which may be technically challenging.

Functional approaches

We thus used a functional approach to quantify recurrent excitation in the glomerular network. Our experimental paradigm relied on measuring auto-evoked glutamatergic potentials as a proxy for glomerular recurrent excitation. We hypothesised that these potentials would become larger with occlusion. Nevertheless, we could not identify any occlusion effect on these potentials (**Fig 9**).

Despite these results, the contribution of increased recurrent excitation to the LLC change in occlusion cannot be excluded. First, due to technical difficulties in maintaining a high-quality recording for long periods of time, it was not possible to analyse glutamate potentials in a highly accurate manner. In an ideal situation, tail potential amplitudes would be calculated by subtracting peak amplitudes from baselines obtained after NBQX/APV wash-in for every cell, in order to quantify the glutamatergic component of this potential accurately. However, we were only able to obtain 6 recordings from cells where both baseline and NBQX/APV wash-in responses were recorded successfully. We thus used these recordings to determine at what time point after evoked spikes most of the glutamatergic potential was eliminated by NBQX/APV on average to quantify tail potentials at these time points in recordings where NBQX and APV wash-in was unsuccessful. In this way, we could have potentially missed an effect of occlusion on recurrent glutamate signalling. It was clear that non-glutamatergic potentials were contributing to the recorded responses, as NBQX and APV did not eliminate the entirety of the post-spike potential. This underlying potential could also have changed with occlusion and thus may have masked occlusion effects on glutamatergic potentials. A more accurate approach to this experiment, perhaps, would have been to perform the protocol in voltage clamp. In this way we would be able to directly isolate individual glutamatergic currents by blocking all others with pharmacological agents (Ma and Lowe, 2007). Nevertheless, it might then be difficult to reliably and reproducibly stimulate the cell to release glutamate under this configuration. This is due to errors in space-clamp; as ETCs are relatively large cells, the holding potential at the site of the recording electrode will radially spread and decay across distance, which means that the membrane more distal to the injection site is not clamped well and is thus difficult to control with voltage steps. Additionally, there is high heterogeneity in the morphology of ETC tufts (chapter 3) which means that space-clamp errors will differ from cell to cell.

Additionally, it has been shown that LLC magnitudes are closely linked to NMDA receptor function (Carlson et al., 2000). Previous reports have shown that NMDA receptors composed of different subunits such as NR2C and NR2D, both expressed in the olfactory bulb (Wenzel et al., 1995), can influence the decay kinetics of NMDA currents (Monyer et al., 1992). It could thus be

entirely possible that the LLC change we observe in occlusion may be due to changes of NMDA receptor density or efficacy. Furthermore, it would be interesting to shine light on whether NMDA mediated potentials or even AMPA mediated potentials are changing. For example, the ratio of AMPA:NMDA mediated currents developmentally increases in OB JGCs and ETCs (Grubb et al., 2008). This change could be so subtle that we would not be able to observe any glutamate potential increases with occlusion in our auto-evoked recordings due to these signals being mixed together with AMPA components and other non-glutamatergic components. It would therefore be beneficial to repeat this experiment in a more controlled manner, where individual wash-in of NBQX and/or APV is performed on every cell recorded. Nevertheless, if such changes occurred in occlusion on a very subtle level, these may not be revealed through our auto-evoked excitation protocol as it is likely they would summate to impact overall recurrent excitation in a glomerulus, resulting in a larger LLC. This would then be difficult to identify through the recorded cell as it may not have enough time to incorporate these increased signals into the auto-evoked response.

Furthermore, the experiment we performed was done in a highly un-physiological setting. In several trial experiments in ACSF (data not shown), we noticed auto-evoked glutamate potentials were very small. Due to the large contribution of NMDA currents in the glomerular excitatory pathway, we therefore aimed to maximise our ability of recording these potentials by relieving the Mg^{2+} block of NMDA receptors by patching in ACSF that contained no Mg^{2+}. This could have resulted in NMDA receptor potentials becoming larger than usual even in control conditions, which may have reached a ceiling level and thus masked occlusion effects. Additionally, different NMDA receptor subunits can change NMDA Mg^{2+} sensitivity levels (Wenzel et al., 1995). Thus elimination of Mg^{2+} in the recording solution could mask potential effects of NMDA receptor subunit composition.

A more direct way of quantifying whether any receptor components on ETCs are adjusted with occlusion would be to obtain paired recordings from two ETCs projecting to the same glomerulus simultaneously. The aim would be to identify whether ETCs are able to ramp up their glutamate sensing or releasing properties with occlusion. Under these conditions, we could record one cell in current-clamp and trigger it to spike, while recording the other in voltage clamp to observe glutamatergic inputs evoked by the first cell's spike. These recordings would be performed in the presence of PTX to block GABAergic currents, and either NBQX or APV to isolate AMPA- and NMDA-mediated currents. If the amplitudes of these currents are increasing with occlusion, this would suggest ETCs are adjusting their AMPA and/or NMDA receptor densities and/or composition that allow them to receive larger glutamatergic currents, which may lead to larger LLCs. It could also imply that presynaptic vesicle packet sizes may be enhanced with occlusion

(Clements and Silver, 2000). Alternatively, or in combination, if the probability of these events increases with occlusion, this would suggest a presynaptic effect, such as an increase in P*r.* A caveat to this approach however, is that there is little evidence for direct synaptic connections between ETCs (De Saint Jan et al., 2009), which would make paired recordings extremely difficult and would produce asynchronous responses that may be difficult to interpret, which is why we did not perform these experiments as part of this thesis. Additionally, it would be difficult to distinguish presynaptic effects from postsynaptic effects. However, changes observed in these recordings would, at least, strongly suggest that recurrent excitation, driven by the excitatory network, are changing with occlusion.

An alternative way to establish whether perhaps ETCs are increasing their P*r* is to observe the magnitude of glutamate spillover occurring at ETC-JGC synapses (Gire et al., 2018). It has previously been suggested that this spillover could actually provide a mechanism by which LLCs are initiated (Gire et al., 2018). In order to observe whether ETC P*r* is increasing with occlusion, we could double patch ETCs and JGCs, initiate an action potential in the ETC in current clamp, and record glutamatergic EPSCs in the JGCs. If the probability of these events occurring increases, it would suggest that ETCs are more likely to release glutamate.

Finally, we did not specifically test for the efficacy of the OSN-ETC connection on a postsynaptic level. It could be possible that ETC LLCs are enhanced with occlusion due to enhanced glutamate sensing capabilities of ETC postsynaptic terminals to OSN input by an increased postsynaptic response to presynaptic release. There are two approaches in which this could be tested. One of these is the use of non-stationary fluctuation analysis (NFSA) (Clements and Silver, 2000), further discussed in chapter 5. Briefly, to obtain measures here, we would electrically stimulate OSNs and record an ETC in voltage clamp. In this method, P*r* is artificially set to different levels with the use of Ca^{2+} chelators or changes in Ca^{2+} concentration in the recording solution. The different levels of P*r* would be used to obtain a curve fitted against the variance of the mean postsynaptically recorded EPSC amplitudes to create a variance-mean (V-M) plot. Observing the plot at the various P*r* levels indicates whether presynaptic or postsynaptic changes result in changes recorded in postsynaptic EPSCs. If the postsynaptic side, so at the ETC level, was increasing quantal size, we would expect to see a change in the initial slope of this plot, as it estimates the average quantal amplitude of the EPSCs. The other approach involves the use of strontium to replace Ca^{2+} in the recording solution. Evoked EPSCs in this medium will reveal individual vesicle release events one by one (Oliet et al., 1996), as opposed to multiple superimposing release events summating to one recorded EPSC (e.g. Grubb et al., 2008). In this way, we could then quantify individual OSN-evoked ETC-EPSC amplitudes recorded in strontium and observe whether they become larger with occlusion. If so, this would suggest that ETCs are

upregulating the function of postsynaptic terminal glutamate sensing machinery after sensory deprivation.

In summary, with our experimental approaches, we did not detect increases in recurrent excitation in the face of occlusion, and thus could not link this as a possible mechanism by which LLCs are increasing in occlusion. Nevertheless, as mentioned above, this possibility cannot be excluded, and further experiments – beyond the scope of the present project – will be required to address this directly.

How could ETC LLCs become larger with occlusion if auto-evoked excitation is not enhanced, and OSN P*r is not increased?*

Due to our observation that LLC increases in magnitudes occurred despite a lack of change in OSN P*r*, this change most likely occurred due to adjustments in the excitatory network. There are several ways in which dendrodendritic amplification can be increased, which mostly rely on somehow strengthening glutamatergic communication, given the lack of passive and morphological properties changing with occlusion (chapter 3). These changes would likely not be apparent with our auto-evoked glutamate release experiment, due to the limitations outlined above, which may further explain why occlusion seemed to have no effect there.

Previous reports have found little evidence for direct ETC-ETC chemical synaptic connections, and much recurrent excitation is thought to occur due to spillover glutamate signalling reaching post-synaptic terminals (De Saint Jan and Westbrook, 2007; Gire et al., 2018; Isaacson, 1999). Indeed, even self-excitation has previously been reported in ETCs through Ca^{2+}-permeable AMPA autoreceptors (Ma and Lowe, 2007). Therefore, as mentioned above, adjusting synaptic properties that sense glutamate could be a tool for LLC manipulation. In the olfactory bulb, short-term sensory deprivation resulted in increased glutamate receptor protein levels on glomerular synapses. This observation was linked to quantal scaling of AMPA and NMDA-mediated currents in JGCs, including ETCs (Tyler et al., 2007). LLC magnitudes are heavily regulated by NMDA receptor currents, as blocking these reduces the amplitude and decay of LLCs (Carlson et al., 2000). Thus, one way ETCs could be increasing LLC size could be by increasing their NMDA receptor density or altering receptor subunit composition of these receptors in order to obtain larger glutamatergic currents that are then amplified across the network. AMPA receptors are required for LLC initiation (Carlson et al., 2000). Thus alternatively, or in combination, ETCs could also increase their AMPA receptor density to allow for more entry of glutamatergic signalling that may act on other excitatory cells which then act to increase the overall glomerular LLC. These properties may also act together. NMDA receptors allow Ca^{2+} to enter the cell which may act to regulate gene expression that influences the density of AMPA

receptors at the terminal (Ghosh and Greenberg, 1995). Thus, if there is a higher density of NMDA receptors, this may act to potentiate AMPA receptor-mediated currents as a result. In M/TCs, NMDA and AMPA autoreceptors enhance spillover glutamatergic signalling between M/TCs projecting to the same glomerulus and are thought to play a role in ensuring reliable M/TC output (Salin et al., 2001; Schoppa and Westbrook, 2002). Therefore, plasticity in the expression or efficacy of ETC Ca^{2+}-permeable AMPA autoreceptors could provide another avenue in which glutamatergic signals may be amplified from cell to cell, resulting in the larger LLCs we observe in occlusion.

Another avenue for LLC changes to occur could be through gap-junction mediated communication. Gap junctions allow for the passage of small molecules such as ions and secondary messengers between connected cells on a relatively fast time-scale and are involved in synchronising neural processes (Dermietzel, 1998). Connexin-36 mediated gap junction coupling in M/TCs has been shown to contribute to the M/TC lateral excitation involved in amplifying sensory input from OSNs (Christie and Westbrook, 2006). Additionally, gap-junctions are involved in defining the magnitude of the M/TC LLC by enhancing glutamate spillover among these cells (Christie and Westbrook, 2006), and indeed LLCs were largely reduced in amplitude and duration in connexin-36 KO animals (De Saint Jan and Westbrook, 2007). Gap-junction mediated communication is also found in ETCs. It has previously been shown that ETCs projecting to the same glomerulus are electrically coupled, a connection that contributes to synchronising ETC activity at one glomerulus (Hayar et al., 2005). Plasticity in gap-junction coupling could therefore impact glutamatergic communication among excitatory cells in glomeruli. Previous studies have found that gap-junctions can indeed strengthen or weaken their conductances as a result of changing input activity through various mechanisms such as NMDA receptor activation (Yang et al., 1990) or mGluR receptor activation (Landisman and Connors, 2005). Thus, perhaps the LLC change we observe is due to increased gap-junction coupling among ETCs, or even ETC-M/TC connections (De Saint Jan et al., 2009). This would allow for a higher passage of excitatory signalling between these cells that would therefore enable an increase in recurrent excitation. Direct evidence for which connexin forms gap junctions on ETCs has not been reported, however it is likely to consist of connexin-36, 45, or 57 (Rash et al., 2005; Zhang, 2011). Interestingly, synchronous activity of M/TCs in connexin-36 KO animals was not eliminated, however stronger stimulations of M/TCs, achieved by glutamate uptake block, was required to maintain this synchrony (Christie et al., 2005). Thus, it would be interesting to observe whether LLCs recorded in ETCs are affected in occlusion in connexin-36 KO animals in order to observe whether connexin-36 also impacts ETC function. Alternatively, to test the strength of gap-junction coupling between ETCs, a dual patch approach could be employed. Two

coupled ETCs would be patched simultaneously in the voltage clamp configuration and in the presence of synaptic blockers. A hyperpolarising step would be induced in one cell, while the resulting outward current would be recorded in the other, while alternating which cell is stimulated. In this way, the coupling coefficient can be calculated, and we would then be able to observe whether this increases with occlusion. If this indeed were the case, we would then be able to tie this effect to LLC changes with further experiments. LLCs would be recorded at baseline in both control and occluded conditions, followed by a wash-in of a gap junction blocker such as carbenoxolone, which has previously been shown to block ETC-ETC gap-junction mediated communication (Hayar et al., 2005). If the occlusion effect on LLCs disappears with the gap junction blocker, it would suggest that this is the locus of the LLC change.

Therefore, though we were unable to pinpoint how the LLC change occurs with occlusion, there are various means in which the excitatory network could adjust to allow for this change.

4.3.4. Occlusion effects on LLCs

Given the importance of LLCs in synchronising M/TC output and defining spike patterns in response to OSN input (Gire and Schoppa, 2009; Vaaga and Westbrook, 2017), a change in LLC magnitude could be an interesting avenue through which occlusion may result in an adjustment in glomerular processing through ETCs. Previous work has shown that larger charge transfer due to strong dendrodendritic glutamatergic amplification, i.e. LLCs, between M/TCs allows them to sustain their firing in response to OSN stimulation, whereas smaller LLCs in ETCS resulted in phase-locked responses (Vaaga and Westbrook, 2017). Therefore, an increase in ETC LLC magnitude could potentially lead to an altered output from these cells. We have shown previously (chapter 3) that intrinsically, ETCs are unaffected by occlusion. Thus, this synaptic LLC phenotype could result in a subtle adjustment to odour responses that is not linked to intrinsic excitability. Since LLCs are received by all M/TCs and ETCs projecting to the same glomerulus, and since ETC LLCs are the most likely target of $GABA_A$ inhibition (Gire and Schoppa, 2009; Whitesell et al., 2013) it is likely they form part of an LLC-modulatory network. It could then be possible that ETCs adjust some of their synaptic properties, discussed above, in order to ramp up recurrent excitation in the entire glomerulus in the face of occlusion, which may feed-forward to M/TCs, resulting in an output change there.

Why do ETC LLCs only become larger with occlusion in the presence of PTX?

When recorded in the presence of PTX, both spontaneous and evoked ETC LLCs become significantly larger both in amplitude and charge in response to occlusion (**Fig 1, Fig 2**). However, when $GABA_A$ signalling persists, the LLC change is no longer evident, or at least, is not as strong

as when $GABA_A$ is blocked (**Fig 12**). Since GABA is thought to directly target ETCs to supress LLCs (Aungst et al., 2003; Gire and Schoppa, 2009; Whitesell et al., 2013), and since $GABA_A$ currents can decrease overall LLC amplitude (Carlson et al., 2000), it could be possible that when recording from ETCs in the presence of $GABA_A$ signalling, this inhibition is so strong that it creates a floor effect on LLC magnitude, which may thus obscure any occlusion effects. Indeed, ETCs directly drive feedback-inhibition in the glomerular network (Hayar et al., 2004a; Murphy et al., 2005). Therefore, if occlusion results in increased excitatory drive between ETCs, this could directly enhance feedback inhibition which then acts on ETC LLCs and may result in the unchanged LLC phenotype we see in ACSF.

M/TC LLCs also become larger with occlusion

Our initial evoked M/TC LLC experiment suggested that looking at ETC LLCs alone does not provide the full story on what is occurring in the glomerular excitatory network with occlusion. We thus wanted to know whether there would be any occlusion effect on the M/TC LLC, that may have arisen due to the changes we saw in ETCs.

Interestingly, under conditions with PTX in the recording solution, M/TC LLC magnitudes were not significantly impacted by occlusion (**Fig 11**). There was however, a very subtle, non-significant, increase in the average charge of M/TC LLCs with occlusion. Therefore, we considered whether perhaps M/TC LLCs were reaching a ceiling level of magnitude when $GABA_A$ modulation is blocked. In contrast to ETCs, M/TC LLCs were larger even under control conditions, thus it could be possible that lack of $GABA_A$ modulation resulted in a ramped-up dendrodendritic amplification in M/TCs that could not become any larger with occlusion.

Indeed, when PTX was excluded from the recording solution, M/TC LLCs did show a significant increase in amplitude and charge in response to occlusion (**Fig 11**). These larger LLCs in occlusion resembled the LLCs recorded in the presence of PTX, whereas control LLCs were much smaller compared to control LLCs in the presence of PTX. This further suggests that M/TCs were reaching a ceiling level of LLC magnitude with PTX.

To test this hypothesis, we could perform an experiment where initial spontaneous LLCs are recorded in ACSF in control and occluded conditions. This would then be followed by a wash-in of PTX. We could then observe whether the inclusion of PTX increase overall LLC magnitude in control conditions and thus eliminated the occlusion effect.

Might the M/TC LLC occlusion effect be linked to the ETC LLC occlusion effect, supporting the idea that ETCs are somehow modulating the initial LLC information M/TCs receive? We hypothesised that ETC LLC differences between control and occluded conditions would reveal

an even larger effect of occlusion when $GABA_A$ modulation was not blocked. The idea behind this was that PTX could also be ramping up the magnitude of the ETC LLC, thus eliminating PTX in our recording solution should allow control ETC LLCs to be even smaller compared to control ETC LLCs in the presence of PTX, mimicking what we see in M/TCs. Our data, however, would suggest otherwise. When ETC LLCs were recorded without PTX in the recording solution, the occlusion effect on LLC magnitude was largely abolished, with only an increased LLC amplitude *trend* remaining (**Fig 12**).

These findings lead to some perplexing questions. If M/TC LLC magnitudes increase with occlusion in the absence of PTX, why is this phenotype not followed by ETCs? Given that the main way of OSN to M/TCs communication is wired through ETCs (Gire and Schoppa, 2009), it is therefore confusing how M/TCs can somehow increase their recurrent excitatory drive without contribution from ETCs.

4.3.5. Models of how occlusion could be impacting the glomerular LLC

Since the glomerular LLC is hypothesised to arise due to regenerative, recurrent excitatory drive (De Saint Jan et al., 2009; Gire et al., 2012), trying to understand the occlusion effect on the glomerular LLC becomes difficult with the mismatch in phenotype in ETCs and M/TCs. ETCs increase their LLC magnitudes with occlusion only if $GABA_A$ signalling is blocked, whereas M/TCs increase their LLC magnitudes with occlusion only when $GABA_A$ signalling is intact. On a cell-type basis, these effects of inhibition could be explained by floor and ceiling effects described above. However, if M/TC LLCs are becoming larger in ACSF, we would expect ETC LLCs to become larger as well, following from the model that ETCs form part of the first amplification step before M/TCs join in with stronger dendrodendritic amplification.

The fact that we do not observe this leads to a number of speculations as to what could be happening in the LLC network. These hypotheses rely heavily on the notion that $GABA_A$ inhibition by JGCs mainly targets ETCs to supress their activity and subdue their LLCs, rather than directly targeting M/TCs. In addition to the finding that JGCs, and especially GABAergic inhibition by these cells, strongly inhibit ETCs (Hayar et al., 2004b; Hayar and Ennis, 2007), recent evidence suggests that intraglomerular GABAergic inhibition directly acts to suppress LLCs at the ETC rather than the M/TC. This study showed that ETCs receiving OSN-evoked LLCs were supressed by GABAergic currents during the same recordings. However, M/TCs never showed inhibitory currents when an LLC did not occur, and when LLCs did occur, M/TCs exhibited IPSCs from GCs rather than JGCs (Gire and Schoppa, 2009). Under the assumption that JGC inhibition is strongly targeted to ETCs, therefore, we propose three scenarios to explain how occlusion may impact the glomerular LLC network:

We *did* observe a trend of ETC LLC amplitudes becoming larger in occlusion when recorded without PTX (**Fig 12**). Perhaps this very subtle increase in ETC LLC amplitude simply was enough to allow M/TCs to integrate this information and drive the changes we observed in M/TC LLCs. In ETCs themselves, this subtle effect may only have been obvious when PTX was included in the recording solution, which would have blocked the effects of feedback inhibition that may have precluded the effect of occlusion on ETC LLCs (scenario A, **Fig 13**). This scenario would also work if there were no intraglomerular cell-type specific differences in $GABA_A$ inhibition on LLCs. Indeed, $GABA_A$ is known to inhibit OSN-evoked M/TC spiking at an intraglomerular locus (Shao et al., 2012), thus at least some of this inhibition will likely target M/TCs as well. Nevertheless, it was specifically shown that intraglomerular $GABA_A$ inhibition supressed the ETC LLC, thus it is unlikely that the functional intraglomerular $GABA_A$ effects targeted to M/TCs would impact the M/TC LLC directly. Additionally, since $GABA_A$-mediated inhibition via GCs does seem to impact M/TC LLCs (Gire and Schoppa, 2009), the ceiling effect of LLC magnitude observed in M/TC LLCs in the presence of PTX could further be due to a block of inhibition at this extraglomerular location. This may not reach ETCs and may thus pose an explanation as to why ETC LLCs do not reach a ceiling level under baseline conditions in PTX, since they would not undergo this "extra" inhibition by GCs.

Alternatively, or in combination, perhaps the glutamate spillover between ETC-JGC connections is increased with occlusion due to increased P*r* of ETCs (scenario B, **Fig 14**). This spillover may act primarily on M/TC dendrites and thus amplify the LLC at the M/TC locus, foregoing the ETC LLC locus as this would be supressed with feedback-inhibition. When PTX is blocking feedback-inhibition onto ETCs, this spillover could then act at the ETC LLC locus (i.e. the ETC recurrent excitation network) and therefore result in us observing the ETC LLC change in occlusion only in PTX. Therefore, even though recurrent excitation may be increasing with occlusion due to increased glutamate spillover at the ETC-JGC synapse, the effect on ETCs themselves may not be evident when $GABA_A$ signalling persists, but still transfers to M/TC processing.

A completely different explanation could also hold true. Perhaps ETCs are only involved in the initial amplification of glutamatergic signalling, which they portray as the ETC LLC, integrated from a relatively limited network of glutamatergic signalling. This is then received by M/TCs that amplify this signal further. With occlusion, perhaps ETC LLCs are not changing at all, and only M/TC dendrodendritic amplification is increasing (scenario C, **Fig 15**). If this is the case, this stronger amplification in M/TCs under baseline conditions could result in a "spillover-LLC" reaching ETCs and enhancing their baseline LLC magnitudes. Under occluded conditions, a further ETC LLC increase in magnitude may only be observed in the presence of PTX because $GABA_A$ strongly targets ETCs (Hayar and Ennis, 2007). When $GABA_A$ signalling is intact, it could

obscure this “feedback excitation” effect in occlusion. This would suggest that the level of LLC magnitude is set by M/TC-M/TC excitation, which may be modulating LLC magnitude by changes in the efficacy of gap junctions or chemical synapses. For example, it has been shown that mGluR1 receptors on M/TC dendrites potentiate the activity of low-voltage activated Ca^{2+} channels (Johnston and Delaney, 2010). With occlusion, it could be possible that more extrasynaptic glutamate (through enhanced M/TC-M/TC recurrent excitation) is accumulated at NMDA or mGluR1 sites. This would allow higher Ca^{2+} entry, providing a way in which gene regulation and/or posttranscriptional modification could be altered in order to produce more extrasynaptic receptors to increase glutamate sensing. If there is more release of glutamate in occlusion, either by M/TCs, ETCs, or both, this could act on these “extra” extrasynaptic receptors on M/TCs rather than ETC receptors, thus increasing the M/TC response without affecting the ETC network.

Several experimental approaches could be used to test these hypotheses. To test whether subtle changes in ETC LLCs lead to large M/TC LLC changes (scenario A), we could artificially increase inhibitory drive onto ETCs in order to explore whether decreased ETC drive onto M/TCs could result in smaller M/TC LLCs. In this case, we could record ETCs and M/TCs in the presence of a benzodiazepine such as diazepam, which increases the efficacy of GABA signalling without flooding the system with GABA (Macdonald and Twyman, 1991). Since GABA likely targets ETCs directly through ETC $GABA_A$ receptors (Aungst et al., 2003; Gire and Schoppa, 2009; Whitesell et al., 2013), but also acts on M/TCs via GC connections (Friedman and Strowbridge, 2003), we would need to target diazepam to single glomeruli via puff application to ensure GC inhibition onto M/TCs is not impacted and only inhibitory action on ETCs is enhanced. We would then record ETC LLCs to observe whether they are becoming slightly smaller under these conditions. At the same time, we would record M/TCs projecting to the same glomerulus and check whether they also follow this phenotype, but respond by drastically reducing their LLC magnitude. This would reveal whether small changes in ETC LLC magnitudes are significantly amplified by the M/TC network to induce large changes in M/TC LLCs.

To test whether glutamate spillover increases between ETC-JGC connections targeting M/TCs and increasing M/TC LLCs while foregoing the ETC network (scenario B), a triple patch approach would need to be employed. We would target a JGC, ETC, and M/TC projecting to the same glomerulus, and induce ETC spiking in current clamp, while recording EPSCs in voltage-clamped JGCs and M/TCs. This approach has been used previously to show that glutamate spillover at ETC-JGC synapses reaches M/TCs due to the time-locked EPSCs recorded in both JGCs and M/TCs upon ETC spiking (Gire et al., 2018). We would thus record in this way in both control and occluded conditions to elucidate whether the recorded EPSC amplitude in M/TCs increases with

occlusion, suggesting a higher rate of glutamate spillover at the ETC-JGC synapse. To then link any effects to LLC changes, we would further, in the same cells, record LLCs and observe whether M/TC LLCs become larger, whereas ETC LLCs potentially only show a slight increase in LLC magnitude. To further strengthen the experiment, we could then wash-in PTX and observe whether occlusion effects on ETC LLCs are now evident, supporting the notion of a "feedback LLC" from M/TCs. This experiment would further show whether the locus of the LLC change is at the ETC or the M/TC level. If glutamate spillover is not increased with occlusion, it points towards M/TCs adjusting their synaptic properties to amplify the M/TC LLC (scenario C), that then is fed back to the ETC network, possibly via spillover glutamate from M/TC-M/TC connections.

To test this latter explanation (scenario C), we would again use a triple patch approach, where two connected M/TCs are recorded, as well as an ETC projecting to the same glomerulus. In this experiment, we would induce one M/TC to fire in current clamp, while recording EPSCs in the other M/TC and the ETC in the voltage clamp configuration. We would then observe whether the amplitude or probability of the M/TC EPSC increases (indicative of whether pre- or post-synaptic properties are changing), and whether this is time-locked to an ETC EPSC. Under occluded conditions, we would then expect the ETC EPSC to become larger, and upon PTX wash-in, we would see a resulting increase in ETC LLC magnitude. The necessity of patching two M/TCs stems from the idea that the glutamate received by the ETC would come due to spillover from the M/TC-M/TC connection. We would thus need to ensure that spillover does indeed occur here by recording coincident EPSCs in the voltage-clamped M/TC.

Therefore, the locus of the LLC change in general could be occurring at various points in this amplification process. As discussed above, this is likely to occur through glutamate sensing enhancements and/or increases in P*r* from ETCs and/or M/TCs. Additionally, since M/TC dendrodendritic amplification appears stronger compared to ETCs, due to the actions of NMDA and mGluR1 receptor-mediated currents (Vaaga and Westbrook, 2017), the function of these receptors could specifically be adjusted on M/TC dendrites to allow them to sense subtle increases in ETC recurrent excitation and transform these to larger M/TC responses.

4.4. Conclusion

Though we were not able to identify the locus of the glomerular LLC change observed in occlusion, we were able to show that OSN inputs do not change presynaptic function with occlusion. This suggests that the glomerular excitatory network may adjust one or more of its glutamate amplification steps to result in larger LLCs. Since OSNs *can* change their presynaptic function with longer-term occlusion, this suggests that LLC changes may be an initial step in this

process, operating after short-term sensory deprivation to prime the postsynaptic network for more efficient glutamate transmission. Alternatively, LLC changes could underlie short-term adjustments in the excitatory network that are in place for overcoming short-term perturbations, perhaps due to less metabolic energy required to produce these changes. If perturbations continue, the network may need to adjust in a more permanent manner by manipulations to OSN synaptic function. The fact that LLCs become larger with occlusion could have a huge impact on the output of the network. The magnitude of an LLC determines the overall spike output M/TCs produce in response to OSN input (Vaaga and Westbrook, 2017). It is thus likely that larger LLCs under occluded conditions would result in M/TCs producing even more prolonged firing responses to OSN stimulation under occluded conditions. Alternatively, LLC changes could ensure that M/TC responses stay consistent across varying odour input levels. Similarly, we would expect ETC firing responses to perhaps adopt a more M/TC-like behaviour when recorded in PTX under occluded conditions. These output changes could be important for enhancing the transmission of limited odour input in sensory deprived environments. In the next chapter, we aim to identify whether ETC and M/TC firing patterns in response to OSN input are changing with occlusion. If so, this may indicate the relevance of LLC changes to glomerular processing across varying input levels experienced through the changing olfactory environment.

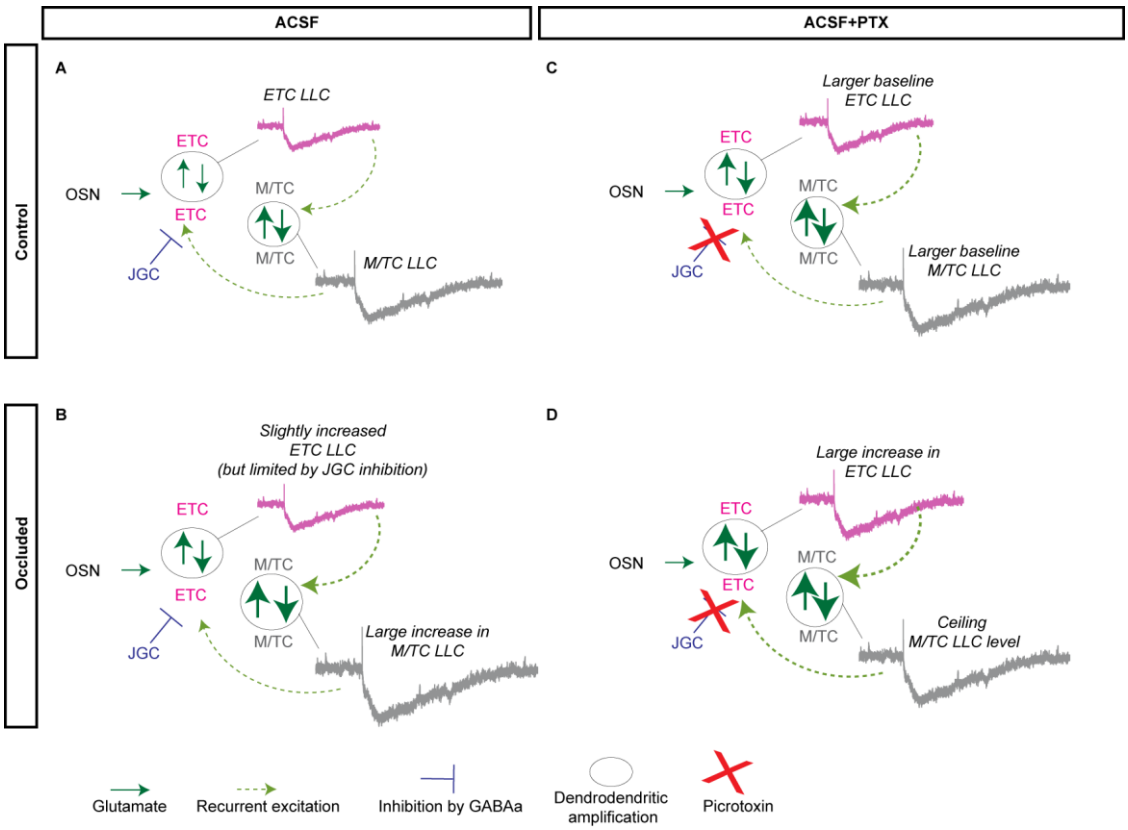

Fig 13. Scenario A.

(**A**) Under control conditions in ACSF, OSN inputs are amplified by recurrent excitation in the ETC network to produce ETC LLCs. This feeds into the M/TC recurrent excitation and dendrodendritic amplification network to produce a larger LLC compared to ETC LLCs, and may also feed back into the ETC network via network recurrent excitation. Under these conditions, $GABA_A$ signalling by JGCs targets ETCs to supress the generation and magnitude of ETC LLCs, which indirectly suppress the magnitude M/TC LLCs can reach. (**B**) Under occluded conditions in ACSF, recurrent excitation between ETCs may be slightly enhanced, which may result in a non-significant increase of the ETC LLC. This further feeds into the M/TC amplification network, which may ramp up the signal even more to generate a large M/TC LLC increase. This increase may not feed back to the ETC network because feedback inhibition by JGCs targets ETCs and thus blocks the effect, thus precluding the observation of a largely enhanced LLC in the ETC network, which may have still fed into the M/TC network and induced changes there. (**C**) Under control conditions in the presence of PTX, recurrent excitation between ETCs, M/TCs, and ETC-to-M/TCs may be enhanced, leading to larger baseline LLCs in both cell types. (**D**) Under occluded conditions in the presence of PTX, the enhanced recurrent excitation in the ETC network can act on ETCs due to lack of inhibition by JGCs, and thus allows for the observation of larger ETC LLCs. This increased amplification is transmitted to M/TCs, which cannot increase their LLC magnitudes any further as they may have reached a ceiling level.

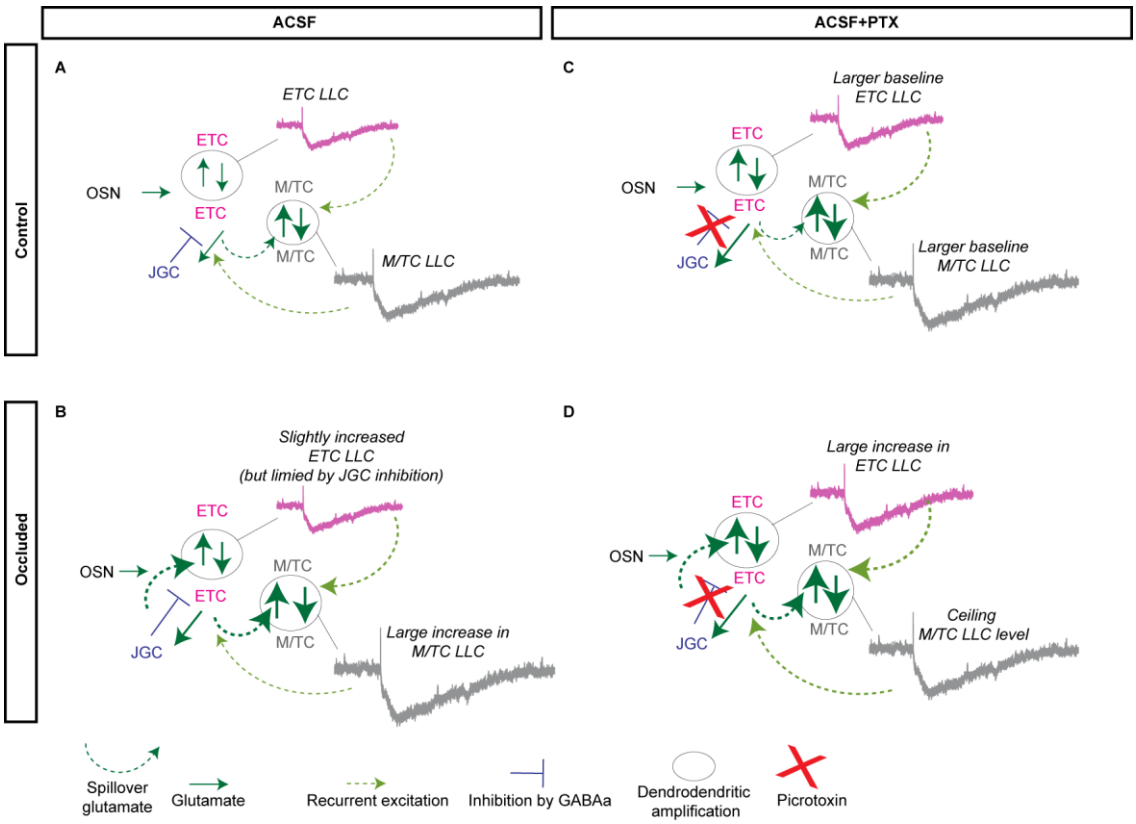

Fig 14. Scenario B.

(**A**) Under control conditions in ACSF, OSN input leads to recurrent excitation among ETCs, generating ETC LLCs which are fed forward to M/TCs. In addition to this, spillover glutamate from ETC-JGC synapses reaches M/TCs, contributing to their dendrodendritic amplification of all the glutamatergic signals they received, resulting in larger M/TC LLCs which may further be fed back into the ETC network via recurrent excitation. (**B**) Under occluded conditions in ACSF, spillover glutamate at ETC-JGC synapses may be enhanced, resulting in more glutamate recurrent excitation at the M/TC level, and thus a larger M/TC LLC. This spillover glutamate may further act on ETCs, however these would be unable to increase their LLC magnitude drastically due to enhanced feedback inhibition by JGCs. (**C**) Under control conditions in the presence of PTX, more recurrent excitation can occur between ETCs and M/TCs due to lack of inhibition onto ETCs. This leads to larger LLCs in both cell types. (**D**) Under occluded conditions in the presence of PTX, spillover glutamate at the ETC-JGC synapse may be enhanced, leading to increased recurrent excitation between ETCs and M/TCs. This may lead to the larger ETC LLC we observe in occlusion as there is no feedback inhibition subduing this increase in response. M/TC LLCs cannot become larger in these conditions due to reaching a ceiling level in LLC magnitude.

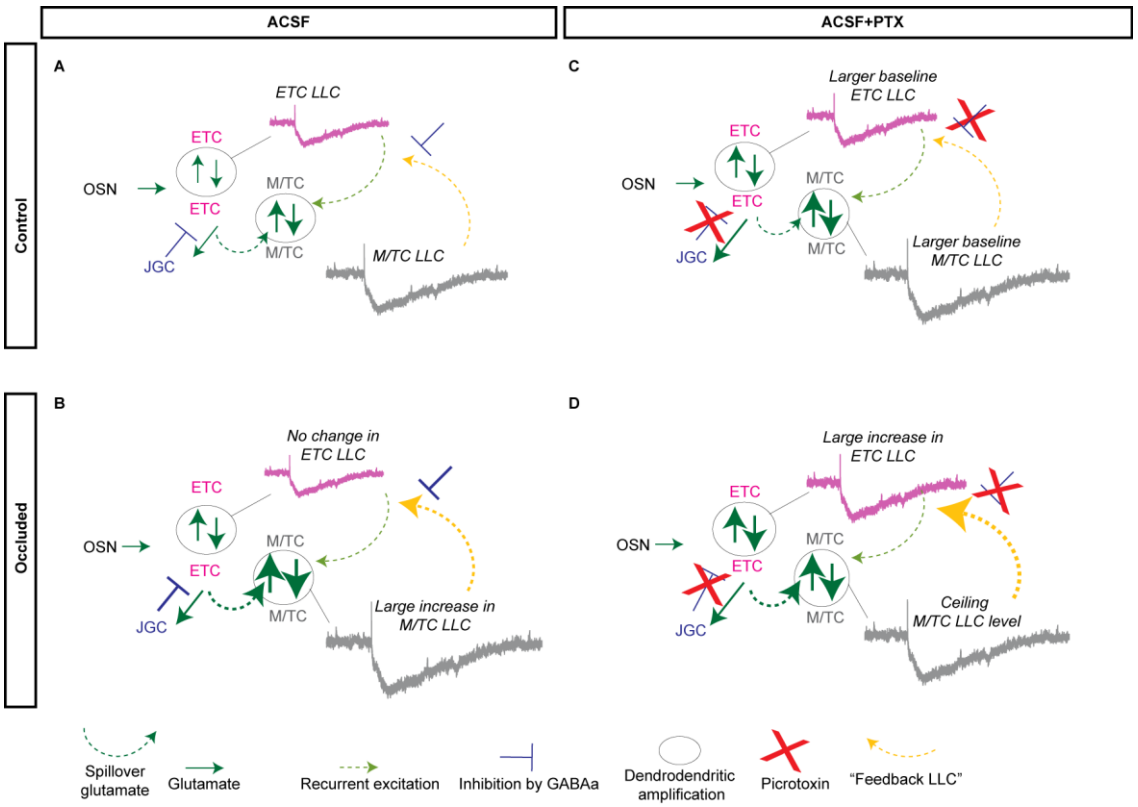

Fig 14. Scenario C.

(**A**) Under control conditions in ACSF, ETCs receive OSN input and initially amplify it to an ETC LLC. This is transmitted to M/TCs, which, along with glutamate spillover from the ETC-JGC synapse amplify this signal, reaching M/TC LLC magnitudes. This additional amplification may lead to "feedback LLCs" reaching ETCs. (**B**) Under occluded conditions in ACSF, initial OSN input amplification by ETCs remains the same, but other factors may change, such as increased synaptic or gap-junction efficacy between M/TCs, or enhanced glutamate sensing capabilities by M/TCs, which does not feed into the ETC LLC network. This is further strongly amplified by M/TCs with dendrodendritic machinery. The resulting larger M/TC LLC could be so strong that it is fed back into the ETC network, however we would not observe this due to inhibition by JGC onto ETCs. (**C**) Under control conditions in the presence of PTX, ETC recurrent excitation can be enhanced due to lack of feedback inhibition. This is further transmitted to M/TCs which are able to dendrodendritically amplify more glutamatergic signal, leading to the larger M/TC LLC found in these conditions. This large magnitude in M/TC LLCs could feedback into the ETC network, resulting in a larger ETC LLC observed in baseline conditions. (**D**) Under occluded conditions in the presence of PTX, the initial amplification of OSN inputs may become stronger, which is fed-forward to M/TCs, that cannot any further amplify their LLC magnitudes due to having reached ceiling level. However, under these conditions, the larger M/TC LLC can still be fed back into the ETC network, allowing us to observe a larger ETC LLC under these conditions.

Chapter 5

Occlusion drives subtle increases during input-evoked firing responses of external tufted cells, but mitral/tufted cell response profiles are unaffected

5.1. Introduction

We have previously shown that, under certain conditions, LLCs in OB glomeruli become larger after 24 h occlusion (chapter 4). Since LLCs are a key component of glomerular feed-forward excitation, we next wanted to establish whether occlusion has an effect on the overall glomerular input-output relationship, and if so, whether that may be correlated with the LLC phenotype. We previously showed that OSN release probability does not increase with 24h naris occlusion (chapter 4), and ETC intrinsic excitability does not change either (chapter 3). Preliminary data further suggests that M/TC intrinsic excitability also does not alter with occlusion (E. Galliano and C. Hahn, unpublished data). Thus, if any glomerular input-output firing is affected by occlusion, it is likely to occur before ET/M/TC firing output, and after initial OSN input. This means that occlusion could impact glomerular processes that are in place for modulating the OSN signal before reaching the output cells.

Several lines of evidence show that M/TCs can adjust their output firing in response to sensory manipulations via various mechanisms. For example, M/TCs can enhance their responses to odours after long-term occlusion (Wilson and Sullivan, 1995). In addition, M/TCs are highly modulated by the GCs, a group of inhibitory cells that undergo life-long neurogenesis, which form synapses onto M/TC lateral dendrites in the external plexiform layer (Chen and Shepherd, 1997). Upon sensory deprivation, the number of new-born GCs in the olfactory bulb is reduced, however, functionally they are more excitable than their control counterparts. This adjustment preserves inhibitory action on M/TCs. This in turn allows M/TCs to continue firing at the same rate and with the same synchrony as in control conditions (Saghatelyan et al., 2005). Conversely, odour over-exposure results in decreased M/TC responses to odours (Buonviso and Chaput, 2000). Though functional studies, to our knowledge, on ETC output in the face of sensory deprivation have not been performed, it is well known that inhibitory and excitatory inputs adjust ETC burst-firing. In slices, blocking ionotropic glutamate transmission reduces the number of spikes per ETC-burst, whereas the opposite is true when $GABA_A$ is blocked (Hayar and Ennis, 2007). Furthermore, ETCs show excitatory rebound responses in response to activation of the GABA/dopaminergic JGCs through D_1-Dopamine receptors present on ETCs (Liu et al., 2013). These mechanisms could thus be implicated in adjusting ETC activity during sensory deprivation. Occlusion-induced ETC and M/TC input-output changes could therefore be achieved through several mechanisms, such as changes in OSN-ET/M/TC (post)synaptic strength, changes in glutamatergic dendro-dendritic amplification between ETCs and M/TCs, and changes in the magnitude of local inhibition or even inhibition by GCs onto M/TCs.

In chapter 4 we show that LLCs become larger, under certain conditions, in occlusion. We have further shown that this effect can occur when $GABA_A$ currents are blocked (chapter 4). Furthermore, we have shown that OSN P*r* and ET/M/TC intrinsic excitability are unaffected by 24h occlusion (chapte3; E. Galliano and C. Hahn, unpublished data; chapter 4). In light of these findings this occlusion effect on LLC magnitude could stem from increased dendro-dendritic amplification in the glomerular excitatory network. Previous work has shown that LLCs are vital for establishing synchronous firing of M/TCs (Gire and Schoppa, 2009). Furthermore, as previously discussed, Vaaga and Westbrook (2017) determined that M/TC and ETC firing output in response to OSN stimulation is cell-type specific and is strongly correlated to LLC size. Therefore, if occlusion can increase the magnitude of LLCs both in ETCs and M/TCs, is there also an occlusion effect on the input-output relationship these cells exhibit? And if so, could it be linked to the occluded LLC phenotype?

In this chapter we aimed to determine whether occlusion had any effect on the evoked output of ETCs and M/TCs. We then wanted to elucidate whether any change here could be linked to the occluded LLC phenotype.

5.2. Results

5.2.1. ETCs and M/TCs respond to both high- and low-frequency OSN stimulation

We wanted to elucidate whether occlusion influences ETC and M/TC evoked firing patterns in the acute slice preparation. In order to investigate this, we electrically stimulated OSN axons while performing on-cell recordings on either ETCs or M/TCs to record OSN-evoked spikes in sham and occluded conditions (**Fig 1A-B**). On-cell recordings are particularly well-suited to study input-output relationships as there is no opportunity for the cells to become dialysed with intracellular recording solution. This provides a more physiological and accurate representation of the cell's response profile while limiting experimental artefacts. The occlusion effects we saw in ETC LLCs occurred when fast inhibitory currents were blocked with PTX, implying a potential change in the excitatory circuitry since rapid $GABA_A$-receptor-dependent feed-forward and feed-back inhibition was blocked. To link these changes to any potential effects of occlusion on input-output relationships, we therefore performed some of the evoked firing response experiments with PTX in the recording solution. Similarly, excluding PTX in some of these recordings allowed us to establish the effects of inhibition on these responses after occlusion (**Fig 1A-B**).

OSNs send their axons from the nasal epithelium to target glomeruli from multiple unpredictable directions (Potter et al., 2001). In the ONL, these axons do coalesce to some degree, but do not form a single tract per glomerulus (Mombaerts et al., 1996; Vassar et al., 1994). This may be due to the fact that in the nasal epithelium, OSNs are dispersed into four broad zones, however within those zones OSNs are apparently randomly distributed (Ressler et al., 1993).

These properties thus hinder the reliable identification of tract paths into glomeruli. In a WT acute slice visualised by DIC it is therefore difficult to distinguish inputs going towards the recorded glomerulus from inputs that do not. More crucially, when placing a stimulating electrode into the ONL, it is impossible to reliably stimulate *all* of the OSN axons terminating in a given target glomerulus, or to always stimulate the exact same proportion of those axons across all samples. One way to ensure stimulation is the same across recordings is to use a minimal stimulation paradigm, where the aim is to use such a low stimulation intensity that only a single axon is stimulated (Takahashi, 1992). However, such a stimulation is not physiological as in the intact animal odours activate multiple OSNs, and many OSNs are spontaneously active, firing at a high rate (Duchamp-Viret et al., 1999), and very weak stimulations evoke unreliable responses (**Fig 1C left**). Furthermore, minimal stimulation is unlikely to produce an action potential because this would require spatial and/or temporal integration of multiple sub-threshold inputs. Additionally, we were aiming to correlate LLC changes to ET/M/TC input-output changes. Evoked LLCs required stimulations stronger than minimal. Thus, in order to be consistent in our experiments we did not want to alter our stimulation paradigm. Finally, to induce the temporal patterns Vaaga and Westbrook (2017) observed, we decided to use the same approach in terms of our stimulations.

Due to this variability in stimulus strength and OSN axon targeting properties, the same electrical stimulus strength will never recruit the same number of fibres between different electrode positions in different slices, making it impossible to use the same stimulus across all recordings. Since OSN stimulation strength could never be identical for each recorded cell in this preparation, a set of strict criteria was established to normalise stimulation strength across cells (**Fig 1C**). The chosen stimulus strength was the weakest strength at which 20-pulse-train stimulation reliably evoked equivalent non-zero numbers of action potentials after the first two pulses, in four out of five sweeps (**Fig 1C**). Two stimulation frequencies were picked to represent high- (Vaaga and Westbrook, 2017) (50Hz) and low-(5Hz) frequency (Burton and Urban, 2014) afferent stimulation. 5Hz stimulus frequency was chosen from pilot data frequency-response curves obtained from 6 M/TCs, which showed that at this frequency, responses could still be reliably produced and were not saturated in terms of overall firing frequency (data not shown). Both stimulation frequencies were given with 20 pulses, with an inter-train interval of 60s to

allow OSN vesicles to replenish (Vaaga and Westbrook, 2017) (**Fig 1Di-Dii**). With high-frequency stimulation, we recorded 24 sham and 15 occluded ETCs in ACSF, 18 sham and 14 occluded ETCs in ACSF+PTX, 18 sham and 15 occluded M/TCs in ACSF, and 15 sham and 15 occluded M/TCs in ACSF+PTX. With low-frequency stimulation, we recorded 15 sham and 9 occluded ETCs in ACSF, 12 sham and 8 occluded ETCs in ACSF+PTX, 11 sham and 10 occluded M/TCs in ACSF, and 12 sham and 12 occluded M/TCs in ACSF+PTX. Before measuring evoked responses however, we first wanted to observe whether occlusion affects ETC and M/TC spontaneous firing (**Fig 2**).

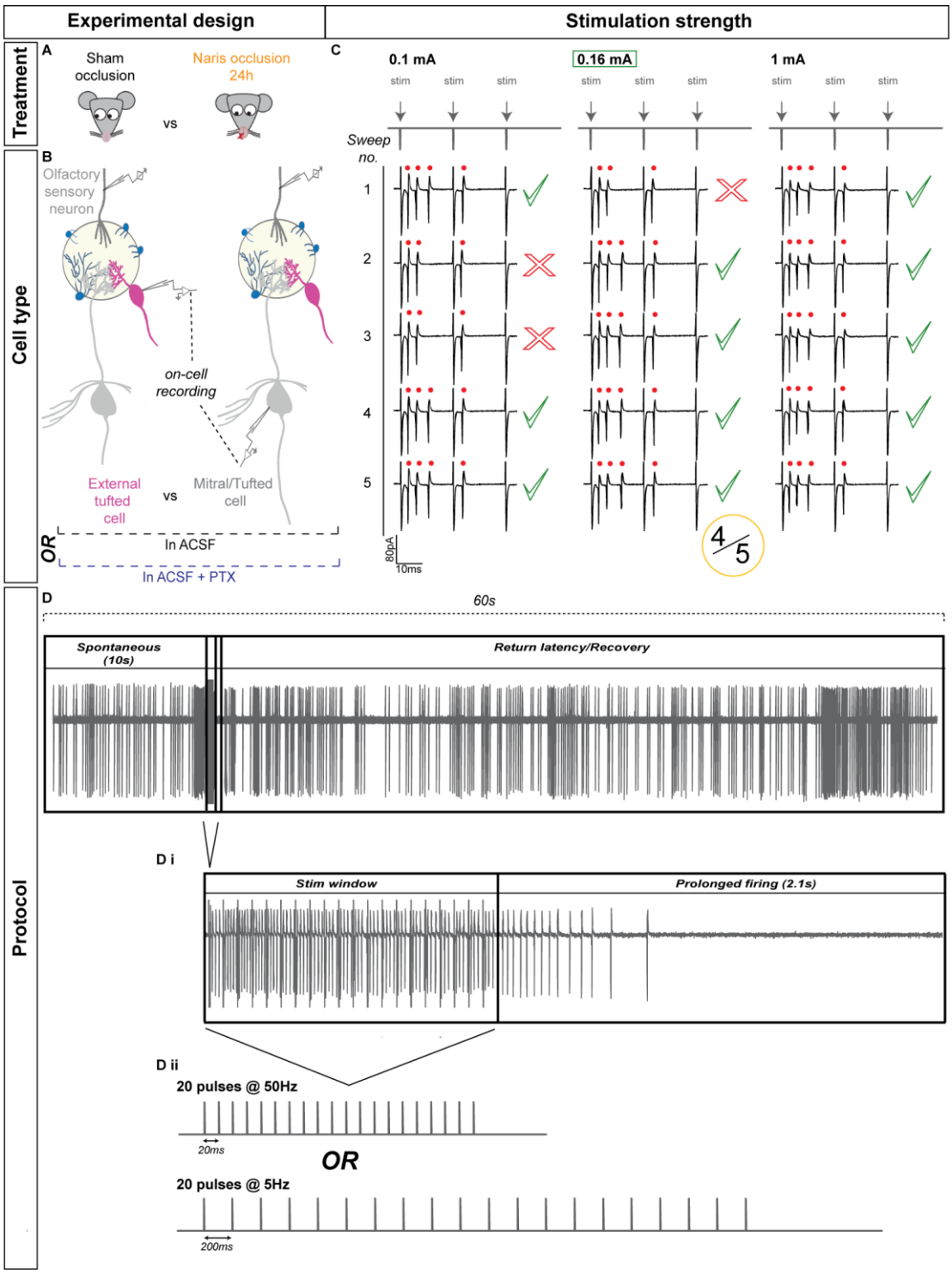
Experimental design
Stimulation strength
Treatment
Cell type
Protocol
A
Sham occlusion
vs
Naris occlusion 24h
B
Olfactory sensory neuron
on-cell recording
External tufted cell
vs
Mitral/Tufted cell
OR
In ACSF
In ACSF + PTX
C
0.1 mA
0.16 mA
1 mA
stim
Sweep no.
1
2
3
4
5
80pA
10ms
4/5
D
60s
Spontaneous (10s)
Return latency/Recovery
D i
Stim window
Prolonged firing (2.1s)
D ii
20 pulses @ 50Hz
20ms
OR
20 pulses @ 5Hz
200ms

Fig 1. Experimental design to compare the output profile of external tufted cells (ETCs) and mitral/tufted cells (M/TCs) in response to olfactory sensory neuron (OSN) stimulation after sham or unilateral naris occlusion.

(**A**) P20-P35 WT mice were either sham occluded or underwent unilateral naris occlusion for 24 hours before acute slices were obtained. (**B**) OSN axons (dark grey) were electrically stimulated while either ETCs (magenta) or M/TCs (grey) were recorded in the on-cell configuration. Recordings were obtained in either artificial cerebral spinal fluid (ACSF) or ACSF containing picrotoxin (10μM PTX). (**C**) Stimulation strength was chosen based on observing the same number of spikes after the first two 20-or 200μs-duration stimuli of a 20-stimulus train for 4/5 sweeps from the recorded cell. Once this was established, the minimum stimulus intensity to evoke this response was used. Red dots indicate spikes. Left: at 0.1mA stimulation strength the cell did not fire consistently in 2/5 sweeps. Middle: at 0.16mA stimulation strength the cell fired reliably in 4/5 sweeps. Right: at 1mA stimulation strength the cell fired reliably for 5/5 sweeps. The weaker stimulus strength (0.16mA) was therefore utilised during this example recording. (**D**) Sweeps were recorded for 60s each. The first 10s of recording was used to obtain a measure of spontaneous firing frequency. The stimulus window incorporated either a 50Hz (**D i**) or 5Hz (**D ii**) train of 20 pulses. After the stimulation window, a 2.1s period was used to calculate prolonged firing. The remainder of the trace was used to observe when cells returned to their baseline firing rate.

5.2.2. 24 hour naris occlusion does not alter spontaneous ET/M/TC firing

ETCs and M/TCs fire spontaneously, shown both in slices (Hayar et al., 2004; Heyward et al., 2001) and *in vivo* (Kaba and Seto, 1993; Tatti et al., 2014). Our previous finding show that LLCs become larger with occlusion and that LLCs can occur spontaneously (chapter 4). Since LLCs drive the firing patterns of ETCs and M/TCs (Vaaga and Westbrook, 2017), we wondered whether occlusion-induced LLC changes could be correlated with alterations in those cells' spontaneous firing. We thus performed on-cell recordings on ETCs and M/TCs in either ACSF or ACSF+PTX external solutions to observe spontaneous firing rate and patterning (**Fig 2A-B**). Spontaneous firing measures were taken from recordings obtained before the OSN-evoked protocol was started. Both ETCs and M/TCs fired spontaneously in ACSF as well as ACSF+PTX.

We started by combining all spontaneous recording data in one statistical test. However, upon performing a 3-way ANOVA to compare cell type, treatment, and drug, we observed that only PTX had a significant and expected (Shao et al., 2012) effect of increasing firing rate (. *3-way ANOVA*: effect of PTX, $F_{(1,265)}$=37.17, p<0.001, all other effects and interactions, p>0.05). We thus chose to separate all further statistical analyses by comparing effects either in ACSF or ACSF+PTX using 2-way ANOVAs in order to observe any differences attributed to occlusion and/or cell-type that may be masked by the large and entirely predicted effect of $GABA_A$ block. However, occlusion still had no significant effect on firing rates in ETCs or M/TCs, in either ACSF or ACSF+PTX (ETCs: sham in ACSF mean ± SEM 4.76 ± 0.65 Hz *n = 43*; occluded in ACSF 5.43 ± 0.68Hz *n=42*; sham in ACSF+PTX 9.06 ± 1.42Hz *n=26*; occluded in ACSF+PTX 12.82 ± 4.45Hz *n=28*; M/TCs: sham in ACSF mean ±SEM 4.76 ± 1.27Hz *n=38*; occluded in ACSF 4.31 ± 0.57Hz *n=38*; sham ± SEM in ACSF+PTX 12.35 ± 1.81Hz *n=27*; occluded ±SEM in ACSF+PTX 12.67 ± 2.67Hz *n=31*; *2-way ANOVAs* on sqrt-transformed data; ACSF: effect of manipulation, $F_{(1,157)}$=0.84, p=0.36; ACSF+PTX: effect of manipulation, $F_{(1,108)}$=0.003, p=0.96). There was also no difference between ETC and M/TC firing rates in either condition, nor any significant interaction between occlusion and cell-type (*2-way ANOVAs* on sqrt-transformed data; ACSF: effect of cell-type, $F_{(1,157)}$=1.17, p=0.28, interaction, $F_{(1,157)}$=0.02, p=0.92; ACSF+PTX: effect of cell-type, $F_{(1,108)}$=1.39, p=0.24, interaction, $F_{(1,108)}$=0.11, p=0.74) (**Fig 2C**).

Though the firing rates of ETCs and M/TCs were not affected by occlusion, the pattern of firing could have been affected. We therefore quantified firing patterns by measuring the coefficient of variation (CV) of inter-spike intervals (ISI), which is a classical measure of burst firing. As with firing rate, occlusion did not affect the burst firing of ETCs and M/TCs, in either ACSF or ACSF+PTX (ETCs: sham in ACSF mean ± SEM 1.82 ± 0.24 *n=36*; occluded in ACSF 1.68 ± 0.20 *n=37*; sham in ACSF+PTX 2.91 ± 0.46 *n=24*; occluded in ACSF+PTX 2.45 ± 0.48 *n=25;* M/TCs: sham in ACSF mean

± SEM 1.51 ± 0.26 *n=30*; occluded in ACSF 1.58 ± 0.22 *n=31*; sham in ACSF+PTX 1.74 ± 0.39 *n=26*; occluded in ACSF+PTX 2.24 ± 0.38 *n=29*; *2-way ANOVAs* on $\log_{10}$-transformed data; ACSF: effect of manipulation $F_{(1,130)}$=0.0004, p=0.98; ACSF+PTX: effect of manipulation, $F_{(1,100)}$=0.20, p=0.65). Similarly, there was no difference between ETC and M/TC burst firing in either condition, nor any significant interaction between occlusion and cell-type (*2-way ANOVAs* on $\log_{10}$-transformed data; ACSF: p=0.98, effect of cell-type, $F_{(1,130)}$=0.44, p=0.51, interaction, $F_{(1,130)}$=0.04, p=0.85; ACSF+PTX: effect of cell-type, $F_{(1,100)}$=4.42, p=0.04, interaction, $F_{(1,100)}$=0.69, p=0.41) (**Fig 2D**). In light of these results, 24h occlusion does not appear to impact spontaneous firing rates or patterns in ETCs and M/TCs in acute slices.

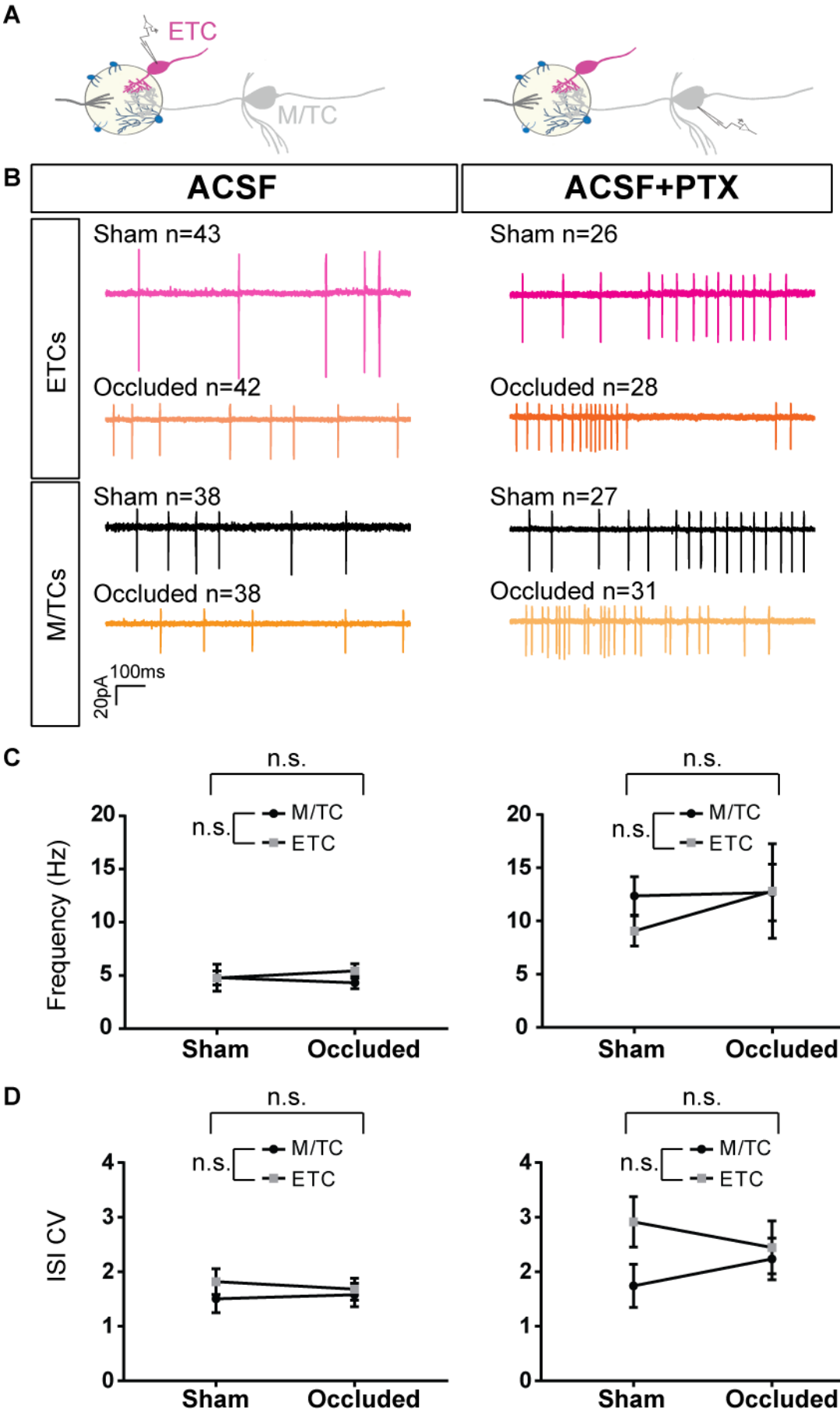
A
ETC
M/TC
B
ACSF
ACSF+PTX
ETCs
M/TCs
Sham n=43
Occluded n=42
Sham n=26
Occluded n=28
Sham n=38
Occluded n=38
Sham n=27
Occluded n=31
100ms
20pA
C
Frequency (Hz)
n.s.
M/TC
ETC
Sham
Occluded
D
ISI CV

Fig 2. 24h naris occlusion does not affect spontaneous firing of external tufted cells (ETCs) or mitral/tufted cells (M/TCs).

(**A**) Either ETC (magenta) or M/TC (grey) spontaneous firing was recorded in the on-cell configuration. (**B**). Example traces of ETC (top) and M/TC (bottom) spontaneous firing in sham and occluded conditions. The recording solution was either artificial cerebrospinal fluid (ACSF) (left) or ACSF + 10μM picrotoxin (PTX) (right). (**C-D**) Graphs showing quantification of spontaneous firing frequency (top) and coefficient of variation (CV) of inter-spike intervals (ISI) (bottom) in ACSF (left) or ACSF + PTX (right). Coloured squares represent means; error bars show SEM. n.s., non-significant.

5.2.3. ETCs and M/TCs do not adjust their basic evoked-firing rates in response to occlusion

To investigate how occlusion affects evoked firing rate in ETCs and M/TCs, we performed on-cell recordings of either cell-type while stimulating OSN axons as described above (**Fig 3Ai, Fig 4Ai**). We examined the evoked response profile by quantifying the firing rate during the stimulation train and the 2.1s period sustained firing window immediately following this (**Fig 3Aii, Fig 4Aii**). This prolonged window was incorporated into the analyses as it is known that M/TCs continue firing well after the stimulus train due to dendro-dendritic amplification via LLCs (Vaaga and Westbrook, 2017), and we wanted to investigate whether occlusion affects this sustained firing. Afferent stimulation at 50Hz is considered strong (Vaaga and Westbrook, 2017; Macridez et al., 1975). We thus considered whether M/TCs could reach a ceiling level of sustained firing with this stimulation protocol, precluding the observation of any changes in firing rate. To increase our chances of observing any change in M/TCs therefore, we looked toward more physiological input frequencies, and additionally performed input-output experiments using a 5Hz afferent stimulus frequency to represent a slightly weaker input strength (Burton and Urban, 2014) (**Fig 4 Ai-Aii**)

Both ETCs and M/TCs reliably fired action potentials throughout the 50Hz (**Fig 3B**) and the 5Hz (**Fig 4B**) stimulation trains, and overall firing patterns were largely consistent across cells. From these recordings, high-frequency stimulation in ACSF revealed the characteristic post-stimulus sustained firing in M/TCs. This was not as pronounced in ETCs, although PTX did appear to prolong this response in this cell type. During low-frequency stimulation, both ETCs and M/TCs appeared to fire at a roughly similar rate. The responses to this 5 Hz stimulus appeared more phase-locked compared to high-frequency afferent stimulation, with negligible post-stimulus sustained spiking.

Occlusion had no effect on total evoked firing rate of ETCs or M/TCs during the stimulation and sustained firing window during *high-frequency* stimulation (**Fig 3C**). Similar to published results (Vaaga and Westbook, 2017), M/TCs showed higher evoked firing rates during the stimulation and sustained firing window compared to ETCs in the shammed condition during recordings made in ACSF (**Fig 3C**) but blocking inhibition allowed ETCs to increase their evoked firing rate to a similar level as M/TCs. (**Fig 3C**; ETCs: sham in ACSF mean ±SEM 16.45 ± 2.59Hz *n=24*; occluded in ACSF 21.41 ± 3.01Hz *n=15*; sham in ACSF+PTX 43.17 ± 6.27Hz *n=18*; occluded in ACSF+PTX 29.07 ± 5.17Hz *n=14*. M/TCs: sham in ACSF mean ±SEM 29.45 ± 4.0Hz *n=18*; occluded in ACSF 20.28 ± 4.46Hz *n=15*; sham in ACSF+PTX 49.01 ± 7.21Hz *n=15*; occluded in ACSF+PTX 45.09 ± 5.43Hz *n=15; 2-way ANOVAs* on sqrt transformed data, ACSF: effect of manipulation,

$F_{(1,68)}$=0.89, p=0.35, effect of cell-type, $F_{(1,68)}$=8.02, p=0.01, interaction, $F_{(1,68)}$=0.87, p=0.35; ACSF+PTX: effect of treatment, $F_{(1,58)}$=1.40, p=0.24, effect of cell-type, $F_{(1,58)}$=3.97, p=0.05, interaction, $F_{(1,58)}$=0.91, p=0.34)

To investigate whether ETC and M/TC firing rates are perhaps impacted by occlusion only during the stimulation period itself, we quantified firing rates only over the high-frequency stimulus train (**Fig 3C**). Again, firing rates during only the high-frequency stimulation period were not significantly impacted by occlusion in either ETCs or M/TCs, and ETC and M/TC firing rates did not differ significantly from each other (**Fig 3C**: ETCs: sham in ACSF mean ±SEM 74.88 ± 9.03Hz *n=24*; occluded in ACSF 91.28 ± 11.42Hz *n=15*; sham in ACSF+PTX 129.9 ± 15.34Hz *n=18*; occluded in ACSF+PTX 99.97 ± 15.25Hz *n=14;* M/TC*s*: sham in ACSF mean ±SEM 92.15 ± 10.53Hz *n=18*; occluded in ACSF 78.35 ± 10.20Hz *n=15*; sham in ACSF+PTX 97.35 ± 12.07Hz *n=15*; occluded in ACSF+PTX 109.5 ± 7.69Hz *n=15; 2-way ANOVAs* on sqrt transformed data*,* ACSF: effect of manipulation, $F_{(1,68)}$=0.08, p=0.78, effect of cell-type, $F_{(1,68)}$=0.08, p=0.78, interaction, $F_{(1,68)}$=2.03, p=0.16. ACSF+PTX: effect of manipulation, $F_{(1,58)}$=0.15, p=0.70, effect of cell-type, $F_{(1,58)}$=0.25, p=0.62, interaction, $F_{(1,58)}$=2.66, p=0.11).

With *low frequency* afferent stimulation, occlusion also did not appear to affect total evoked firing rate throughout the stimulation and sustained firing window in ETCs and M/TCs, and there were overall no significant differences between M/TC and ETC total evoked firing rate (**Fig 4C**) (ETCs: sham in ACSF mean ±SEM 14.77 ± 2.46Hz *n=15*; occluded in ACSF 14.15 ± 3.24Hz *n=9*; sham in ACSF+PTX 35.57 ± 6.93Hz *n=12*; occluded in ACSF+PTX 19.62 ± 4.53Hz *n=8*; M/TCs: sham in ACSF mean ±SEM 15.34 ± 2.90Hz *n=11*; occluded in ACSF 20.68 ± 4.18Hz *n=10*; sham in ACSF+PTX 35.43 ± 5.74Hz n=*12*; occluded in ACSF+PTX 28.72 ± 2.98Hz *n=12*; *2-way ANOVAs* on $\log_{10}$ transformed data, ACSF: effect of manipulation, $F_{(1,41)}$=0.40, p=0.53, effect of cell-type, $F_{(1,41)}$=1.01, p=0.32, interaction, $F_{(1,41)}$=0.31, p=0.58. ACSF+PTX: effect of manipulation, $F_{(1,40)}$=1.84, p=0.18, effect of cell-type, $F_{(1,40)}$=2.42, p=0.13, interaction, $F_{(1,40)}$=0.95, p=0.34).

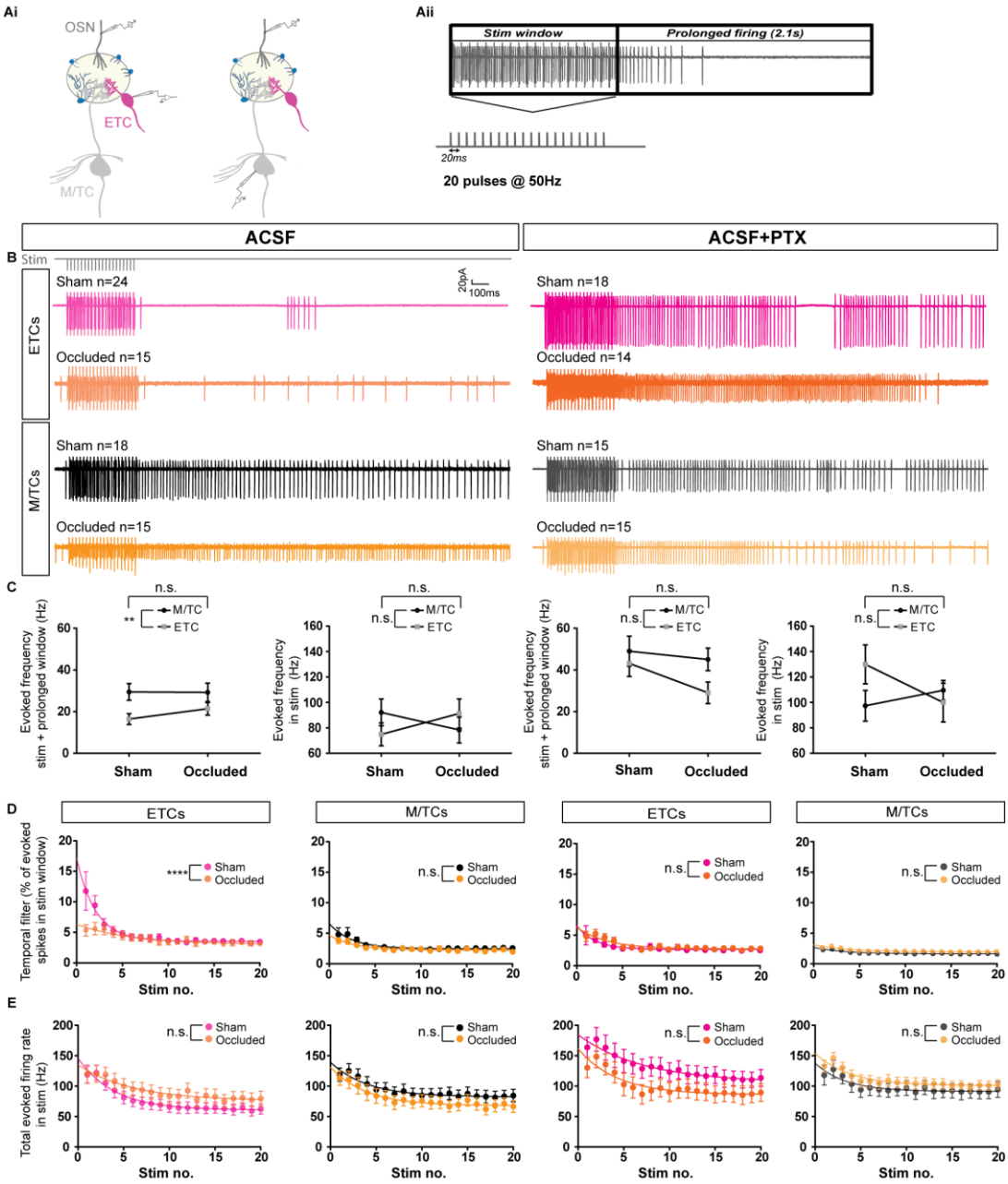
Ai
OSN
ETC
M/TC
Aii
Stim window
Prolonged firing (2.1s)
20ms
20 pulses @ 50Hz
ACSF
ACSF+PTX
B
Stim
ETCs
M/TCs
Sham n=24
Occluded n=15
Sham n=18
Occluded n=14
Sham n=18
Occluded n=15
Sham n=15
Occluded n=15
20pA
100ms
C
Evoked frequency stim + prolonged window (Hz)
Evoked frequency in stim (Hz)
n.s.
**
M/TC
ETC
Sham
Occluded
D
ETCs
M/TCs
Temporal filter (% of evoked spikes in stim window)
****
Sham
Occluded
Stim no.
E
Total evoked firing rate in stim (Hz)
Stim no.

Fig 3. Occlusion alters external tufted cell (ETC) temporal filter in response to high-frequency input when inhibition is blocked.

(**Ai**) Olfactory sensory neuron (OSN) axons, shown in dark grey, were stimulated while either ETCs (magenta) or mitral/tufted cells (M/TCs), shown in grey, were recorded in the on-cell configuration. (**Aii**) Firing rates were obtained from spikes occurring during the stimulation window (20 pulses at 50Hz) and the 2.1s post-stimulus prolonged firing window. (**B**) Example traces of ETC (top) and M/TC (bottom) evoked firing in sham and occluded conditions. The recording solution was either artificial cerebrospinal fluid (ACSF) (left) or ACSF + 10μm picrotoxin (PTX) (right). Stimulation protocol shown on top left (grey); stimulus artefacts have not been removed from the recordings. (**C**) Graphs showing quantification of evoked firing rates during stimulation + 2.1s window and evoked firing rates during the stimulation window in ACSF on the left two graphs, and in ACSF+PTX on the right two graphs. Coloured squares represent means; error bars show SEM. (**D**) Graphs displaying mean temporal filters of ETCs and M/TCs recorded in ACSF (two left graphs) or ACSF+PTX (two right graphs), fit with one-phase decays. Error bars indicate SEM. Temporal filters were obtained by calculating the percentage of spikes evoked after each stimulus from the total evoked spikes during the stimulation window. (**E**) Plots showing mean evoked firing rates during the stimulus train for ETCs and M/TCs recorded in ACSF (two left graphs) or ACSF+PTX (two right graphs), fit with one-phase decays. Error bars indicate SEM. **, $p<0.01$; ****, $p<0.0001$; n.s., non-significant.

As observed with high-frequency afferent stimulation, occlusion also had no significant effect on directly evoked firing rates during the low-frequency stimulation train in ETCs and M/TCs, and no ETC/M/TC evoked firing rate differences throughout the stimulus window were observed (**Fig 4C**) (ETCs: sham in ACSF mean ±SEM 24.48 ± 3.48Hz *n=15*; occluded in ACSF 24.24 ± 5.71Hz *n=9*; sham in ACSF+PTX 51.47 ± 11.81 *n=12*; occluded in ACSF+PTX 30.58 ± 5.95Hz *n=8*; M/TCs: sham in ACSF mean ±SEM 24.21 ± 4.27Hz *n=11*; occluded in ACSF 32.99 ± 5.73Hz *n=10*; sham in ACSF+PTX 55.08 ± 8.96Hz *n=12*; occluded in ACSF+PTX 46.12 ± 3.70Hz *n=12*; *2-way ANOVAs* on $\log_{10}$ transformed data, ACSF: effect of manipulation, $F_{(1,41)}$=0.69, p=0.41, effect of cell-type, $F_{(1,41)}$=0.85, p=0.36, interaction, $F_{(1,41)}$=0.51, p=0.48. ACSF+PTX: effect of manipulation, $F_{(1,40)}$=0.34, p=0.56, effect of cell-type, $F_{(1,40)}$=0.39, p=0.07, interaction, $F_{(1,40)}$=0.21, p=0.65). These results demonstrate that occlusion does not seem to impact ETC and M/TC basic firing rates in response to high- or low-frequency afferent stimulation.

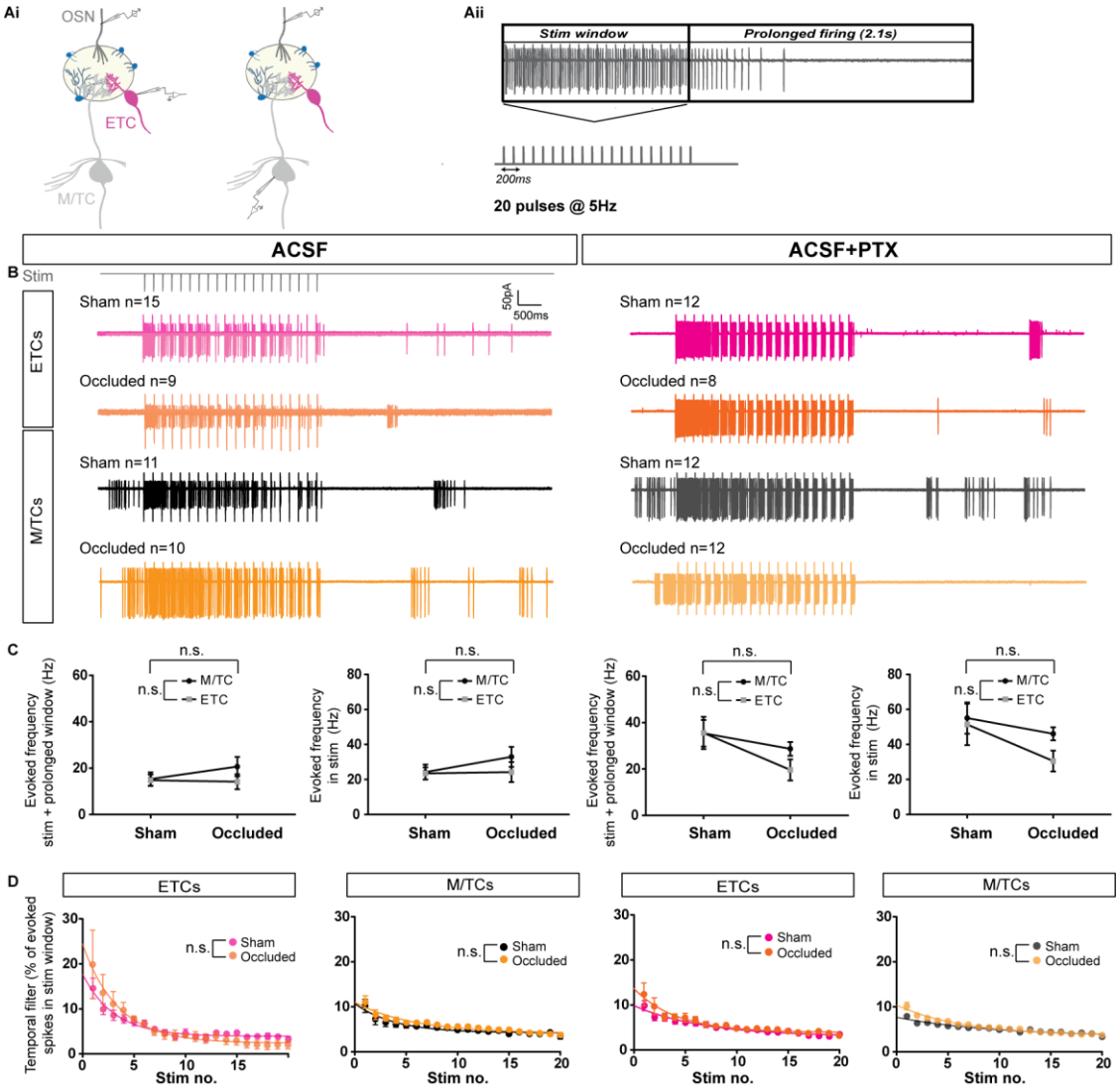

Fig 4. External tufted cells (ETCs) and mitral/tufted cells (M/TCs) do not adapt their temporal filter in response to low-frequency input after occlusion.

(**Ai**) Olfactory sensory neuron (OSN) axons, shown in dark grey, were stimulated while either ETCs (magenta) or M/TCs (grey), were recorded in the on-cell configuration. (**Aii**) Firing rates were obtained from spikes occurring during the stimulation window (20 pulses at 5Hz) and the 2.1s post-stimulus prolonged firing window. (**B**) Example traces of ETC (top) and M/TC (bottom) evoked firing in sham and occluded conditions. The recording solution was either artificial cerebrospinal fluid (ACSF) (left) or ACSF + 10µm picrotoxin (PTX) (right). Stimulation protocol shown on top left (grey); stimulus artefacts have not been removed from the recordings. (**C**) Graphs showing quantification of evoked firing rates during stimulation + 2.1s window and evoked firing rates during the stimulation window in ACSF on the left two graphs, and in ACSF+PTX on the right two graphs. Coloured squares represent means, error bars show SEM. (**D**) Graphs displaying temporal filters of ETCs and M/TCs recorded in ACSF (two left graphs) or ACSF+PTX (two right graphs), fit with one-phase decays. Error bars indicate SEM. Temporal filters were obtained by calculating the percentage of spikes evoked after each stimulus from the total evoked spikes during the stimulation window. n.s., non-significant

5.2.4. ETCs increase sustained transmission in response to high frequency afferent stimulation after occlusion

The measures examined above indicate that occlusion does not affect ETC and M/TC overall firing rate in response to high- or low-frequency afferent stimulation. However, these measurements did not quantify more subtle changes in firing profiles. Vaaga and Westbrook (2017) showed a clear difference in M/TC versus ETC firing patterns in response to high-frequency stimulation of OSNs, where ETCs produced a transient response but M/TCs prolonged their elevated firing to produce a more sustained response. They measured this phenomenon by quantifying the temporal filters of these cells, by calculating the percentage of spikes fired in response to each individual stimulus over the spikes fired during the entire stimulation window. In this approach, if cells are firing most of their evoked action potentials early in the stimulus train, their temporal filter is steeper, indicative of a transient response. Conversely, if cells fire steadily throughout the stimulus train, their temporal filter is shallower, indicative of a sustained response. M/TC temporal filters were shallow (Vaaga and Westbrook, 2017), implying that they continuously generate action potentials at a similar rate throughout the stimulus window. M/TCs were able to prolong their response because of dendro-dendritic amplification of glutamatergic signal in the shape of their much larger LLCs compared to ETC LLCs. The direct link between LLC magnitude and temporal filter pattern was evident, since blocking mGluR1 and NMDA receptors, known to inhibit M/TC LLCs (De Saint Jan and Westbrook, 2007), refined M/TC spiking to a less sustained response (Vaaga and Westbrook, 2017). Because LLCs are so highly relevant for determining the temporal filter in ETCs and M/TCs, and because we had clear occlusion effects on LLCs in both cell-types (chapter 4), we next wanted to analyse evoked firing patterns during the stimulation window in ETCs and M/TCs in a similar fashion to Vaaga and Westbrook's (2017) technique to observe whether the temporal filters of these cells are affected by occlusion.

We quantified temporal filters by calculating the percentage of spikes evoked after each stimulus from the total evoked spikes during the stimulation window. The average response curves could be fit by a one-phase decay where a relatively steep input-output relationship is representative of a transient response and is reflected in a high value of the fitted *k* parameter. Steepness of these mean response curves could then be compared with an extra sum of squares F-test on *k* values (Vaaga and Westbrook, 2017). Since this involved performing 6 separate pairwise comparisons for both our 5 and 5Hz stimulation data, we needed to employ Bonferroni correction of our significance threshold, meaning that the new α-value was 0.05/6 = 0.008.

In response to high-frequency OSN stimulation, occlusion significantly increased ETC sustained firing when inhibition was left intact (**Fig 3D**) (ETC sham τ=2.08 stimuli, *k*=0.48, *n=24;* ETC occluded τ=6.16 stimuli, *k*=0.16, *n=15; extra sum of squares F-test*, comparing *k* values p<0.0001). This occlusion effect in ETCs was not as pronounced in ACSF+PTX, and though there was a trend towards more prolonged firing in occlusion, it was not significantly different to sham conditions (**Fig 3D**) (sham τ=2.03 stimuli, *k*=0.49, *n=18*; occluded τ=3.35 stimuli, *k*=0.30, *n=14; extra sum of squares F-test*, comparing *k* values p=0.09). Therefore, with high-frequency OSN stimulation, the occlusion effect we see on the ETC temporal filter seems to be at least partly dependent on inhibition via $GABA_A$ signalling, as no significant effect was observed when $GABA_A$ signalling was blocked. Contrastingly, occlusion did not significantly impact M/TC temporal filters in response to high-frequency afferent stimulation with or without $GABA_A$ inhibition (**Fig 3D**). (ACSF: sham τ=2.45 stimuli, *k*=0.41 *n=18*; occluded τ=2.76 stimuli, *k*=0.36, *n=15; extra sum of squares F-test*, comparing *k* values p=0.65. ACSF+PTX: sham τ=3.39 stimuli, *k*=0.29, *n=15*; occluded τ=3.61 stimuli, *k*=0.28, *n=15; extra sum of squares F-test*, comparing *k* values, p=0.85). No significant differences were observed between ETCs and M/TCs in any condition (ACSF: sham ETC vs sham M/TC *extra sum of squares F-test*, comparing *k* values p=0.29, occluded ETC vs occluded M/TC *extra sum of squares F-test*, comparing *k* values p=0.02, ACSF+PTX: sham ETC vs sham M/TC *extra sum of squares F-test*, comparing *k* values p=0.14, occluded ETC vs occluded M/TC *extra sum of squares F-test*, comparing *k* values p=0.89). However, there does seem to be a trend towards a shallower curve in M/TCs compared to ETCs in sham ACSF conditions, corresponding with Vaaga and Westbrook's (2017) findings, but this slight difference was not statistically significant in our hands.

In response to *low-frequency* stimulation, ETCs and M/TCs did not alter their temporal filter with occlusion either with or without inhibition (**Fig 4D**) (ACSF: ETCs: sham τ=3.06 stimuli, *k*=0.32, *n=15*; occluded τ=3.45 stimuli, *k*=0.29, *n=9; extra sum of squares F-test*, comparing *k* values p=0.39 , M/TCs: sham τ=3.88 stimuli, *k*=0.26, *n=11*; occluded τ=5.70 stimuli, *k*=0.17, *n=10*, *extra sum of squares F-test*, comparing *k* values p=0.23; ACSF+PTX: ETCs: sham τ=6.78 stimuli, *k*=0.15, *n=12*; occluded τ=4.17 stimuli, *k*=0.24, *n=8*; *extra sum of squares F-test*, comparing *k* values p=0.39; M/TCs: sham τ=9.66 stimuli, *k*=0.10, *n=12*; occluded τ=6.40 stimuli, *k*=0.16, *n=12; extra sum of squares F-test*, comparing *k* values p=0.22). Additionally, no cell-type differences were observed in any conditions (**Fig 4D**) (ACSF: sham ETC vs sham M/TC *extra sum of squares F-test*, comparing *k* values p=0.43; occluded ETC vs occluded M/TC *extra sum of squares F-test*, comparing *k* values p=0.07; ACSF+PTX: sham ETC vs sham M/TC *extra sum of squares F-test*, comparing *k* values p=0.38; occluded ETC vs occluded M/TC extra sum of squares F-test, comparing *k* values p=0.06).

These data suggest that occlusion has no effect on M/TC sustained firing nor firing pattern either with high- or low-frequency afferent stimulation. ETCs however, though not changing their overall evoked firing rate, are able to change their firing pattern throughout a stimulus train after occlusion.

5.2.4. Occlusion does not affect post-input prolonged firing in ETCs and M/TCs

Since low-frequency stimulation did not reveal any occlusion effects on ETC and M/TC temporal filters, and the only occlusion effect occurred during high-frequency OSN stimulation, we decided to focus further analysis on prolonged firing induced/evoked by high-frequency stimulation. Above, we show that ETC responses to high-frequency OSN stimulation became more sustained with occlusion. Could this be linked to a more sustained response after the stimulus offset? To investigate whether this indeed occurs, we quantified evoked firing rates occurring solely during the 2.1s sustained firing window (**Fig 5 Ai-Aii**). M/TCs always produced action potentials during this time-window whereas for ETCs this was not always the case -rarely, ETCs were silent in this window (<10% of cells) (**Figure 5B**).

M/TCs fired at a significantly higher rate in the post-stimulus period compared to ETCs, both with and without inhibition. However, occlusion did not affect prolonged firing in either cell-type (**Fig 5C**). (ACSF: ETCs: sham mean ±SEM 6.19 ± 1.90Hz *n=24;* occluded 8.99 ± 1.83Hz *n=15;* M/TCs*:* sham mean ±SEM 17.62 ± 3.36Hz *n=18*; occluded 19.93 ± 3.88Hz *n=15; 2-way ANOVA* on sqrt transformed data: effect of treatment, $F_{(1,68)}$=2.10, p=0.15, effect of cell-type, $F_{(1,68)}$=16.94, p=0.0001, interaction, $F_{(1,68)}$=0.57, p=0.45; ACSF+PTX: ETCs: sham mean ±SEM 26.77 ± 5.2Hz *n=18;* occluded 15.91 ± 3.85Hz *n=14;* M/TCs: sham mean ±SEM 39.81 ± 6.44Hz *n=15;* occluded 32.9 ± 5.37Hz *n=15; 2-way ANOVA* on sqrt transformed data: effect of manipulation, $F_{(1,58)}$=1.82, p=0.18, effect of cell-type, $F_{(1,58)}$=9.97, p=0.003, interaction, $F_{(1,58)}$=0.25, p=0.62).

These results agree with those in **Fig 3C**, seen in the left graph under ACSF and left graph under ACSF+PTX, where firing rates during the stimulation window *and* sustained firing window were not affected by occlusion. The lack of occlusion effect on post-stimulus prolonged firing indicates that the occlusion effect on the ETC temporal filter is likely a very subtle one, that may be occurring only *during* the later stages of high-frequency OSN stimulation, and only in the presence of $GABA_A$ signalling.

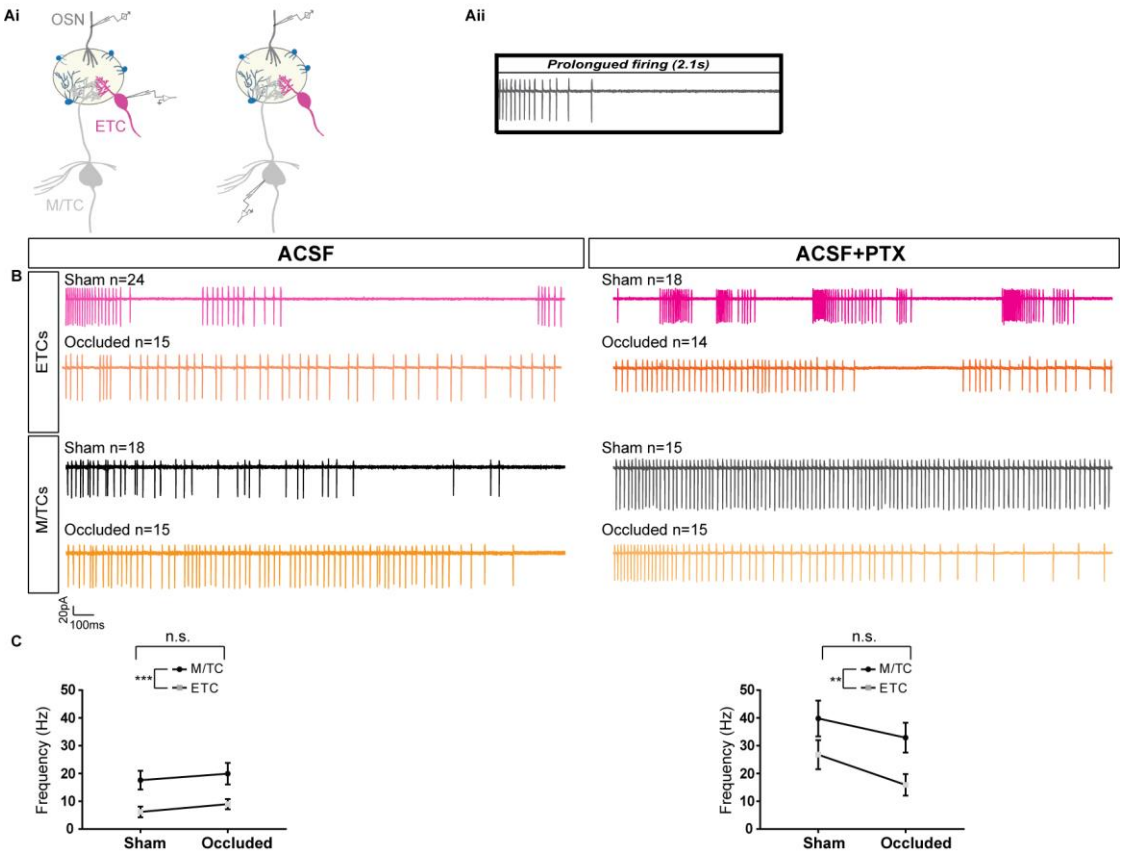

Fig 5. Occlusion does not alter external tufted cell (ETC) or mitral/tufted cell (M/TC) prolonged firing.

(**Ai**) Olfactory sensory neuron (OSN) axons, shown in dark grey, were stimulated while either ETCs (magenta) or M/TCs (grey), were recorded in the on-cell configuration. (**Aii**) Firing rates were obtained from spikes occurring during the 2.1s post-stimulus prolonged firing window. (**B**) Example traces of ETC (top) and M/TC (bottom) post-stimulus firing in sham and occluded conditions. The recording solution was either artificial cerebrospinal fluid (ACSF) (left) or ACSF + 10µm picrotoxin (PTX) (right). (**C**) Graphs showing quantification of 2.1s post-stimulus firing rates recorded in ACSF on the left, and in ACSF+PTX on the right. Coloured squares represent means, error bars show SEM. **, p<0.01; ****, p<0.0001; n.s., non-significant.

5.2.5. ETCs show a subtle increase in firing rate during high-frequency afferent stimulation after occlusion

If ETC firing rates throughout the high-frequency stimulation window and the combined stimulation and sustained firing window were unaffected by occlusion when recording in ACSF, how could the temporal filter of these cells be changing as a response to occlusion? This could occur due to a subtle prolongation of firing rate *during* the stimulation train which may not be strong enough to reveal a significant increase in overall firing rate. Indeed, when comparing evoked *firing rates* (rather than temporal filter) during the stimulation window against stimulation number, there does appear to be a slight but non-significant prolongation of firing in ETCs with occlusion throughout the stimulus train (**Fig 3E**) which may be strong enough to explain the temporal filter phenotype we see (sham τ=3,94 stimuli, *k*=0.25; occluded τ=5.94 stimuli, *k*=0.17; *extra sum of squares F-test*, comparing *k* values, p=0.04). Though the temporal filter change is most obvious following the first 5 stimuli (**Fig 3D**), this is not matched by an increase in ETC firing after the same stimuli (**Fig 3E**). However, due to the subtle increase in firing *throughout* the stimulus train in occlusion, this may serve to even out the number of spikes fired after each stimulus. This may drive the flattening of the temporal filter in occlusion because it may contribute to similar numbers of action potentials being fired in response to all stimuli, which may be most evident after the first 5 stimuli because under control conditions, most spikes are fired here, whereas under occluded conditions firing seems to be more evenly distributed throughout the stimulus train (**Fig 3E**). This trend is not evident in ETCs recorded in ACSF+PTX, nor M/TCs recorded in ether condition (**Fig 3E**), where temporal filters were not affected by occlusion either (ETCs: sham τ=7.10 stimuli, *k*=0.13; occluded τ=4.25 stimuli, *k*=0.23; *extra sum of squares F-test*, comparing *k* values, p=0.10; M/TCs: ACSF: sham τ=4.01 stimuli, *k*=0.25; occluded τ=3.89 stimuli, *k*=0.26; *extra sum of squares F-test*, comparing *k* values, p=0.89; ACSF+PTX: sham τ=3.32 stimuli, *k*=0.30; occluded τ=3.79 stimuli, *k*=0.26; *extra sum of squares F-test*, comparing *k* values, p=0.68).

These observations indicate that after 24 h sensory deprivation, ETCs subtly prolong their firing *only during* high-frequency OSN stimulation, and only in the presence of $GABA_A$ signalling. This implies that inhibition plays a role in adapting ETC temporal filters, and that when it is absent the subtle changes produced by occlusion on ETC prolonged firing are obscured.

5.3. Discussion

In this chapter we explored whether 24h naris occlusion impacts the glomerular input-output relationship at the ETC and M/TC level. OSNs form synapses onto both ETCs and M/TCs, however

these connections appear to be stronger with ETCs (De Saint Jan et al., 2009; Gire et al., 2012) and there is more and more evidence pointing toward ETCs playing a vital role in amplifying initial OSN inputs before this information reaches M/TCs (De Saint Jan et al., 2009, Gire et al., 2012, Gire and Schoppa, 2009; Gire et al., 2018; Najac et al., 2011). Our previous work suggests that attenuated odour input increases synaptic excitatory drive, as observed by increases in LLC magnitude under certain conditions (chapter 4). Under control conditions this amplification of glutamatergic signalling enables M/TCs to exhibit sustained firing in response to relatively transient input (Vaaga and Westbrook, 2017), thus we hypothesised that larger LLCs would be associated with more sustained transmission by ETCs and M/TCs after occlusion.

Our results however, revealed that M/TC evoked sustained firing rates are resistant to occlusion, and ETCs only deviate from phase locked responses to slightly sustained transmission when inhibition remains intact. Furthermore, this change in ETCs is a very subtle increase in firing rates *during* high-frequency OSN stimulation. This small change was enough to drive an overall change in the ETC temporal filter to portray a more sustained response, however this was not coupled with an increase in sustained firing post-stimulus.

5.3.1. Spontaneous firing is unaffected by occlusion

Both ETCs and M/TCs portray spontaneous rhythmic activity (Hayar et al., 2004; Heyward et al., 2001). Slice physiology has shown that ETC spontaneous firing is intrinsic (Hayar et al., 2004). However, glomerular circuitry can affect these spontaneous firing properties. ETCs form synapses onto inhibitory JGCs and it has been shown that ETC spike bursts can drive GABAergic JGCs. This creates feedback inhibition onto ETCs and shunts their responses (Hayar et al., 2008). Additionally, $GABA_A$ and glutamate have been shown to modulate the firing rate within an ETC spontaneous burst, where $GABA_A$ decreases the number of spikes in a burst, and glutamate increases them (Hayar and Ennis, 2007). Additionally, dopamine can act on ETC D_1-Dopamine receptors to increase I_h-coupled increases in re-bound spiking (Liu et al., 2013). ETC spontaneous firing is crucial for maintaining synchronous activity in the glomerulus (Hayar et al., 2004; Wachowiak and Shipley, 2006). Therefore, the regulation of this property provides a potential avenue for adjusting glomerular processing upon changes in sensory input. M/TC spontaneous firing is also highly regulated by several mechanisms both within the glomerulus as well as by GCs in the external plexiform layer. ETCs provide feed-forward excitation to M/TCs and tonic GABAergic inhibition from JGCs onto ETCs indirectly reduces M/TC spike output (Shao et al., 2012). Furthermore, lateral inhibition by GCs onto M/TC lateral dendrites also shapes M/TC spontaneous firing (Chen and Shepherd, 1997). Therefore, since spontaneous firing in ETCs and

M/TCs can be heavily regulated, we wanted to know whether this modulation is changed in occlusion by observing spontaneous firing rates.

With 24h naris occlusion, we observed no changes in the release probability of OSNs and can thus exclude their contribution to any occlusion effects we observe on spontaneous firing (chapter 4). We can further exclude the contribution of intrinsic excitability changes after occlusion, as membrane properties also did not change in ETCs and M/TCs (chapter 3; E. Galliano and C. Hahn, unpublished data). Our results show that spontaneous firing also remains unaffected by occlusion (**Fig 2**), both with and without $GABA_A$-mediated inhibition. This finding supports the findings from whole-cell recordings of spontaneous firing in ETCs that also showed no changes with occlusion (chapter 3). This implies that the modulation of spontaneous activity of ETCs and M/TCs by excitatory and inhibitory local circuitry is also not impacted by occlusion.

One caveat of studying spontaneous activity in a slice is that centrifugal inputs are cut off during the slicing preparation. Modulation of ETC and M/TC responses by these inputs is well-known (Devore and Linster, 2012). For example, acetylcholine received from cholinergic fibres arriving from the horizontal limb of the diagonal band of Broca has been shown to increase M/TC excitability (Castillo et al., 1999). Serotonin received from projections in the raphe nuclei has an indirect excitatory effect on ETCs (Liu et al., 2012). Thus, eliminating these inputs could obscure our spontaneous firing measures. Additionally, *in vivo*, odours are continuously being received by OSNs either through breathing or active sniffing. This provides a relatively constant activation drive on glomerular circuitry. This cannot be reproduced in a slice, but has impacts on M/TC spontaneous firing, as spontaneous M/TC firing is reduced in slices compared to in an intact animal (Ciombor et al., 1999). Therefore, although we did not observe any occlusion effects on ETC and M/TC spontaneous firing in slices, this may not represent what could be happening with occlusion in the *in vivo* situation.

5.3.2. High-frequency afferent input in occluded conditions allows ETCs to adjust their temporal filter

It has previously been shown that whereas M/TCs produce a prolonged transmission in response to high frequency input, ETC responses are more phase-locked to stimuli (Vaaga and Westbrook, 2017). The prolonged transmission observed in M/TCs occurs due to strong dendro-dendritic amplification of OSN signals that can be observed in the much larger M/TC LLC compared to the ETC LLC (Vaaga and Westbrook, 2017; chapter 4). Given that occlusion can increase LLC magnitude, suggesting recurrent excitation is enhanced in these conditions, we hypothesised that this adaptation would translate to a more prolonged firing response at the output cells.

ETCs drive M/TC activity (De Saint Jan et al., 2009), so we wanted to observe whether evoked output from these cells would be adjusted in response to occlusion. Indeed, when inhibition was left intact and afferents were evoked with a high-frequency stimulus, ETCs changed their temporal filter from a more phasic stimulus-locked response, to a slightly more sustained response resembling a M/TC response to this kind of stimulus (**Fig 3**). This shift in temporal filter is likely due to a subtle prolongation of ETC firing over the course of the stimulus train (**Fig 3**). Under low-frequency OSN stimulation, this change in ETC temporal filter is not observed. The inter-pulse intervals in our low-frequency stimulation (200ms) were much longer compared to the high-frequency stimulation (20ms). Therefore, having more time between stimulation pulses allows for more modulation of the evoked response by the circuitry. For example, OSNs may have replenished more of their vesicles between the inter-pulse intervals in our low-frequency stimulation compared to high-frequency stimulation. This means that more OSN signal can be received by ETCs in both control and occluded conditions. OSN release probability does not change with short-term occlusion (chapter 4), and the prolongation of ETC firing with high-frequency stimulation is only very subtle. This small adjustment in ETC firing may therefore not be evident with low-frequency stimulation, as more time is given for ETCs to receive OSN input, where under these conditions both ETCs and M/TCs already fire more spikes between pulses under base-line conditions compared to high-frequency stimulation (**Fig 4**).

The occlusion effect on ETC temporal filter cannot be seen when $GABA_A$ receptors are blocked. This effect could occur due to two possibilities. First, occlusion could be producing changes in local inhibition that influence the ETC temporal filter during high-frequency afferent stimulation. The juxtaglomerular GABA/dopaminergic interneurons can change their properties in an activity-dependent manner (Baker 1990), and glomerular inhibitory circuitry is known to regulate ETC activity (Hayar et al., 2008; Liu et al., 2013). In fact, Hayar and Ennis (2007) showed a strong connection between $GABA_A$ and ETC firing properties, where blocking $GABA_A$ receptors increased ETC spikes per burst. Therefore, ETCs could be prolonging their firing response during stimulus trains if less inhibition is acting on these cells. In our recordings in ACSF, this is indeed the effect that we see (**Fig 3**). In addition, it has recently been shown that ETC-M/TC glutamate transmission occurring in glomeruli largely stems from ETC-PGC glutamate spillover that reaches M/TC apical dendrites via extra-synaptic glutamate receptors (Gire et al., 2018). In this scenario, a strong stimulus would allow excitatory extra-synaptic signalling to “win” over PGC inhibitory drive, whereas a weak stimulus would allow inhibitory drive to override excitation. Gire and colleagues (2018) suggest that spillover at the ETC-PGC synapse could provide a mechanism for triggering recurrent excitation in the form of LLCs. In light of this, under occluded conditions, we could imagine a scenario where JGCs, notably the GABA/dopaminergic JGCs, may presumably

be less active and therefore release less inhibitory signal that shunts this excitatory drive. With less inhibition, perhaps ETCs are then able to receive larger intraglomerular excitatory signals, leading to a prolonged firing response during high-frequency afferent stimulation. Therefore, if $GABA_A$ currents are blocked, we would be unable to see any differences between sham and occluded ETC temporal filters, because the inhibitory circuitry responsible for producing this change is blocked in both conditions.

In a second scenario, inhibition may not play a direct role in adjusting ETC temporal filter, but rather, blocking inhibition could preclude us from observing any occlusion effects produced purely by changes in the excitatory network. We can imagine that inhibitory drive is responsible for reducing the already high excitatory responses of ETCs to OSN stimulation, resulting in the steep temporal filter we see in ACSF control conditions. Upon blocking $GABA_A$ currents in control conditions, we observed that ETC temporal filters were more shallow compared to ACSF conditions (**Fig 3**). Thus, by removing the inhibitory drive on ETC temporal filter in control conditions, we are seeing a more sustained response during the stimulation window. This "uninhibited" temporal filter could then be at a maximum level of shallowness, and therefore could hide any effects occlusion may have on the temporal filter generated by excitatory drive. Indeed, the ETC temporal filter in sham ACSF+PTX condition mimics the ETC temporal filter in occluded ACSF conditions (**Fig 3**).

How could we distinguish between these two scenarios? One powerful experiment to perform would be to record evoked firing rates in the same way as in the experiments in this chapter, but record each cells' response with $GABA_A$ agonists in the recording solution. This would produce different effects according to the two scenarios discussed above. First, if the mechanism adjusting ETC temporal filter in occlusion is purely GABAergic, then the addition of $GABA_A$ agonists should result in no difference between sham and occluded ETC temporal filters. If however, the mechanism is glutamatergic, the addition of $GABA_A$ agonists should not affect the ETC temporal filter change we see with occlusion, and may even enhance the difference observed between control and occluded temporal filters. This is because if $GABA_A$ serves to limit the ETC temporal filter, the addition of $GABA_A$ agonists in control conditions would potentially result in an even steeper ETC temporal filter. The effects of occlusion on temporal filter would then be even more obvious. However, the addition of $GABA_A$ agonists could, in theory, boost inhibition so much that the temporal filter effects become equalised. One could consider using a benzodiazepine such as diazepam, which serves to increase the frequency of $GABA_A$ receptor opening (Macdonald et al., 1991). This would then enhance GABA effects on ETCs without flooding the entire system with GABA. At an optimised concentration, this could then enhance the ETC temporal filter effect in occlusion, as the increased actions of GABA are limited. This

would then give a convincing indication that temporal filter changes are largely happening due to the excitatory circuitry.

Interestingly, there seems to be a mismatch of LLC phenotype and ETC temporal filter phenotype, even though LLC magnitude is closely linked to temporal filter patterns (Vaaga and Westbrook, 2017). In ACSF, ETC LLCs are unaffected by occlusion whereas the ETC temporal filter becomes shallower. If there is less $GABA_A$ modulating ETC temporal filters in occlusion, why do we not also see this matched with a larger LLC? This observation adds another level of complexity in how temporal filters may be modulated. It has previously been suggested that M/TC dendro-dendritic amplification is stronger compared to ETCs (Vaaga and Westbrook, 2017), and indeed M/TC LLCs are larger compared to ETCs (Vaaga and Westbrook, 2017; chapter 4). We have shown that occlusion increases the magnitude of the M/TC LLC in ACSF but not the ETC LLC. Thus, perhaps M/TC-M/TC dendro-dendritic amplification is increased under these conditions and feeds back to ETCs which are able to use this signal to prolong their firing in response to strong afferent stimulation. The lack of occlusion effect we would then expect to see on ETC LLCs could be explained in three scenarios. First, ETCs and M/TCs are coupled electrically via gap junctions (De Saint Jan et al., 2009). The M/TC excitatory currents could then be reaching ETCs through gap junctions rather than LLCs. Secondly, M/TC release probability could be increasing, allowing ETCs to receive more direct excitatory current. Recent evidence suggests that there are few, if any, ETC-M/TC chemical synapses (Bourne and Schoppa, 2017), which may explain why the ETC temporal filter effects are so small. Third, perhaps ETCs *are* in fact increasing their LLC magnitude, but since $GABA_A$ is still present under these conditions, and it is known that GABA immunoreactivity does not change with sensory deprivation (Baker, 1990), GABA can still act to subdue this effect and preclude us from observing it. Since ETC activity creates feedback inhibition, perhaps their "hidden" LLC increases could act upon these inhibitory JGCs to achieve more inhibition and thus result in an unchanged LLC phenotype. In addition to this, inhibition may be reduced under occluded conditions, and these effects may at least in part produce the ETC temporal filter effects we see (see above). When $GABA_A$ signalling is blocked, the presumed effect of the M/TC LLC on ETCs (discussed in chapter 4) may be uninhibited, allowing ETCs to read-out a larger LLC. Nevertheless, because ETC temporal filters are perhaps already at a ceiling level of shallowness in these conditions, this larger LLC effect may not be observed at the temporal filter level.

Nevertheless, if the temporal filter change in occlusion is affected by any of the mechanisms discussed above, how can they leave the ETC LLC unaltered?

This could be due to an entirely different explanation. LLCs are highly NMDA dependent (De Saint Jan and Westbrook, 2007), however OSN responses in ETCs also depend strongly on AMPA

receptor activation. Thus, perhaps the temporal filter adjustment we see is due to changes in AMPA conductances which would not be evident in the LLC. In occlusion, ETCs could be increasing their post-synaptic AMPA receptor density at OSN-ETC, ETC-ETC, or ETC-M/TC synapses, or all of these. In this case ETCs would receive a slightly higher glutamatergic signal from any of these connections. This could then indirectly impact ETC temporal filters without adjusting LLCs, since NMDA receptor properties theoretically remain unchanged.

To test for all these possibilities, we could perform whole-cell recordings of ETCs with several pharmacological agents in the solution. To test whether AMPA receptor density is increasing at ETCs, we could record miniature EPSCs (mEPSCs) that represent AMPA currents. These are recorded in the presence of TTX to eliminate any sodium currents, APV to eliminate glutamatergic currents coming through NMDA receptors, and PTX to block any $GABA_A$ currents. If the amplitude of the AMPA-mEPSCs increases with occlusion, it would suggest that indeed there are more AMPA receptors present post-synaptically. To distinguish where these inputs are coming from we would need to do further testing.

To quantify whether the post-synaptic AMPA receptor density is changed at the OSN-ETC connection, we could employ non-stationary fluctuation analysis. With this protocol, we would record multiple OSN-evoked AMPA-EPSCs at different average OSN release probability (P*r*) settings which are reduced by either reducing extracellular Ca^{2+} or adding cadmium (a Ca^{2+} chelator) to the recording solution. We would then calculate the EPSC variance at each P*r* setting, which is then plotted against the mean EPSC amplitude to form a variance-mean (V-M) plot which can then be fit with a parabola. The initial slope of this curve represents an estimate of the average quantal size, the curvature of the plot is related to P*r*, and the size of the curve is related to the number of independent transmitter release sites that make up the synaptic connection (Clements and Silver, 2000). Using these measures, we would then be able to see whether the slope of the V-M plot changes, which would suggest that ETCs are changing the density of their AMPA receptors at the OSN-ETC synapse. This calculation would also provide us with an additional estimate of OSN P*r* that could be included in our analysis of OSN P*r* changes in occlusion. Furthermore, this method of calculating OSN P*r* and possible post-synaptic contributions has been validated in the glomerular circuit previously (Murphy et al., 2004).

Though the chemical synaptic connection between ETCs and M/TCs has been shown to be unidirectional from ETC to M/TC (De Saint Jan et al., 2009), the consequent glutamate release by M/TCs upon ETC activation likely spills back onto ETC AMPA receptors (Christie and Westbrook, 2006; Hayar et al., 2005; Schoppa and Westbrook, 2002). Thus, to quantify whether post-synaptic AMPA-receptor density on ETCs is altered, we could double-patch ETCs and M/TCs. In this experiment, we would need to isolate the AMPA receptor-mediated current by

recording in APV and PTX. We would then stimulate the M/TC to fire an action potential and record the AMPA-mediated EPSC at the ETC. If the amplitude of this EPSC increases with occlusion, it wold suggest that ETCs are increasing the density of their AMPA receptors at the M/TC-ETC connection. This approach would also reveal whether perhaps M/TCs are in fact increasing their release probability of glutamate, that may account for the changes we see in ETCs. If this were the case, we would expect to see an increase in the frequency of ETC EPSCs in response to M/TC spikes.

With the same experimental approach, we could check whether the AMPA receptor density is changed specifically at the ETC-ETC synapse, though this is complicated by the fact that there is little evidence suggesting chemical synapses exist between ETCs (Hayar et al., 2005), thus finding connected pairs may be technically challenging.

To test the gap-junction-mediated hypothesis, we would again double patch ETCs and M/TCs, but this time with all chemical synaptic transmission and I*h* current blocked. Under whole-cell configuration we would inject a hyperpolarising current into each cell alternatively and observe whether the voltage deflection in the other cell becomes larger in occlusion. Alternatively, we could perform our input-output experiments in a transgenic mouse-line that lacks gap-junctional coupling between ETCs and M/TCs, such as the Cx36 mouse-line (Christie et al., 2005). If the occlusion effect on ETC temporal filter is abolished, it could indicate that a gap-junction mediated change is responsible for this small increase in ETC spike responses during high-frequency OSN stimulation in occlusion.

If none of these experiments revealed any changes, it would seem highly likely that $GABA_A$ currents are responsible for modulating the ETC temporal filter with short-term occlusion.

In summary, despite the ETC and M/TC temporal filter differences Vaaga and Westbrook (2017) reported in their study, the differences we saw were not significant. However, *within* cell-types, the relationship between experience-dependent changes in LLCs and evoked firing responses are not so evident.

5.3.3. M/TCs do not adjust their evoked firing properties in response to occlusion

Previous reports have stated that M/TCs are able to adjust their spike output in response to input in the face of sensory manipulations. For example, long-term sensory deprivation enhances M/TC responses (Wilson and Sullivan 1995), and sensory over-exposure can decrease M/TC responsiveness (Buonviso and Chaput, 2000). Furthermore, long-term sensory deprivation increases OSN release probability, which also enhances M/TC spiking (Tyler et al., 2007). GCs

greatly regulate M/TC activity (Friedman and Strowbridge, 2003; Lagier et al., 2004) and thus sensory experience can also alter the M/TC-GC-M/TC network. Upon long-term sensory deprivation, the number of new-born GCs is reduced, but a compensatory increased excitability of new-born GCs results in an unchanged M/TC output (Shagatelyan et al., 2005). Contrastingly, early unilateral naris occlusion results in lower M/TC output due to increased inhibition by GCs in these conditions (Wilson et al., 1990). Here, we used comparatively short-term sensory deprivation (24h) to drive changes in the OB. This does not allow for a lot of time to drive network changes that affect M/TC output. Nevertheless, we did observe an increase in LLC magnitude in occluded conditions (chapter 4). In addition, 24h naris occlusion reduced intrinsic excitability of GABA/dopaminergic JGCs, and there was decreased c-Fos immunoreactivity in these cells (D. Byrne and E. Galliano, unpublished data). Thus, this time-frame does allow for some adjustments to occur. We were thus curious to see what would happen to M/TC firing output under occluded conditions.

Interestingly, M/TC sustained firing in response to OSN stimulation remained unaffected by occlusion in both ACSF as well as ACSF+PTX (**Fig 3**). We also tested M/TC responses in response to low-frequency afferent stimulation due to the possibility that M/TCs were reaching a ceiling firing output with high-frequency stimulation (**Fig 4**). Nevertheless, even in these conditions, M/TC sustained firing was unaffected by occlusion.

The question arises therefore, as to why M/TCs retain their temporal filters with short-term occlusion, when ETCs can adjust their firing during stimulation trains? The occlusion effect we see in the ETC temporal filter is very subtle and may not be translated to M/TC output due to the counteracting inhibitory effects targeted at M/TCs. Perhaps confounding this is the small ETC effect which may not be seen in our M/TC recordings because they already have such a prolonged firing response. As discussed above, M/TC output can be shaped by multiple mechanisms, not just by ETC feedforward excitation. Indeed, these other circuit mechanisms *could* offset the influence of ETC temporal filter changes on M/TCs.

Long-term sensory deprivation can adjust M/TC spiking by changes in the inhibitory network (Shagatelyan et al., 2005; Wilson et al., 1990; Wilson and Sullivan, 1995). However, a key difference in our study is that we used very short-term naris occlusion. Though GC activity impacts M/TC output (Friedman and Strowbridge, 2003; Lager et al., 2004), GC activity-dependent plasticity may not have yet occurred after 24h of sensory deprivation, and thus may not have impacted the temporal filter in such a short time period. In addition to this, glomerular inhibitory neurons may play more of a key role in affecting the ETC temporal filter rather than the M/TC temporal filter during such a short manipulation. Similarly, we have shown that OSN

release probability is not affected with 24h naris occlusion (chapter 4), thus any presynaptic occlusion effects on M/TC output (Tyler et al., 2007) are likely not yet in place.

As observed in ETCs, there also appears to be a mismatch between M/TC LLC changes and M/TC spiking output.

Though LLCs are heavily involved in shaping the M/TC temporal filter (Vaaga and Westbrook, 2017), occlusion effects on LLCs may not be directly targeted at the M/TC temporal filter. Alternatively, due to the shortness of the sensory manipulation, the LLC effect on the M/TC temporal filter in ACSF may be limited by feedback inhibition from GCs. If M/TCs are receiving stronger recurrent excitation, they would activate their GC partners more strongly, resulting in stronger feedback inhibition. Thus, perhaps M/TCs do change their temporal filters, but we would be unable to see this effect because the increased feedback inhibition ensures M/TCs retain their temporal filter response. As with ETCs, when $GABA_A$ signalling is blocked, perhaps M/TCs already reached their maximum sustained firing capabilities under control conditions thus rendering no effect of occlusion. Indeed, though the effect is not as strong as in ETCs, M/TCs do portray a shallower temporal filter in PTX compared to ACSF responses (**Fig 3**).

To test whether GCs are indeed increasing their inhibitory drive on M/TCs on a population-wide level we could do an experiment where IPSCs are recorded in M/TCs in the whole-cell configuration while the GC layer is stimulated electrically. To record IPSCs, the recording solution would need to contain TTX, NBQX and APV to block glutamatergic and Na^+ currents, and we would need to hold M/TCs at 0mV in voltage clamp to increase the GABAergic driving force and thus see IPSCs clearly. If the amplitude of IPSCs becomes larger with occlusion, this would suggest GCs are increasing their inhibitory drive on M/TCs. We would then perform another experiment to check that LLC changes are not affected by this increased GC inhibition. Again, we would be stimulating the GC layer and recording responses in M/TCs in the whole-cell configuration. We would also evoke LLCs by electrical stimulation of OSNs. First, we would record evoked LLCs, as these cannot occur in the presence of TTX (Carlson et al., 2000). After a baseline has been established, we would wash in TTX, NBQX and APV to block glutamatergic currents. Then, we would hold the cell at 0mV in voltage clamp to record IPSCs. If the IPSCs become larger with occlusion, and we still see an increase in the evoked LLC in those same cells compared to control cells, this would show us that the larger M/TC LLC in occlusion may indeed drive increased GC inhibition onto M/TCs, without affecting the observed LLC.

In vivo, M/TC dendro-dendritic amplification of OSN input is an important feature to allow signals to be reliably transmitted to the piriform cortex. OSNs have an unusually high release probability (Murphy et al., 2004; Vaaga and Westbrook, 2017) meaning that they only contribute

to a transient post-synaptic activation. To overcome this, many OSNs are activated upon odour stimulation, leading to a low signal-to-noise ratio. M/TC dendro-dendritic amplification of this signal is part of a mechanism that boosts signals in this "noisy" environment (De Saint Jan and Westbrook, 2007; Vaaga and Westbrook, 2016). Under plug-occluded conditions, less odours reach the OSNs, thus less input reaches the glomeruli. Perhaps an increase in LLC magnitude under these conditions allows M/TCs to amplify the reduced amount of signal entering the glomerulus, which ensures M/TC firing responses are not reduced during occlusion.

Perhaps the temporal filter changes in ETCs are more relevant to circuit processes that do not directly affect M/TC spiking output. For example, ETCs project their axons to isofunctional odour columns (Belluscio et al., 2002), and though the functional properties of these connections have not been investigated, it could be possible that ETC temporal filter changes are an important feature of adjusting inter-glomerular circuit amplification. Alternatively, or in addition to this, ETC temporal filters could be involved in adjusting the actions of inter-glomerular GABA/dopaminergic JGCs. Since occlusion increases ETC sustained firing during afferent stimulation, this could act on the GABA/dopaminergic JGCs and increase their ability to provide inter-glomerular inhibition.

5.3.4. Technical considerations

While there are many potential biological mechanisms that may explain a lack of M/TC evoked firing changes after 24h occlusion, there is also a significant technical consideration to bear in mind. An important caveat to comparing electrically-stimulated responses across acute slices and cells is control of stimulus strength. Though we were able to define stimulus frequency and pulses, it is not possible to stimulate the same number of afferents with the exact same stimulus strength for each recording. For this reason, we designed a set of strict criteria to control for this stimulus strength variability. Due to the need to control our stimulus strength in this way, we may have normalised our recordings to such an extent that small differences that may be occurring in occlusion are normalised out of significance.

There are several approaches that might be used in future to stimulate ONSs more comprehensively in slices. For example, a transgenic mouse line expressing ChR2 in OSNs could be used instead of WT mice. This would allow for a more reliable stimulation of OSNs across samples as a similar number of OSN fibres would be stimulated each time (Dhawale et al., 2010). However, this method still relies on all relevant OSNs projecting to the target glomerulus being present and functional in the slice, which may not necessarily be the case. Another method could be to use a minimal stimulation protocol that always stimulates just one OSN axon, however as mentioned above, this would likely not produce spiking responses and thus be ineffective for

our experiment. Additionally, minimal stimulation was not used to evoke LLCs, and since we wanted to correlate our LLC phenotype with any input-output changes we did not want to alter the stimulus paradigm. To compare cell-type differences, a neat method to ensure exactly the same stimulus reaches the recorded ETCs and M/TCs would be to double-patch these cells while stimulating afferents.

In vivo experiments, especially in awake animals, could further provide a better technical approach and more physiologically relevant results. In these experiments, stimuli could be presented as simple odours of known concentrations, thus every recorded cell would be evoked by the same input across samples. However, to record from ETCs in these conditions, one would need to use a transgenic mouse line, such as CCK-tdT, where ETCs are clearly labelled, as it is difficult to identify these in WT tissue. To be even more precise, a transgenic animal that has particular glomeruli with known ligands labelled (Bozza et al., 2002; Mombaerts et al., 1996) could be used to record responses across cells that are always part of the same glomerular circuit. Alternatively, *in vivo* experiments on mice expressing ChR2 in their OSNs could further provide stimulation strength control. As opposed to a slice, this method would ensure that all relevant OSN axons are present.

5.4. Conclusion

This chapter explored how 24 h naris occlusion affects glomerular output in terms of the firing rate and pattern of ETCs and M/TCs. We have shown that occlusion can subtly impact the firing pattern of ETCs during high-frequency afferent stimulation, an effect not seen when inhibition is blocked. We propose two scenarios that could explain this phenomenon. First, these results could imply that the inhibitory circuit is involved in shaping the ETC temporal filter. Second, it is possible that we are unable to see excitatory effects on ETC temporal filters because when inhibition is blocked, these responses could be at their maximum, and thus the effect of occlusion is not seen. The occlusion effect on ETC temporal filter is not translated to a prolonged response in ETCs after a stimulus train. Similarly, this ETC effect is not directly translated to M/TC firing, as M/TCs do not alter their stimulus responses or patterning at all with occlusion.

Under certain conditions, LLCs become larger with occlusion in both ETCs and M/TCs. It is clear that there is heavy involvement of LLCs in shaping ETC and M/TC firing output in response to afferent stimulation. In light of this, we predicted that ETC and M/TC firing responses would become more prolonged with occlusion. However, only very subtle output changes in ETCs can be observed, suggesting that other regulatory mechanisms are in place to adjust the network to short-term sensory deprivation.

Chapter 6

Discussion

The aim of this thesis was to determine whether ETCs, central to OB glomerular odour processing, exhibit activity-dependent plasticity, and whether any changes observed in ETCs would impact the subsequent interpretation of input integrated by the OB circuitry. In chapter 3, we found that ETCs do not adjust any of the various intrinsic functional and morphological properties we probed in the face of short-term sensory deprivation. However, in chapter 4 we found that odour deprivation results in a striking increase in the magnitude of the synaptically-driven glomerular LLC read out by ETCs and M/TCs, which we could observe under certain conditions. Given the importance of the glomerular LLC in providing feedforward excitation that drives M/TC activity, in chapter 5 we explored the possibility that the occlusion effect on LLC magnitude may affect the overall output of a glomerulus in response to stimuli. Interestingly, though ETCs appear to *subtly* increase their spike responses to OSN input in occlusion, an effect only observed when the inhibitory circuitry is left intact, M/TCs retain remarkably stable response profiles after this short-term sensory manipulation.

Our results suggest that 24 hours of olfactory deprivation likely induces a synaptic change in the excitatory circuitry within glomeruli. Though we could not identify the specific role of ETCs in this adjustment, we *were* able to show that this change likely does not occur due to adjustments in OSN terminals. Therefore, we posit that short-term occlusion drives the post-synaptic targets of these cells, specifically ETCs and M/TCs, to somehow enhance the efficacy of glomerular glutamatergic signalling, resulting in larger LLCs, that *may* be responsible for regulating the overall output these principal cells exhibit with this manipulation.

If spiking responses to input are unchanged at the M/TC level with short-term sensory deprivation, what is the function of a larger LLC under these circumstances? Indeed, on a broad scale, what could this sort of adjustment in excitatory signalling mean for a neural network in terms of computing environmental changes? In this chapter, we will first discuss some limitations with our approach that may hinder the interpretations of our findings. We will then explore possible answers to the questions above. We will further underline how this study could be strengthened with future experimental techniques. These may broaden our knowledge in understanding how the changes we observe in the OB may specifically occur, and what they may translate to on a functional level for odour perception.

6.1. Are processes in acute slices representative of intact OB function?

Acute slices provide a great medium for studying relatively physiological processes occurring at the cellular level, since some network integrity is preserved, as opposed to dissociated cultures

of cells, but the ability to target specific cell-types is more straight forward than in a whole brain. Additionally, as opposed to an intact OB, acute slices allow for greater control of the extracellular environment, where recording solutions with the addition of various pharmacological agents can easily be adjusted to suit the experiment. Specifically in the OB, due to glomeruli forming microcircuits and sensory input axons still being functionally present, acute OB slices preserve glomerular processes that can therefore be studied on a network level.

Nevertheless, during the preparation of slices, many important neural projections are likely to be severed. These include more long-distance interglomerular processes, and centrifugal inputs, known to backpropagate signal to the OB (Lowe, 2013), which are (functionally) eliminated from the OB. Therefore, though it is possible to comprehensively observe cellular properties on a glomerular level in an acute slice preparation, the full effects of interglomerular and top-down processes are not present.

Additionally, when wishing to observe response profiles to input in the acute slice preparation, which is dissociated from the sensory transduction machinery in the nose, it becomes difficult to mimic the olfactory environment artificially. This usually involves electrically or optogenetically stimulating OSN fibres, which necessarily need to be stimulated simultaneously and en-masse to observe spike responses in recorded cells. Nevertheless, with these protocols it is impossible to stimulate *all* of the inputs that would normally be activated by a given stimulus. Therefore, this artificial stimulation paradigm does not represent the patterns of odour input experienced *in vivo* (Duchamp-Viret et al., 1999). Indeed, it also prohibits the study of how odour identity or concentration may be differently interpreted in a circuit that has undergone sensory manipulations, or even under baseline conditions.

In the scope of this thesis, the use of acute slices therefore limits the functional interpretations we can draw from the plastic changes in excitatory drive we observe. Though LLCs are becoming larger with occlusion, and ETC responses to OSN input appear to be subtly enhanced, we cannot conclusively state whether this effect occurs *in vivo*, as we cannot predict how feedback cortical communication might modulate this effect in the intact OB. In addition to this, since we cannot mimic the olfactory environment by electrical stimulation of OSNs, we also cannot state whether changes in LLCs, if they do indeed occur physiologically, exhibit functional consequences on odour detection and discrimination.

Nevertheless, from these experiments we can deduce that the excitatory circuitry likely has the *capability*, at least, to adjust post-input glutamatergic drive. The implications of how this may function to alter the circuitry are discussed below.

6.2. The usefulness of OB glomerular circuitry as a model to study plasticity

The OB poses as an attractive circuit in which to study plasticity. This is because it receives direct input from sensory neurons and is thus anatomically close to the periphery, making manipulations of activity via alterations of sensory experience straightforward and reliable. Additionally, the OB consists of microcircuits (glomeruli), that can be targeted with electrophysiological/imaging approaches both *in* and *ex vivo* due to the genetic tractability many of its components possess (Coppola, 2012; Imai, 2014). This allows for the comprehensive study of how individual cell-types in a circuit may functionally adjust to impact network processing in response to input (Wilson et al., 2004).

6.2.1. Limitations of using the OB to study plasticity

The usefulness of the glomerular circuit in studies on plasticity on a cellular level may be limited to an extent. For instance, there appears to be a large dependence on spillover neurotransmitter communication between both inhibitory and excitatory components of the circuit (De Saint Jan and Westbrook, 2007; Gire et al., 2018; Smith and Jahr, 2002). This may complicate interpretations of plastic changes observed as spillover communication may be "hidden" in these investigations. For example, in this thesis, we show that excitatory signalling is enhanced with sensory deprivation, however determining the locus of this polysynaptic change is extremely difficult when multiple components including synaptic, extrasynaptic, and gap-junctional communication have all been implicated in LLC generation (De Saint Jan and Westbrook, 2007; De Saint Jan et al., 2009; Gire et al., 2012). In addition to this, members of the OB circuitry are still being identified (Bywalez et al., 2017), thus we still do not know how the entirety of the circuit functions to process input.

To untangle single processes, it is often therefore necessary to employ a cocktail of pharmacological agents and/or specific stimulation paradigms that allow for the isolation of particular mechanisms. While useful in determining individual cellular processes, they preclude the effects of the network and thus make it difficult to make clear conclusions about *in vivo* signal transmission. In the case of the glomerular LLC, this phenomenon arises due to recurrent excitation among the principal cells. This limits the use of pharmacological agents to study where and how LLC changes may be originating, as this approach would preclude the appearance of LLCs and thus make it difficult to relate any cellular effects to the generation of LLC changes.

Though many components of the OB *are* genetically tractable, we do not (yet) have a molecular handle on the major excitatory subtypes of the glomerular circuitry. This makes it difficult to

artificially perturb or enhance the activity of whole populations, or even subpopulations of these cell-types via, for example, optogenetic or chemogenetic manipulations. When molecular markers and associated mouse lines are finally established, they will provide useful future tools for determining how changing activity levels in these cells impact the network, and may provide a more direct avenue by which we can elucidate the specific function of LLC changes.

6.2.2. Strengths of studying glomerular circuitry to decipher sensory signalling mechanisms

Despite these limitations, the glomerular circuit is still a strong model system in which to study plasticity. With the technological advancement in imaging techniques, it is now possible to monitor neurons in awake behaving animals. Due to its anatomical proximity to the periphery, the OB is a particularly "visible" brain region to image. It is even possible to track individual cells for months, to observe how these may be impacted by variations in sensory input (Livneh and Mizrahi, 2011; Mizrahi and Katz, 2003).

In addition to this, the fact that OB processing centres are so anatomically close to sensory input allows us to study interesting phenomena that may occur elsewhere in less accessible parts of the brain. In sensory circuits, regenerative and recurrent excitation is in place to encode a continuous stream of analogue information. This may be important for sensing, and reliably transmitting fast and transient inputs that occur regularly as an organism moves through the environment, without missing important information. It is argued that inhibition is in place to dampen this feedforward excitation, ensuring minimal "littering" of the sensory system with unnecessary background noise. It is hypothesised that the summated activity of recurrent excitation and inhibition in neural circuits is transmitted to downstream processing centres to interpret a cohesive whole percept (Ganguli and Latham, 2009).

In the OB, the output cells are only one, or a few, synapses away from direct sensory input. Additionally, OB processes can be tracked to measurable behavioural readouts (Imai, 2014). This circuit therefore provides a highly accessible platform in which to study how sensory signal transduction, such as the process described above, occurs and is transmitted to higher processing areas, and how this process may be plastic. For instance, the glomerular LLC appears to be the physiological substrate for recurrent glomerular excitation and performs the function of entraining local excitatory components to portray synchronous patterned activity on a glomerular scale. Similar long-lasting depolarising events in response to input have been reported in other neural systems, such as in hippocampal granule cells (Mistry and Mellor, 2008) and in medioventral medulla neurons (Mamiya et al., 2005). However, in these systems, it is difficult to alter sensory experience to reliably drive plastic changes under "physiological"

conditions, making it difficult to interpret what these events may mean for basic input processing. Therefore, studying this phenomenon in the glomerular circuit of the OB may shine light on how sensory systems could function to encode changes in the environment.

Overall, although there are difficulties in detangling specific processes that arise due to input changes to OB glomeruli, the plastic changes we find here have the potential to provide valuable lessons of how the brain may encode the changing environment to maintain functional perception and behavioural output.

6.3. The role of larger LLCs in glomerular processing

The glomerular LLC is a crucial regenerative mechanism that ensures M/TCs are able to reliably respond to OSN input (Gire and Schoppa, 2009; Vaaga and Westbrook, 2017). The role of LLCs in amplifying initial, transient, OSN input is well-described (Carlson et al., 2000; De Saint Jan and Westbrook, 2007; De Saint Jan et al., 2009; Gire and Schoppa, 2009; Gire et al., 2012; Najac et al., 2011; Vaaga and Westbrook, 2017), and highlights the importance of these events in ensuring glutamatergic currents are transmitted to M/TCs. Due to LLCs, M/TCs can synchronise their sustained firing output and transmit robust signals to olfactory cortical areas. However, on a functional level, what do changes in LLC magnitudes actually mean for OB processing? If LLC changes do not appear, in our experiments, to impact M/TC output in response to OSN input, what is their function in the changing glomerulus?

Network stability in the face of changing activity levels is maintained by homeostatic plasticity. This mechanism ensures that network activity does not exhibit inappropriate and functionally detrimental high or low activity levels (Turrigiano and Nelson, 2004). Therefore, the enhanced excitatory glomerular drive by larger LLCs and subtle OSN-evoked increase of ETC firing demonstrated in this thesis, as well as the decreased inhibitory drive (D. Byrne, E. Galliano, unpublished data) observed during sensory-deprived conditions may be a homeostatic response that increases gain to ensure M/TC output remains functionally intact.

This may have important consequences for downstream signal processing. Since the olfactory cortical areas translate M/TC inputs into sensory perception, the output M/TCs present to cells in olfactory cortex heavily impacts how odours are interpreted. Odour identity appears to be encoded by the activity of distinct M/TC ensembles that respond to particular odours with synchronised firing (Kashiwadani et al., 1999). The activity of several M/TC ensembles creates oscillations in the OB (~40Hz in mammals) (McGann, 2013), and the detection of coincident M/TC activation during defined temporal windows throughout these oscillations appears to be necessary for olfactory cortex to “recognise” odorants. In addition to this, the concentration of

odorants seems to be coded by the spike response latencies M/TCs portray in response to input (Bolding and Franks, 2017). Therefore, even a small change in M/TC spiking behaviour in response to odours could change the percept of olfactory information. With *short-term* changes in sensory input, it may be beneficial for the organism to maintain the level of odour discrimination in terms of identity and concentration it portrays, as it would consequently be able to navigate through an ever-changing olfactory environment without significantly impacting its capability to sense odorants.

Therefore, the concerted action of increased excitatory synaptic drive, i.e. larger LLCs, and decreased inhibitory drive may provide a means of adjusting the glomerular network to a sensory deprived environment and ensures the outcome of processing at the M/TC level remains the same. Of course, while occlusion is in place, it may not be possible for the circuit to fully compensate for the huge reduction in incoming signal during that time, which may render any adjustments futile. However, this compensatory machinery may be in place to allow the network to be functionally "prepared" for when the perturbation is relieved.

Interpreting what LLC changes may mean becomes difficult when considering the basic lack in understanding of how these events are generated. Though the events have been well characterised in terms of mechanism (at the M/TC level) (De Saint Jan and Westbrook 2007; Vaaga and Westbrook, 2017), function (De Saint Jan et al., 2009; Gire and Schoppa, 2009; Gire et al., 2012; Vaaga and Westbrook, 2017), and requirement for recurrent excitation (Carlson et al., 2000; De Saint Jan et al., 2009), we still do not have concrete evidence as to the source of LLC generation. Additionally, no one, to our knowledge, has determined the mechanism of build-up of LLCs in the ETC network, which may display crucial processes in the functional effects LLCs have on M/TCs. Therefore, when changes occur in LLC magnitude, it could imply a multitude of processes that may be occurring. However, due to our lack in basic understanding of the mechanisms behind these events, it is difficult to pin-point the functional source of this change, and extrapolate the meaning of this on a network level.

6.4. The role of synaptically plastic ETCs in glomerular excitatory drive

Although ETCs do not appear to be intrinsically plastic with short term changes in input activity, they could represent the locus or are at least major contributors to synaptically adjusting excitatory drive in glomerular processing. This is because many studies point toward ETCs being at the heart of driving the recurrent feedforward excitation responsible for triggering M/TC responses to odorants (De Saint Jan et al., 2009; Gire and Schoppa, 2009; Gire et al., 2012; Najac

et al., 2011; Vaaga and Westbrook, 2016). We further strengthen this argument with our observation of a "multi-state" M/TC LLC, that we hypothesise to show the build up of M/TC LLCs utilising individual ETC-dependent LLCs.

Nevertheless, one may wonder why ETCs are at the centre of this processing in the first place, when M/TCs are anatomically connected to OSNs and inhibitory feedback loops. Indeed, in the AOB, there seems to be a lack of multi-step excitatory processing as seen in the main OB. Interestingly, differences between main OB M/TC and AOB MC firing responses to stimuli have recently been found, suggesting that these cells show some differences in their intrinsic properties and in their ability to integrate input information. In response to brief afferent stimulation, whereas main OB M/TCs respond with comparatively short, but intense, bursts of spikes, AOB MCs sustain low-frequency firing for a prolonged period of time, and require relatively strong stimulation (Luo et al., 2003; Shpak et al., 2012). This difference is due to the expression of TRPM4 channels on AOB MC dendrites (not found on main OB M/TC dendrites), which allow the influx of the persistent-spike associated non-selective cationic current (*I*can) (Shpak et al., 2012). This difference in odour-evoked responses may underlie key differences in how these circuits need to process incoming information.

In the main OB, it may be beneficial to dissect individual components of incoming odorants on a glomerular level, which may increase the discriminatory abilities of the olfactory cortex in depicting and integrating the multitude of the olfactory environment, extracting relevant information from these inputs on a relatively fast time-scale (Dulac and Wagner, 2006). Therefore, the prevalent multi-step excitatory pathway, via ETCs, in the glomeruli of the main OB may function to ensure distinct messages are transmitted to olfactory cortex. The inclusion of an ETC-mediated pathway in this case would aid this distinct transmission, because fine-scale mediation by inhibition is targeted to limiting feedforward excitation, i.e. LLCs, arriving through ETCs (Gire and Schoppa, 2009). In this case, while ETCs are important for amplifying initial excitatory input, the importance of which may arise because main OB M/TCs may not have this ability (perhaps due to a lack of TRPM4 channels on their dendrites), they may also provide a locus by which the glomerular circuitry can limit this amplification. This would then drive M/TCs to portray sustained odour-evoked response profiles that are however limited to a degree, ensuring that there is a distinct and relatively fast interpretation of odour information at the olfactory cortex level.

In contrast, the AOB is highly implicated in processing social signals, thus it may be beneficial to integrate signals over a much longer period of time to perceptually understand the social context (Dulac and Wagner, 2006; Shpak et al., 2012). Indeed, in the AOB, some MCs sample from different VR-associated glomeruli (Holy, 2018), thus integrating multiple input signals may need

more integrative time. In this case, the presence of an intermediary modulator, such as an ETC, may hinder this capability. This is because the inclusion of ETCs could provide another platform by which inhibition can limit excitatory drive to MCs. This may prevent MCs from responding to input with very long responses because the feedforward excitatory path could be intercepted by inhibition at the ETC locus, in addition to the MC locus which is already targeted by $GABA_A$ (presumably from local interneurons) to reduce prolonged firing (Shpak et al., 2012).

Therefore, in the main OB, modulation of excitatory drive through ETCs may be a mechanism that refines M/TC response profiles in the face of changing olfactory environments to produce relatively "transient" inputs to olfactory cortex, allowing cells there to distinguish odour identity and concentration throughout varying degrees of olfactory input. In contrast, this step may not be necessary in the AOB, and may in fact hinder the ability for MCs there to respond with the sustained patterns needed to integrate complex social cues.

6.4. Conforming to models of homeostatic plasticity?

Neurons function in networks that are continuously processing input from the environment. Since sensory experience is constantly changing, it is not surprising that network processing needs to adapt to encode these changes. In the OB, many components of initial processing have been shown to be plastic. These changes often happen in synchrony, where several components must adjust in a delicate balance of excitation and inhibition to ensure functional odour processing persists. With this thesis, we provide evidence for another avenue in which glomerular processing adjusts to sensory experience, which portrays the ability of the glomerular excitatory network to enhance glutamatergic drive in sensory-deprived conditions.

In the study of homeostatic network plasticity of mature circuits, a common finding is that plasticity in the excitatory components of a network occurs after the reduction of synaptic input by inhibitory neurons. This allows for excitatory components to retain their activity levels with changing environmental input (Barnes et al., 2015; Chen et al., 2011; Keck et al., 2011). Indeed, it has been shown that in the adult cortex, the ratio of excitation and inhibition remains relatively stable despite changes in cortical activity levels. When excitation is increased, inhibition is proportionally enhanced through the increased activity of inhibitory cells (Xue et al., 2014).

With 24 hours of activity level changes, similar plastic processes seem to occur in the OB. GABA/dopaminergic JGCs in dissociated cultures show inverted AIS plasticity (Chand et al., 2015). Whereas excitatory neurons usually portray a shortening of AISs in the face of increased activity levels (Evans et al., 2015), GABA/dopaminergic inhibitory neurons lengthen their AISs. A lengthening of AISs has been linked to increased excitability (Kaphzan et al., 2011; Kuba et al.,

2010), thus this phenotype could be in place to increase inhibitory drive onto the "over-excited" glomerular network. Unpublished *ex vivo* data further support this notion and demonstrate that with 24 hours of sensory deprivation, GABA/dopaminergic JGCs shorten their AISs, a phenotype linked to decreased excitability (D. Byrne, E. Galliano, unpublished data). Meanwhile, under the same conditions, the excitatory components of glomerular processing, the ETCs and M/TCs, do not adjust their AISs, and portray no change in their intrinsic excitability as partially discussed in this thesis (E. Galliano, C. Hahn, unpublished data). However, upon 3 days of occlusion, ETCs undergo AMPAergic and NMDAergic synaptic scaling (Tyler et al., 2007), and even broaden their axonal targeting specificity after longer periods (weeks) of sensory deprivation (Cummings and Belluscio, 2010). Thus, this circuit fits into the model that inhibitory cells may adjust their properties before the excitatory cells show such changes.

Nevertheless, we show here that synaptically, excitation in the circuit *is* increased with short-term sensory deprivation during similar time-frames in which inhibitory cells have been shown to adjust their properties (D. Byrne, E. Galliano, unpublished data; Chand et al., 2015). Thus, it may be possible that while the inhibitory circuitry adjusts first on a larger scale, the excitatory circuitry can adjust fine-scale properties that subtly enhance the shift of excitation and inhibition at this initial time point.

This form of network plasticity may be a solution to maintaining processing of odours under *short-term* environmental changes. If sensory experience remains changed for longer periods of time, multiple components of the network adjust their properties in several ways. For example, OSNs can adjust their release probability of glutamate (Tyler et al., 2007) and ETCs can change the broadness of their axonal targeting specificity (Cummings and Belluscio, 2010) (chapter 1, Introduction). These alterations may function to achieve a more permanent change to odour processing, and may be involved in ensuring odour processing functionally continues in a consistently sensory deprived or enriched environment.

6.5. The use of 24 hours of sensory deprivation to interpret the meaning of plastic changes

Naris occlusion has been a highly used sensory manipulation to drive plastic changes in the OB circuit (Coppola, 2012). In light of recent findings that 24 hours of sensory deprivation was enough time to drive plasticity in the inhibitory JGC circuitry (D. Byrne, E. Galliano, unpublished data), we predicted that ETCs, given their central role in glomerular processing, could adjust some of their properties in this time-frame. Indeed, we found that excitatory synaptic drive in a glomerulus can be enhanced after 24h occlusion.

One may be tempted to presume that longer periods of sensory deprivation may drive the excitatory circuit to enhance glutamatergic signalling even more, potentially to enhance the detection of a limited amount of odour input as much as possible. However, this may lead to an "over-stimulated" circuit, where most input is drastically amplified by an enhanced recurrent circuit, and transmitted as signal due to run-away excitatory signalling (Ganguli and Latham, 2009). This could lead to a massive reduction of the signal to noise ratio, and thus greatly perturb the sense of smell. In this study, we suggest LLCs can reach a ceiling level of magnitude. This ceiling level may be set intrinsically by the glomerular circuitry to prevent such runaway signalling under conditions that enhance the excitatory circuitry. In light of homeostatic plasticity, under long-term sensory deprivation, if excitatory signalling remains enhanced for long periods of time, i.e. LLCs remain at ceiling levels, it could trigger compensatory upregulation of the inhibitory circuitry (Turrigiano and Nelson, 2004). This would thus "re-set" the glomerular LLC to original levels. Thus, with long-term occlusion, the adjustability of LLC magnitude may be missed. Perhaps even 24 hours of sensory deprivation was too long to observe the critical change that enhances glomerular LLCs in the first place. Creating a time-line of LLC magnitudes under different periods of sensory deprivation may shine some light on where this change originates, and how it develops through varying periods of sensory deprivation.

What might be the impact of longer-term sensory deprivation on ETCs? Was 24 hours of sensory deprivation enough time to follow crucial plastic changes that may result in a change of the input-output relationship? From a homeostatic plasticity view-point, we may predict that given long-term sensory manipulations, the excitatory components of glomerular processing may portray further adjustments. Nevertheless, the findings that M/TCs retain remarkable dendritic stability in the face of sensory manipulations (Mizrahi and Katz, 2003) suggest that these cells are reluctant to adjust in an activity-dependent manner. However, axonal targeting (Cummings and Belluscio, 2010) and synaptic properties (Tyler et al., 2007) of ETCs *can* change with longer sensory manipulations. Additionally, we observed a very subtle increase in OSN-evoked ETC firing with our short-term occlusion paradigm, which may display the beginning of another property ETCs are adjusting that may not be fully evident with such short-term manipulation. Thus, it would be of profound interest to inspect ETC properties after longer-term sensory deprivations, to observe whether ETCs do play into circuit plasticity with other adjustments, such as in their intrinsic excitability or structural properties, and what the functions of these changes may be on glomerular processing.

Contrastingly, do other sensory manipulations that enrich the circuit result in changes occurring in the opposite direction? To this end, it would be interesting to observe whether LLC magnitudes can be decreased under enriched conditions. Corresponding to our hypothesis, we

would predict that with 24 hours of enrichment, M/TC OSN-evoked output again is unchanged, but the excitatory drive would be decreased, i.e. smaller LLCs, while the inhibitory drive increases. This would show us the bidirectional properties of glomerular input processing. Nevertheless, enrichment is a difficult sensory manipulation to robustly drive plastic changes across the entire OB. Unlike occlusion, where sensory input is blocked to the whole OB, it is not possible to expose animals to all possible odours glomeruli could respond to, as different odour identities and intensities drive differential glomerular pattern activation (Bozza et al., 2004). To this end, retaining control over which glomeruli are enriched and which are not, as well as the extent to which individual glomeruli are "enriched", becomes difficult without the use of transgenic animals that have particular glomeruli with known ligands fluorescently labelled (Mombaerts et al., 1996). With the use of transgenic animals, the scope of study then becomes limited, as only two or a few glomeruli would be fluorescently labelled per animal, limiting the number of observations the experimenter can obtain from a single experiment.

Therefore, elevating glomerular activity will aid the interpretation of the plastic changes we observe in this thesis and allow us to study this phenotype further. However, driving controlled elevated activity levels with sensory enrichment is not straightforward.

6.5. Future directions

6.5.1. Determining the origin of the LLC change

To fully interpret what enhanced excitatory signalling may mean for the glomerular circuit, it is imperative to determine the source of this plastic change. With the available experimental techniques to date, this feat may be complicated due to the difficulty in untangling single processes in glomerular communication (see section 6.2.1. above). However, with the advent of new genetic techniques, such as patch-seq and CRISPR, we may be able to study these processes more specifically in the future.

With techniques such as single-cell sequencing, it will be possible to identify particular molecular markers of ETCs, M/TCs, and the various subtypes of these populations. This would provide us with genetic access to these cells which we could then artificially modulate to decipher key processes.

In the case of LLCs, and the involvement of ETCs in their malleability, being able to genetically target ETCs would allow us to drive the expression of genetic probes specifically in these cells. In a slice, this could allow us to monitor ETC glutamate release for example, by expressing a glutamate-sensitive fluorescent reporter (GluSnFR) (Marvin et al., 2013), which would answer

our question about whether perhaps ETCs are responsible for the LLC change in occlusion due to higher rates of glutamate release. In addition to this, GluSnFRs can be used to track glutamate spillover and monitor the temporal patterns of this transmission (Hires et al., 2008). Thus, being able to specifically visualise the dynamics of glutamate release and transmission portrayed by individual cell-types in a glomerulus will undoubtedly allow us to decipher where and how an enhancement in this transmission occurs.

With further technological advancement, it may soon be possible to genetically target multiple cell-types in the same animal, all labelled with different fluorescent probes (Livet et al., 2007). This could allow us to directly map the dynamic transmission of LLCs among the glomerular circuitry, observing the effects this has on individual cell-types. Not only will this enhance our knowledge of the generation and specific function of the glomerular LLC, but it will also show us how sensory manipulations impact cell-specific LLC changes. With the use of these tools together with multi-photon imaging techniques, we would further be able to observe whether the LLC occurs *in vivo*, and whether enhancements or reductions in LLC magnitude in response to sensory manipulations can be observed in the awake, behaving animal.

6.5.2. Deciphering the functional consequences of activity-dependent plasticity in glomerular excitatory signalling

With the knowledge of where the LLC change occurs, we could design experiments that specifically manipulate the magnitude of an LLC (ideally genetically or optogenetically, by the application of light to increase or reduce activity of specific conductances distinctly linked to LLC generation). In this way, we could artificially precisely control LLC changes – either in the slice, or perhaps in the intact, behaving animal – and observe what the consequences are on M/TC responses to real odorants presented at different concentrations.

We could then link these manipulations to changes in the olfactory cortex. If we can manipulate the LLC in such a way that it drives changes in M/TC output in response to odorants, we could artificially replicate these changed response profiles by targeting these cells with ChR2 and stimulating them to fire at precise frequencies and latencies that would be defined by a particular glomerular LLC. At the same time, we could observe how these responses translate to olfactory cortical responses, and whether changes in these M/TC responses, that originate from a changed LLC, may alter the “interpretation” at these down-stream processing centres. This would provide key knowledge as to whether a change in glomerular excitatory signalling really impacts odour coding.

6.5.3. Behavioural consequences

It would further be interesting to observe whether glomerular LLC changes impact odour perception. To this end, it would first be compelling to observe whether 24 hours of sensory deprivation in itself results in changed odour perception, given the lack of M/TC output changes we observed with our experimental techniques. To explore this, we could train mice to discriminate between odorants, and determine whether the discrimination or detection of these odorants is impacted by short-term occlusion.

To tie any effects here to changes in glomerular excitatory signalling, we would again turn to our cell-type targeting techniques. In this way, we could present odorants to awake animals and artificially enhance or reduce glomerular LLC magnitudes. We could then observe whether an enhanced glomerular LLC results in the same perceptual changes observed under occluded conditions, and what the functional consequences are if an LLC change does not occur, i.e. artificially reduce the occluded LLC to a control LLC magnitude. In the same way, we could artificially induce a wide variety of LLC magnitudes, expressed by different cell-types, and observe their effects on odour perception.

These studies may reveal how the population activity in sensory systems, and key players within it, function to amplify stochastic and noisy sensory input to summate this information into a cohesive percept. Furthermore, they would shine some light on what mechanisms are in place to allow neural networks to adjust to changes in environmental stimuli.

6.6. Concluding remarks

Studies on activity-dependent plasticity in the excitatory circuit of the OB have so far been scarce. Contrasting the idea that activity-dependent plasticity first encompasses the inhibitory circuitry (Xue et al., 2014), we show here that the excitatory network *can* undergo short-term plastic synaptic changes, though these may not be as drastic as the changes observed in the inhibitory circuitry in the same time-frame.

The findings in this thesis suggest that short-term odour deprivation leads to a subtle adjustment in glomerular excitatory signalling, portrayed by a larger glomerular LLC experienced by ETCs and M/TCs, and a subtle increase in ETC firing in response to OSN stimulation, under certain conditions. This enhancement likely does not arise due to changes in the properties of OSN terminals, and suggests that the excitatory circuitry synaptically enhances recurrent excitation with mechanisms yet to be determined. Given the importance of LLCs in shaping ETC and M/TC responses to input, and their role in synchronising glomerular excitatory activity, the finding that

LLC magnitudes can be adjusted in an activity-dependent manner suggests malleable LLCs may functionally impact odour processing. These functional implications are yet to be determined, and future studies utilising novel experimental techniques will be useful in deciphering what this relatively fast adjustment in excitatory signalling in response to sensory manipulation means for a neural network.

References

AARTS, E., VERHAGE, M., VEENVLIET, J. V., DOLAN, C. V. & VAN DER SLUIS, S. 2014. A solution to dependency: using multilevel analysis to accommodate nested data. *Nature Neuroscience,* 17**,** 491.

ABRAHAM, N. M., EGGER, V., SHIMSHEK, D. R., RENDEN, R., FUKUNAGA, I., SPRENGEL, R., SEEBURG, P. H., KLUGMANN, M., MARGRIE, T. W., SCHAEFER, A. T. & KUNER, T. 2010. Synaptic Inhibition in the Olfactory Bulb Accelerates Odor Discrimination in Mice. *Neuron,* 65**,** 399-411.

ADAM, Y., LIVNEH, Y., MIYAMICHI, K., GROYSMAN, M., LUO, L. & MIZRAHI, A. 2014. Functional transformations of odor inputs in the mouse olfactory bulb. *Frontiers in Neural Circuits,* 8.

ADAM, Y. & MIZRAHI, A. 2011. Long-Term Imaging Reveals Dynamic Changes in the Neuronal Composition of the Glomerular Layer. *The Journal of Neuroscience,* 31**,** 7967-7973.

AIZENMAN, C. D. & LINDEN, D. J. 2000. Rapid, synaptically driven increases in the intrinsic excitability of cerebellar deep nuclear neurons. *Nature Neuroscience,* 3**,** 109.

ALKON, D. L. 1984. Calcium-mediated reduction of ionic currents: a biophysical memory trace. *Science,* 226**,** 1037-45.

ALTMAN, J. 1969. Autoradiographic and histological studies of postnatal neurogenesis. IV. Cell proliferation and migration in the anterior forebrain, with special reference to persisting neurogenesis in the olfactory bulb. *Journal of Comparative Neurology,* 137**,** 433-457.

ANGELO, K. & MARGRIE, T. W. 2011. Population diversity and function of hyperpolarization-activated current in olfactory bulb mitral cells. *Scientific Reports,* 1**,** 50.

ANGELO, K., RANCZ, E. A., PIMENTEL, D., HUNDAHL, C., HANNIBAL, J., FLEISCHMANN, A., PICHLER, B. & MARGRIE, T. W. 2012. A biophysical signature of network affiliation and sensory processing in mitral cells. *Nature,* 488**,** 375.

ANTAL, M., EYRE, M., FINKLEA, B. & NUSSER, Z. 2006. External tufted cells in the main olfactory bulb form two distinct subpopulations. *Eur J Neurosci,* 24**,** 1124-36.

ARNEODO, E. M., PENIKIS, K. B., RABINOWITZ, N., LICATA, A., CICHY, A., ZHANG, J., BOZZA, T. & RINBERG, D. 2018. Stimulus dependent diversity and stereotypy in the output of an olfactory functional unit. *Nature Communications,* 9**,** 1347.

ARONIADOU-ANDERJASKA, V., ZHOU, F., PRIEST, C., ENNIS, M. & T. SHIPLEY, M. 2000. *Tonic and Synaptically Evoked Presynaptic Inhibition of Sensory Input to the Rat Olfactory Bulb Via GABABHeteroreceptors*.

AUNGST, J. L., HEYWARD, P. M., PUCHE, A. C., KARNUP, S. V., HAYAR, A., SZABO, G. & SHIPLEY, M. T. 2003. Centre–surround inhibition among olfactory bulb glomeruli. *Nature,* 426**,** 623.

BAKER, H., MOREL, K., STONE, D. M. & MARUNIAK, J. A. 1993. Adult naris closure profoundly reduces tyrosine hydroxylase expression in mouse olfactory bulb. *Brain Res,* 614**,** 109-16.

BANERJEE, A., MARBACH, F., ANSELMI, F., KOH, MATTHEW S., DAVIS, MARTIN B., GARCIA DA SILVA, P., DELEVICH, K., OYIBO, HASSANA K., GUPTA, P., LI, B. & ALBEANU, DINU F. 2015. An Interglomerular Circuit Gates Glomerular Output and Implements Gain Control in the Mouse Olfactory Bulb. *Neuron,* 87**,** 193-207.

BARNES, SAMUEL J., SAMMONS, ROSANNA P., JACOBSEN, R. I., MACKIE, J., KELLER, GEORG B. & KECK, T. 2015. Subnetwork-Specific Homeostatic Plasticity in Mouse Visual Cortex In Vivo. *Neuron,* 86**,** 1290-1303.

BASTIEN-DIONNE, P.-O., DAVID, L. S., PARENT, A. & SAGHATELYAN, A. 2010. Role of sensory activity on chemospecific populations of interneurons in the adult olfactory bulb. *Journal of Comparative Neurology,* 518**,** 1847-1861.

BEAN, B. P. 2007. The action potential in mammalian central neurons. *Nature Reviews Neuroscience,* 8**,** 451.

BELLOCCHIO, E. E., REIMER, R. J., FREMEAU, R. T. & EDWARDS, R. H. 2000. Uptake of glutamate into synaptic vesicles by an inorganic phosphate transporter. *Science (New York, N.Y.),* 289**,** 957-960.

BELLUSCIO, L., LODOVICHI, C., FEINSTEIN, P., MOMBAERTS, P. & KATZ, L. C. 2002. Odorant receptors instruct functional circuitry in the mouse olfactory bulb. *Nature,* 419**,** 296-300.

BENDER, K. J. & TRUSSELL, L. O. 2012. The Physiology of the Axon Initial Segment. *Annual Review of Neuroscience,* 35**,** 249-265.

BEPARI, A. K., WATANABE, K., YAMAGUCHI, M., TAMAMAKI, N. & TAKEBAYASHI, H. 2012. Visualization of odor-induced neuronal activity by immediate early gene expression. *BMC Neuroscience,* 13**,** 140.

BOLDING, K. A. & FRANKS, K. M. 2017. Complementary codes for odor identity and intensity in olfactory cortex. *Elife,* 6.

BONZANO, S., BOVETTI, S., FASOLO, A., PERETTO, P. & DE MARCHIS, S. 2014. Odour enrichment increases adult-born dopaminergic neurons in the mouse olfactory bulb. *European Journal of Neuroscience,* 40**,** 3450-3457.

BORISOVSKA, M., BENSEN, A. L., CHONG, G. & WESTBROOK, G. L. 2013. Distinct Modes of Dopamine and GABA Release in a Dual Transmitter Neuron. *The Journal of Neuroscience,* 33**,** 1790-1796.

BOURNE, J. N. & SCHOPPA, N. E. 2017. Three-dimensional synaptic analyses of mitral cell and external tufted cell dendrites in rat olfactory bulb glomeruli. *Journal of Comparative Neurology,* 525**,** 592-609.

BOVETTI, S., VEYRAC, A., PERETTO, P., FASOLO, A. & DE MARCHIS, S. 2009. *Olfactory Enrichment Influences Adult Neurogenesis Modulating GAD67 and Plasticity-Related Molecules Expression in Newborn Cells of the Olfactory Bulb*.

BOYD, ALISON M., STURGILL, JAMES F., POO, C. & ISAACSON, JEFFRY S. 2012. Cortical Feedback Control of Olfactory Bulb Circuits. *Neuron,* 76**,** 1161-1174.

BOZZA, T., MCGANN, J. P., MOMBAERTS, P. & WACHOWIAK, M. 2004. In Vivo Imaging of Neuronal Activity by Targeted Expression of a Genetically Encoded Probe in the Mouse. *Neuron,* 42**,** 9-21.

BRENNAN, P. A. & KEVERNE, E. B. 2004. Something in the Air? New Insights into Mammalian Pheromones. *Current Biology,* 14**,** R81-R89.

BRENNAN, P. A., SCHELLINCK, H. M., DE LA RIVA, C., KENDRICK, K. M. & KEVERNE, E. B. 1998. Changes in neurotransmitter release in the main olfactory bulb following an olfactory conditioning procedure in mice. *Neuroscience,* 87**,** 583-590.

BRETON-PROVENCHER, V., BAKHSHETYAN, K., HARDY, D., BAMMANN, R. R., CAVARRETTA, F., SNAPYAN, M., CÔTÉ, D., MIGLIORE, M. & SAGHATELYAN, A. 2016. Principal cell activity induces spine relocation of adult-born interneurons in the olfactory bulb. *Nature Communications,* 7**,** 12659.

BRONS, J. F. & WOODY, C. D. 1980. Long-term changes in excitability of cortical neurons after Pavlovian conditioning and extinction. *J Neurophysiol,* 44**,** 605-15.

BUCK, L. & AXEL, R. 1991. A novel multigene family may encode odorant receptors: a molecular basis for odor recognition. *Cell,* 65**,** 175-87.

BUCK, L. B. 2004. Olfactory Receptors and Odor Coding in Mammals. *Nutrition Reviews,* 62**,** S184-S188.

BUONVISO, N., AMAT, C., LITAUDON, P., ROUX, S., ROYET, J. P., FARGET, V. & SICARD, G. 2003. Rhythm sequence through the olfactory bulb layers during the time window of a respiratory cycle. *Eur J Neurosci,* 17**,** 1811-9.

BUONVISO, N., GERVAIS, R., CHALANSONNET, M. & CHAPUT, M. 1998. Short-lasting exposure to one odour decreases general reactivity in the olfactory bulb of adult rats. *European Journal of Neuroscience,* 10**,** 2472-2475.

BURTON, S. D. & URBAN, N. N. 2014. Greater excitability and firing irregularity of tufted cells underlies distinct afferent-evoked activity of olfactory bulb mitral and tufted cells. *The Journal of Physiology,* 592**,** 2097-2118.

BYWALEZ, W. G., ONA-JODAR, T., LUKAS, M., NINKOVIC, J. & EGGER, V. 2017. Dendritic Arborization Patterns of Small Juxtaglomerular Cell Subtypes within the Rodent Olfactory Bulb. *Frontiers in Neuroanatomy,* 10.

CADWELL, C. R., PALASANTZA, A., JIANG, X., BERENS, P., DENG, Q., YILMAZ, M., REIMER, J., SHEN, S., BETHGE, M., TOLIAS, K. F., SANDBERG, R. & TOLIAS, A. S. 2015. Electrophysiological, transcriptomic and morphologic profiling of single neurons using Patch-seq. *Nature Biotechnology,* 34**,** 199.

CANSLER, H. L., MAKSIMOVA, M. A. & MEEKS, J. P. 2017. Experience-Dependent Plasticity in Accessory Olfactory Bulb Interneurons following Male–Male Social Interaction. *The Journal of Neuroscience,* 37**,** 7240-7252.

CARLSON, G. C., SHIPLEY, M. T. & KELLER, A. 2000. Long-Lasting Depolarizations in Mitral Cells of the Rat Olfactory Bulb. *The Journal of Neuroscience,* 20**,** 2011-2021.

CHAND, A. N., GALLIANO, E., CHESTERS, R. A. & GRUBB, M. S. 2015. A Distinct Subtype of Dopaminergic Interneuron Displays Inverted Structural Plasticity at the Axon Initial Segment. *The Journal of Neuroscience,* 35**,** 1573-1590.

CHAUDHURY, D., MANELLA, L., ARELLANOS, A., ESCANILLA, O., CLELAND, T. A. & LINSTER, C. 2010. Olfactory bulb habituation to odor stimuli. *Behav Neurosci,* 124**,** 490-9.

CHEETHAM, C., PARK, U. & BELLUSCIO, L. 2016. *Rapid and continuous activity-dependent plasticity of olfactory sensory input*.

CHEETHAM, C. E. J., GRIER, B. D. & BELLUSCIO, L. 2015. Bulk regional viral injection in neonatal mice enables structural and functional interrogation of defined neuronal populations throughout targeted brain areas. *Frontiers in Neural Circuits,* 9.

CHEN, W. R. & SHEPHERD, G. M. 1997. Membrane and synaptic properties of mitral cells in slices of rat olfactory bulb. *Brain Research,* 745**,** 189-196.

CHEUNG, M. C., JANG, W., SCHWOB, J. E. & WACHOWIAK, M. 2013. Functional recovery of odor representations in regenerated sensory inputs to the olfactory bulb. *Front Neural Circuits,* 7**,** 207.

CHITTAJALLU, R., CRAIG, M. T., MCFARLAND, A., YUAN, X., GERFEN, S., TRICOIRE, L., ERKKILA, B., BARRON, S. C., LOPEZ, C. M., LIANG, B. J., JEFFRIES, B. W., PELKEY, K. A. & MCBAIN, C. J. 2013. Dual origins of functionally distinct O-LM interneurons revealed by differential 5-HT3AR expression. *Nature Neuroscience,* 16**,** 1598.

CHO, J. Y., MIN, N., FRANZEN, L. & BAKER, H. 1996. Rapid down-regulation of tyrosine hydroxylase expression in the olfactory bulb of naris-occluded adult rats. *J Comp Neurol,* 369**,** 264-76.

CHONG, E. & RINBERG, D. 2018. Behavioral readout of spatio-temporal codes in olfaction. *Current Opinion in Neurobiology,* 52**,** 18-24.

CHRISTIE, J. M., BARK, C., HORMUZDI, S. G., HELBIG, I., MONYER, H. & WESTBROOK, G. L. 2005. Connexin36 Mediates Spike Synchrony in Olfactory Bulb Glomeruli. *Neuron,* 46**,** 761-772.

CHRISTIE, J. M., SCHOPPA, N. E. & WESTBROOK, G. L. 2001. Tufted cell dendrodendritic inhibition in the olfactory bulb is dependent on NMDA receptor activity. *J Neurophysiol,* 85**,** 169-73.

CHRISTIE, J. M. & WESTBROOK, G. L. 2006. Lateral Excitation within the Olfactory Bulb. *The Journal of Neuroscience,* 26**,** 2269-2277.

CLELAND, T. A. & LINSTER, C. 2012. On-Center/Inhibitory-Surround Decorrelation via Intraglomerular Inhibition in the Olfactory Bulb Glomerular Layer. *Front Integr Neurosci,* 6**,** 5.

CLEMENTS, J. D. & SILVER, R. A. 2000. Unveiling synaptic plasticity: a new graphical and analytical approach. *Trends in Neurosciences,* 23**,** 105-113.

COCKERHAM, R. E., MARGOLIS, F. L. & MUNGER, S. D. 2009. Afferent activity to necklace glomeruli is dependent on external stimuli. *BMC Research Notes,* 2**,** 31.

COPPOLA, D., M WAGUESPACK, A., R REEMS, M., L BUTMAN, M. & CHERRY, J. 2006. *Naris occlusion alters transducory protein immunoreactivity in olfactory epithelium*.

COPPOLA, D. M. 2012. Studies of Olfactory System Neural Plasticity: The Contribution of the Unilateral Naris Occlusion Technique. *Neural Plasticity,* 2012**,** 14.

COPPOLA, D. M. & WAGGENER, C. T. 2012. The Effects of Unilateral Naris Occlusion on Gene Expression Profiles in Mouse Olfactory Mucosa. *Journal of Molecular Neuroscience,* 47**,** 604-618.

CUDMORE, R. H. & TURRIGIANO, G. G. 2004. Long-Term Potentiation of Intrinsic Excitability in LV Visual Cortical Neurons. *Journal of Neurophysiology,* 92**,** 341-348.

CUMMINGS, D. M. & BELLUSCIO, L. 2010. Continuous Neural Plasticity in the Olfactory Intrabulbar Circuitry. *The Journal of Neuroscience,* 30**,** 9172-9180.

CUMMINGS, D. M., HENNING, H. E. & BRUNJES, P. C. 1997. Olfactory Bulb Recovery after Early Sensory Deprivation. *The Journal of Neuroscience,* 17**,** 7433-7440.

CUMMINGS, D. M., SNYDER, J. S., BREWER, M., CAMERON, H. A. & BELLUSCIO, L. 2014. Adult Neurogenesis Is Necessary to Refine and Maintain Circuit Specificity. *The Journal of Neuroscience,* 34**,** 13801-13810.

DAHLEN, J., JIMENEZ, D., GERKIN, R. & URBAN, N. 2011. Morphological Analysis of Activity-Reduced Adult-Born Neurons in the Mouse Olfactory Bulb. *Frontiers in Neuroscience,* 5.

DE SAINT JAN, D., HIRNET, D., WESTBROOK, G. L. & CHARPAK, S. 2009. External Tufted Cells Drive the Output of Olfactory Bulb Glomeruli. *The Journal of Neuroscience,* 29**,** 2043-2052.

DE SAINT JAN, D. & WESTBROOK, G. L. 2007. Disynaptic amplification of metabotropic glutamate receptor 1 responses in the olfactory bulb. *J Neurosci,* 27**,** 132-40.

DERMIETZEL, R. 1998. Gap junction wiring: a `new' principle in cell-to-cell communication in the nervous system?1Published on the World Wide Web on 4 November 1997.1. *Brain Research Reviews,* 26**,** 176-183.

DHAWALE, A. K., HAGIWARA, A., BHALLA, U. S., MURTHY, V. N. & ALBEANU, D. F. 2010. Non-redundant odor coding by sister mitral cells revealed by light addressable glomeruli in the mouse. *Nat Neurosci,* 13**,** 1404-12.

DIAS, B. G. & RESSLER, K. J. 2014. Parental olfactory experience influences behavior and neural structure in subsequent generations. *Nat Neurosci,* 17**,** 89-96.

DUCHAMP-VIRET, P., CHAPUT, M. A. & DUCHAMP, A. 1999. Odor Response Properties of Rat Olfactory Receptor Neurons. *Science,* 284**,** 2171-2174.

DULAC, C. & WAGNER, S. 2006. Genetic Analysis of Brain Circuits Underlying Pheromone Signaling. *Annual Review of Genetics,* 40**,** 449-467.

DUMITRESCU, A. S., EVANS, M. D. & GRUBB, M. S. 2016. Evaluating Tools for Live Imaging of Structural Plasticity at the Axon Initial Segment. *Frontiers in Cellular Neuroscience,* 10.

ECONOMO, M. N., HANSEN, K. R. & WACHOWIAK, M. 2016. Control of Mitral/Tufted Cell Output by Selective Inhibition among Olfactory Bulb Glomeruli. *Neuron,* 91**,** 397-411.

ELMQVIST, D. & QUASTEL, D. M. 1965. A quantitative study of end-plate potentials in isolated human muscle. *J Physiol,* 178**,** 505-29.

ENNIS, M., LINSTER, C., ARONIADOU-ANDERJASKA, V., CIOMBOR, K. & SHIPLEY, M. T. 1998. Glutamate and Synaptic Plasticity at Mammalian Primary Olfactory Synapsesa. *Annals of the New York Academy of Sciences,* 855**,** 457-466.

ENNIS, M., ZIMMER, L. A. & SHIPLEY, M. T. 1996. Olfactory nerve stimulation activates rat mitral cells via NMDA and non-NMDA receptors in vitro. *NeuroReport,* 7**,** 989-992.

EVANS, M. D., DUMITRESCU, A. S., KRUIJSSEN, D. L. H., TAYLOR, S. E. & GRUBB, M. S. 2015. Rapid Modulation of Axon Initial Segment Length Influences Repetitive Spike Firing. *Cell Rep,* 13**,** 1233-1245.

FAN, Y., FRICKER, D., BRAGER, D. H., CHEN, X., LU, H.-C., CHITWOOD, R. A. & JOHNSTON, D. 2005. Activity-dependent decrease of excitability in rat hippocampal neurons through increases in Ih. *Nature Neuroscience,* 8**,** 1542.

FARBMAN, A., BRUNJES, P., RENTFRO, L., MICHAS, J. & RITZ, S. 1988. The effect of unilateral naris occlusion on cell dynamics in the developing rat olfactory epithelium. *The Journal of Neuroscience,* 8**,** 3290-3295.

FERREIRA, T., BLACKMAN, A., OYRER, J., JAYABAL, S., J CHUNG, A., WATT, A., SJÖSTRÖM, P. & J VAN MEYEL, D. 2014. *Neuronal morphometry directly from bitmap images*.

FLETCHER, M. L. & WILSON, D. A. 2003. Olfactory bulb mitral-tufted cell plasticity: odorant-specific tuning reflects previous odorant exposure. *J Neurosci,* 23**,** 6946-55.

FRIEDMAN, D. & STROWBRIDGE, B. W. 2003. Both electrical and chemical synapses mediate fast network oscillations in the olfactory bulb. *J Neurophysiol,* 89**,** 2601-10.

FUKUNAGA, I., HERB, J., KOLLO, M., BOYDEN, E. S. & SCHAEFER, A. T. 2014. Independent control of gamma and theta activity by distinct interneuron networks in the olfactory bulb. *Nature neuroscience,* 17**,** 1208-1216.

FUZIK, J., ZEISEL, A., MÁTÉ, Z., CALVIGIONI, D., YANAGAWA, Y., SZABÓ, G., LINNARSSON, S. & HARKANY, T. 2016. Integration of electrophysiological recordings with single-cell RNA-seq data identifies neuronal subtypes. *Nature biotechnology,* 34**,** 175-183.

GABELLEC, M.-M., PANZANELLI, P., SASSOÈ-POGNETTO, M. & LLEDO, P.-M. 2007. Synapse-specific localization of vesicular glutamate transporters in the rat olfactory bulb. *European Journal of Neuroscience,* 25**,** 1373-1383.

GALLIANO, E., FRANZONI, E., BRETON, M., CHAND, A. N., BYRNE, D. J., MURTHY, V. N. & GRUBB, M. S. 2018. Embryonic and postnatal neurogenesis produce functionally distinct subclasses of dopaminergic neuron. *eLife,* 7**,** e32373.

GANGULI, S. & LATHAM, P. 2009. Feedforward to the Past: The Relation between Neuronal Connectivity, Amplification, and Short-Term Memory. *Neuron,* 61**,** 499-501.

GANGULY, K., KISS, L. & POO, M.-M. 2000. *Enhancement of presynaptic neuronal excitability by correlated presynaptic and postsynaptic spiking*.

GARCIA-SEGURA, L. M. & PEREZ-MARQUEZ, J. 2014. A new mathematical function to evaluate neuronal morphology using the Sholl analysis. *Journal of Neuroscience Methods,* 226**,** 103-109.

GHOSH, A. & GREENBERG, M. 1995. Calcium signaling in neurons: molecular mechanisms and cellular consequences. *Science,* 268**,** 239-247.

GIRE, D. H., FRANKS, K. M., ZAK, J. D., TANAKA, K. F., WHITESELL, J. D., MULLIGAN, A. A., HEN, R. & SCHOPPA, N. E. 2012. Mitral cells in the olfactory bulb are mainly excited through a multistep signaling path. *The Journal of neuroscience : the official journal of the Society for Neuroscience,* 32**,** 2964-2975.

GIRE, D. H. & SCHOPPA, N. E. 2009. Control of On/Off Glomerular Signaling by a Local GABAergic Microcircuit in the Olfactory Bulb. *The Journal of Neuroscience,* 29**,** 13454-13464.

GOLDFARB, M., SCHOORLEMMER, J., WILLIAMS, A., DIWAKAR, S., WANG, Q., HUANG, X., GIZA, J., TCHETCHIK, D., KELLEY, K., VEGA, A., MATTHEWS, G., ROSSI, P., ORNITZ, D. M. & D'ANGELO, E. 2007. Fibroblast Growth Factor Homologous Factors Control Neuronal Excitability through Modulation of Voltage-Gated Sodium Channels. *Neuron,* 55**,** 449-463.

GRAZIADEI, P. P. & GRAZIADEI, G. A. 1979. Neurogenesis and neuron regeneration in the olfactory system of mammals. I. Morphological aspects of differentiation and structural organization of the olfactory sensory neurons. *J Neurocytol,* 8**,** 1-18.

GRIER, B. D., BELLUSCIO, L. & CHEETHAM, C. E. J. 2016. Olfactory Sensory Activity Modulates Microglial-Neuronal Interactions during Dopaminergic Cell Loss in the Olfactory Bulb. *Frontiers in Cellular Neuroscience,* 10.

GROSS, GARRETT G., JUNGE, JASON A., MORA, RUDY J., KWON, H.-B., OLSON, C. A., TAKAHASHI, TERRY T., LIMAN, EMILY R., ELLIS-DAVIES, GRAHAM C. R., MCGEE,

AARON W., SABATINI, BERNARDO L., ROBERTS, RICHARD W. & ARNOLD, DON B. 2013. Recombinant Probes for Visualizing Endogenous Synaptic Proteins in Living Neurons. *Neuron,* 78**,** 971-985.

GRUBB, M. S. & BURRONE, J. 2010a. Activity-dependent relocation of the axon initial segment fine-tunes neuronal excitability. *Nature,* 465**,** 1070-1074.

GRUBB, M. S. & BURRONE, J. 2010b. Building and maintaining the axon initial segment. *Curr Opin Neurobiol,* 20**,** 481-8.

GRUBB, M. S., NISSANT, A., MURRAY, K. & LLEDO, P.-M. 2008. Functional Maturation of the First Synapse in Olfaction: Development and Adult Neurogenesis. *The Journal of Neuroscience,* 28**,** 2919-2932.

GSCHWEND, O., ABRAHAM, N. M., LAGIER, S., BEGNAUD, F., RODRIGUEZ, I. & CARLETON, A. 2015. Neuronal pattern separation in the olfactory bulb improves odor discrimination learning. *Nature Neuroscience,* 18**,** 1474.

GUENTHNER, CASEY J., MIYAMICHI, K., YANG, HELEN H., HELLER, H. C. & LUO, L. 2013. Permanent Genetic Access to Transiently Active Neurons via TRAP: Targeted Recombination in Active Populations. *Neuron,* 78**,** 773-784.

GUTHRIE, K., WILSON, D. & LEON, M. 1990. Early unilateral deprivation modifies olfactory bulb function. *The Journal of Neuroscience,* 10**,** 3402-3412.

HALPERN, M. & MARTINEZ-MARCOS, A. 2003. Structure and function of the vomeronasal system: an update. *Prog Neurobiol,* 70**,** 245-318.

HAYAR, A. & ENNIS, M. 2007. Endogenous GABA and glutamate finely tune the bursting of olfactory bulb external tufted cells. *J Neurophysiol,* 98**,** 1052-6.

HAYAR, A., KARNUP, S., ENNIS, M. & SHIPLEY, M. T. 2004a. External Tufted Cells: A Major Excitatory Element That Coordinates Glomerular Activity. *The Journal of Neuroscience,* 24**,** 6676-6685.

HAYAR, A., KARNUP, S., SHIPLEY, M. T. & ENNIS, M. 2004b. Olfactory Bulb Glomeruli: External Tufted Cells Intrinsically Burst at Theta Frequency and Are Entrained by Patterned Olfactory Input. *The Journal of Neuroscience,* 24**,** 1190-1199.

HAYAR, A., SHIPLEY, M. T. & ENNIS, M. 2005. Olfactory bulb external tufted cells are synchronized by multiple intraglomerular mechanisms. *The Journal of neuroscience : the official journal of the Society for Neuroscience,* 25**,** 8197-8208.

HEYWARD, P., ENNIS, M., KELLER, A. & SHIPLEY, M. T. 2001. Membrane Bistability in Olfactory Bulb Mitral Cells. *The Journal of Neuroscience,* 21**,** 5311-5320.

HIRES, S. A., ZHU, Y. & TSIEN, R. Y. 2008. Optical measurement of synaptic glutamate spillover and reuptake by linker optimized glutamate-sensitive fluorescent reporters. *Proceedings of the National Academy of Sciences,* 105**,** 4411-4416.

HOLY, T. E. 2018. The Accessory Olfactory System: Innately Specialized or Microcosm of Mammalian Circuitry? *Annual Review of Neuroscience,* 41**,** 501-525.

IBARRA-SORIA, X., LEVITIN, M. O., SARAIVA, L. R. & LOGAN, D. W. 2014. The Olfactory Transcriptomes of Mice. *PLOS Genetics,* 10**,** e1004593.

IGARASHI, K. M., IEKI, N., AN, M., YAMAGUCHI, Y., NAGAYAMA, S., KOBAYAKAWA, K., KOBAYAKAWA, R., TANIFUJI, M., SAKANO, H., CHEN, W. R. & MORI, K. 2012. Parallel mitral and tufted cell pathways route distinct odor information to different targets in the olfactory cortex. *J Neurosci,* 32**,** 7970-85.

IMAI, T. 2014. Construction of functional neuronal circuitry in the olfactory bulb. *Seminars in Cell & Developmental Biology,* 35**,** 180-188.

IMAMURA, K., MATAGA, N. & MORI, K. 1992. Coding of odor molecules by mitral/tufted cells in rabbit olfactory bulb. I. Aliphatic compounds. *Journal of Neurophysiology,* 68**,** 1986-2002.

ISAACSON, J. S. 1999. Glutamate spillover mediates excitatory transmission in the rat olfactory bulb. *Neuron,* 23**,** 377-84.

ISAACSON, J. S. & STROWBRIDGE, B. W. 1998. Olfactory Reciprocal Synapses: Dendritic Signaling in the CNS. *Neuron,* 20**,** 749-761.

J MURPHY, G., P DARCY, D. & S ISAACSON, J. 2005. *Intraglomerular inhibition: Signaling mechanisms of an olfactory microcircuit*.

JAHR, C. E. & NICOLL, R. A. 1982. An intracellular analysis of dendrodendritic inhibition in the turtle in vitro olfactory bulb. *The Journal of Physiology,* 326**,** 213-234.

JENKINS, S. M. & BENNETT, V. 2001. Ankyrin-G coordinates assembly of the spectrin-based membrane skeleton, voltage-gated sodium channels, and L1 CAMs at Purkinje neuron initial segments. *J Cell Biol,* 155**,** 739-46.

JOHNSON, B. A. & LEON, M. 2000. Modular representations of odorants in the glomerular layer of the rat olfactory bulb and the effects of stimulus concentration. *Journal of Comparative Neurology,* 422**,** 496-509.

JOHNSON, M. C., BIJU, K. C., HOFFMAN, J. & FADOOL, D. A. 2013. Odor enrichment sculpts the abundance of olfactory bulb mitral cells. *Neuroscience Letters,* 541**,** 173-178.

JOHNSTON, J. & DELANEY, K. R. 2010. Synaptic activation of T-type Ca2+ channels via mGluR activation in the primary dendrite of mitral cells. *J Neurophysiol,* 103**,** 2557-69.

JONES, S. V., CHOI, D. C., DAVIS, M. & RESSLER, K. J. 2008. Learning-Dependent Structural Plasticity in the Adult Olfactory Pathway. *The Journal of Neuroscience,* 28**,** 13106-13111.

K JIN, B., FRANZEN, L. & BAKER, H. 1996. *Regulation of C-Fos mRNA and fos protein expression in olfactory bulbs from unilaterally odor-deprived adult mice*.

KAPHZAN, H., BUFFINGTON, S. A., JUNG, J. I., RASBAND, M. N. & KLANN, E. 2011. Alterations in Intrinsic Membrane Properties and the Axon Initial Segment in a Mouse Model of Angelman Syndrome. *The Journal of Neuroscience,* 31**,** 17637-17648.

KASHIWADANI, H., SASAKI, Y. F., UCHIDA, N. & MORI, K. 1999. Synchronized Oscillatory Discharges of Mitral/Tufted Cells With Different Molecular Receptive Ranges in the Rabbit Olfactory Bulb. *Journal of Neurophysiology,* 82**,** 1786-1792.

KASS, M. D., POTTACKAL, J., TURKEL, D. J. & MCGANN, J. P. 2013a. Changes in the neural representation of odorants after olfactory deprivation in the adult mouse olfactory bulb. *Chemical senses,* 38**,** 77-89.

KASS, M. D., ROSENTHAL, M. C., POTTACKAL, J. & MCGANN, J. P. 2013b. Fear Learning Enhances Neural Responses to Threat-Predictive Sensory Stimuli. *Science,* 342**,** 1389-1392.

KATO, HIROYUKI K., CHU, MONICA W., ISAACSON, JEFFRY S. & KOMIYAMA, T. 2012. Dynamic Sensory Representations in the Olfactory Bulb: Modulation by Wakefulness and Experience. *Neuron,* 76**,** 962-975.

KAUER, J. S., SENSEMAN, D. M. & COHEN, L. B. 1987. Odor-elicited activity monitored simultaneously from 124 regions of the salamander olfactory bulb using a voltage-sensitive dye. *Brain Research,* 418**,** 255-261.

KAWANO, T. & MARGOLIS, F. L. 1982. Transsynaptic regulation of olfactory bulb catecholamines in mice and rats. *J Neurochem,* 39**,** 342-8.

KAWASHIMA, T., OKUNO, H. & BITO, H. 2014. A new era for functional labeling of neurons: activity-dependent promoters have come of age. *Frontiers in neural circuits,* 8**,** 37-37.

KAY, L. M. & LAURENT, G. 1999. Odor- and context-dependent modulation of mitral cell activity in behaving rats. *Nat Neurosci,* 2**,** 1003-9.

KELSCH, W., LIN, C.-W., MOSLEY, C. P. & LOIS, C. 2009. A Critical Period for Activity-Dependent Synaptic Development during Olfactory Bulb Adult Neurogenesis. *The Journal of Neuroscience,* 29**,** 11852-11858.

KENT, P. F., MOZELL, M. M., MURPHY, S. J. & HORNUNG, D. E. 1996. The interaction of imposed and inherent olfactory mucosal activity patterns and their composite representation in a mammalian species using voltage-sensitive dyes. *J Neurosci,* 16**,** 345-53.

KIKUTA, S., FLETCHER, M. L., HOMMA, R., YAMASOBA, T. & NAGAYAMA, S. 2013. Odorant response properties of individual neurons in an olfactory glomerular module. *Neuron,* 77**,** 1122-35.

KIKUTA, S., SAKAMOTO, T., NAGAYAMA, S., KANAYA, K., KINOSHITA, M., KONDO, K., TSUNODA, K., MORI, K. & YAMASOBA, T. 2015. Sensory Deprivation Disrupts Homeostatic Regeneration of Newly Generated Olfactory Sensory Neurons after Injury in Adult Mice. *The Journal of Neuroscience,* 35**,** 2657-2673.

KIMBELL, J. S., GODO, M. N., GROSS, E. A., JOYNER, D. R., RICHARDSON, R. B. & MORGAN, K. T. 1997. Computer Simulation of Inspiratory Airflow in All Regions of the F344 Rat Nasal Passages. *Toxicology and Applied Pharmacology,* 145**,** 388-398.

KIYOKAGE, E., PAN, Y. Z., SHAO, Z., KOBAYASHI, K., SZABO, G., YANAGAWA, Y., OBATA, K., OKANO, H., TOIDA, K., PUCHE, A. C. & SHIPLEY, M. T. 2010. Molecular identity of periglomerular and short axon cells. *J Neurosci,* 30**,** 1185-96.

KONDO, K., SUZUKAWA, K., SAKAMOTO, T., WATANABE, K., KANAYA, K., USHIO, M., YAMAGUCHI, T., NIBU, K.-I., KAGA, K. & YAMASOBA, T. 2010. Age-related changes in cell dynamics of the postnatal mouse olfactory neuroepithelium: Cell proliferation, neuronal differentiation, and cell death. *Journal of Comparative Neurology,* 518**,** 1962-1975.

KOSAKA, K. & KOSAKA, T. 2007. Chemical properties of type 1 and type 2 periglomerular cells in the mouse olfactory bulb are different from those in the rat olfactory bulb. *Brain Research,* 1167**,** 42-55.

KOSAKA, T. & KOSAKA, K. 2011. "Interneurons" in the olfactory bulb revisited. *Neurosci Res,* 69**,** 93-9.

KOSAKA, T., KOSAKA, K., HAMA, K., WU, J.-Y. & NAGATSU, I. 1987. Differential effect of functional olfactory deprivation on the GABAergic and catecholaminergic traits in the rat main olfactory bulb. *Brain Research,* 413**,** 197-203.

KUBA, H., OICHI, Y. & OHMORI, H. 2010. Presynaptic activity regulates Na(+) channel distribution at the axon initial segment. *Nature,* 465**,** 1075-8.

L KOSTER, N., NORMAN, A., RICHTAND, N., NICKELL, W., PUCHE, A. C., PIXLEY, S. & T SHIPLEY, M. 1999. *Olfactory receptor neurons express D2 dopamine receptors*.

LAGIER, S., CARLETON, A. & LLEDO, P. M. 2004. Interplay between local GABAergic interneurons and relay neurons generates gamma oscillations in the rat olfactory bulb. *J Neurosci,* 24**,** 4382-92.

LAMPRECHT, R. & LEDOUX, J. 2004. *Structural plasticity and memory*.

LANDISMAN, C. E. & CONNORS, B. W. 2005. Long-Term Modulation of Electrical Synapses in the Mammalian Thalamus. *Science,* 310**,** 1809-1813.

LAU, C. G. & MURTHY, V. N. 2012. Activity-Dependent Regulation of Inhibition via GAD67. *The Journal of Neuroscience,* 32**,** 8521-8531.

LEPOUSEZ, G., NISSANT, A., BRYANT, A. K., GHEUSI, G., GREER, C. A. & LLEDO, P.-M. 2014. Olfactory learning promotes input-specific synaptic plasticity in adult-born neurons. *Proceedings of the National Academy of Sciences,* 111**,** 13984-13989.

LI, C. S., KABA, H., SAITO, H. & SETO, K. 1990. Neural mechanisms underlying the action of primer pheromones in mice. *Neuroscience,* 36**,** 773-778.

LIN, C. W., SIM, S., AINSWORTH, A., OKADA, M., KELSCH, W. & LOIS, C. 2010. Genetically increased cell-intrinsic excitability enhances neuronal integration into adult brain circuits. *Neuron,* 65**,** 32-9.

LINK, W., KONIETZKO, U., KAUSELMANN, G., KRUG, M., SCHWANKE, B., FREY, U. & KUHL, D. 1995. Somatodendritic expression of an immediate early gene is regulated by synaptic activity. *Proc Natl Acad Sci U S A,* 92**,** 5734-8.

LINSTER, C. & CLELAND, T. A. 2002. Cholinergic modulation of sensory representations in the olfactory bulb. *Neural Netw,* 15**,** 709-17.

LIU, S., AUNGST, J., C PUCHE, A. & T SHIPLEY, M. 2012. *Serotonin modulates the population activity profile of olfactory bulb external tufted cells*.

LIU, S., PLACHEZ, C., SHAO, Z., PUCHE, A. & SHIPLEY, M. T. 2013. Olfactory bulb short axon cell release of GABA and dopamine produces a temporally biphasic inhibition-excitation response in external tufted cells. *J Neurosci,* 33**,** 2916-26.

LIU, S., PUCHE, A. C. & SHIPLEY, M. T. 2016. The Interglomerular Circuit Potently Inhibits Olfactory Bulb Output Neurons by Both Direct and Indirect Pathways. *The Journal of Neuroscience,* 36**,** 9604-9617.

LIU, S. & SHIPLEY, M. T. 2008. Multiple Conductances Cooperatively Regulate Spontaneous Bursting in Mouse Olfactory Bulb External Tufted Cells. *The Journal of Neuroscience,* 28**,** 1625-1639.

LIU, W. L. & SHIPLEY, M. T. 1994. Intrabulbar associational system in the rat olfactory bulb comprises cholecystokinin-containing tufted cells that synapse onto the dendrites of GABAergic granule cells. *J Comp Neurol,* 346**,** 541-58.

LIVET, J., WEISSMAN, T. A., KANG, H., DRAFT, R. W., LU, J., BENNIS, R. A., SANES, J. R. & LICHTMAN, J. W. 2007. Transgenic strategies for combinatorial expression of fluorescent proteins in the nervous system. *Nature,* 450**,** 56-62.

LIVNEH, Y., ADAM, Y. & MIZRAHI, A. 2014. Odor Processing by Adult-Born Neurons. *Neuron,* 81**,** 1097-1110.

LIVNEH, Y., FEINSTEIN, N., KLEIN, M. & MIZRAHI, A. 2009. Sensory Input Enhances Synaptogenesis of Adult-Born Neurons. *The Journal of Neuroscience,* 29**,** 86-97.

LIVNEH, Y. & MIZRAHI, A. 2011. Experience-dependent plasticity of mature adult-born neurons. *Nature Neuroscience,* 15**,** 26.

LODOVICHI, C., BELLUSCIO, L. & KATZ, L. C. 2003. Functional topography of connections linking mirror-symmetric maps in the mouse olfactory bulb. *Neuron,* 38**,** 265-276.

LOIS, C. & ALVAREZ-BUYLLA, A. 1994. Long-distance neuronal migration in the adult mammalian brain. *Science,* 264**,** 1145-1148.

LONGAIR, M. H., BAKER, D. A. & ARMSTRONG, J. D. 2011. Simple Neurite Tracer: open source software for reconstruction, visualization and analysis of neuronal processes. *Bioinformatics,* 27**,** 2453-2454.

LUO, M., FEE, M. S. & KATZ, L. C. 2003. Encoding Pheromonal Signals in the Accessory Olfactory Bulb of Behaving Mice. *Science,* 299**,** 1196-1201.

LYFORD, G. L., YAMAGATA, K., KAUFMANN, W. E., BARNES, C. A., SANDERS, L. K., COPELAND, N. G., GILBERT, D. J., JENKINS, N. A., LANAHAN, A. A. & WORLEY, P. F. 1995. Arc, a growth factor and activity-regulated gene, encodes a novel cytoskeleton-associated protein that is enriched in neuronal dendrites. *Neuron,* 14**,** 433-445.

LYNCH, J. W. & BARRY, P. H. 1989. Action potentials initiated by single channels opening in a small neuron (rat olfactory receptor). *Biophys J,* 55**,** 755-68.

MA, J. & LOWE, G. 2007. Calcium permeable AMPA receptors and autoreceptors in external tufted cells of rat olfactory bulb. *Neuroscience,* 144**,** 1094-1108.

MA, M. & LUO, M. 2012. Optogenetic activation of basal forebrain cholinergic neurons modulates neuronal excitability and sensory responses in the main olfactory bulb. *J Neurosci,* 32**,** 10105-16.

MACDONALD, R. L. & TWYMAN, R. E. 1991. Biophysical properties and regulation of GABAA receptor channels. *Seminars in Neuroscience,* 3**,** 219-230.

MACKAY-SIM, A. & KITTEL, P. W. 1991. On the Life Span of Olfactory Receptor Neurons. *European Journal of Neuroscience,* 3**,** 209-215.

MACRIDES, F. & SCHNEIDER, S. P. 1982. Laminar organization of mitral and tufted cells in the main olfactory bulb of the adult hamster. *Journal of Comparative Neurology,* 208**,** 419-430.

MADISEN, L., ZWINGMAN, T. A., SUNKIN, S. M., OH, S. W., ZARIWALA, H. A., GU, H., NG, L. L., PALMITER, R. D., HAWRYLYCZ, M. J., JONES, A. R., LEIN, E. S. & ZENG, H. 2009. A robust and high-throughput Cre reporting and characterization system for the whole mouse brain. *Nature Neuroscience,* 13**,** 133.

MAGAVI, S. S., MITCHELL, B. D., SZENTIRMAI, O., CARTER, B. S. & MACKLIS, J. D. 2005. Adult-born and preexisting olfactory granule neurons undergo distinct experience-dependent modifications of their olfactory responses in vivo. *J Neurosci,* 25**,** 10729-39.

MAHER, B. & L WESTBROOK, G. 2008. *Co-Transmission of Dopamine and GABA in Periglomerular Cells*.

MAHER, B., MCGINLEY, M. & L WESTBROOK, G. 2009. *Experience-dependent maturation of the glomerular microcircuit*.

MALNIC, B., HIRONO, J., SATO, T. & BUCK, L. B. 1999. Combinatorial Receptor Codes for Odors. *Cell,* 96**,** 713-723.

MAMIYA, K., BAY, K., SKINNER, R. D. & GARCIA-RILL, E. 2005. Induction of long-lasting depolarization in medioventral medulla neurons by cholinergic input from the pedunculopontine nucleus. *Journal of Applied Physiology,* 99**,** 1127-1137.

MANDAIRON, N., DIDIER, A. & LINSTER, C. 2008. Odor enrichment increases interneurons responsiveness in spatially defined regions of the olfactory bulb correlated with perception. *Neurobiol Learn Mem,* 90**,** 178-84.

MANDAIRON, N., SACQUET, J., JOURDAN, F. & DIDIER, A. 2006. Long-term fate and distribution of newborn cells in the adult mouse olfactory bulb: Influences of olfactory deprivation. *Neuroscience,* 141**,** 443-51.

MARKOPOULOS, F., ROKNI, D., GIRE, DAVID H. & MURTHY, VENKATESH N. 2012. Functional Properties of Cortical Feedback Projections to the Olfactory Bulb. *Neuron,* 76**,** 1175-1188.

MARKS, C. A., CHENG, K., CUMMINGS, D. M. & BELLUSCIO, L. 2006. Activity-Dependent Plasticity in the Olfactory Intrabulbar Map. *The Journal of Neuroscience,* 26**,** 11257-11266.

MARTONČÍKOVÁ, M., LIEVAJOVÁ, K., ORENDÁČOVÁ, J., BLAŠKO, J. & RAČEKOVÁ, E. 2011. Odor enrichment influences neurogenesis in the rostral migratory stream of young rats. *Acta Histochemica,* 113**,** 326-332.

MARUNIAK, J. A., HENEGAR, J. R. & SWEENEY, T. P. 1990. Effects of long-term unilateral naris closure on the olfactory epithelia of adult mice. *Brain Research,* 526**,** 65-72.

MARVIN, J. S., BORGHUIS, B. G., TIAN, L., CICHON, J., HARNETT, M. T., AKERBOOM, J., GORDUS, A., RENNINGER, S. L., CHEN, T.-W., BARGMANN, C. I., ORGER, M. B., SCHREITER, E. R., DEMB, J. B., GAN, W.-B., HIRES, S. A. & LOOGER, L. L. 2013. An optimized fluorescent probe for visualizing glutamate neurotransmission. *Nature Methods,* 10**,** 162.

MASUYAMA, K., ZHANG, Y., RAO, Y. & WANG, J. W. 2012. Mapping Neural Circuits with Activity-Dependent Nuclear Import of a Transcription Factor. *Journal of Neurogenetics,* 26**,** 89-102.

MCQUISTON, A. R. & KATZ, L. C. 2001. Electrophysiology of interneurons in the glomerular layer of the rat olfactory bulb. *J Neurophysiol,* 86**,** 1899-907.

MEISAMI, E. & SAFARI, L. 1981. A quantitative study of the effects of early unilateral olfactory deprivation on the number and distribution of mitral and tufted cells and of glomeruli in the rat olfactory bulb. *Brain Res,* 221**,** 81-107.

MEREDITH, M. 1994. Chronic recording of vomeronasal pump activation in awake behaving hamsters. *Physiology & Behavior,* 56**,** 345-354.

MISTRY, R. & MELLOR, J. R. 2008. Bidirectional activity-dependent plasticity of membrane potential and the influence on spiking in rat hippocampal dentate granule cells. *Neuropharmacology,* 54**,** 290-299.

MITSUI, S., IGARASHI, K. M., MORI, K. & YOSHIHARA, Y. 2011. Genetic visualization of the secondary olfactory pathway in Tbx21 transgenic mice. *Neural Systems & Circuits,* 1**,** 5.

MIYAMICHI, K., AMAT, F., MOUSSAVI, F., WANG, C., WICKERSHAM, I., WALL, N. R., TANIGUCHI, H., TASIC, B., HUANG, Z. J., HE, Z., CALLAWAY, E. M., HOROWITZ, M. A. & LUO, L. 2011. Cortical representations of olfactory input by transsynaptic tracing. *Nature,* 472**,** 191-196.

MIZRAHI, A. 2007a. *Dendritic development and plasticity of adult-born neurons in the mouse olfactory bulb*.

MIZRAHI, A. 2007b. Dendritic development and plasticity of adult-born neurons in the mouse olfactory bulb. *Nature Neuroscience,* 10**,** 444.

MIZRAHI, A. & C KATZ, L. 2003. *Dendritic stability in the adult olfactory bulb*.
MIZRAHI, A. & KATZ, L. C. 2003. Dendritic stability in the adult olfactory bulb. *Nature Neuroscience,* 6**,** 1201.
MOLINAS, A., AOUDE, I., SOUBEYRE, V., TAZIR, B., CADIOU, H. & GROSMAITRE, X. 2016. Anatomical and molecular consequences of Unilateral Naris Closure on two populations of olfactory sensory neurons expressing defined odorant receptors. *Neurosci Lett,* 626**,** 42-7.
MOMBAERTS, P., WANG, F., DULAC, C., CHAO, S. K., NEMES, A., MENDELSOHN, M., EDMONDSON, J. & AXEL, R. 1996. Visualizing an Olfactory Sensory Map. *Cell,* 87**,** 675-686.
MONYER, H., SPRENGEL, R., SCHOEPFER, R., HERB, A., HIGUCHI, M., LOMELI, H., BURNASHEV, N., SAKMANN, B. & SEEBURG, P. H. 1992. Heteromeric NMDA Receptors: Molecular and Functional Distinction of Subtypes. *Science,* 256**,** 1217-1221.
MORATALLA, R., VICKERS, E. A., ROBERTSON, H. A., COCHRAN, B. H. & GRAYBIEL, A. M. 1993. Coordinate expression of c-fos and jun B is induced in the rat striatum by cocaine. *J Neurosci,* 13**,** 423-33.
MORI, K., KISHI, K. & OJIMA, H. 1983. Distribution of dendrites of mitral, displaced mitral, tufted, and granule cells in the rabbit olfactory bulb. *J Comp Neurol,* 219**,** 339-55.
MORI, K., NAGAO, H. & YOSHIHARA, Y. 1999. The Olfactory Bulb: Coding and Processing of Odor Molecule Information. *Science,* 286**,** 711-715.
MOURET, A., LEPOUSEZ, G., GRAS, J., GABELLEC, M. M. & LLEDO, P. M. 2009. Turnover of newborn olfactory bulb neurons optimizes olfaction. *J Neurosci,* 29**,** 12302-14.
MOZELL, M. M., KENT, P. F. & MURPHY, S. J. 1991. The effect of flow rate upon the magnitude of the olfactory response differs for different odorants. *Chemical Senses,* 16**,** 631-649.
MUGNAINI, E., OERTEL, W. H. & WOUTERLOOD, F. F. 1984. Immunocytochemical localization of GABA neurons and dopamine neurons in the rat main and accessory olfactory bulbs. *Neuroscience Letters,* 47**,** 221-226.
MURAI, A., IWATA, R., FUJIMOTO, S., AIHARA, S., TSUBOI, A., MUROYAMA, Y., SAITO, T., NISHIZAKI, K. & IMAI, T. 2016. Distorted Coarse Axon Targeting and Reduced Dendrite Connectivity Underlie Dysosmia after Olfactory Axon Injury. *eneuro,* 3.
MURPHY, G. J., GLICKFELD, L. L., BALSEN, Z. & ISAACSON, J. S. 2004. Sensory Neuron Signaling to the Brain: Properties of Transmitter Release from Olfactory Nerve Terminals. *The Journal of Neuroscience,* 24**,** 3023-3030.
MURTHY, V. N., SCHIKORSKI, T., STEVENS, C. F. & ZHU, Y. 2001. Inactivity Produces Increases in Neurotransmitter Release and Synapse Size. *Neuron,* 32**,** 673-682.
MUTOH, H., YUAN, Q. & KNÖPFEL, T. 2005. Long-Term Depression at Olfactory Nerve Synapses. *The Journal of Neuroscience,* 25**,** 4252-4259.
NADI, N. S., HEAD, R., GRILLO, M., HEMPSTEAD, J., GRANNOT-REISFELD, N. & MARGOLIS, F. L. 1981. Chemical deafferentation of the olfactory bulb: Plasticity of the levels of tyrosine hydroxylase, dopamine and norepinephrine. *Brain Research,* 213**,** 365-377.
NAGAI, Y., SANO, H. & YOKOI, M. 2005. Transgenic expression of Cre recombinase in mitral/tufted cells of the olfactory bulb. *genesis,* 43**,** 12-16.
NAGAYAMA, S., ENERVA, A., FLETCHER, M. L., MASURKAR, A. V., IGARASHI, K. M., MORI, K. & CHEN, W. R. 2010. Differential axonal projection of mitral and tufted cells in the mouse main olfactory system. *Front Neural Circuits,* 4.
NAGAYAMA, S., HOMMA, R. & IMAMURA, F. 2014. Neuronal organization of olfactory bulb circuits. *Frontiers in Neural Circuits,* 8.
NAGAYAMA, S., TAKAHASHI, Y. K., YOSHIHARA, Y. & MORI, K. 2004. Mitral and tufted cells differ in the decoding manner of odor maps in the rat olfactory bulb. *J Neurophysiol,* 91**,** 2532-40.
NAJAC, M., JAN, D., REGUERO, L., GRANDES, P. & CHARPAK, S. 2011. *Monosynaptic and Polysynaptic Feed-Forward Inputs to Mitral Cells from Olfactory Sensory Neurons*.

NAKAMURA, T. & GOLD, G. H. 1987. A cyclic nucleotide-gated conductance in olfactory receptor cilia. *Nature,* 325**,** 442-4.
NARITSUKA, H., SAKAI, K., HASHIKAWA, T., MORI, K. & YAMAGUCHI, M. 2009. Perisomatic-targeting granule cells in the mouse olfactory bulb. *Journal of Comparative Neurology,* 515**,** 409-426.
NIZAK, C., MONIER, S., DEL NERY, E., MOUTEL, S., GOUD, B. & PEREZ, F. 2003. Recombinant antibodies to the small GTPase Rab6 as conformation sensors. *Science,* 300**,** 984-7.
NOLAN, M. F., DUDMAN, J. T., DODSON, P. D. & SANTORO, B. 2007. HCN1 channels control resting and active integrative properties of stellate cells from layer II of the entorhinal cortex. *The Journal of neuroscience : the official journal of the Society for Neuroscience,* 27**,** 12440-12451.
OHMOMO, H., INA, A., YOSHIDA, S., SHUTOH, F., UEDA, S. & HISANO, S. 2009. Postnatal changes in expression of vesicular glutamate transporters in the main olfactory bulb of the rat. *Neuroscience,* 160**,** 419-426.
OKA, Y., KATADA, S., OMURA, M., SUWA, M., YOSHIHARA, Y. & TOUHARA, K. 2006. Odorant Receptor Map in the Mouse Olfactory Bulb: In Vivo Sensitivity and Specificity of Receptor-Defined Glomeruli. *Neuron,* 52**,** 857-869.
OLIET, S. H. R., MALENKA, R. C. & NICOLL, R. A. 1996. Bidirectional Control of Quantal Size by Synaptic Activity in the Hippocampus. *Science,* 271**,** 1294-1297.
ORONA, E., SCOTT, J. W. & RAINER, E. C. 1983. Different granule cell populations innervate superficial and deep regions of the external plexiform layer in rat olfactory bulb. *J Comp Neurol,* 217**,** 227-37.
PADMANABHAN, K. & URBAN, N. N. 2010. Intrinsic biophysical diversity decorrelates neuronal firing while increasing information content. *Nat Neurosci,* 13**,** 1276-82.
PANZANELLI, P., PERAZZINI, A. Z., FRITSCHY, J. M. & SASSOE-POGNETTO, M. 2005. Heterogeneity of gamma-aminobutyric acid type A receptors in mitral and tufted cells of the rat main olfactory bulb. *J Comp Neurol,* 484**,** 121-31.
PARRISH-AUNGST, S., KIYOKAGE, E., SZABO, G., YANAGAWA, Y., SHIPLEY, M. T. & PUCHE, A. C. 2011. Sensory experience selectively regulates transmitter synthesis enzymes in interglomerular circuits. *Brain Res,* 1382**,** 70-6.
PARRISH-AUNGST, S., SHIPLEY, M. T., ERDELYI, F., SZABO, G. & PUCHE, A. C. 2007. Quantitative analysis of neuronal diversity in the mouse olfactory bulb. *J Comp Neurol,* 501**,** 825-36.
PETREANU, L. & ALVAREZ-BUYLLA, A. 2002. Maturation and death of adult-born olfactory bulb granule neurons: role of olfaction. *J Neurosci,* 22**,** 6106-13.
PETZOLD, G. C., HAGIWARA, A. & MURTHY, V. N. 2009. Serotonergic modulation of odor input to the mammalian olfactory bulb. *Nat Neurosci,* 12**,** 784-91.
PIGNATELLI, A. & BELLUZZI, O. 2008. *Cholinergic Modulation of Dopaminergic Neurons in the Mouse Olfactory Bulb*.
PIGNATELLI, A., KOBAYASHI, K., OKANO, H. & BELLUZZI, O. 2005. Functional properties of dopaminergic neurones in the mouse olfactory bulb. *J Physiol,* 564**,** 501-14.
PIMENTEL, D. O. & MARGRIE, T. W. 2008. Glutamatergic transmission and plasticity between olfactory bulb mitral cells. *The Journal of Physiology,* 586**,** 2107-2119.
PINCHING, A. J. & POWELL, T. P. S. 1971. The Neuron Types of the Glomerular Layer of the Olfactory Bulb. *Journal of Cell Science,* 9**,** 305-345.
PLATEL, J.-C., ANGELOVA, A., BUGEON, S., GANAY, T., CHUDOTVOROVA, I., DELOULME, J.-C., BECLIN, C., TIVERON, M.-C., CORE, N. & CREMER, H. 2018. Neuronal integration in the adult olfactory bulb is a non-selective addition process. *bioRxiv*.
POPOV, V. I., BOCHAROVA, L. S. & BRAGIN, A. G. 1992. Repeated changes of dendritic morphology in the hippocampus of ground squirrels in the course of hibernation. *Neuroscience,* 48**,** 45-51.
PREIBISCH, S., SAALFELD, S. & TOMANCAK, P. 2009. Globally optimal stitching of tiled 3D microscopic image acquisitions. *Bioinformatics,* 25**,** 1463-1465.

PRESSLER, R. T., INOUE, T. & STROWBRIDGE, B. W. 2007. Muscarinic Receptor Activation Modulates Granule Cell Excitability and Potentiates Inhibition onto Mitral Cells in the Rat Olfactory Bulb. *The Journal of Neuroscience,* 27**,** 10969-10981.

PRICE, J. L. & POWELL, T. P. S. 1970a. The Mitral and Short Axon Cells of the Olfactory Bulb. *Journal of Cell Science,* 7**,** 631-651.

PRICE, J. L. & POWELL, T. P. S. 1970b. The Morphology of the Granule Cells of the Olfactory Bulb. *Journal of Cell Science,* 7**,** 91-123.

PUCHE, A. C. & SHIPLEY, M. T. 1999. Odor-Induced, Activity-Dependent Transneuronal Gene InductionIn Vitro: Mediation by NMDA Receptors. *The Journal of Neuroscience,* 19**,** 1359-1370.

QUAST, K. B., UNG, K., FROUDARAKIS, E., HUANG, L., HERMAN, I., ADDISON, A. P., ORTIZ-GUZMAN, J., CORDINER, K., SAGGAU, P., TOLIAS, A. S. & ARENKIEL, B. R. 2016. Developmental broadening of inhibitory sensory maps. *Nature Neuroscience,* 20**,** 189.

RALL, W., SHEPHERD, G. M., REESE, T. S. & BRIGHTMAN, M. W. 1966. Dendrodendritic synaptic pathway for inhibition in the olfactory bulb. *Experimental Neurology,* 14**,** 44-56.

RAMÓN-CUETO, A. & AVILA, J. 1998. Olfactory ensheathing glia: properties and function. *Brain Research Bulletin,* 46**,** 175-187.

RASH, J. E., DAVIDSON, K. G. V., KAMASAWA, N., YASUMURA, T., KAMASAWA, M., ZHANG, C., MICHAELS, R., RESTREPO, D., OTTERSEN, O. P., OLSON, C. O. & NAGY, J. I. 2005. Ultrastructural localization of connexins (Cx36, Cx43, Cx45), glutamate receptors and aquaporin-4 in rodent olfactory mucosa, olfactory nerve and olfactory bulb. *Journal of Neurocytology,* 34**,** 307-341.

RESSLER, K. J., SULLIVAN, S. L. & BUCK, L. B. 1993. A zonal organization of odorant receptor gene expression in the olfactory epithelium. *Cell,* 73**,** 597-609.

ROCHEFORT, C., GHEUSI, G., VINCENT, J. D. & LLEDO, P. M. 2002. Enriched odor exposure increases the number of newborn neurons in the adult olfactory bulb and improves odor memory. *J Neurosci,* 22**,** 2679-89.

ROSSELLI-AUSTIN, L. & WILLIAMS, J. 1990. *Enriched neonatal odor exposure leads to increased numbers of olfactory bulb mitral and granule cells*.

ROYET, J. P., SICARD, G., SOUCHIER, C. & JOURDAN, F. 1987. Specificity of spatial patterns of glomerular activation in the mouse olfactory bulb: computer-assisted image analysis of 2-deoxyglucose autoradiograms. *Brain Research,* 417**,** 1-11.

RUBIN, B. D. & KATZ, L. C. 1999. Optical Imaging of Odorant Representations in the Mammalian Olfactory Bulb. *Neuron,* 23**,** 499-511.

SAFFEN, D. W., COLE, A. J., WORLEY, P. F., CHRISTY, B. A., RYDER, K. & BARABAN, J. M. 1988. Convulsant-induced increase in transcription factor messenger RNAs in rat brain. *Proceedings of the National Academy of Sciences,* 85**,** 7795-7799.

SAGHATELYAN, A., ROUX, P., MIGLIORE, M., ROCHEFORT, C., DESMAISONS, D., CHARNEAU, P., SHEPHERD, G. M. & LLEDO, P.-M. 2005. Activity-Dependent Adjustments of the Inhibitory Network in the Olfactory Bulb following Early Postnatal Deprivation. *Neuron,* 46**,** 103-116.

SAILOR, K. A., VALLEY, M. T., WIECHERT, M. T., RIECKE, H., SUN, G. J., ADAMS, W., DENNIS, J. C., SHARAFI, S., MING, G.-L., SONG, H. & LLEDO, P.-M. 2016. Persistent Structural Plasticity Optimizes Sensory Information Processing in the Olfactory Bulb. *Neuron,* 91**,** 384-396.

SALIN, P.-A., LLEDO, P.-M., VINCENT, J.-D. & CHARPAK, S. 2001. Dendritic Glutamate Autoreceptors Modulate Signal Processing in Rat Mitral Cells. *Journal of Neurophysiology,* 85**,** 1275-1282.

SAWADA, M., KANEKO, N., INADA, H., WAKE, H., KATO, Y., YANAGAWA, Y., KOBAYASHI, K., NEMOTO, T., NABEKURA, J. & SAWAMOTO, K. 2011. Sensory Input Regulates Spatial and Subtype-Specific Patterns of Neuronal Turnover in the Adult Olfactory Bulb. *The Journal of Neuroscience,* 31**,** 11587-11596.

SCHILLING, K., LUK, D., MORGAN, J. I. & CURRAN, T. 1991. Regulation of a fos-lacZ fusion gene: a paradigm for quantitative analysis of stimulus-transcription coupling. *Proceedings of the National Academy of Sciences,* 88**,** 5665-5669.

SCHINDELIN, J., ARGANDA-CARRERAS, I., FRISE, E., KAYNIG, V., LONGAIR, M., PIETZSCH, T., PREIBISCH, S., RUEDEN, C., SAALFELD, S., SCHMID, B., TINEVEZ, J. Y., WHITE, D. J., HARTENSTEIN, V., ELICEIRI, K., TOMANCAK, P. & CARDONA, A. 2012. Fiji: an open-source platform for biological-image analysis. *Nat Methods,* 9**,** 676-82.

SCHINDELIN, J., RUEDEN, C. T., HINER, M. C. & ELICEIRI, K. W. 2015. The ImageJ ecosystem: An open platform for biomedical image analysis. *Molecular Reproduction and Development,* 82**,** 518-529.

SCHNEGGENBURGER, R., SAKABA, T. & NEHER, E. 2002. Vesicle pools and short-term synaptic depression: lessons from a large synapse. *Trends Neurosci,* 25**,** 206-12.

SCHNELL, E., SIZEMORE, M., KARIMZADEGAN, S., CHEN, L., BREDT, D. S. & NICOLL, R. A. 2002. Direct interactions between PSD-95 and stargazin control synaptic AMPA receptor number. *Proceedings of the National Academy of Sciences,* 99**,** 13902-13907.

SCHOENFELD, T. A. & CLELAND, T. A. 2005. The anatomical logic of smell. *Trends in Neurosciences,* 28**,** 620-627.

SCHOENFELD, T. A., MARCHAND, J. E. & MACRIDES, F. 1985. Topographic organization of tufted cell axonal projections in the hamster main olfactory bulb: An intrabulbar associational system. *Journal of Comparative Neurology,* 235**,** 503-518.

SCHOPPA, N. E. & WESTBROOK, G. L. 2001. Glomerulus-Specific Synchronization of Mitral Cells in the Olfactory Bulb. *Neuron,* 31**,** 639-651.

SCHOPPA, N. E. & WESTBROOK, G. L. 2002a. AMPA autoreceptors drive correlated spiking in olfactory bulb glomeruli. *Nature Neuroscience,* 5**,** 1194.

SCHOPPA, N. E. & WESTBROOK, G. L. 2002b. AMPA autoreceptors drive correlated spiking in olfactory bulb glomeruli. *Nat Neurosci,* 5**,** 1194-202.

SCHWOB, J. E. 2002. Neural regeneration and the peripheral olfactory system. *The Anatomical Record,* 269**,** 33-49.

SCHWOB, J. E., YOUNGENTOB, S. L., RING, G., IWEMA, C. L. & MEZZA, R. C. 1999. Reinnervation of the rat olfactory bulb after methyl bromide-induced lesion: Timing and extent of reinnervation. *Journal of Comparative Neurology,* 412**,** 439-457.

SEROOGY, K. B., BRECHA, N. & GALL, C. 1985. Distribution of cholecystokinin-like immunoreactivity in the rat main olfactory bulb. *Journal of Comparative Neurology,* 239**,** 373-383.

SHAO, Z., PUCHE, A. C., LIU, S. & SHIPLEY, M. T. 2012. Intraglomerular inhibition shapes the strength and temporal structure of glomerular output. *Journal of Neurophysiology,* 108**,** 782-793.

SHEPHERD, G. M., CHEN, W. R., WILLHITE, D., MIGLIORE, M. & GREER, C. A. 2007. The olfactory granule cell: From classical enigma to central role in olfactory processing. *Brain Research Reviews,* 55**,** 373-382.

SHOLL, D. A. 1953. Dendritic organization in the neurons of the visual and motor cortices of the cat. *J Anat,* 87**,** 387-406.

SHPAK, G., ZYLBERTAL, A., YAROM, Y. & WAGNER, S. 2012. Calcium-Activated Sustained Firing Responses Distinguish Accessory from Main Olfactory Bulb Mitral Cells. *The Journal of Neuroscience,* 32**,** 6251-6262.

SIN, W. C., HAAS, K., RUTHAZER, E. S. & CLINE, H. T. 2002. Dendrite growth increased by visual activity requires NMDA receptor and Rho GTPases. *Nature,* 419**,** 475.

SMITH, T. C. & JAHR, C. E. 2002. Self-inhibition of olfactory bulb neurons. *Nature Neuroscience,* 5**,** 760.

SOBEL, N., KHAN, R. M., HARTLEY, C. A., SULLIVAN, E. V. & GABRIELI, J. D. E. 2000. Sniffing Longer rather than Stronger to Maintain Olfactory Detection Threshold. *Chemical Senses,* 25**,** 1-8.

SOBEL, N., KHAN, R. M., SALTMAN, A., SULLIVAN, E. V. & GABRIELI, J. D. E. 1999. The world smells different to each nostril. *Nature,* 402**,** 35.

SPORS, H., ALBEANU, D. F., MURTHY, V. N., RINBERG, D., UCHIDA, N., WACHOWIAK, M. & FRIEDRICH, R. W. 2012. Illuminating Vertebrate Olfactory Processing. *The Journal of Neuroscience,* 32**,** 14102-14108a.

SPORS, H. & GRINVALD, A. 2002. Spatio-Temporal Dynamics of Odor Representations in the Mammalian Olfactory Bulb. *Neuron,* 34**,** 301-315.

SPORS, H., WACHOWIAK, M., COHEN, L. B. & FRIEDRICH, R. W. 2006. Temporal Dynamics and Latency Patterns of Receptor Neuron Input to the Olfactory Bulb. *The Journal of Neuroscience,* 26**,** 1247-1259.

STATHAKIS, D. G., HOOVER, K. B., YOU, Z. & BRYANT, P. J. 1997. Human postsynaptic density-95 (PSD95): location of the gene (DLG4) and possible function in nonneural as well as in neural tissues. *Genomics,* 44**,** 71-82.

TAKAHASHI, Y. K., KUROSAKI, M., HIRONO, S. & MORI, K. 2004. Topographic Representation of Odorant Molecular Features in the Rat Olfactory Bulb. *Journal of Neurophysiology,* 92**,** 2413-2427.

TAN, J., SAVIGNER, A., MA, M. & LUO, M. 2010. Odor Information Processing by the Olfactory Bulb Analyzed in Gene-Targeted Mice. *Neuron,* 65**,** 912-926.

TANIGUCHI, H., HE, M., WU, P., KIM, S., PAIK, R., SUGINO, K., KVITSANI, D., FU, Y., LU, J., LIN, Y., MIYOSHI, G., SHIMA, Y., FISHELL, G., NELSON, SACHA B. & HUANG, Z. J. 2011. A Resource of Cre Driver Lines for Genetic Targeting of GABAergic Neurons in Cerebral Cortex. *Neuron,* 71**,** 995-1013.

TATTI, R., BHAUKAURALLY, K., GSCHWEND, O., SEAL, R. P., EDWARDS, R. H., RODRIGUEZ, I. & CARLETON, A. 2014. A population of glomerular glutamatergic neurons controls sensory information transfer in the mouse olfactory bulb. *Nature communications* [Online], 5. Available: http://europepmc.org/abstract/MED/24804702

http://europepmc.org/articles/PMC4028618?pdf=render

http://europepmc.org/articles/PMC4028618

https://doi.org/10.1038/ncomms4791 [Accessed 2014/05//].

THANAWALA, M. S. & REGEHR, W. G. 2016. Determining synaptic parameters using high-frequency activation. *Journal of Neuroscience Methods,* 264**,** 136-152.

TOBIN, V. A., HASHIMOTO, H., WACKER, D. W., TAKAYANAGI, Y., LANGNAESE, K., CAQUINEAU, C., NOACK, J., LANDGRAF, R., ONAKA, T., LENG, G., MEDDLE, S. L., ENGELMANN, M. & LUDWIG, M. 2010. An intrinsic vasopressin system in the olfactory bulb is involved in social recognition. *Nature,* 464**,** 413-7.

TRIPATHY, S. J., PADMANABHAN, K., GERKIN, R. C. & URBAN, N. N. 2013. Intermediate intrinsic diversity enhances neural population coding. *Proceedings of the National Academy of Sciences,* 110**,** 8248-8253.

TROMBLEY, P. & SHEPHERD, G. 1992. Noradrenergic inhibition of synaptic transmission between mitral and granule cells in mammalian olfactory bulb cultures. *The Journal of Neuroscience,* 12**,** 3985-3991.

TURRIGIANO, G. G. & NELSON, S. B. 2004. Homeostatic plasticity in the developing nervous system. *Nature Reviews Neuroscience,* 5**,** 97.

TYLER, W. J., PETZOLD, G. C., PAL, S. K. & MURTHY, V. N. 2007. Experience-Dependent Modification of Primary Sensory Synapses in the Mammalian Olfactory Bulb. *The Journal of Neuroscience,* 27**,** 9427-9438.

VAAGA, C. E. & WESTBROOK, G. L. 2016. Parallel processing of afferent olfactory sensory information. *J Physiol,* 594**,** 6715-6732.

VAAGA, C. E. & WESTBROOK, G. L. 2017. Distinct temporal filters in mitral cells and external tufted cells of the olfactory bulb. *The Journal of Physiology,* 595**,** 6349-6362.

VAAGA, C. E., YORGASON, J. T., WILLIAMS, J. T. & WESTBROOK, G. L. 2017. Presynaptic gain control by endogenous cotransmission of dopamine and GABA in the olfactory bulb. *Journal of Neurophysiology,* 117**,** 1163-1170.

VAN WELIE, I., VAN HOOFT, J. A. & WADMAN, W. J. 2004. Homeostatic scaling of neuronal excitability by synaptic modulation of somatic hyperpolarization-activated I_h channels. *Proceedings of the National Academy of Sciences of the United States of America,* 101**,** 5123-5128.

VARGAS-BARROSO, V., ORDAZ-SÁNCHEZ, B., PEÑA-ORTEGA, F. & LARRIVA-SAHD, J. A. 2016. Electrophysiological Evidence for a Direct Link between the Main and Accessory Olfactory Bulbs in the Adult Rat. *Frontiers in Neuroscience,* 9.

VASSAR, R., CHAO, S. K., SITCHERAN, R., NUN˜EZ, J. M., VOSSHALL, L. B. & AXEL, R. 1994. Topographic organization of sensory projections to the olfactory bulb. *Cell,* 79**,** 981-991.

VAZDARJANOVA, A., RAMIREZ-AMAYA, V., INSEL, N., PLUMMER, T. K., ROSI, S., CHOWDHURY, S., MIKHAEL, D., WORLEY, P. F., GUZOWSKI, J. F. & BARNES, C. A. 2006. Spatial exploration induces ARC, a plasticity-related immediate-early gene, only in calcium/calmodulin-dependent protein kinase II-positive principal excitatory and inhibitory neurons of the rat forebrain. *J Comp Neurol,* 498**,** 317-29.

WACHOWIAK, M. & COHEN, L. B. 1999. Presynaptic Inhibition of Primary Olfactory Afferents Mediated by Different Mechanisms in Lobster and Turtle. *The Journal of Neuroscience,* 19**,** 8808-8817.

WACHOWIAK, M. & SHIPLEY, M. T. 2006. Coding and synaptic processing of sensory information in the glomerular layer of the olfactory bulb. *Semin Cell Dev Biol,* 17**,** 411-23.

WALLACE, J. L., WIENISCH, M. & MURTHY, V. N. 2017. Development and Refinement of Functional Properties of Adult-Born Neurons. *Neuron,* 96**,** 883-896.e7.

WEFELMEYER, W., CATTAERT, D. & BURRONE, J. 2015. Activity-dependent mismatch between axo-axonic synapses and the axon initial segment controls neuronal output. *Proceedings of the National Academy of Sciences*.

WENZEL, A., SCHEURER, L., KUNZI, R., FRITSCHY, J. M., MOHLER, H. & BENKE, D. 1995. Distribution of NMDA receptor subunit proteins NR2A, 2B, 2C and 2D in rat brain. *Neuroreport,* 7**,** 45-8.

WHITESELL, J. D., SORENSEN, K. A., JARVIE, B. C., HENTGES, S. T. & SCHOPPA, N. E. 2013. Interglomerular lateral inhibition targeted on external tufted cells in the olfactory bulb. *J Neurosci,* 33**,** 1552-63.

WILSON, D. & SULLIVAN, R. 1995. The D2 antagonist spiperone mimics the effects of olfactory deprivation on mitral/tufted cell odor response patterns. *The Journal of Neuroscience,* 15**,** 5574-5581.

WILSON, D. A., BEST, A. R. & SULLIVAN, R. M. 2004. Plasticity in the Olfactory System: Lessons for the Neurobiology of Memory. *The Neuroscientist,* 10**,** 513-524.

WILSON, D. A., SULLIVAN, R. M., GALL, C. M. & GUTHRIE, K. M. 1996. NMDA-Receptor modulation of lateral inhibition and c-fos expression in olfactory bulb. *Brain Research,* 719**,** 62-71.

WILSON, R. I. & MAINEN, Z. F. 2006. EARLY EVENTS IN OLFACTORY PROCESSING. *Annual Review of Neuroscience,* 29**,** 163-201.

WINPENNY, E., LEBEL-POTTER, M., FERNANDEZ, M. E., BRILL, M. S., GÖTZ, M., GUILLEMOT, F. & RAINETEAU, O. 2011. Sequential generation of olfactory bulb glutamatergic neurons by Neurog2-expressing precursor cells. *Neural Development,* 6**,** 12.

XUE, M., ATALLAH, B. V. & SCANZIANI, M. 2014. Equalizing excitation–inhibition ratios across visual cortical neurons. *Nature,* 511**,** 596.

YAMAGUCHI, M. 2014. Interneurons in the Olfactory Bulb: Roles in the Plasticity of Olfactory Information Processing. *In:* MORI, K. (ed.) *The Olfactory System: From Odor Molecules to Motivational Behaviors.* Tokyo: Springer Japan.

YAMAGUCHI, M. & MORI, K. 2005. Critical period for sensory experience-dependent survival of newly generated granule cells in the adult mouse olfactory bulb. *Proc Natl Acad Sci U S A,* 102**,** 9697-702.

YAN, Z., TAN, J., QIN, C., LU, Y., DING, C. & LUO, M. 2008. Precise Circuitry Links Bilaterally Symmetric Olfactory Maps. *Neuron,* 58**,** 613-624.

YANG, X.-D., KORN, H. & FABER, D. S. 1990. Long-term potentiation of electrotonic coupling at mixed synapses. *Nature,* 348**,** 542.

YASSIN, L., BENEDETTI, B. L., JOUHANNEAU, J.-S., WEN, J. A., POULET, J. F. A. & BARTH, A. L. 2010. An Embedded Subnetwork of Highly Active Neurons in the Neocortex. *Neuron,* 68**,** 1043-1050.

YU, C. R., POWER, J., BARNEA, G., O'DONNELL, S., BROWN, H. E. V., OSBORNE, J., AXEL, R. & GOGOS, J. A. 2004. Spontaneous Neural Activity Is Required for the Establishment and Maintenance of the Olfactory Sensory Map. *Neuron,* 42**,** 553-566.

ZHANG, C. 2011. Expression of connexin 57 in the olfactory epithelium and olfactory bulb. *Neuroscience Research,* 71**,** 226-234.

ZHANG, W. & LINDEN, D. 2003. *The other side of the engram: Experience-driven changes in neuronal intrinsic excitability*.

ZHOU, Z. & BELLUSCIO, L. 2008. Intrabulbar Projecting External Tufted Cells Mediate a Timing-Based Mechanism That Dynamically Gates Olfactory Bulb Output. *The Journal of Neuroscience,* 28**,** 9920-9928.

ZHU, Y.-Y., NI, D.-F. & XU, C.-M. 2009. *Gene Expression Profiles in the Olfactory Bulb from a Rat Model of Alzheimer's Disease*.

ZOU, D. J., FEINSTEIN, P., RIVERS, A. L., MATHEWS, G. A., KIM, A., GREER, C. A., MOMBAERTS, P. & FIRESTEIN, S. 2004. Postnatal refinement of peripheral olfactory projections. *Science,* 304**,** 1976-9.